NASA TECHNICAL MEMORANDUM



NASA TM X-1840

NASA TM X-1840

CASE FILE COPY

EFFECT OF HYPERSONIC RESEARCH ENGINE INSTALLATION ON AERODYNAMIC CHARACTERISTICS OF 0.0667-SCALE MODEL OF X-15A-2 AIRPLANE AT MACH NUMBERS FROM 1.75 TO 4.63

by Ernald B. Graves

Langley Research Center
Langley Station, Hampton, Va.

NATIONAL AERONAUTICS AND SPACE ADMINISTRATION • WASHINGTON, D. C. • AUGUST 1969

1. Report No. NASA TM X-1840	2. Government Accession No.	3. Recipient's Catalog No.
4. Title and Subtitle EFFECT OF HYPERSONIC RESEARCH ENGINE INSTALLATION ON AERODYNAMIC CHARACTERISTICS OF 0.0667-SCALE MODEL OF X-15A-2 AIRPLANE AT MACH NUMBERS FROM 1.75 to 4.63		5. Report Date August 1969 6. Performing Organization Code
7. Author(s) Ernald B. Graves		8. Performing Organization Report No. L-6347
9. Performing Organization Name and Address NASA Langley Research Center Hampton, Va. 23365		10. Work Unit No. 722-03-00-06-23 11. Contract or Grant No. 13. Type of Report and Period Covered Technical Memorandum
12. Sponsoring Agency Name and Address National Aeronautics and Space Administration Washington, D.C. 20546		14. Sponsoring Agency Code
15. Supplementary Notes		

16. Abstract

An investigation has been conducted in the Langley Unitary Plan wind tunnel to determine the effect of the proposed NASA hypersonic research engine (HRE) installation on the aerodynamic characteristics of a 0.0667-scale model of the X-15A-2 research vehicle. Test Mach numbers ranged from 1.75 to 4.63 at a constant Reynolds number of 3.0×10^6 per foot (9.84×10^6 per meter). The angle-of-attack range was from about -5^0 to 20^0 and the angle-of-sideslip range was from about -4^0 to 9^0.

Test results indicate that the installation of the hypersonic research engine on the X-15A-2 research vehicle will not generally produce any significant adverse effects on the static stability and control characteristics of the airplane. As expected, there is a small drag increase due to the presence of the engine. Shock patterns emanating from the leading edges of the wing and landing skid appear to be interacting with the flow field forward of the HRE inlet. This interaction would significantly influence the performance of the HRE.

17. Key Words Suggested by Author(s)	18. Distribution Statement
Static aerodynamic characteristics X-15 aircraft Hypersonic research engine	Unclassified – Unlimited

19. Security Classif. (of this report)	20. Security Classif. (of this page)	21. No. of Pages	22. Price
Unclassified	Unclassified	185	$3.00

EFFECT OF HYPERSONIC RESEARCH ENGINE INSTALLATION ON AERODYNAMIC CHARACTERISTICS OF 0.0667-SCALE MODEL OF X-15A-2 AIRPLANE AT MACH NUMBERS FROM 1.75 TO 4.63

By Ernald B. Graves
Langley Research Center

SUMMARY

An investigation has been conducted in the Langley Unitary Plan wind tunnel to determine the effect of the proposed NASA hypersonic research engine (HRE) installation on the aerodynamic characteristics of a 0.0667-scale model of the X-15A-2 research vehicle. Test Mach numbers ranged from 1.75 to 4.63 at a constant Reynolds number of 3.0×10^6 per foot (9.84×10^6 per meter). The angle-of-attack range was from about -5° to 20° and the angle-of-sideslip range was from about -4° to 9°.

Test results indicate that the installation of the hypersonic research engine on the X-15A-2 research vehicle will not generally produce any significant adverse effects on the static stability and control characteristics of the airplane. As expected, there is a small drag increase due to the presence of the engine. Shock patterns emanating from the leading edges of the wing and landing skid appear to be interacting with the flow field forward of the HRE inlet. This interaction would significantly influence the performance of the HRE.

INTRODUCTION

The Langley Research Center is currently pursuing the development of a hypersonic research engine (HRE). As a part of this project, the X-15A-2 airplane was selected as the flight test facility and a wind-tunnel test program was initiated to determine the stability and control characteristics of a 0.0667-scale model of the X-15A-2 airplane with an HRE model installed.

The tests, results presented herein, were performed in the Langley Unitary Plan Wind tunnel at Mach numbers from 1.75 to 4.63 through an angle-of-attack range from about -5° to 20° and an angle-of-sideslip range from about -4° to 9° at a constant Reynolds number of 3.0×10^6 per foot (9.84×10^6 per meter). Results of tests on the model with speed brakes deployed are also included.

SYMBOLS

The longitudinal and lateral data are presented about the stability and body axes system, respectively. The moment reference center is located at the 20-percent wing mean geometric chord (24.96 inches (63.40 centimeters) aft of the model nose, see fig. 1(a)).

b	wing span
C_D	drag coefficient, $\frac{\text{Drag}}{qS}$
$C_{D,o}$	drag coefficient at $C_L = 0$
C_L	lift coefficient, $\frac{\text{Lift}}{qS}$
C_{L_α}	lift-curve slope per degree
$C_{L,\alpha=0}$	lift coefficient at $\alpha = 0^o$
C_Y	side-force coefficient, $\frac{\text{Side force}}{qS}$
C_{Y_β}	side-force parameter, $\frac{\Delta C_Y}{\Delta\beta}$, per degree
C_l	rolling-moment coefficient, $\frac{\text{Rolling moment}}{qSb}$
C_{l_β}	effective-dihedral parameter, $\frac{\Delta C_l}{\Delta\beta}$, per degree
C_m	pitching-moment coefficient, $\frac{\text{Pitching moment}}{qS\bar{c}}$
$C_{m,o}$	pitching-moment coefficient at $C_L = 0$
C_{m_δ}	control effectiveness parameter, $\frac{\Delta C_m}{\Delta\delta_h}$, per degree
C_n	yawing-moment coefficient, $\frac{\text{Yawing moment}}{qSb}$
C_{n_β}	directional-stability parameter, $\frac{\Delta C_n}{\Delta\beta}$, per degree
$\bar{c}$	wing mean geometric chord

L/D	lift-drag ratio, C_L/C_D
M	free-stream Mach number
q	free-stream dynamic pressure
S	wing plan-form area
x_{ac}	aerodynamic center, $\frac{\partial C_m}{\partial C_L}$
α	angle of attack, degrees
β	angle of sideslip, degrees
δ_J	deflection of speed brakes, degrees
δ_h	deflection of horizontal tail, positive trailing edge down, degrees

Model nomenclature:

B_{11}	modified fuselage
H_9	horizontal stabilizer
J_{L4}	lower speed brakes: integral with ramjet pylon
J_{U2}	upper speed brakes: integral with vertical stabilizer

} Brakes deployed simultaneously

N_{12}	hypersonic research engine: simulated open inlet (spike retracted), pylon-mounted to aft fuselage underside
N_{13}	hypersonic research engine: simulated closed inlet (spike extended), pylon-mounted to aft fuselage underside
T_{12}	tank, spherical helium bottle located aft the upper speed brake well
T_{13}	fuel tanks: two tanks, one mounted to the lower surface of each fuselage fairing

V_{L8} lower vertical stabilizer

V_{U5} upper vertical stabilizer

V_{U6} extended upper vertical stabilizer

W_2 wing

X_{16} modified side fairings

Y_5 ramjet pylon: support for hypersonic research engine, attaches to aft fuselage underside, replaces lower vertical stabilizer, incorporates lower speed brakes

APPARATUS AND METHODS

Model

Drawings of the 0.0667-scale model of the X-15A-2 airplane used in this investigation and of the HRE are presented in figure 1 and a photograph of the model is presented as figure 2. Additional information on the X-15A-2 model geometry may be found in reference 1.

The basic test configuration is designated by the code $B_{11}X_{16}W_2H_9T_{12}V_{U5}Y_5N_{13}$, where $B_{11}X_{16}W_2H_9T_{12}$ are common to all test configurations. Although there is no code designation, a fuselage nozzle was installed on the model and is a part of the basic configuration. The removable external fuel tanks T_{13} are an integral part of the X-15A-2 vehicle and are not a part of the HRE installation.

The model ventral fin could be replaced by a pylon for supporting the hypersonic research engine. Provision was made for mounting the HRE simulating an inlet open position (inlet spike retracted) or an inlet closed position (inlet spike extended). Model simulation did not include airflow through the HRE. Unless otherwise noted, the HRE simulating the inlet closed position was used for these tests. A vertical tail with an extended span and speed brakes housed within the vertical surfaces were also provided.

Tunnel

Tests were conducted in both the low and high Mach number test sections of the Langley Unitary Plan wind tunnel which is a closed-loop, variable-pressure facility. Each test section is about 4 feet (1.22 meters) square and about 7 feet (2.13 meters) long. The nozzle leading to each test section is of the asymmetric sliding-block type which

permits a continuous variation in Mach number from about 1.5 to 2.9 in the low Mach number test section and from about 2.3 to 4.7 in the high Mach number test section.

Test Conditions and Corrections

Tests were conducted at Mach numbers from 1.75 to 4.63 at a constant Reynolds number of 3.0×10^6 per foot (9.84×10^6 per meter). The angles of attack ranged from about -5° to 20° and angles of sideslip ranged from about -4° to 9°. Forces and moments on the model were measured by means of an internally mounted, six-component electrical strain-gage balance which was connected to a sting support system. Pressure in the model chamber was measured by means of a single static orifice. Transition strips in 1/16-inch (0.16 centimeter) bands were affixed to the model 1.2 inches (3.05 centimeters) aft of the model and fuel tank nose apexes and 0.4 inch (1.02 centimeters) aft of all the airfoil sections in a streamwise direction. No. 60 sand was used at Mach numbers from 1.75 to 2.86. No. 35 sand was used at the higher Mach numbers. The test-section dew-point temperature was maintained sufficiently low to avoid any significant condensation effects.

Angles of attack and sideslip were corrected for sting-balance deflections due to aerodynamic loads. Angles of attack were also corrected for tunnel-flow angularity. The drag-coefficient data presented have been adjusted to free-stream conditions acting over the base of the fuselage nozzle and over the base of the fuselage when fuselage nozzle is off. No corrections were applied for the pressures acting over the base of the HRE.

PRESENTATION OF RESULTS

The results of the investigation are presented as follows:

	Figure
Effect of HRE components and fuel tanks on longitudinal aerodynamic characteristics	3
Longitudinal control effectiveness for $B_{11}X_{16}W_2H_9T_{12}V_{U5}Y_5N_{13}$ (HRE on)	4
Longitudinal control effectiveness for $B_{11}X_{16}W_2H_9T_{12}V_{U5}Y_5$ (HRE off)	5
Longitudinal control effectiveness for $B_{11}X_{16}W_2H_9T_{12}V_{U5}Y_5N_{13}T_{13}$ (HRE and tanks on)	6
Effect of HRE spike position on longitudinal aerodynamic characteristics	7
Effect of fuselage nozzle on longitudinal aerodynamic characteristics	8
Effect of extended vertical tail on longitudinal aerodynamic characteristics	9
Effect of speed-brake deflection on longitudinal control for $B_{11}X_{16}W_2H_9T_{12}V_{U5}Y_5N_{13}$ (HRE on) with $\delta_h = 0^\circ$	10
Effect of speed-brake deflection on longitudinal control for $B_{11}X_{16}W_2H_9T_{12}V_{U5}Y_5N_{13}$ (HRE on) with $\delta_h = -10^\circ$	11

Figure

Effect of speed-brake deflection on longitudinal control for $B_{11}X_{16}W_2H_9T_{12}V_{U5}Y_5N_{13}$ (HRE on) with $\delta_h = -20^o$ 12
Effect of speed-brake deflection on longitudinal control for $B_{11}X_{16}W_2H_9T_{12}V_{U5}Y_5$ (HRE off) with $\delta_h = 0^o$ 13
Effect of speed-brake deflection on longitudinal control for $B_{11}X_{16}W_2H_9T_{12}V_{U5}Y_5$ (HRE off) with $\delta_h = -10^o$ 14
Effect of speed-brake deflection on longitudinal control for $B_{11}X_{16}W_2H_9T_{12}V_{U5}Y_5$ (HRE off) with $\delta_h = -20^o$ 15
Summary of longitudinal aerodynamic characteristics 16
Variation of lateral aerodynamic coefficients with sideslip angle 17
Effect of HRE components and fuel tanks on lateral stability parameters 18
Effect of horizontal-tail deflection on lateral stability parameters for $B_{11}X_{16}W_2H_9T_{12}V_{U5}Y_5N_{13}$ (HRE on) 19
Effect of horizontal-tail deflection on lateral stability parameters for $B_{11}X_{16}W_2H_9T_{12}V_{U5}Y_5$ (HRE off) 20
Effect of horizontal-tail deflection on lateral stability parameters for $B_{11}X_{16}W_2H_9T_{12}V_{U5}Y_5N_{13}T_{13}$ (HRE and tanks on) 21
Effect of HRE spike position on lateral stability parameters 22
Effect of fuselage nozzle on lateral stability parameters 23
Effect of extended vertical tail on lateral stability parameters 24
Effect of speed-brake deflection on lateral stability parameters for $B_{11}X_{16}W_2H_9T_{12}V_{U5}Y_5N_{13}$ (HRE on) 25
Effect of speed-brake deflection on lateral stability parameters for $B_{11}X_{16}W_2H_9T_{12}V_{U5}Y_5$ (HRE off) 26
Roll control effectiveness of the horizontal tail for $B_{11}X_{16}W_2H_9T_{12}V_{U5}Y_5N_{13}$ (HRE on) 27
Roll control effectiveness of the horizontal tail for $B_{11}X_{16}W_2H_9T_{12}V_{U5}Y_5$ (HRE off) 28
Roll control effectiveness of the horizontal tail for $B_{11}X_{16}W_2H_9T_{12}V_{U5}Y_5N_{13}T_{13}$ (HRE and tanks on) 29
Summary of lateral stability parameters 30
Schlieren photographs 31

DISCUSSION

Longitudinal Aerodynamic Characteristics

The effects of the HRE components and the external fuel tanks on the longitudinal aerodynamic characteristics of the X-15A-2 model are shown in figure 3. The data

indicate that the engine causes a slight increase in $C_{L,\alpha=0}$ which leads to a noticeable decrease in $C_{m,o}$. These effects, however, decrease with increase in Mach number. As expected, installation of the HRE adds to the drag of the model and thus reduces the lift-drag ratio. These adverse effects, however, would probably not be as large as shown if airflow were provided through the inlet. The large external fuel tanks lead to a significant decrease in the stability level with an accompanying noticeable increase in $C_{m,o}$. The data indicate marginal stability for the test center-of-gravity location at angles of attack in excess of about 10° with the external fuel tanks installed.

The longitudinal control effectiveness of the horizontal tail is shown in figures 4, 5, and 6 for the basic, HRE off, and the tanks-on configurations, respectively. The horizontal tail is effective in producing pitching moment throughout the test Mach number range, and there appears to be little effect of the HRE or the tanks on C_m. There is, however, a slight decrease in C_{m_δ} with increase in control deflection and a significant decrease in C_{m_δ} with increase in Mach number for each of the configurations.

There are no significant effects on the longitudinal aerodynamic characteristics due to the HRE inlet spike position, due to the fuselage nozzle, or due to the extended vertical tail. (See figs. 7, 8, and 9, respectively).

Figures 10 to 12 and 13 to 15 present the effects of speed-brake deflection on the longitudinal control of the engine-on and engine-off configurations, respectively, for horizontal-tail deflections of 0°, -10°, and -20°. The speed brakes are effective in producing large drag increments for the model provided large deflections are used. The drag-coefficient increment due to δ_J is not linear since a 10° speed-brake deflection produces only a small ΔC_D in comparison with a 35° deflection, and at the higher Mach numbers, the ΔC_D due to δ_J is almost negligible for the 10° deflection. Deflection of the speed brakes also leads to a slight increase in the stability level of the model. Horizontal-tail deflection has little or no effect on the speed-brake capabilities.

A summary of the longitudinal data is presented in figure 16. The familiar decrease in C_{L_α}, $C_{D,o}$, and C_{m_δ} with increase in Mach number may be noted in the figure. In addition, there is a forward shift in aerodynamic-center position of about 14 percent mean aerodynamic chord from the lowest to the highest test Mach number for the configuration without external tanks.

Lateral Aerodynamic Characteristics

Some examples of variation of lateral aerodynamic coefficients with sideslip angle are shown in figure 17. At an angle of attack of 0° the data are relatively linear; however, with an increase in α to 10°, the variation becomes nonlinear particularly for the yawing-moment coefficients. Data for the ensuing figures showing lateral stability parameters were obtained from pitch polars at $\beta = 0^o$ and 4°, and although the basic data were

not linear through this β range at discrete angles of attack, it is felt that the comparative data are qualitatively correct.

The effects of the HRE components and the external fuel tanks on the lateral stability parameters are shown in figure 18. In general, the HRE installation produces an increase in directional stability and a decrease in effective dihedral at all test Mach numbers and throughout the angle-of-attack range. The external tanks, however, generally cause a decrease in directional stability and an increase in effective dihedral. This decrease in directional stability obviously results from a forward shift in center-of-pressure location due to the tanks since C_{Y_β} for this configuration is considerably more negative than even that with the HRE installed.

The data in figures 19, 20, and 21 generally indicate that neither the HRE nor the external tanks have any significant effect on the directional stability or effective dihedral of the model with various tail deflections.

There are no large effects of the HRE inlet spike position or the fuselage nozzle on the lateral stability parameters of the test configuration throughout the angle-of-attack and Mach number range (figs. 22 and 23). The extended vertical tail (fig. 24) however leads to significant increases in both directional stability and effective dihedral for the model at all test Mach numbers.

Deploying the speed brakes to an angle of 35° leads to significant increases in directional stability at all test Mach numbers and angles of attack. A 10° speed-brake deflection produces only a small increase in C_{n_β} (figs. 25 and 26).

Differential settings of the horizontal tail are effective in producing rolling moment at all test conditions, and neither the HRE nor the external fuel tanks have any significant effect on this capability. In addition, differential settings of the horizontal tail generally cause a favorable yawing moment to accompany the roll. These results may be found in figures 27 to 29.

A summary of the lateral stability parameter data is presented in figure 30. The variations of the lateral parameters with Mach number for the various test configurations are essentially the same, only the levels are different as previously noted.

Interference Effects

Schlieren photographs were taken of many of the test configurations with particular emphasis on the flow field in the vicinity of the HRE. From the photographs in figure 31, it appears that shock waves emanating from the leading edges of the wing and landing skid of the model are interacting with the flow field forward of the HRE inlet. This, of course, would significantly influence the performance of the HRE. The need for further study of this phenomenon is indicated. In flight tests at the NASA Flight Research Center,

Burcham and Nugent noted shock impingement on a pylon-mounted dummy ramjet engine mounted under the X-15-2 airplane; thus, the schlieren photographic data presented herein is substantiated.

CONCLUSIONS

Supersonic tests of a 0.0667-scale model of the X-15A-2 airplane, with and without the hypersonic research engine (HRE) attached, lead to the following conclusions:

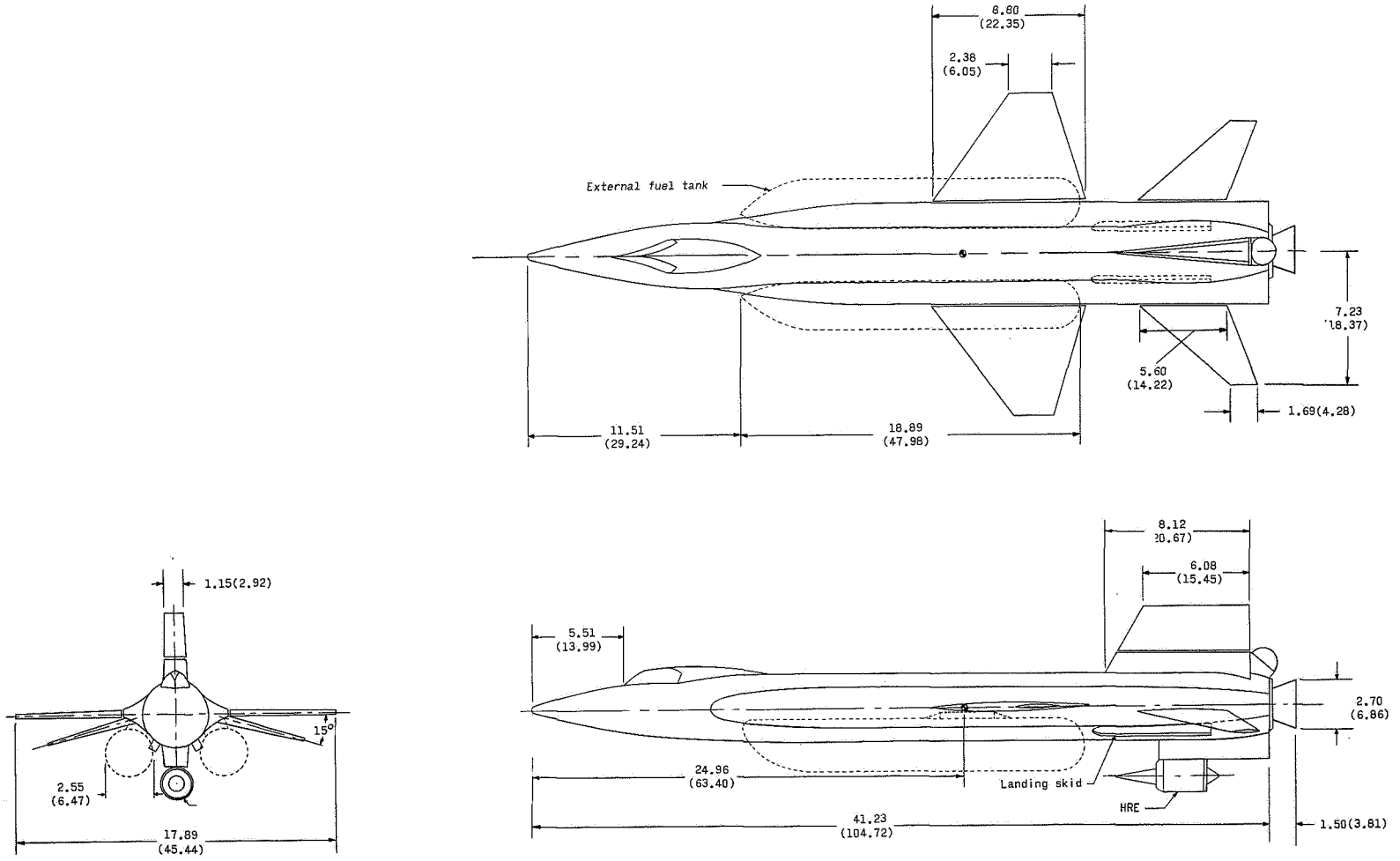
1. Installation of the HRE on the X-15A-2 model produces no significant adverse effects on the static stability and control characteristics of the vehicle. There exists, however, a noticeable increase in drag coefficient.

2. Shock patterns emanating from the leading edges of the wing and landing skid appear to be interacting with the flow field forward of the HRE inlet. This interaction would significantly influence the performance of the HRE.

Langley Research Center,
National Aeronautics and Space Administration,
Langley Station, Hampton, Va., May 12, 1969,
722-03-00-06-23.

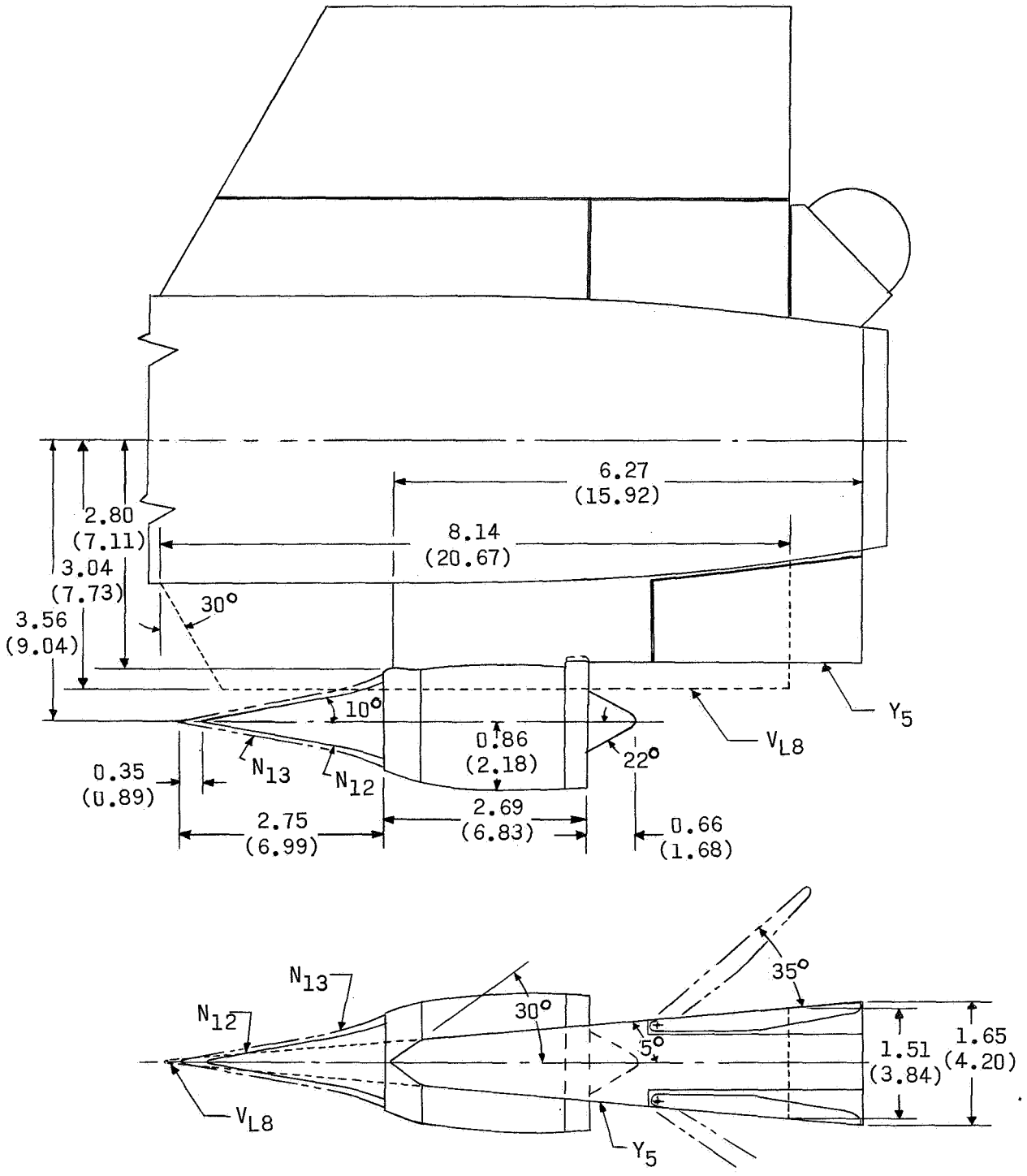
REFERENCE

1. Patterson, James C., Jr.: Aerodynamic Characteristics of a 0.0667-Scale Model of the X-15A-2 Research Airplane at Transonic Speeds. NASA TM X-1198, 1966.



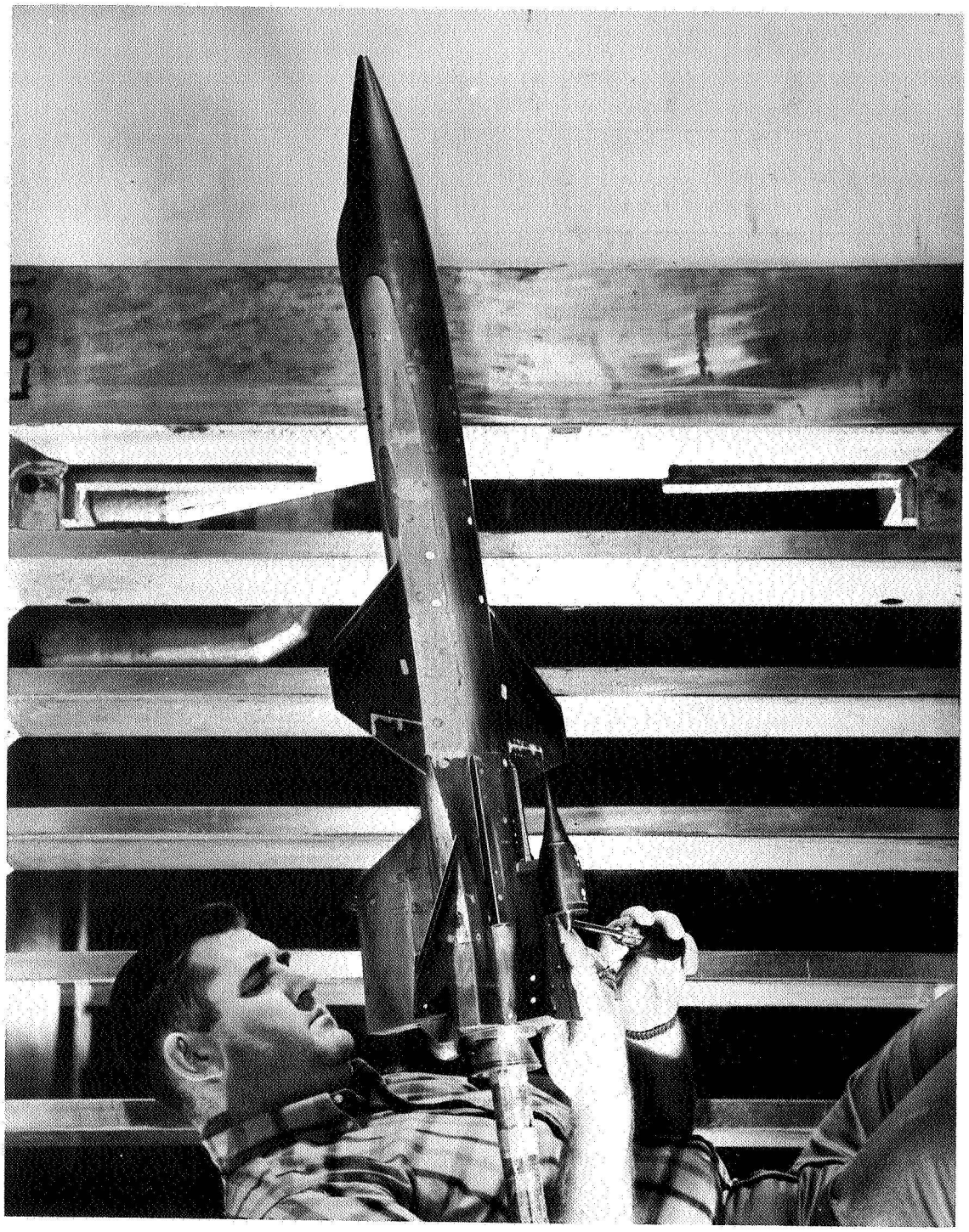
(a) Complete model.

Figure 1.- Details of model. All dimensions are in inches (centimeters) unless otherwise noted.



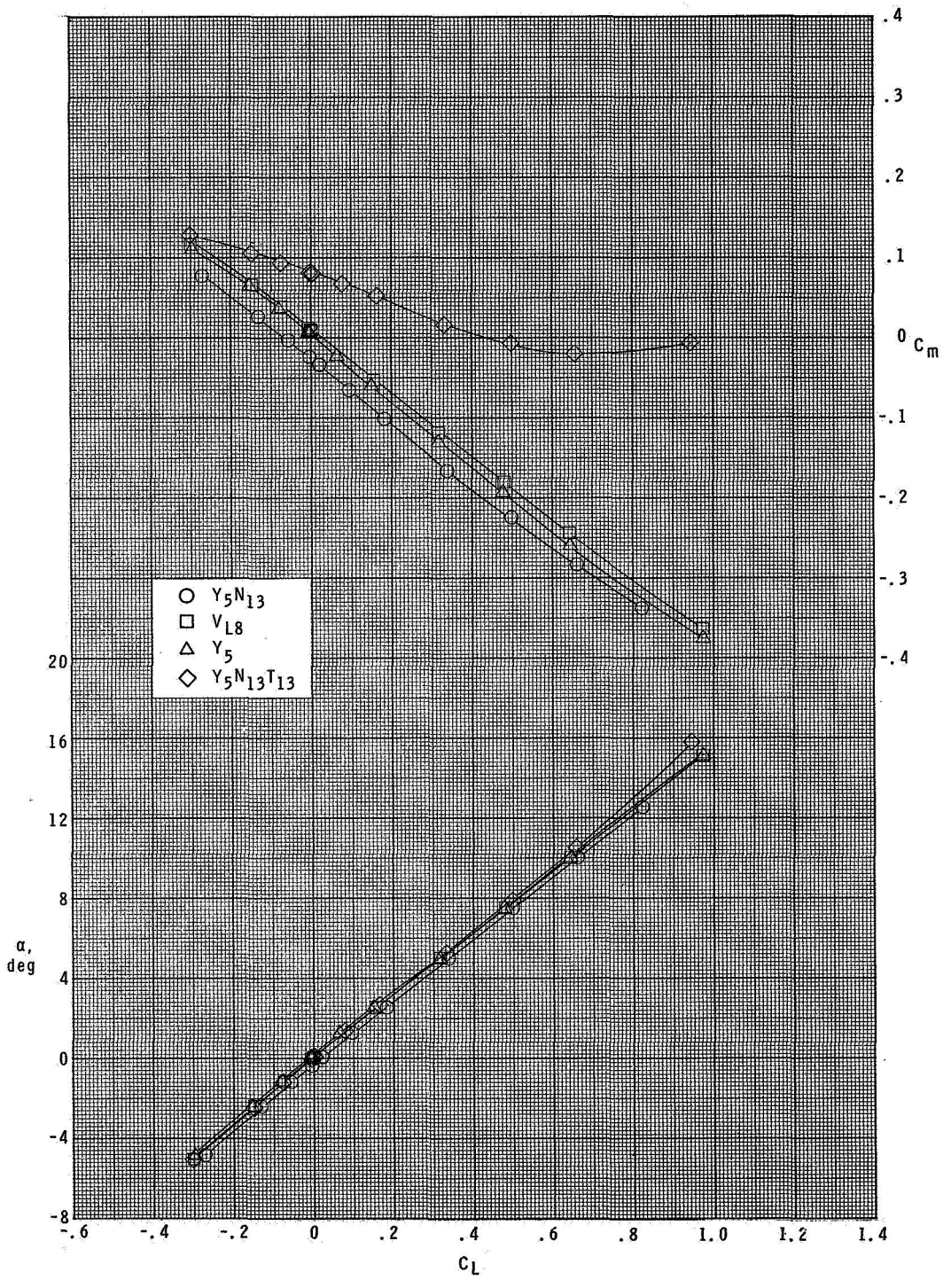
(b) Hypersonic research engine.

Figure 1.- Concluded.



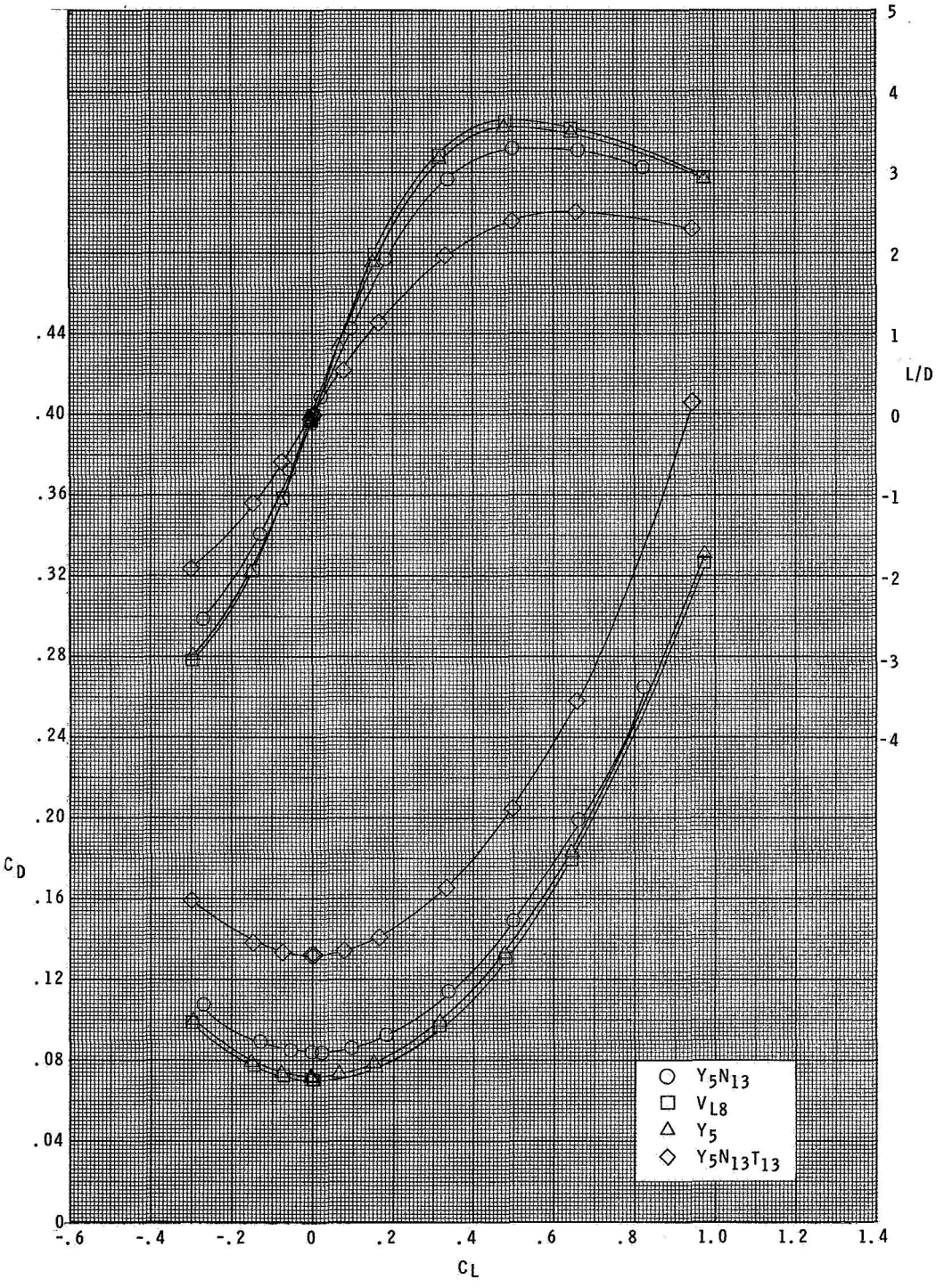
L-67-8518

Figure 2.- Photograph of model.



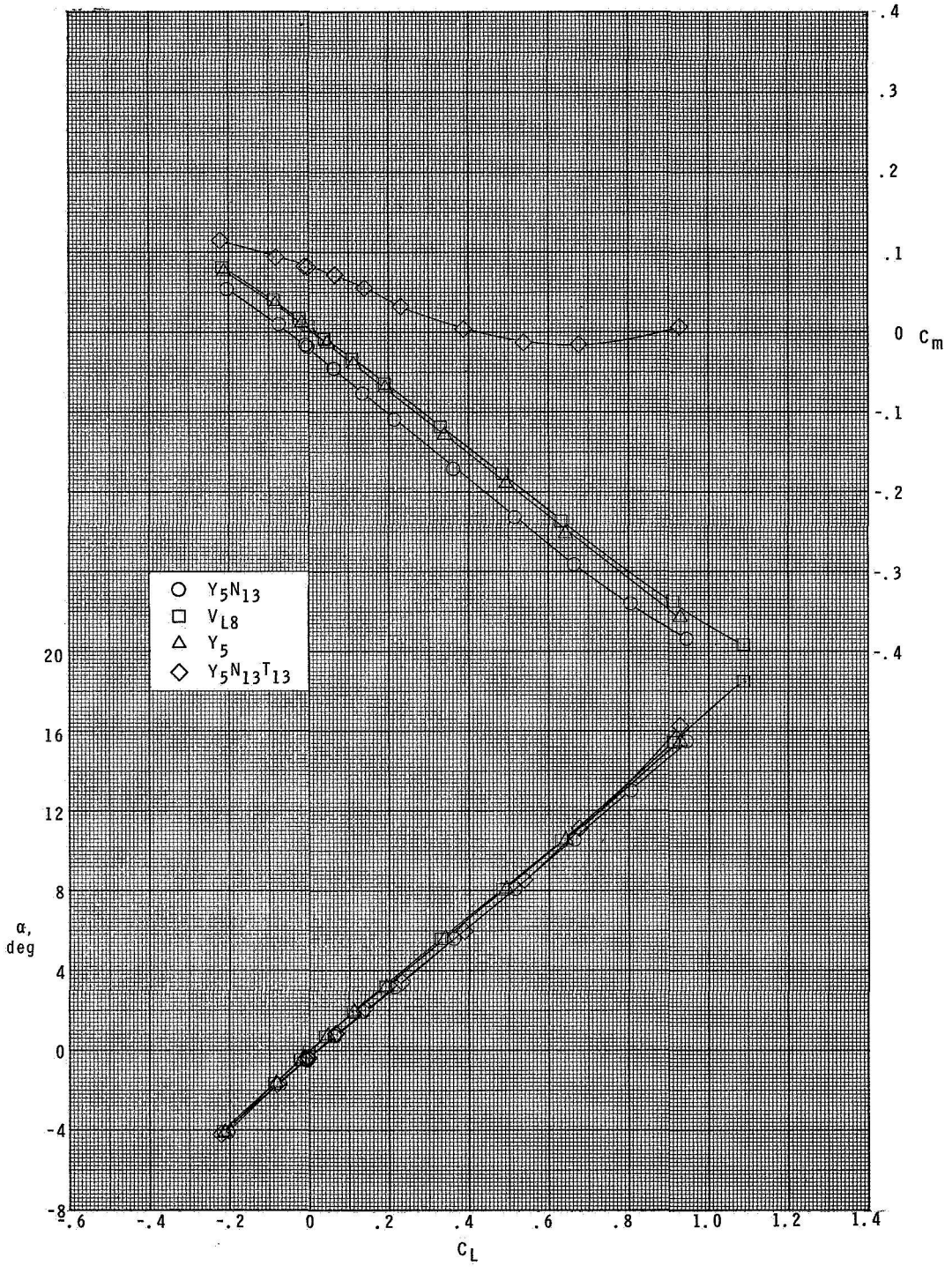
(a) M = 1.75.

Figure 3.- Effect of HRE components and fuel tanks on longitudinal aerodynamic characteristics for $B_{11}X_{16}W_2H_9T_{12}V_{U5}$. $\delta_h = 0^o$.



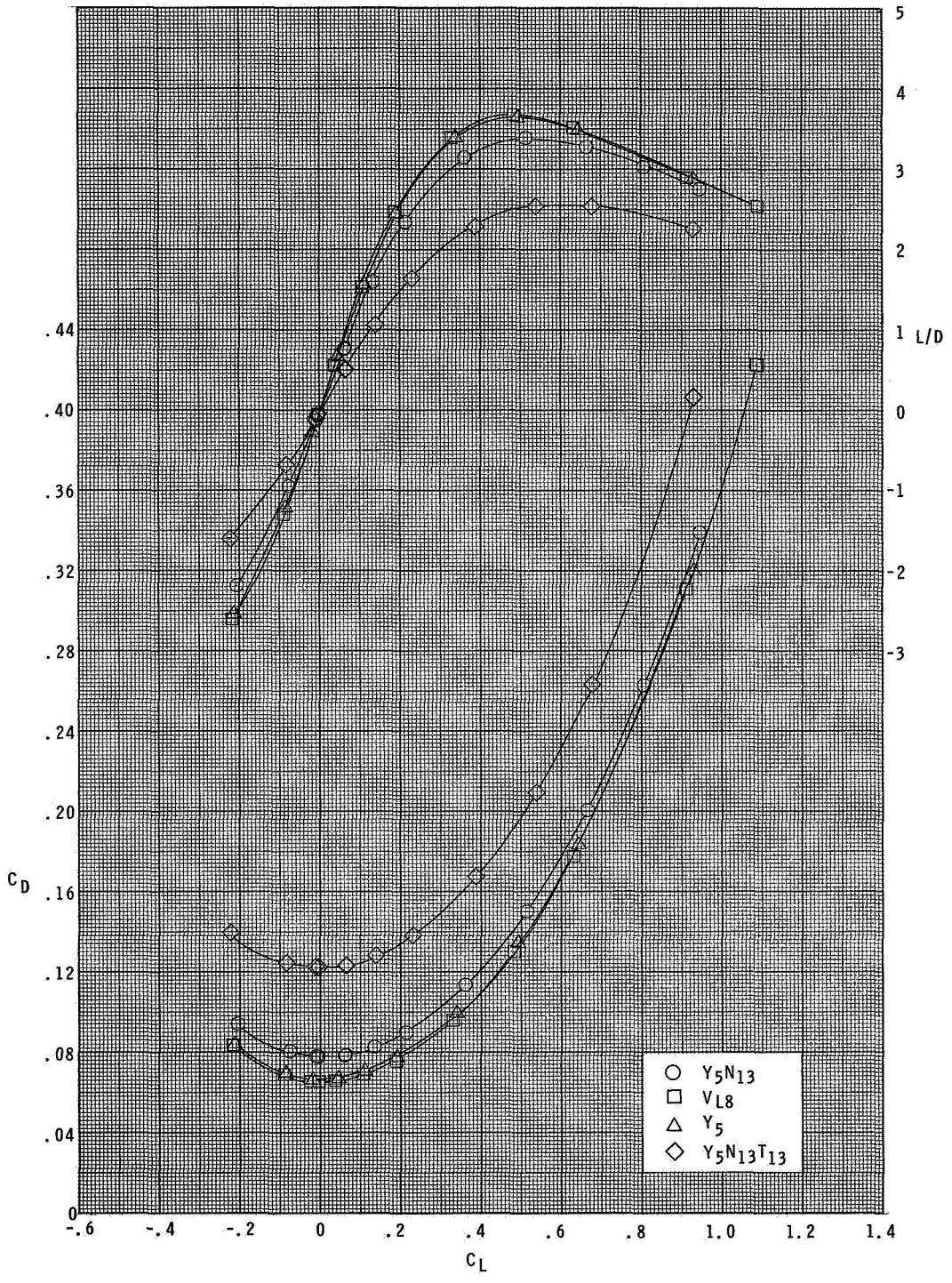
(a) Concluded.

Figure 3.- Continued.



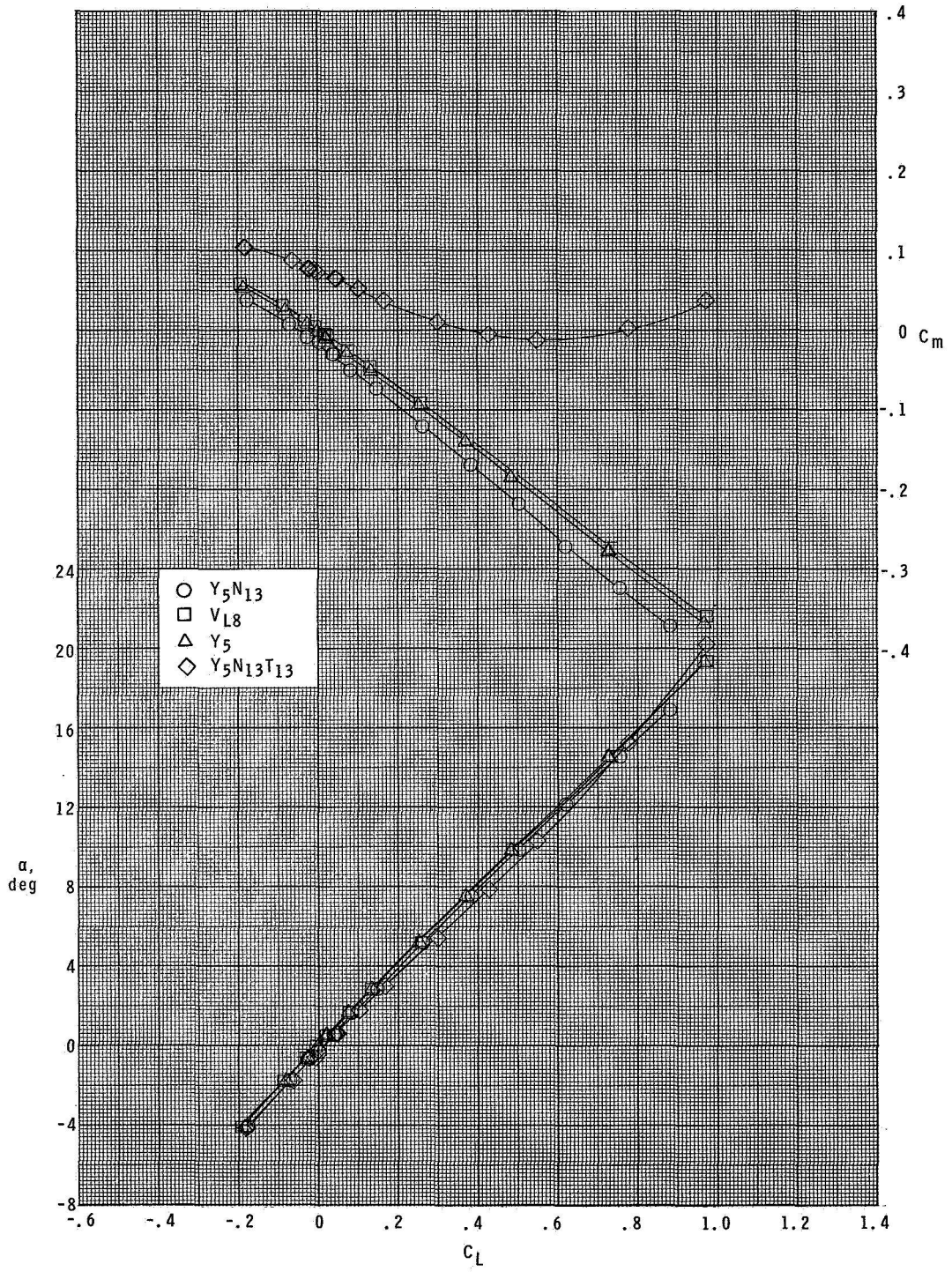
(b) M = 2.00.

Figure 3.- Continued.



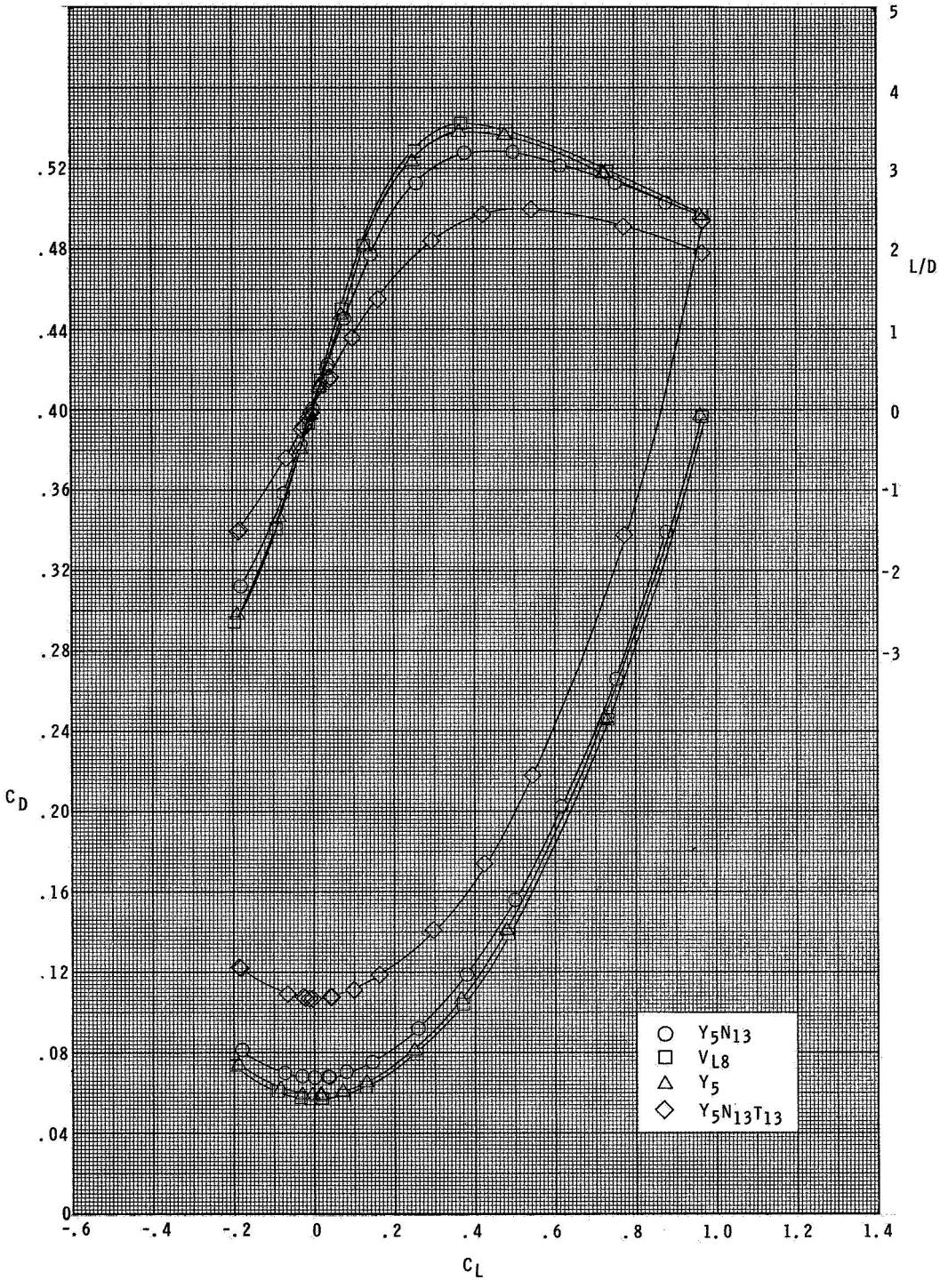
(b) Concluded.

Figure 3.- Continued.



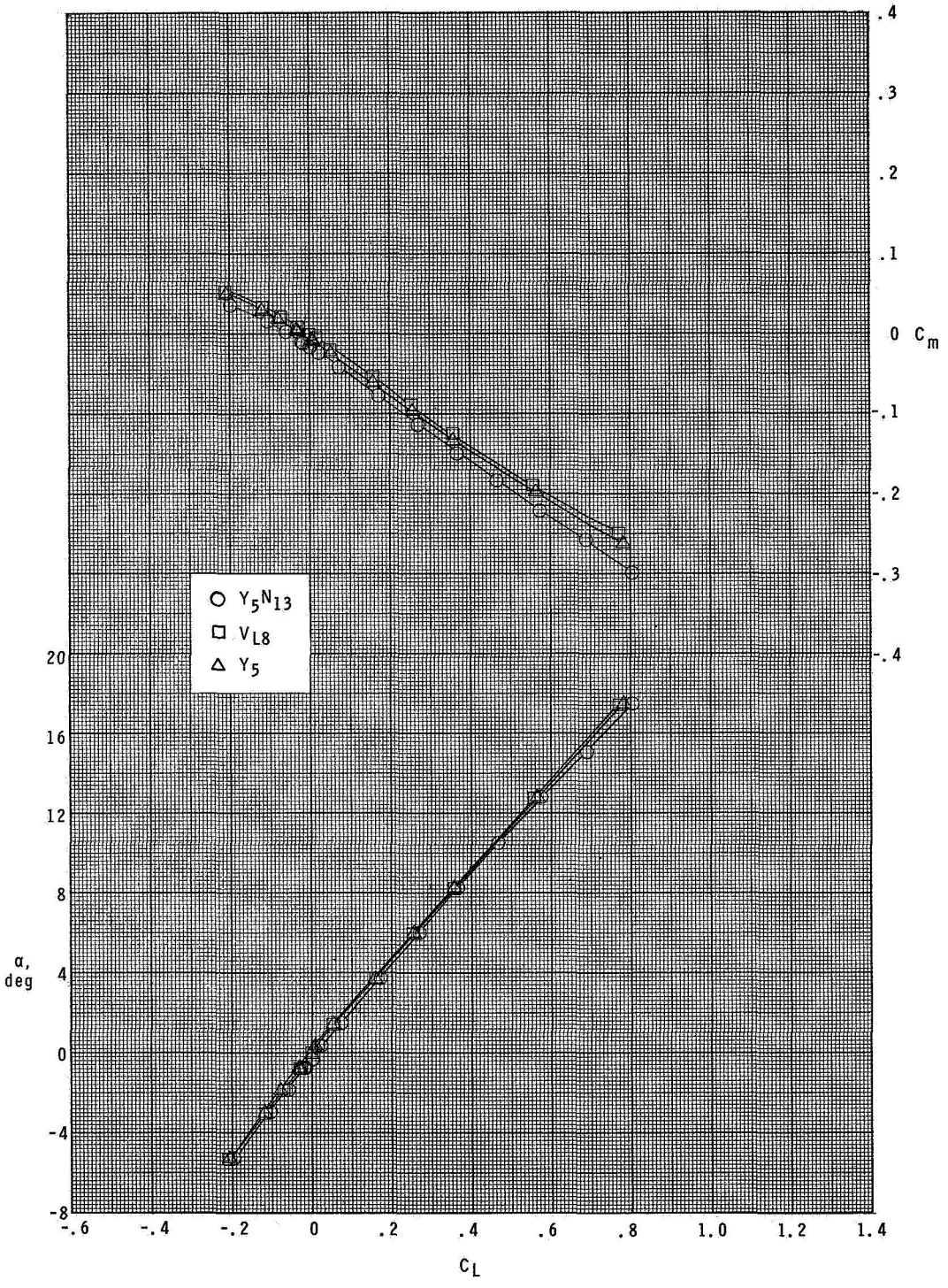
(c) M = 2.50.

Figure 3.- Continued.



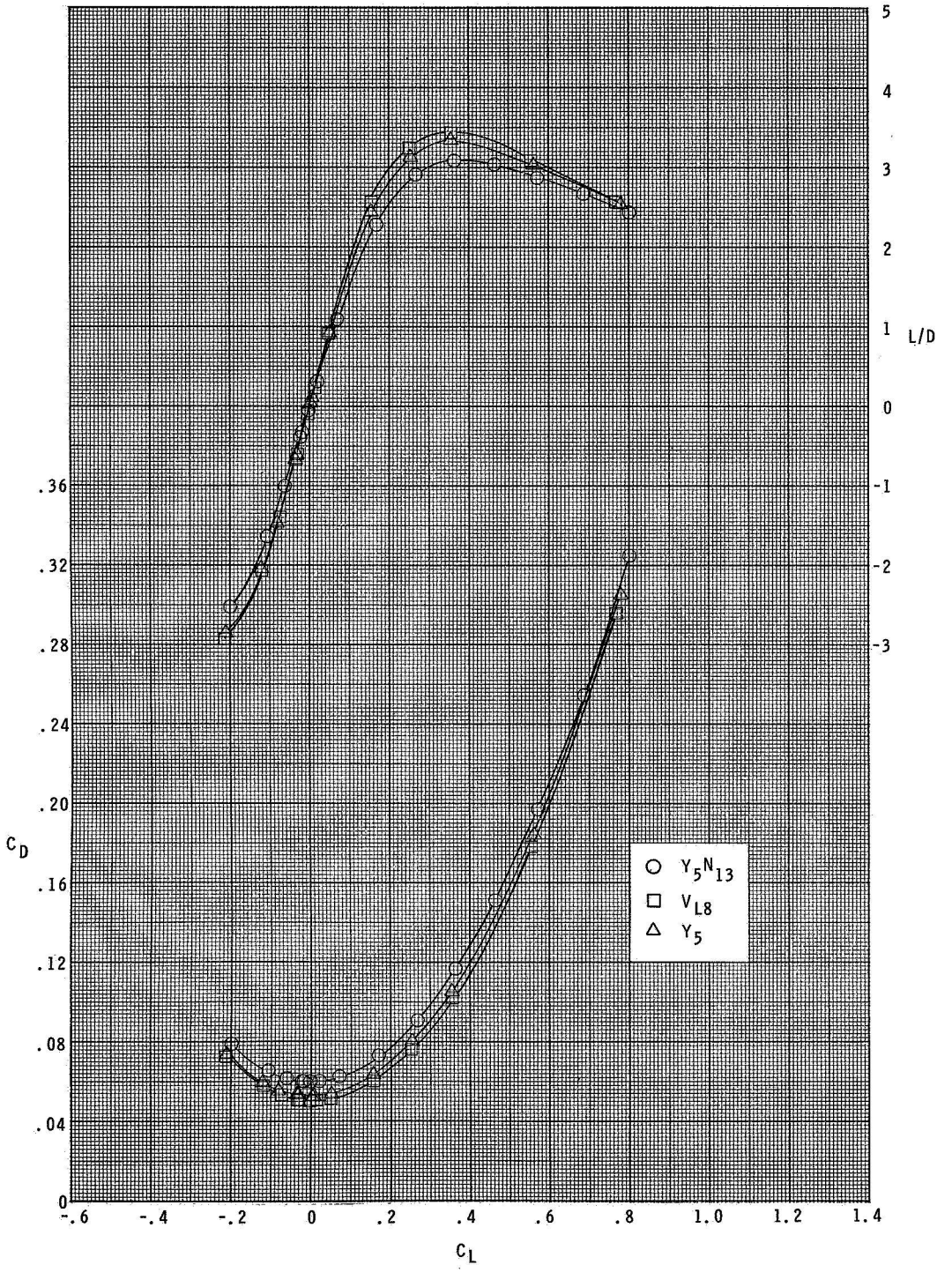
(c) Concluded.

Figure 3.- Continued.



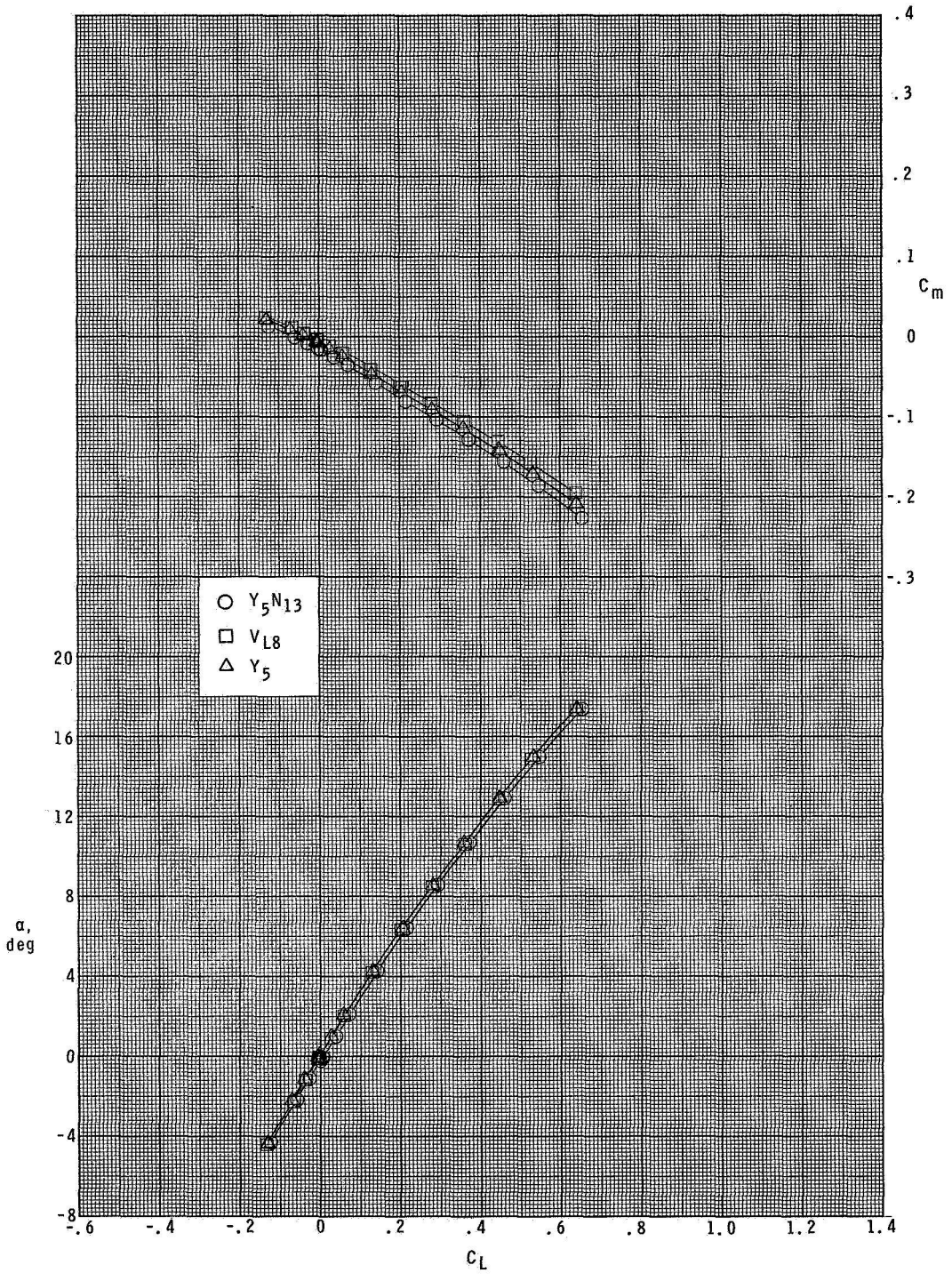
(d) M = 2.86.

Figure 3.- Continued.



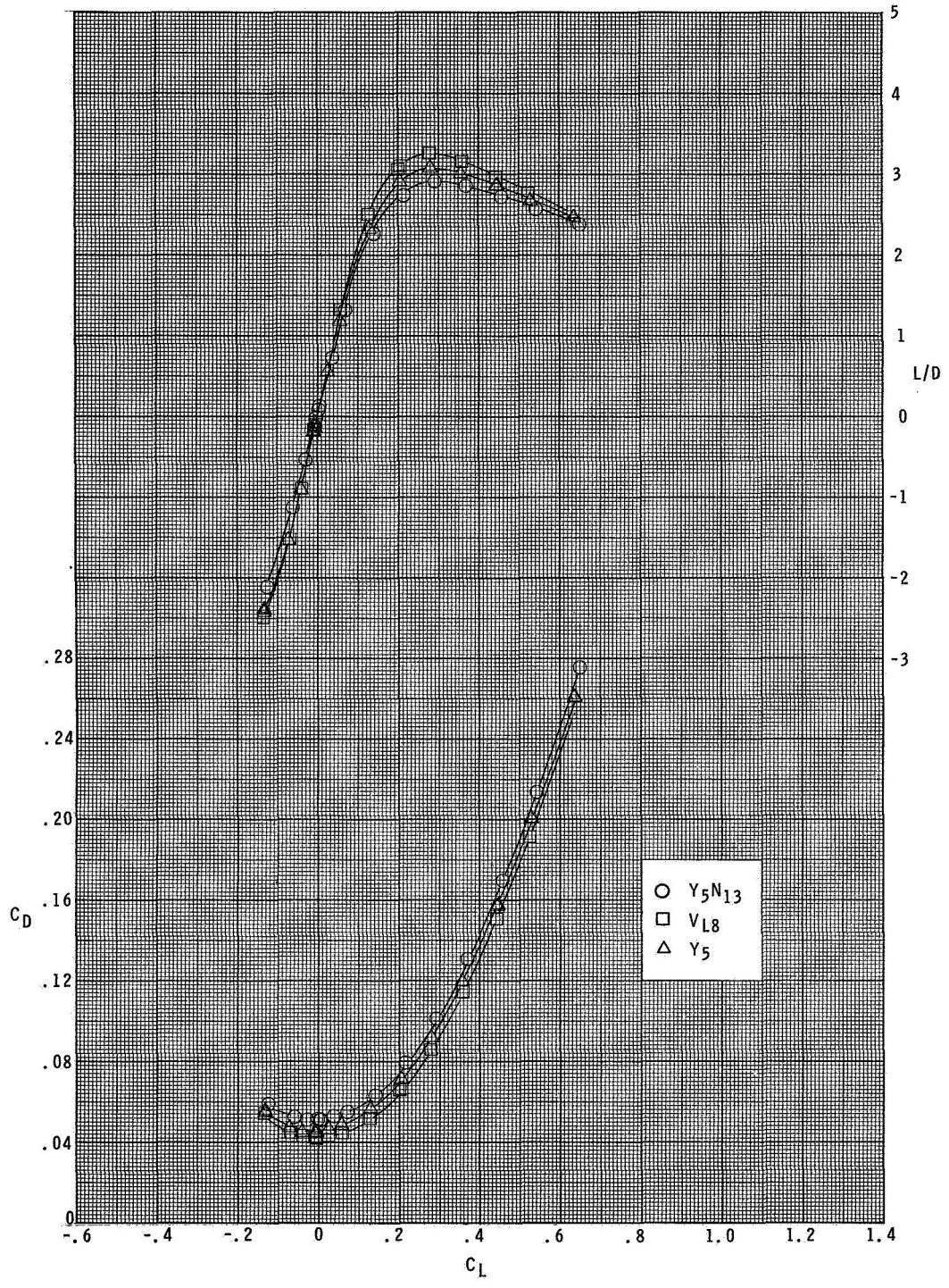
(d) Concluded.

Figure 3.- Continued.



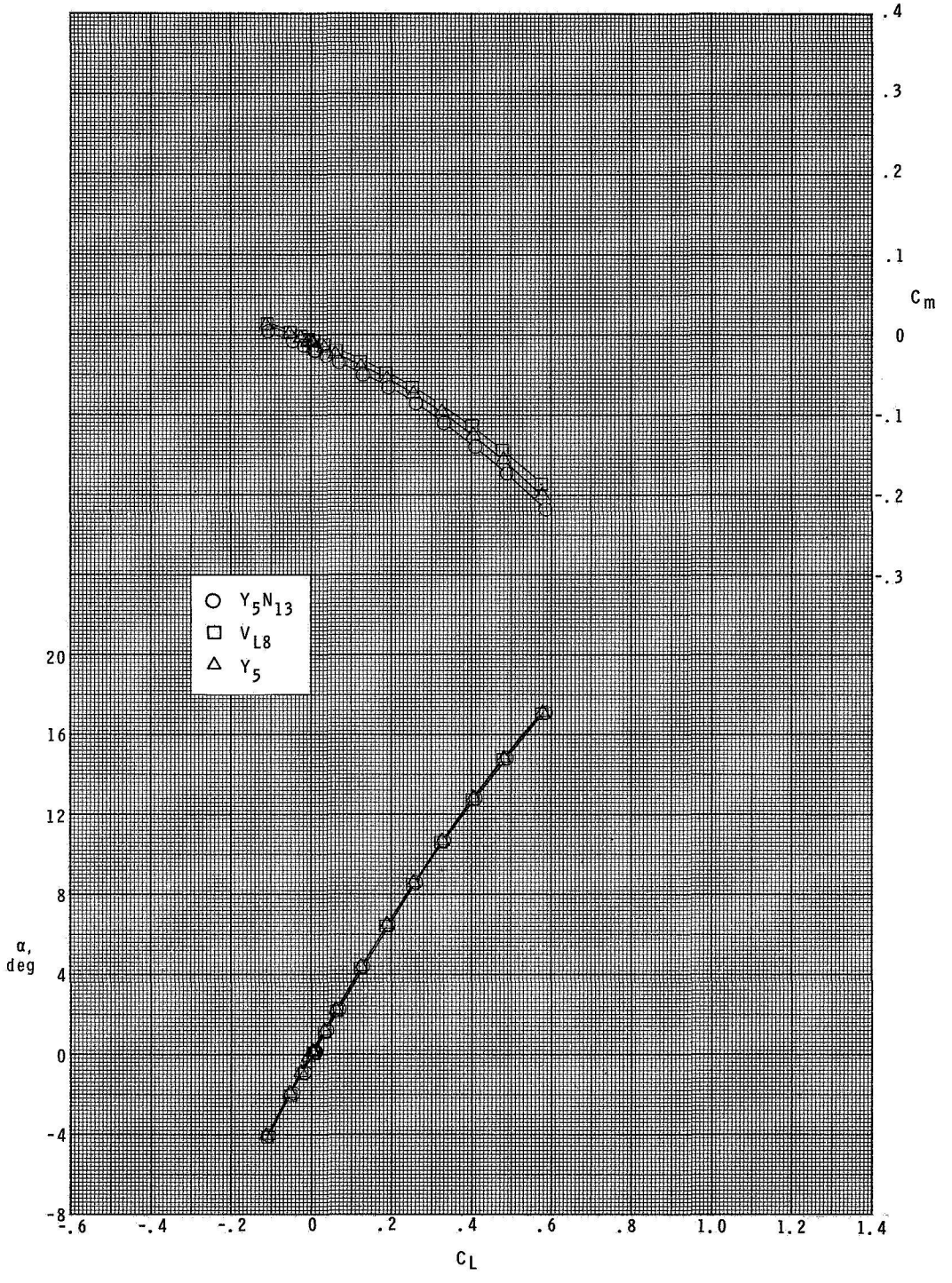
(e) M = 3.95.

Figure 3.- Continued.



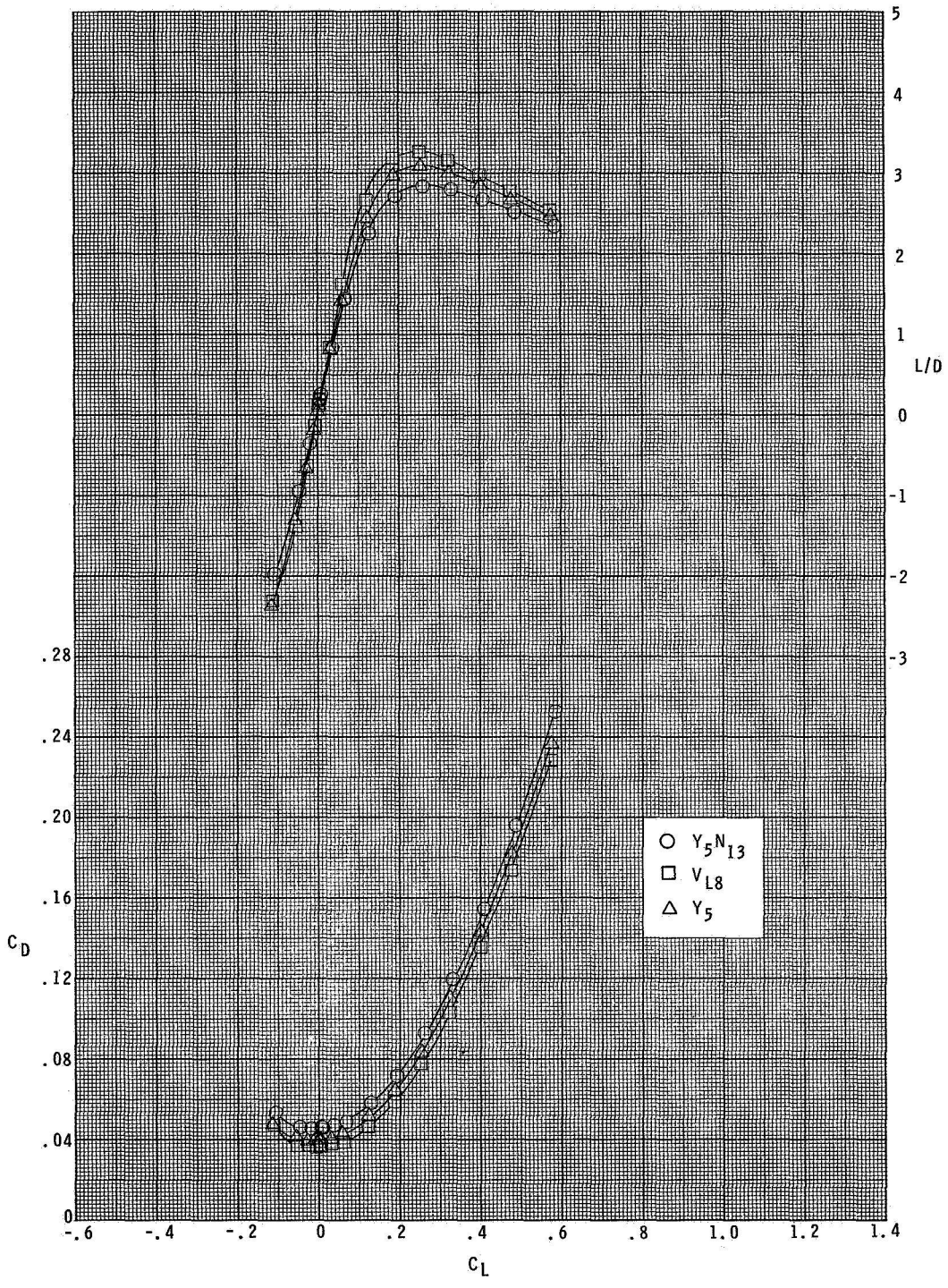
(e) Concluded.

Figure 3.- Continued.



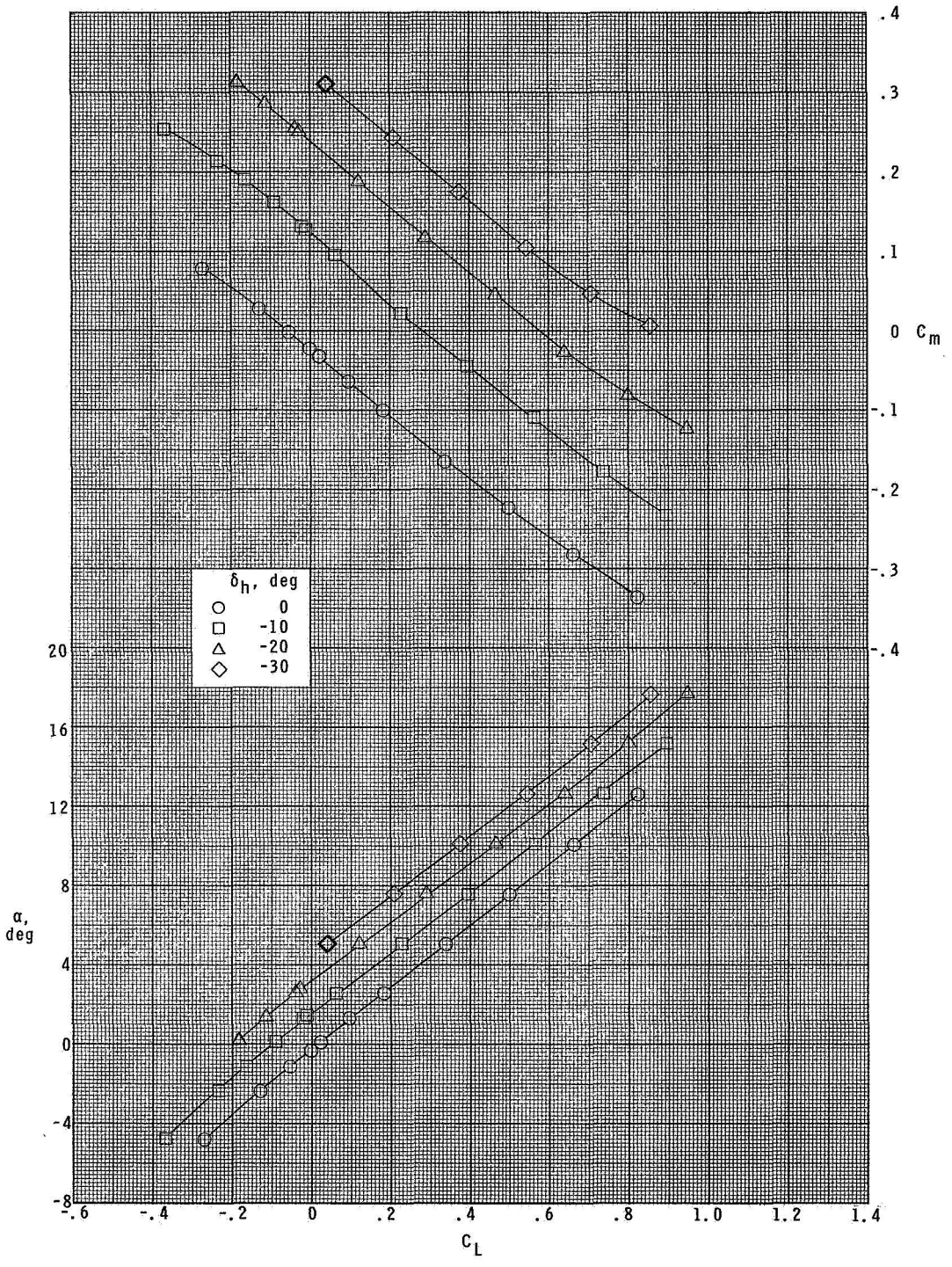
(f) M = 4.63.

Figure 3.- Continued.



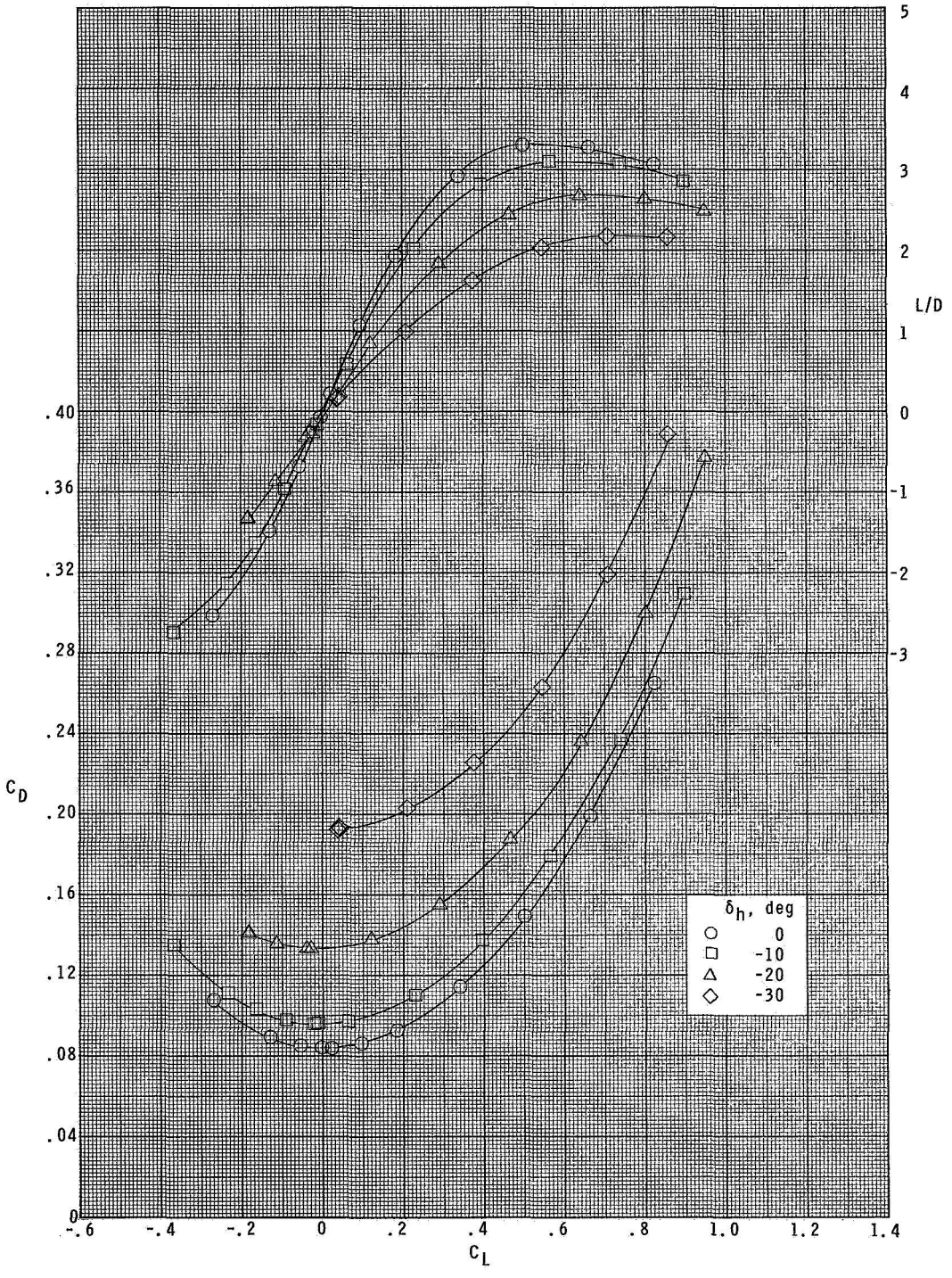
(f) Concluded.

Figure 3.- Concluded.



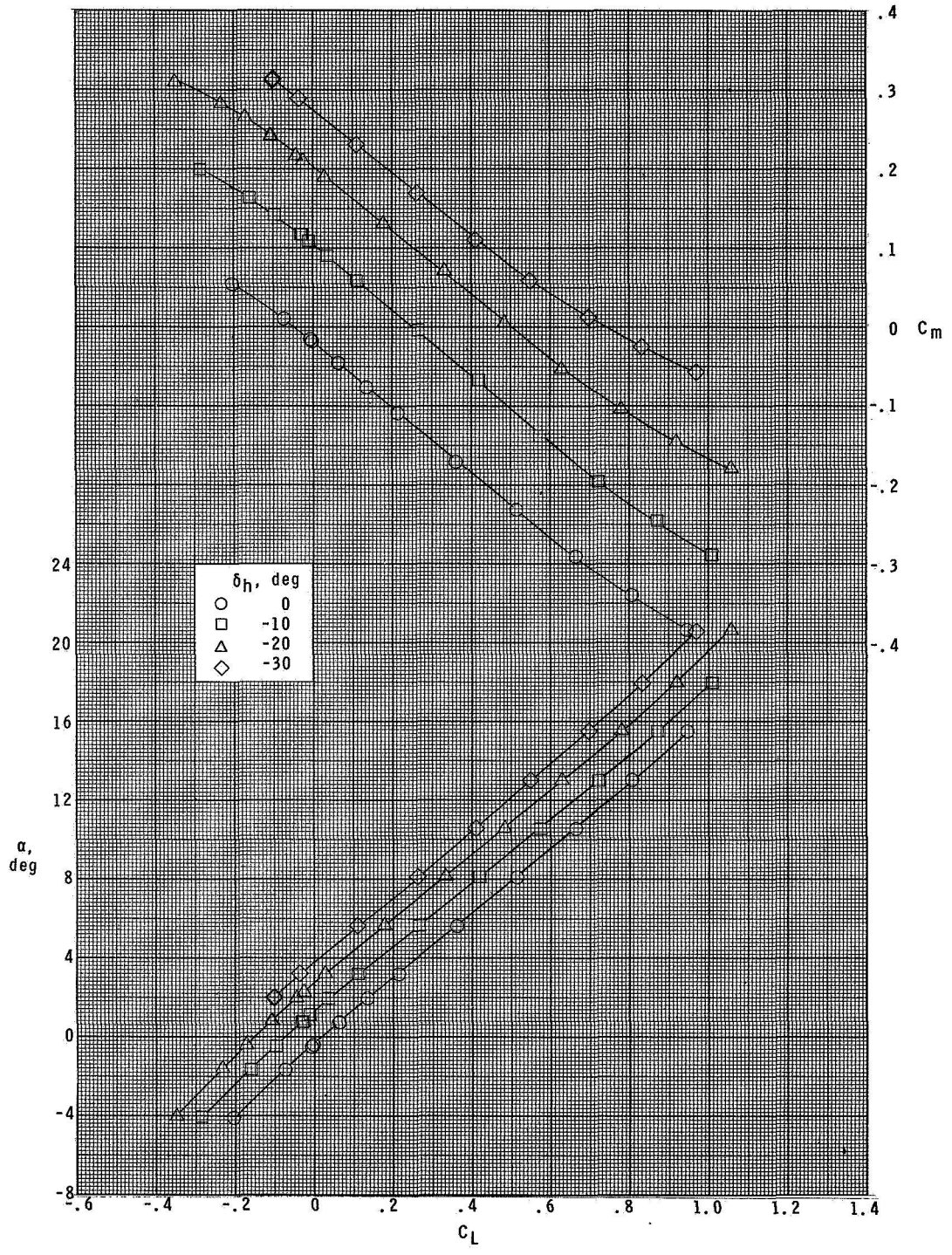
(a) M = 1.75.

Figure 4.- Longitudinal control effectiveness for $B_{11}X_{16}W_2H_9T_{12}V_{U5}Y_5N_{13}$ (HRE on).



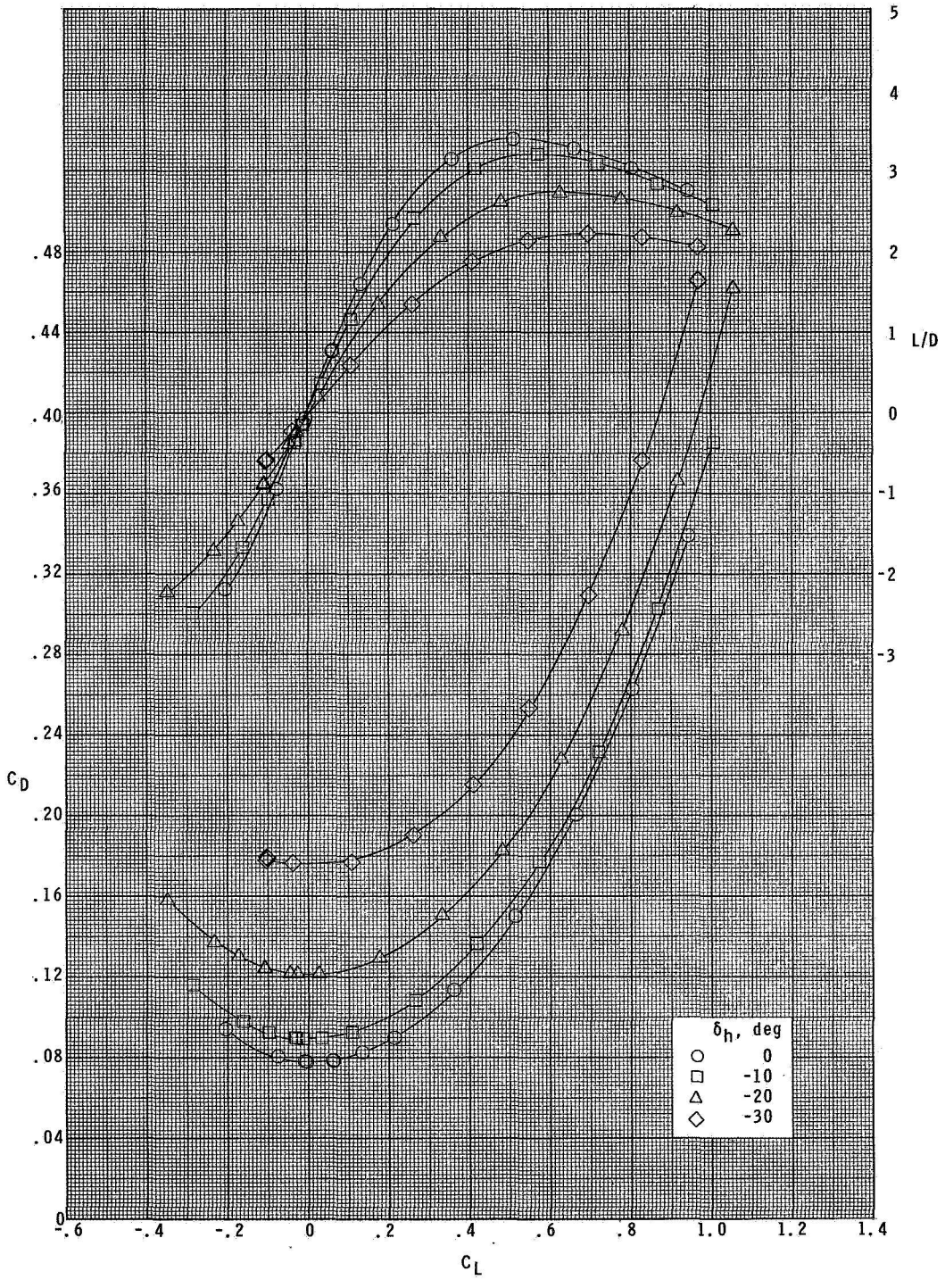
(a) Concluded.

Figure 4.- Continued.



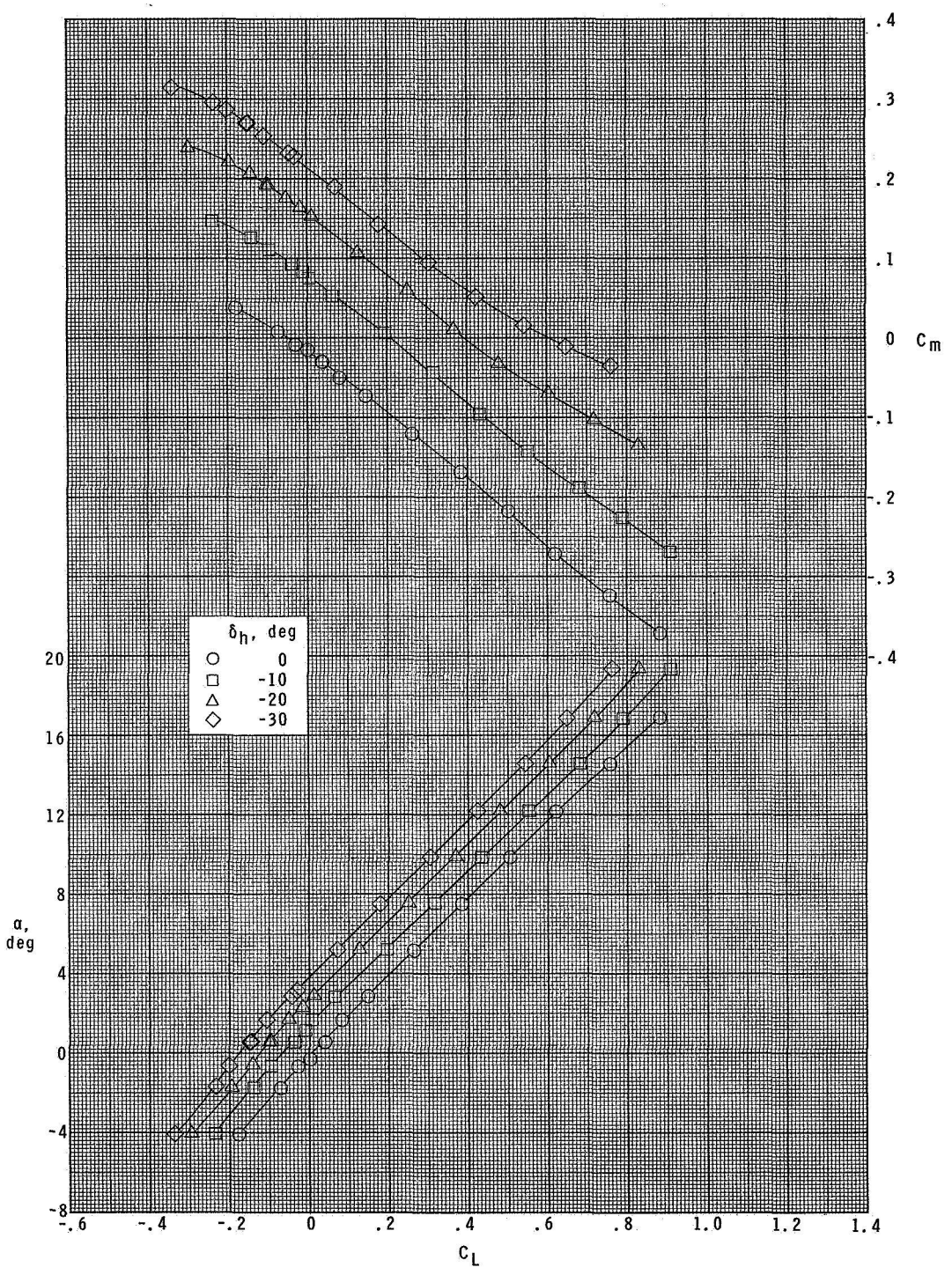
(b) M = 2.00.

Figure 4.- Continued.



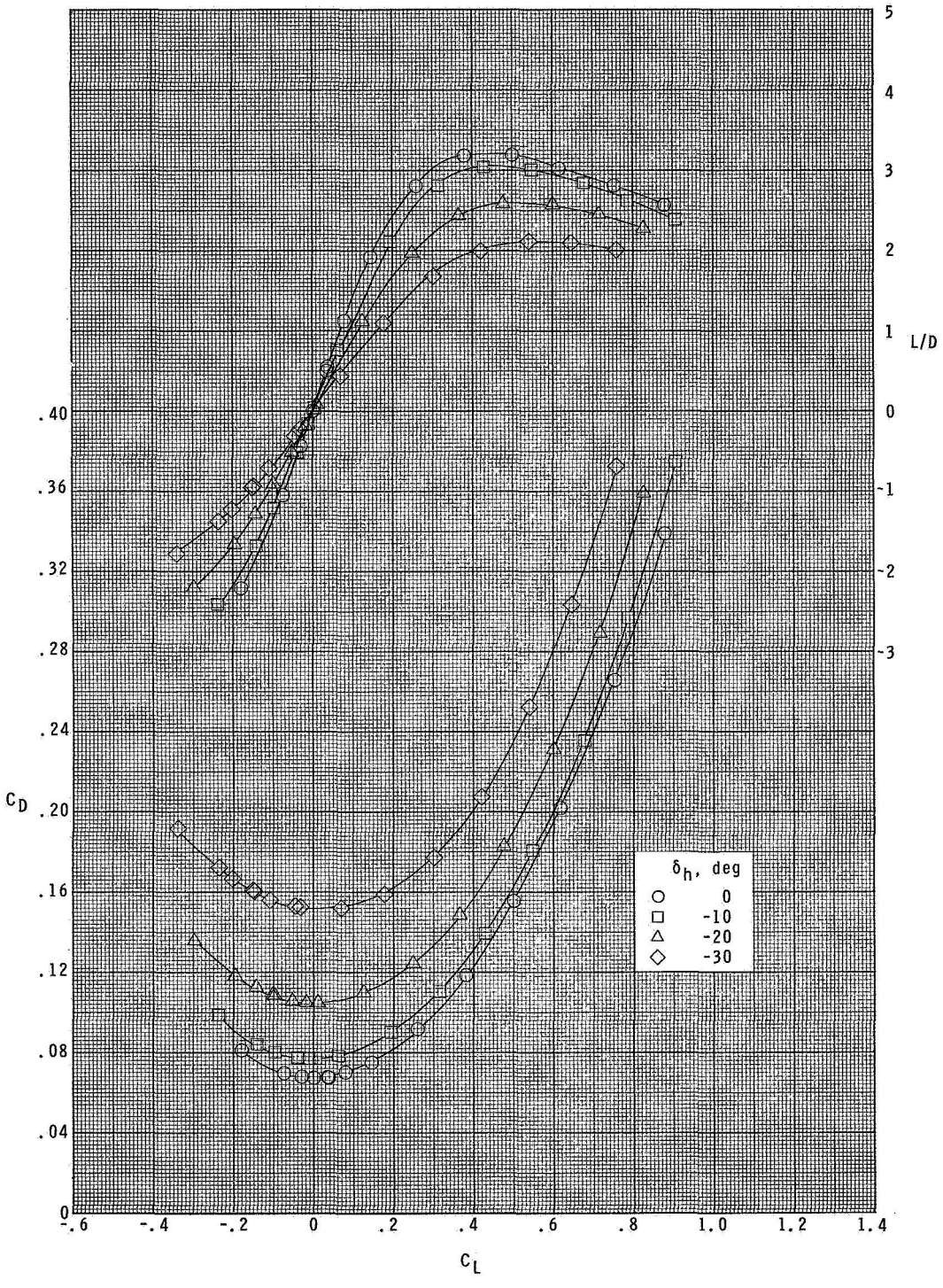
(b) Concluded.

Figure 4.- Continued.



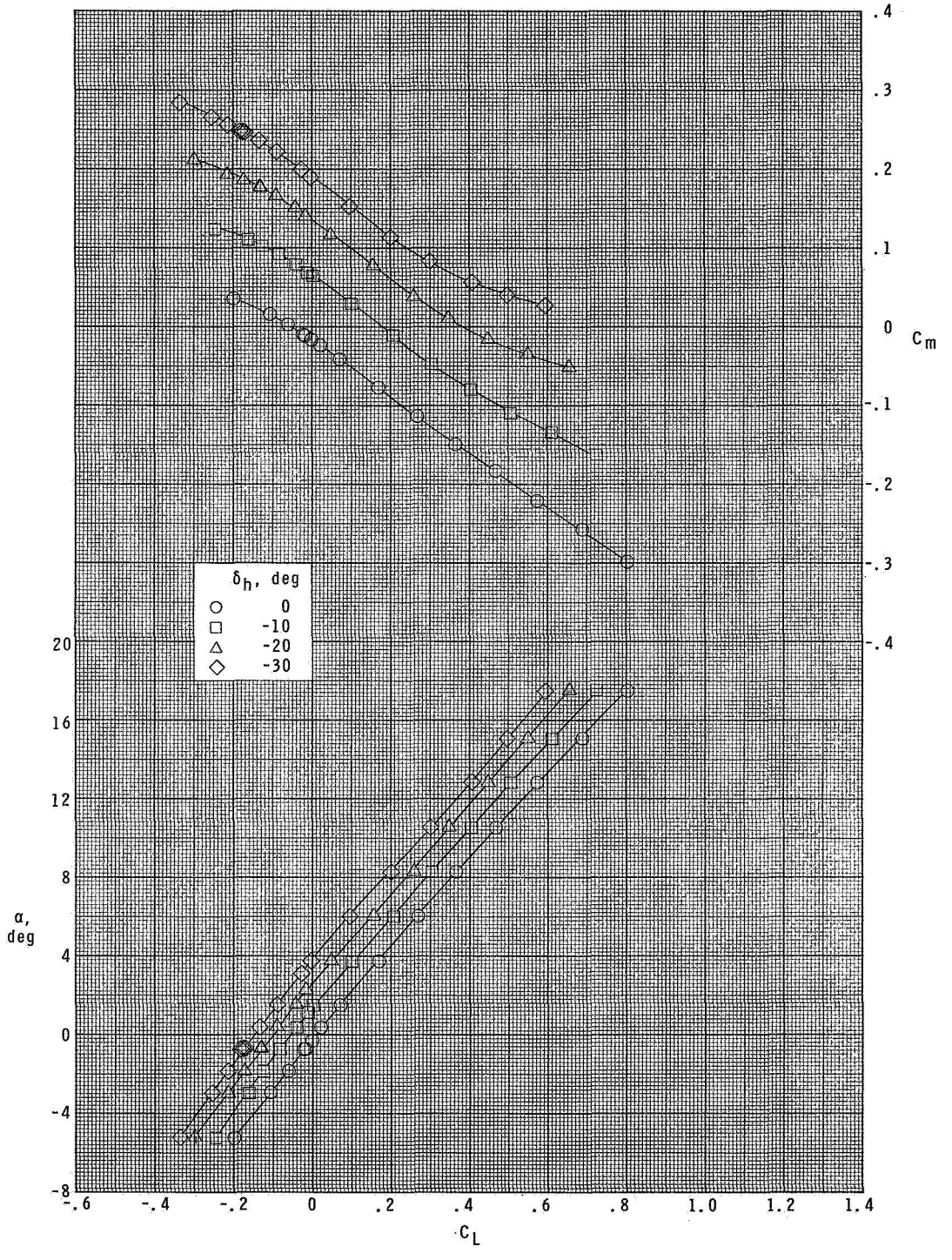
(c) M = 2.50.

Figure 4.- Continued.



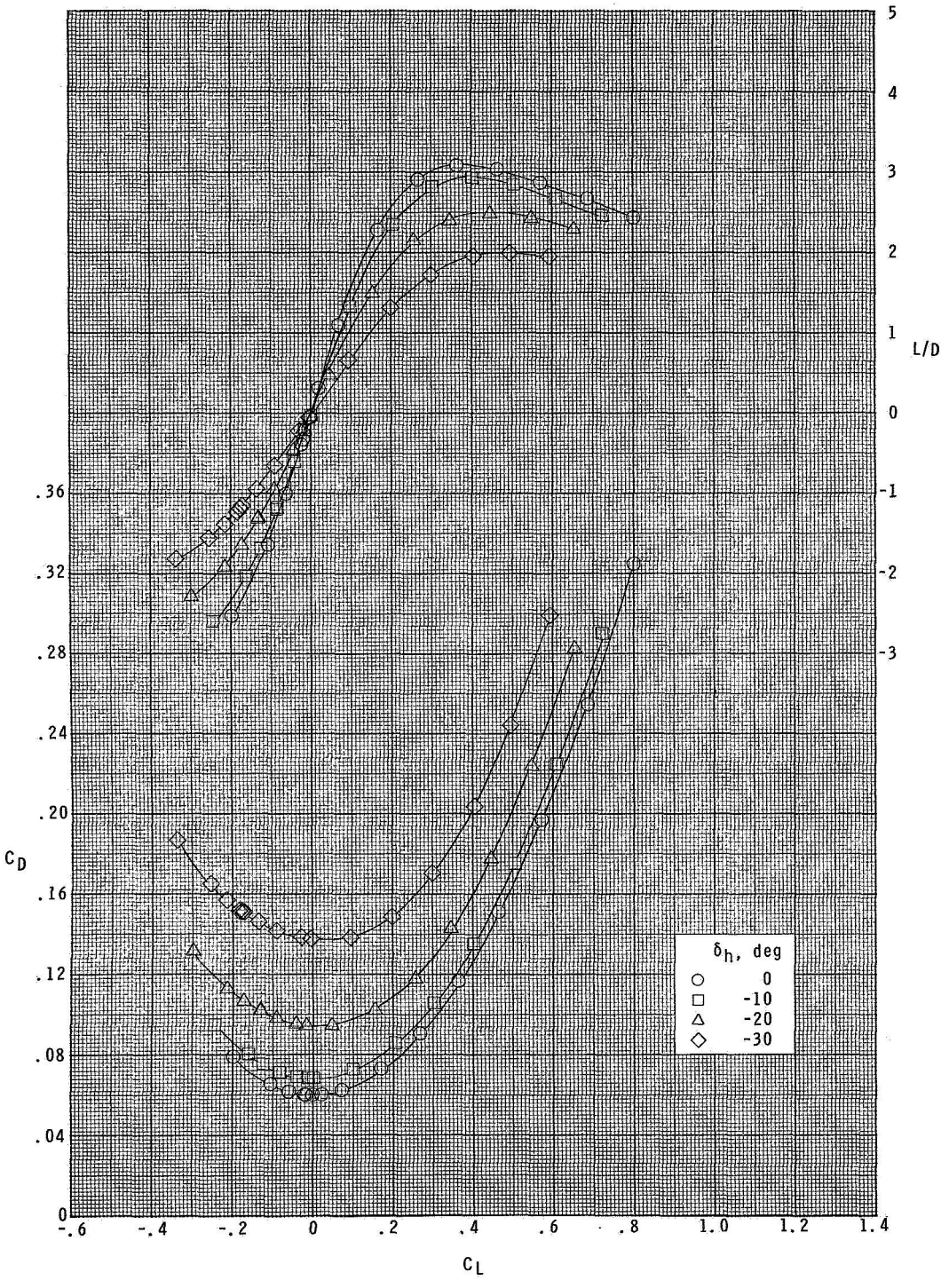
(c) Concluded.

Figure 4.- Continued.



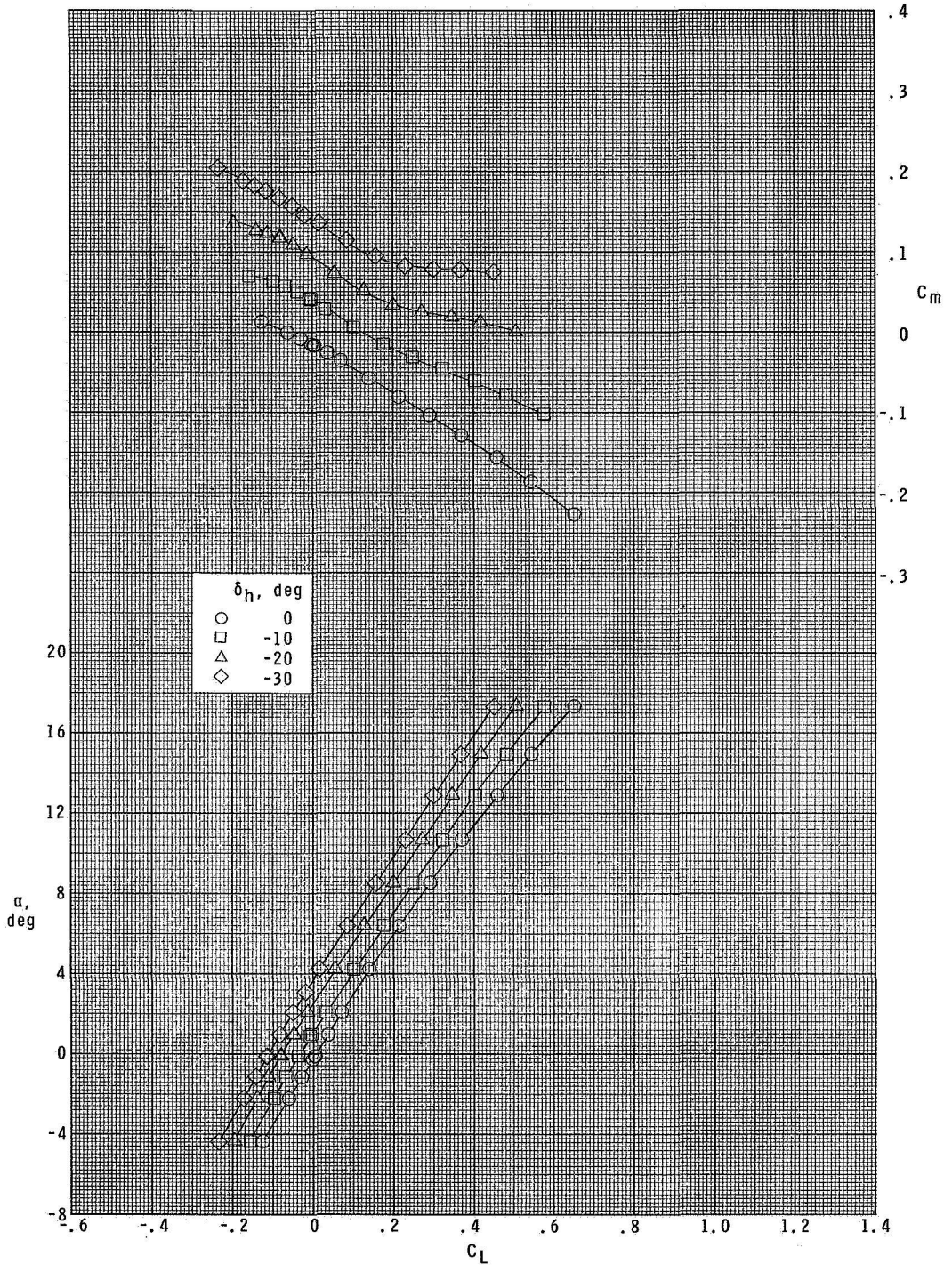
(d) M = 2.86.

Figure 4.- Continued.



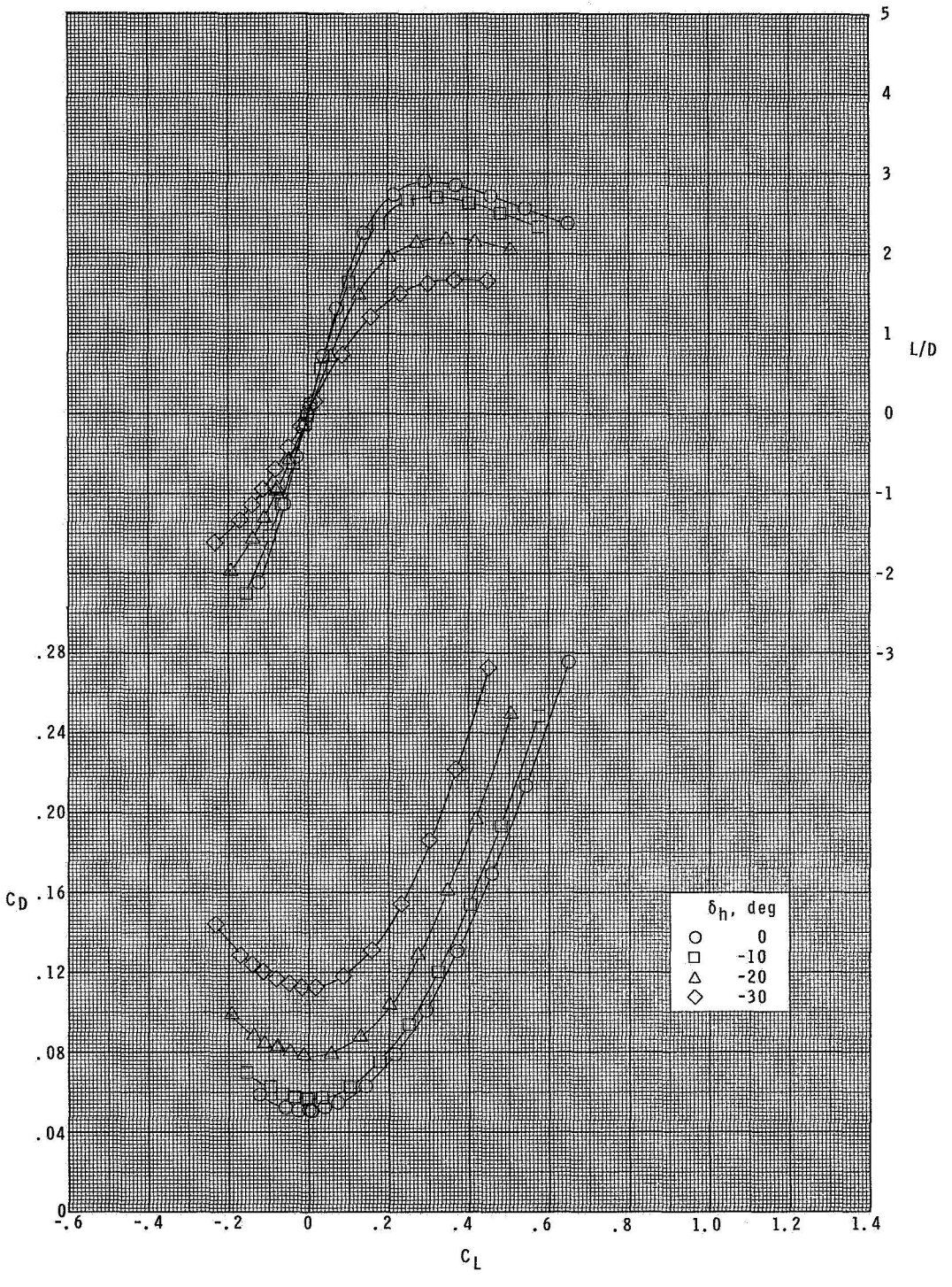
(d) Concluded.

Figure 4.- Continued.



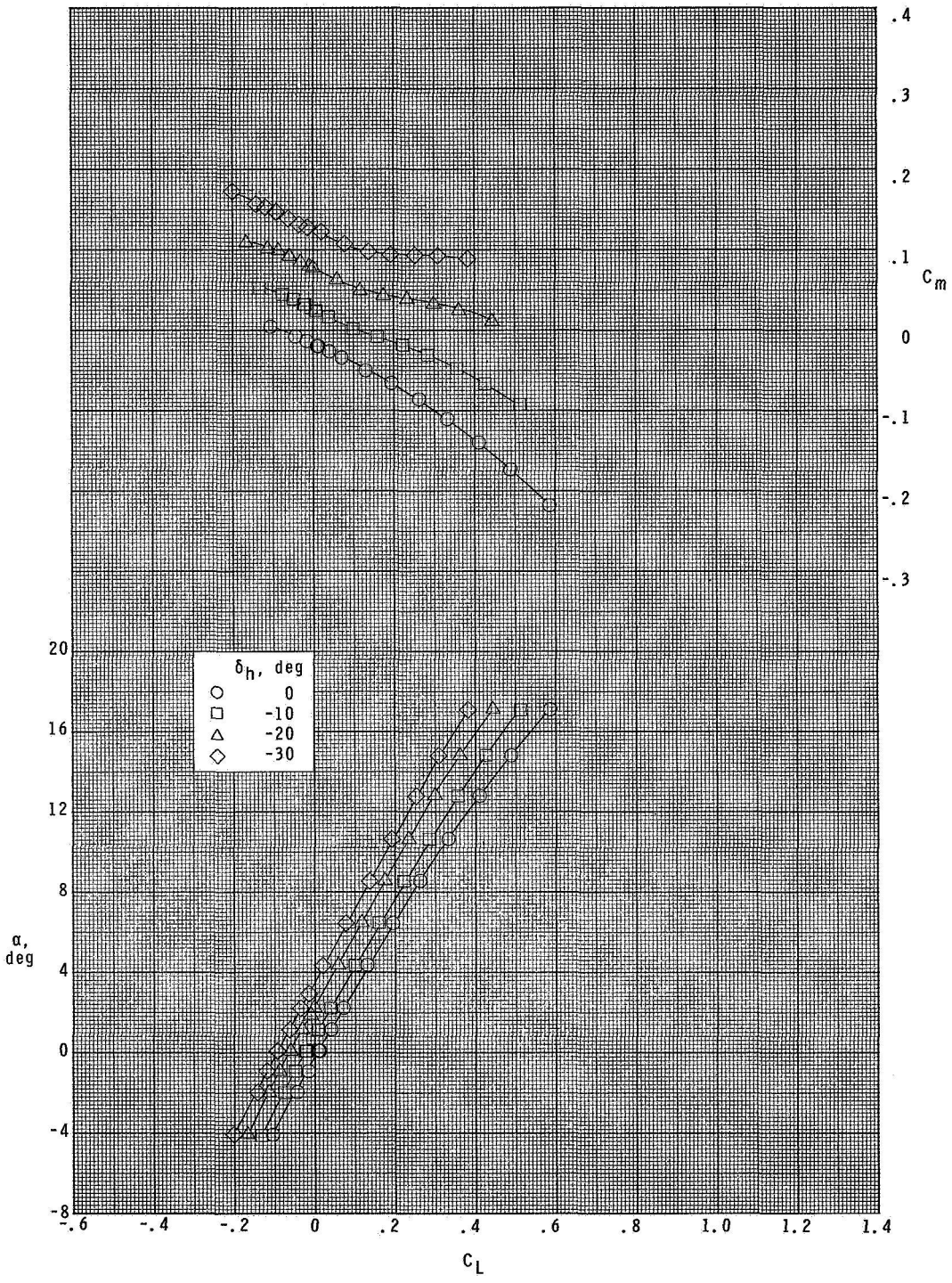
(e) M = 3.95.

Figure 4.- Continued.



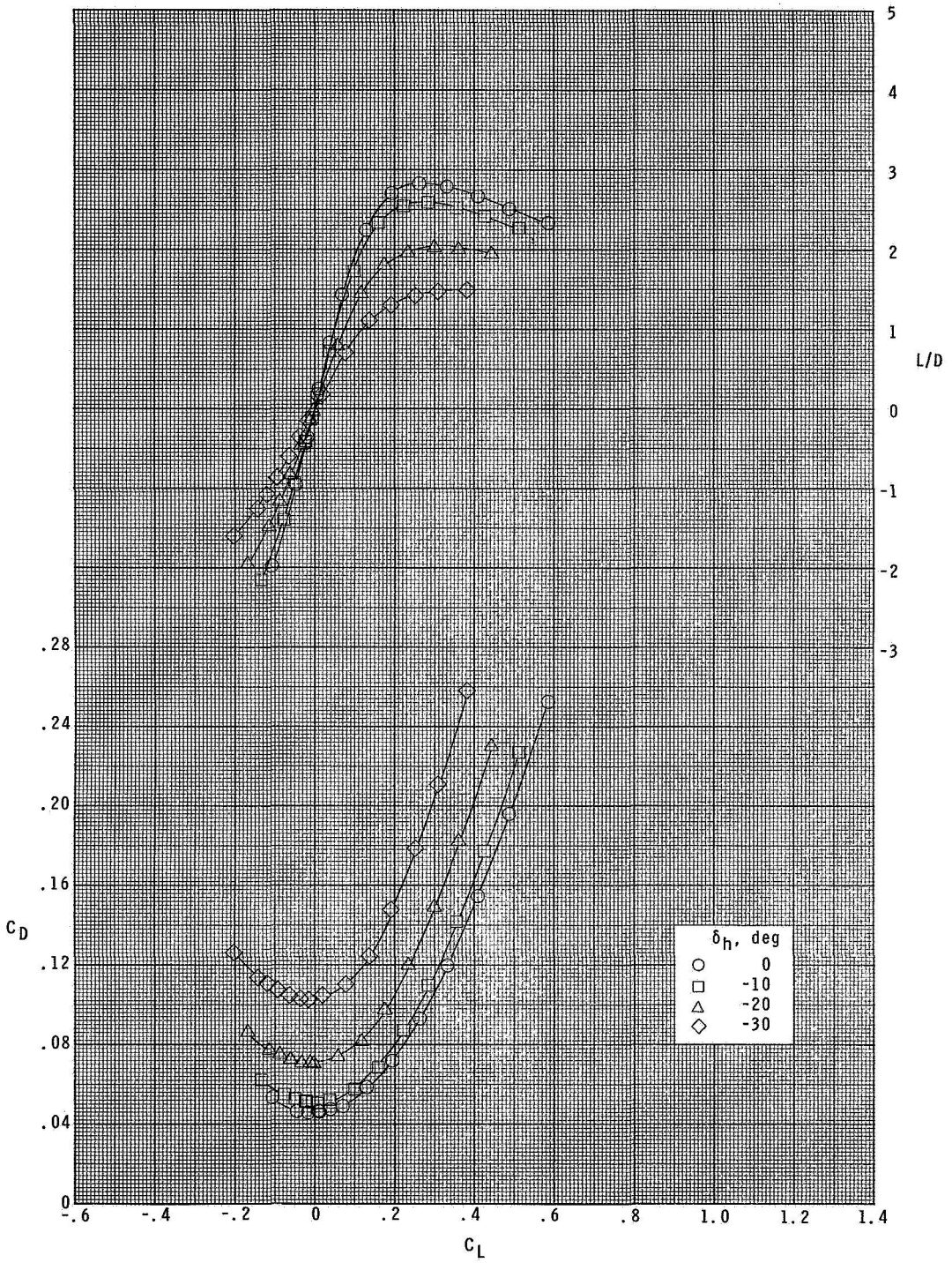
(e) Concluded.

Figure 4.- Continued.



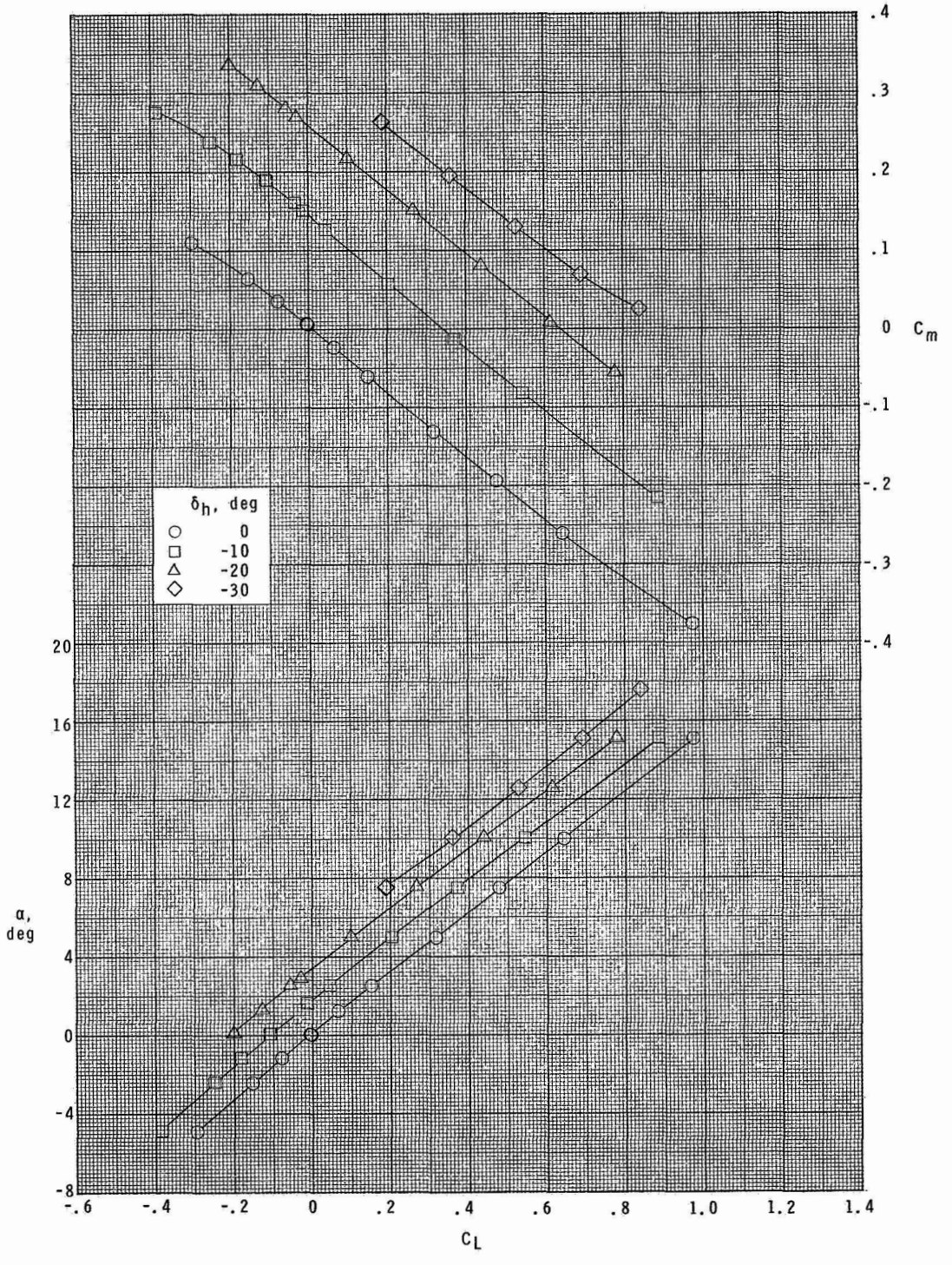
(f) M = 4.63.

Figure 4.- Continued.



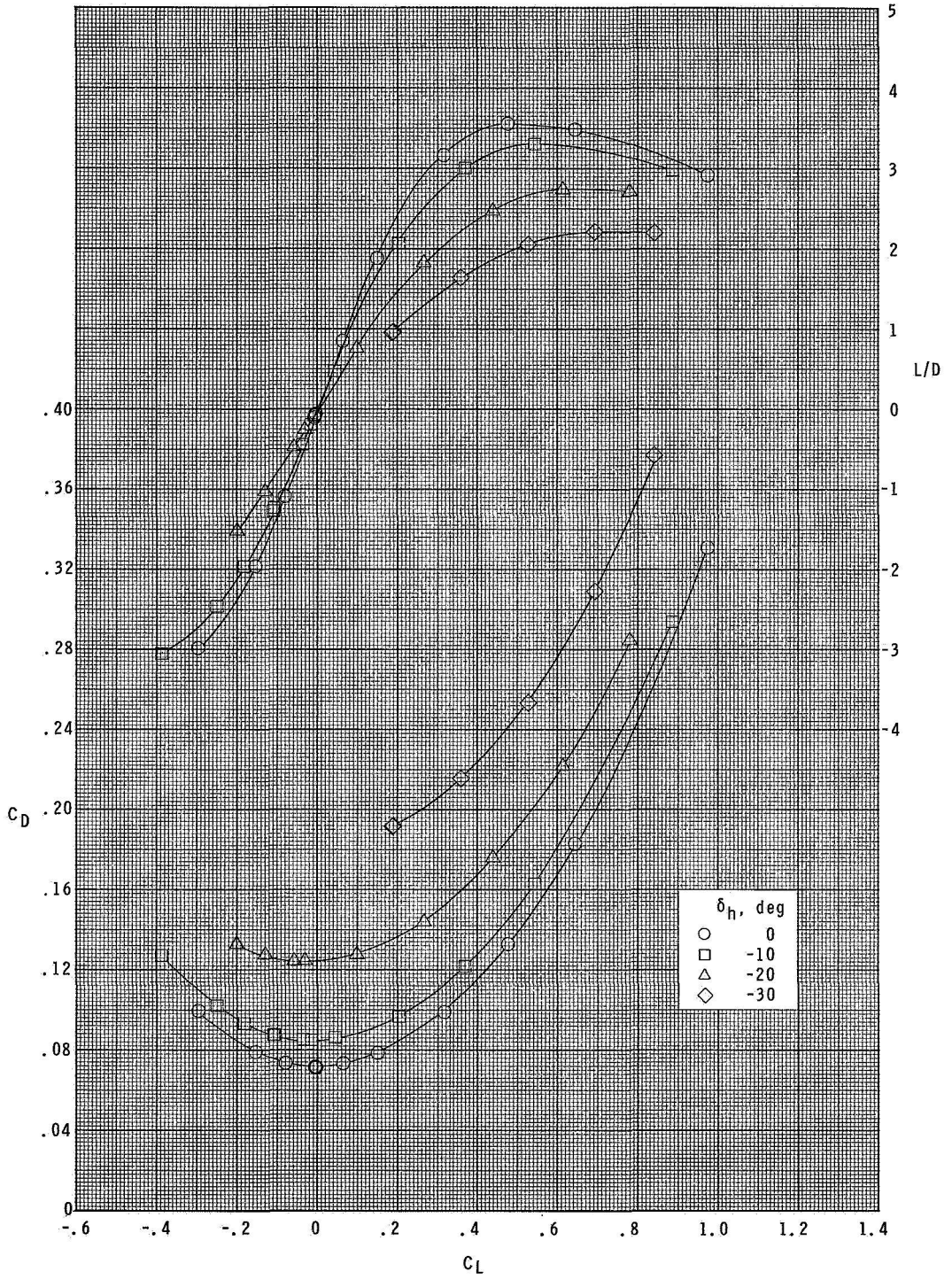
(f) Concluded.

Figure 4.- Concluded.



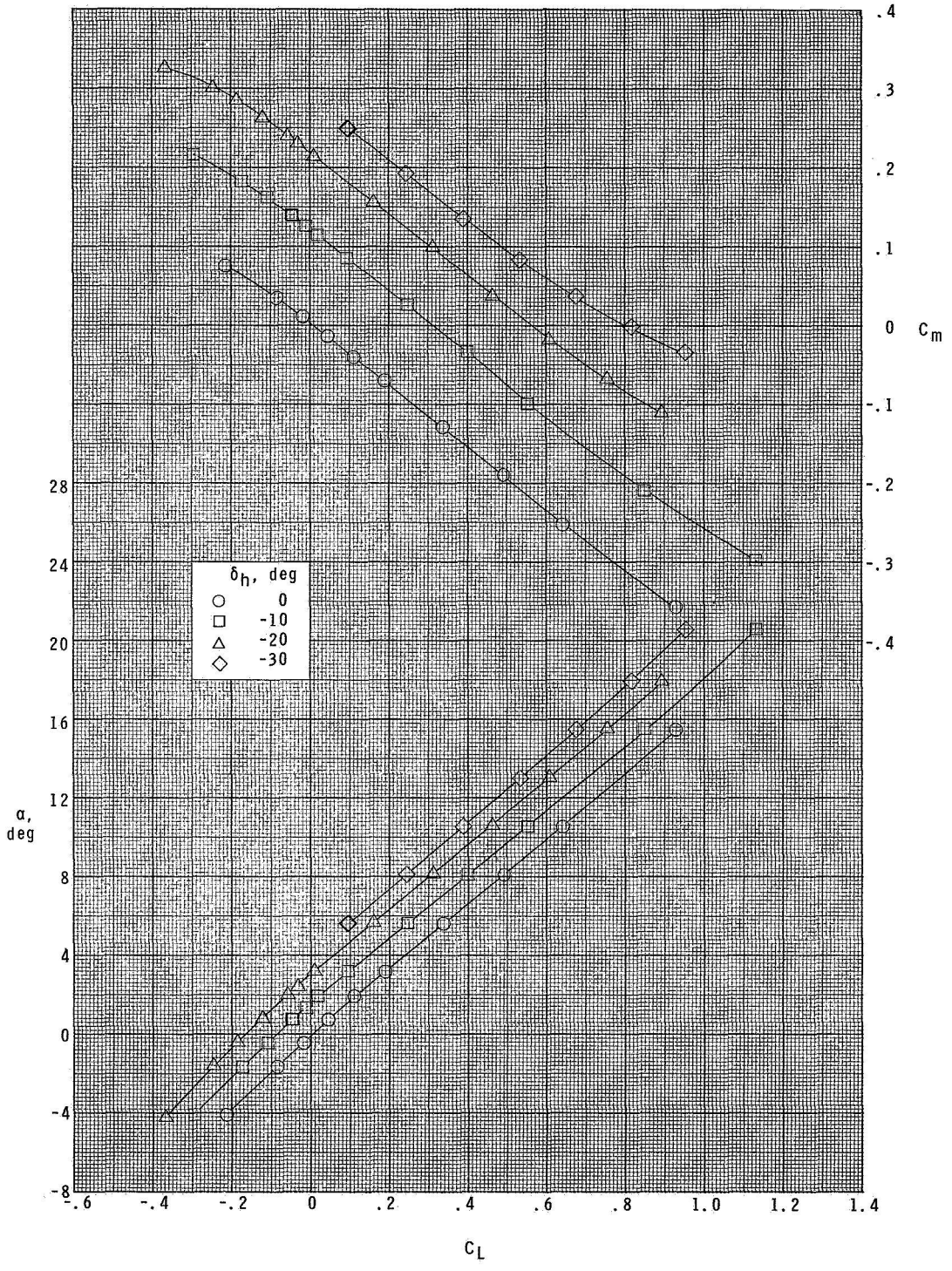
(a) M = 1.75.

Figure 5.- Longitudinal control effectiveness for $B_{11}X_{16}W_2H_9T_{12}V_{U5}Y_5$ (HRE off).



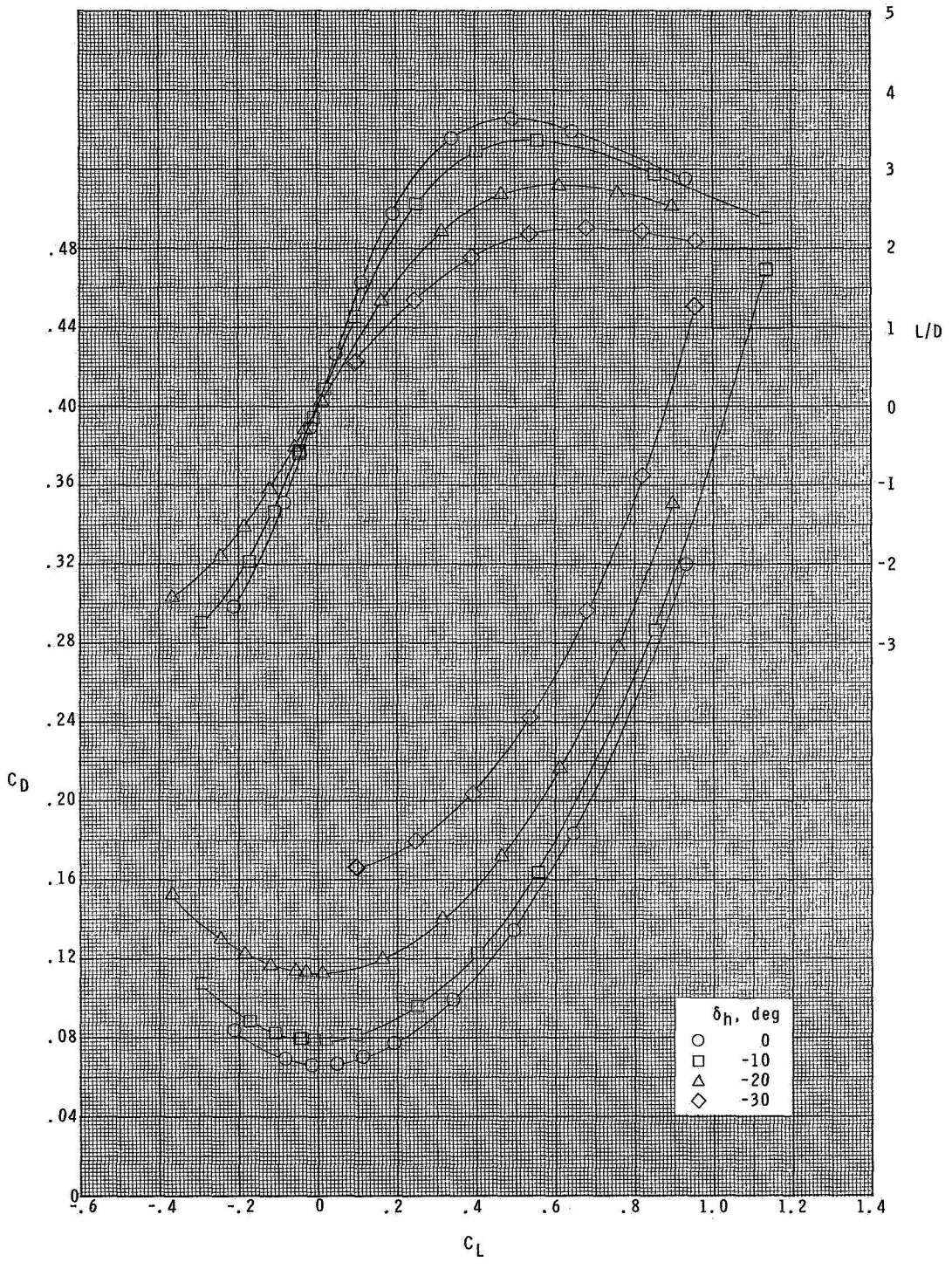
(a) Concluded.

Figure 5.- Continued.



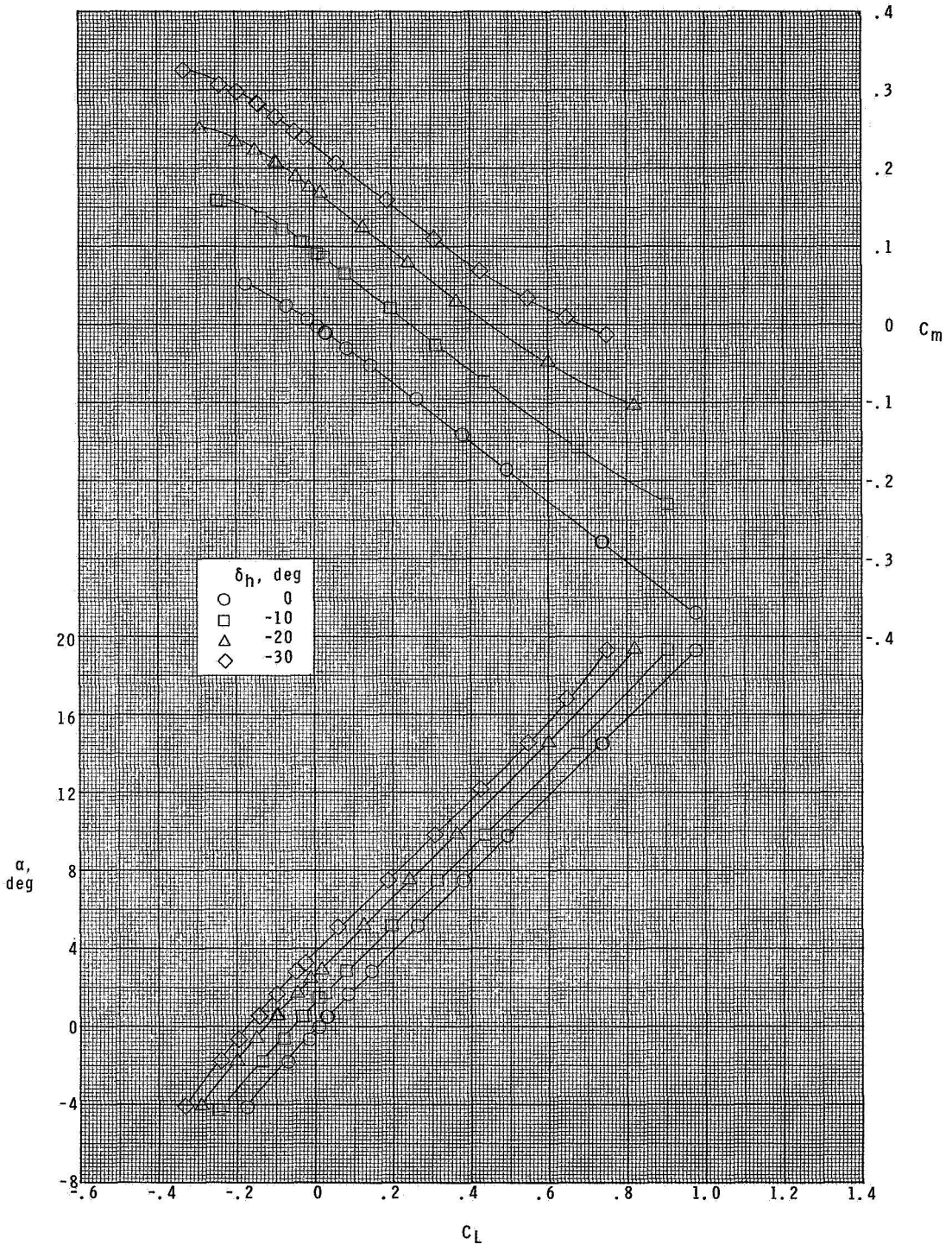
(b) M = 2.00.

Figure 5.- Continued.



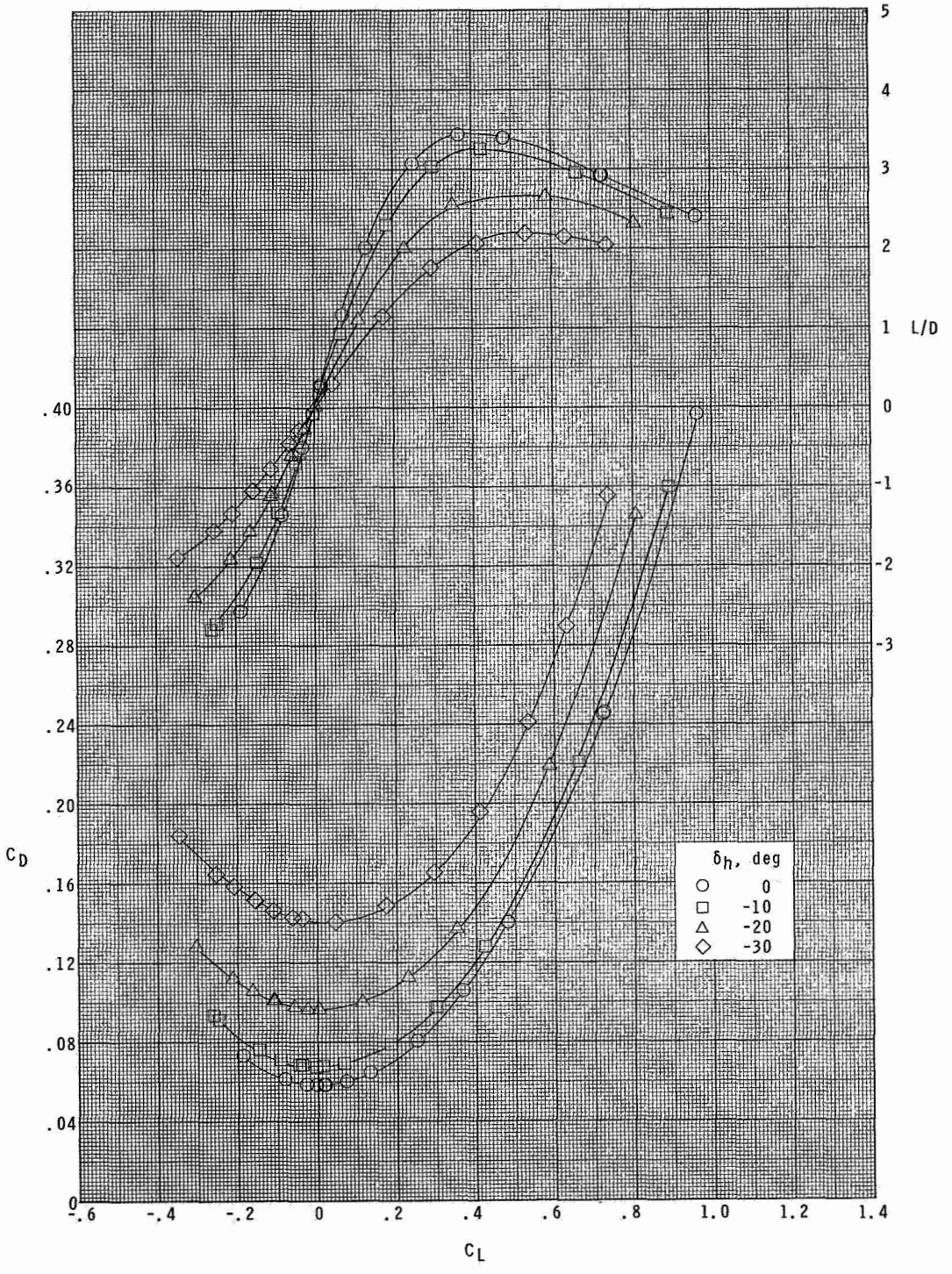
(b) Concluded.

Figure 5.- Continued.



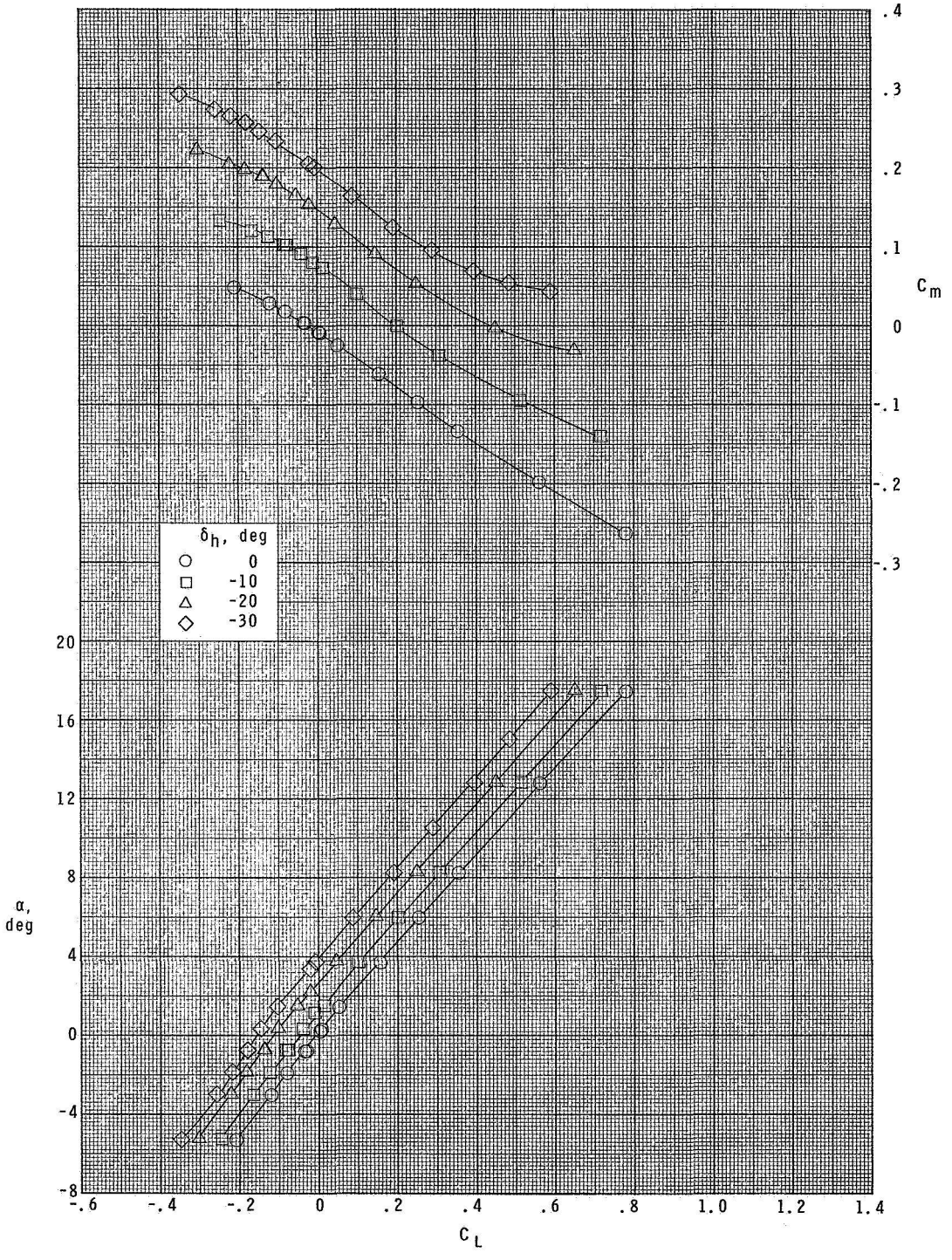
(c) M = 2.50.

Figure 5.- Continued.



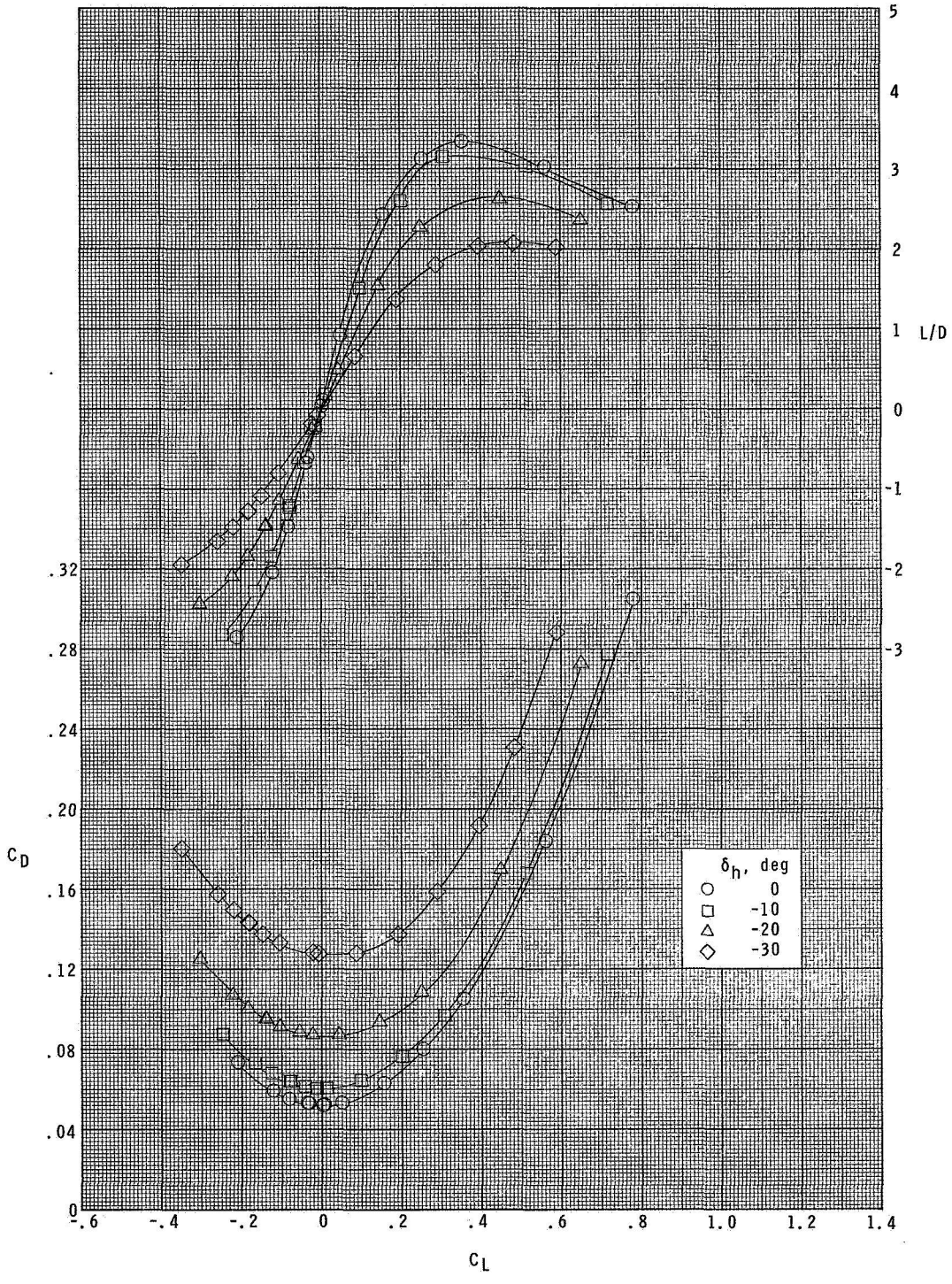
(c) Concluded.

Figure 5.- Continued.



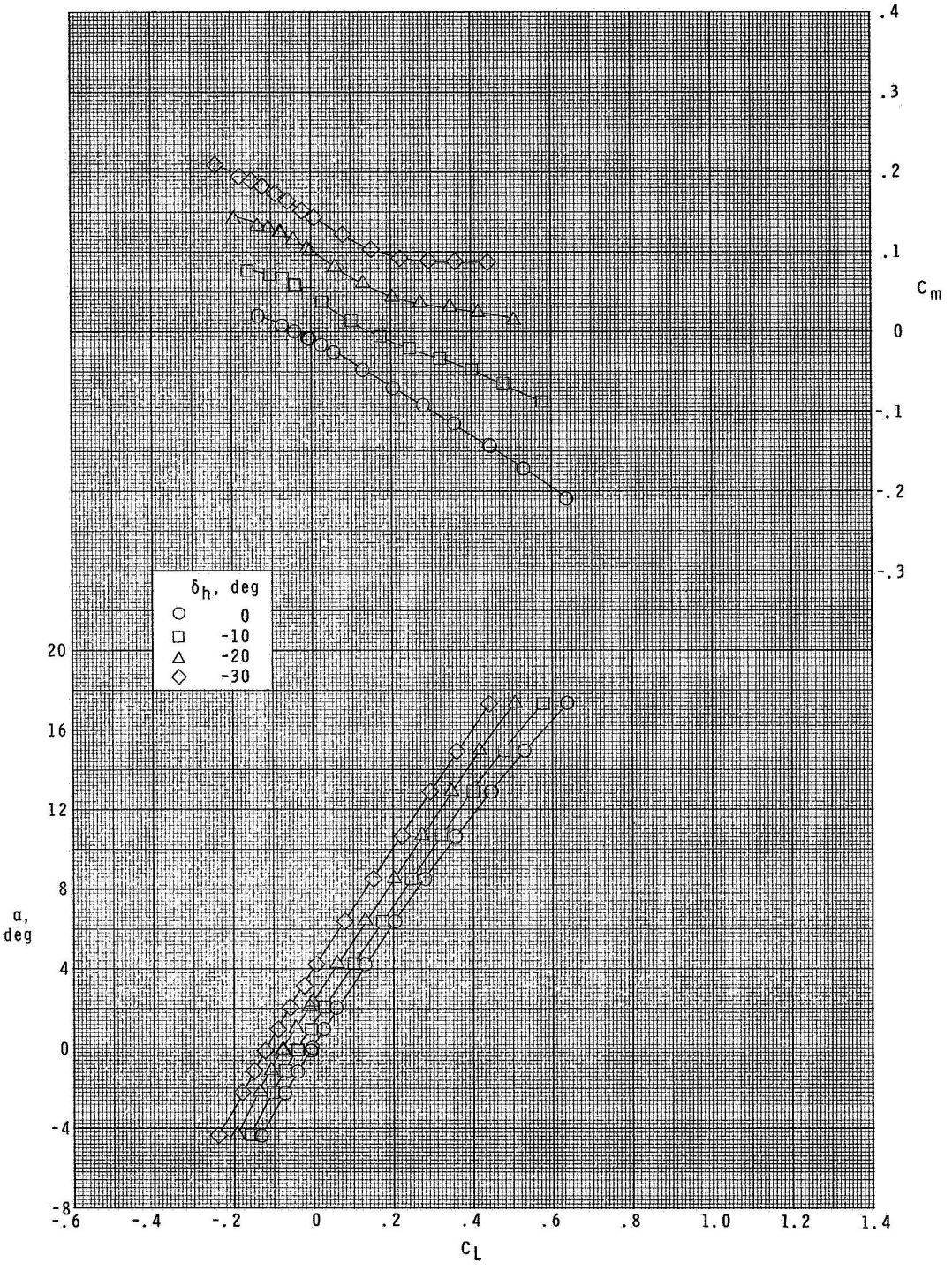
(d) M = 2.86.

Figure 5.- Continued.



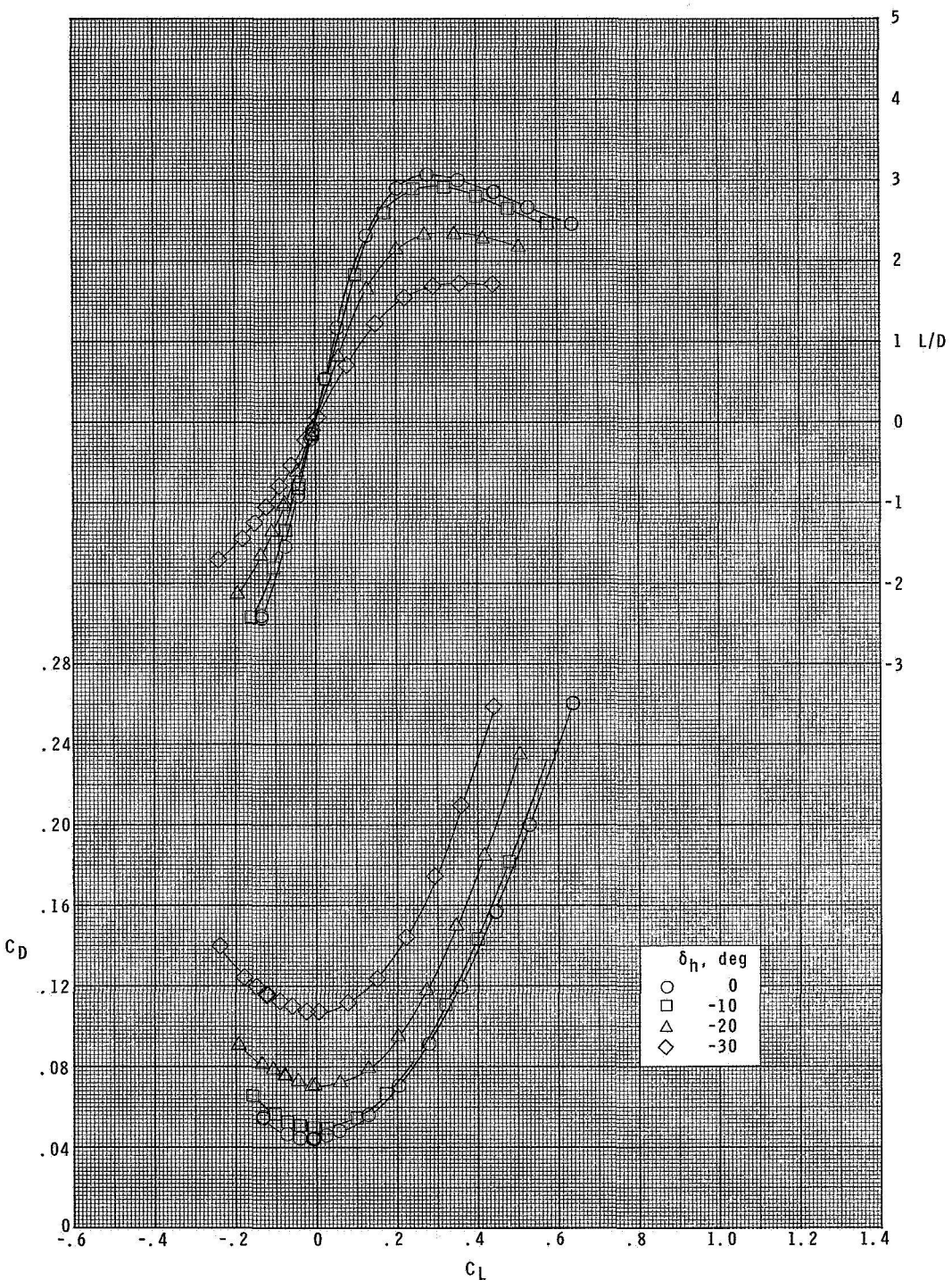
(d) Concluded.

Figure 5.- Continued.



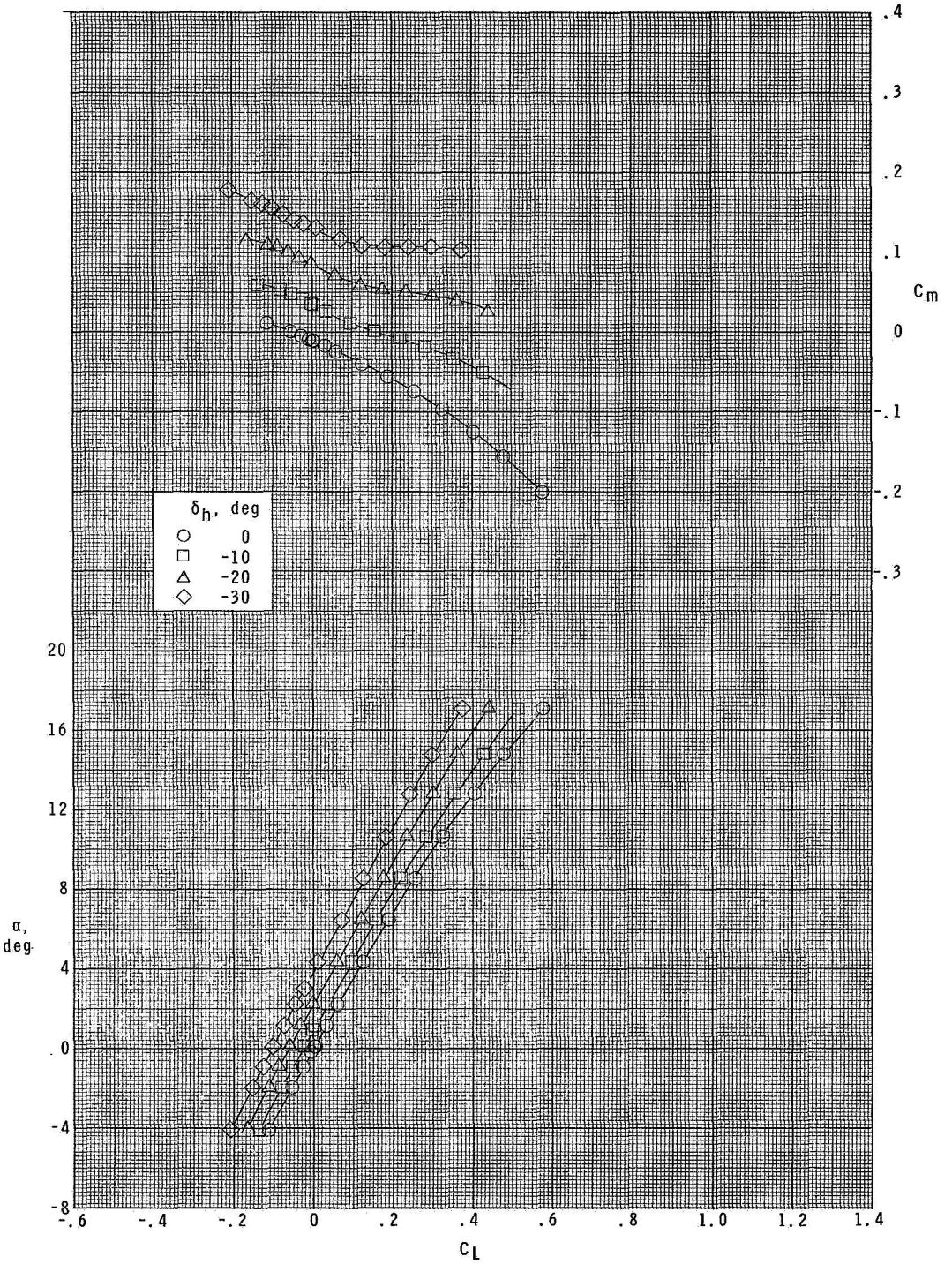
(e) M = 3.95.

Figure 5.- Continued.



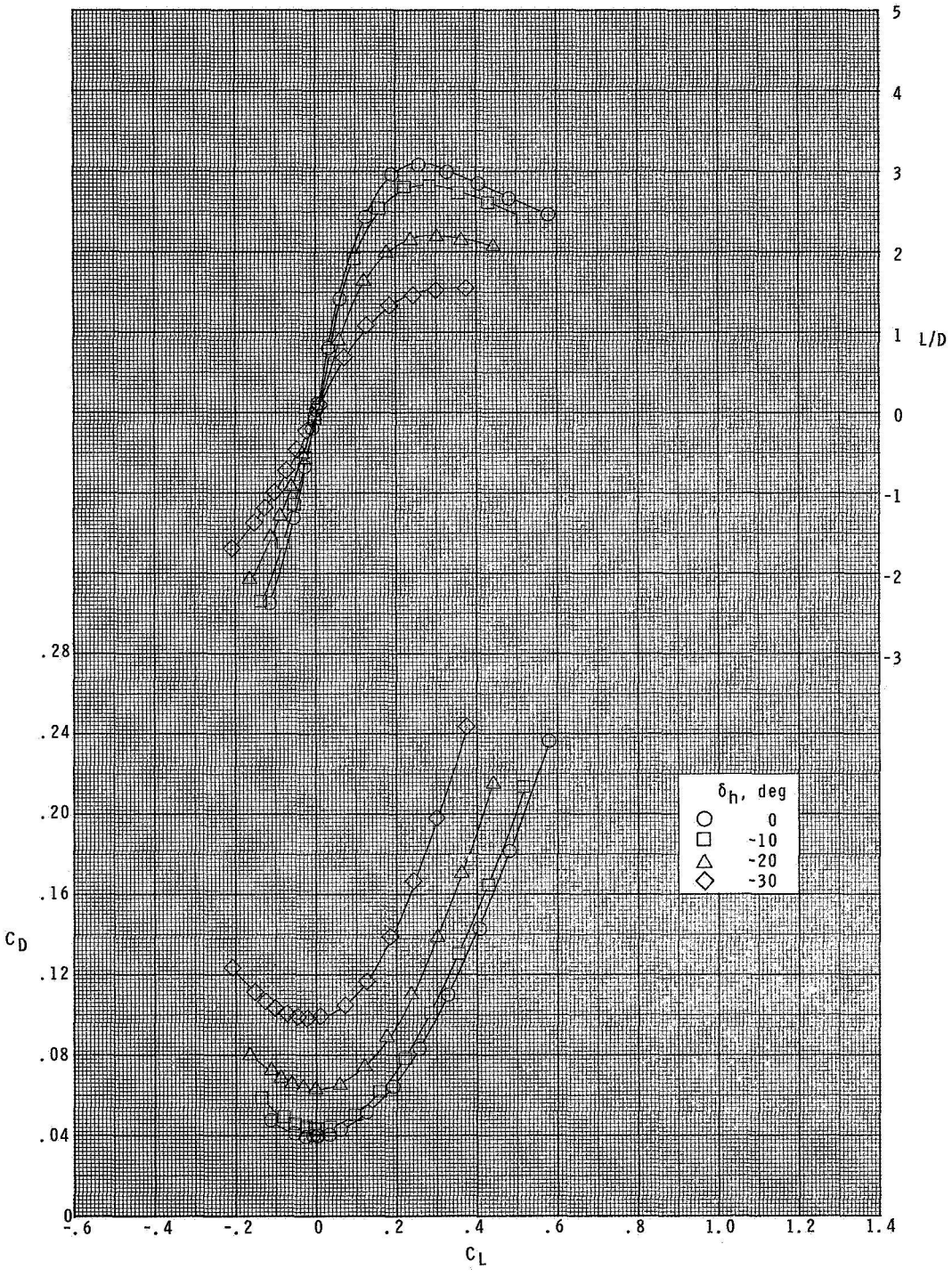
(e) Concluded.

Figure 5.- Continued.



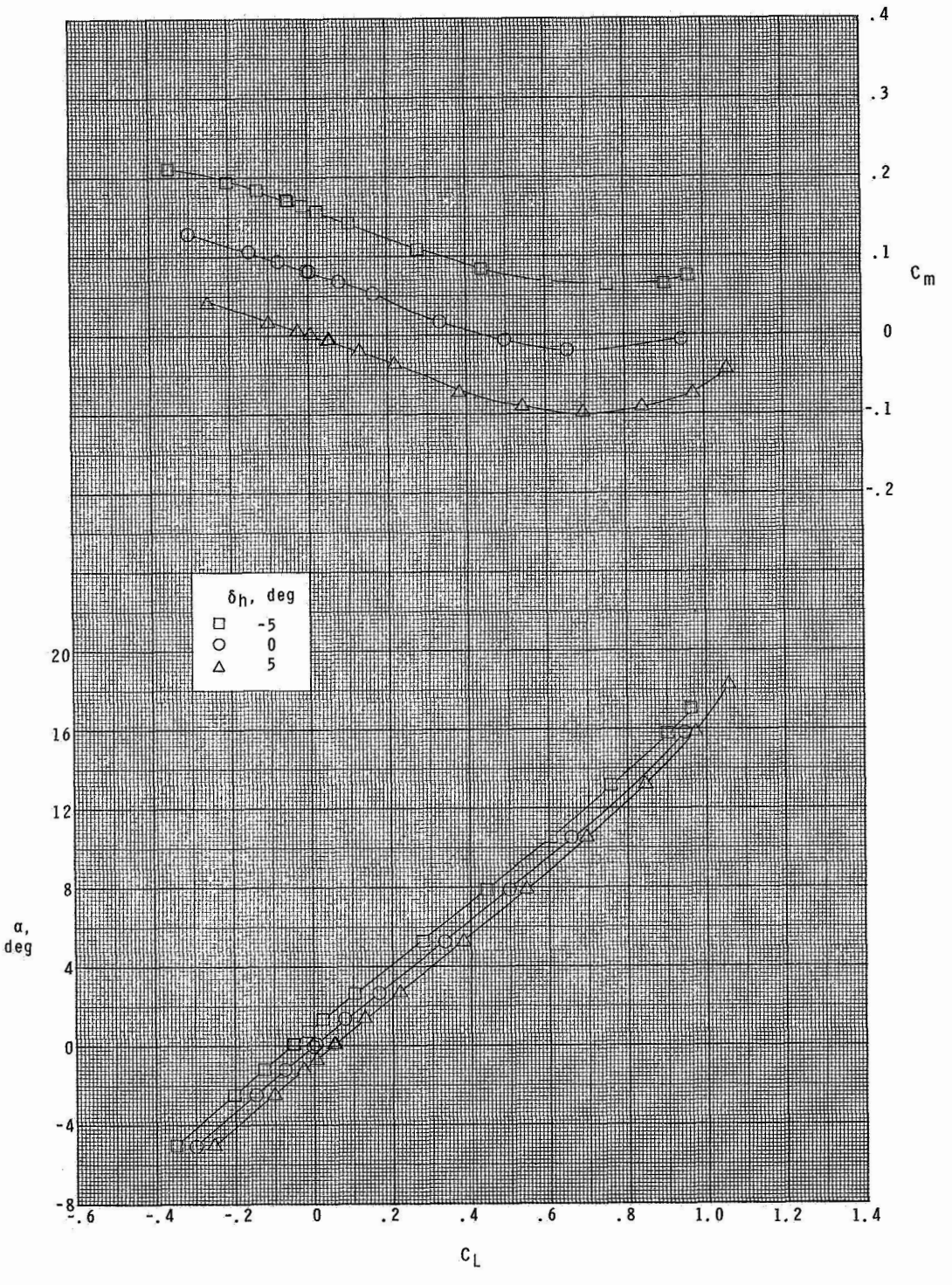
(f) M = 4.63.

Figure 5.- Continued.



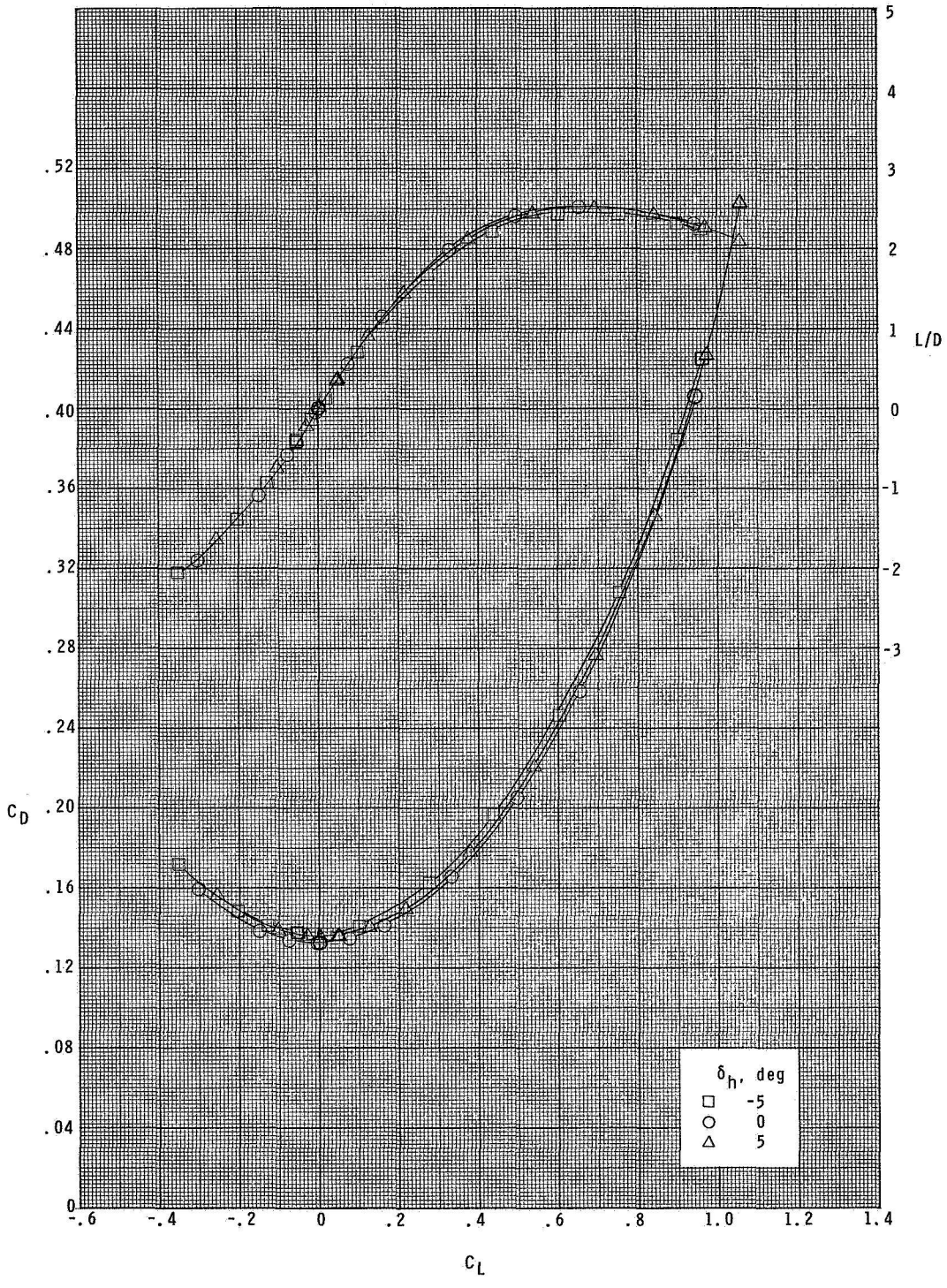
(f) Concluded.

Figure 5.- Concluded.



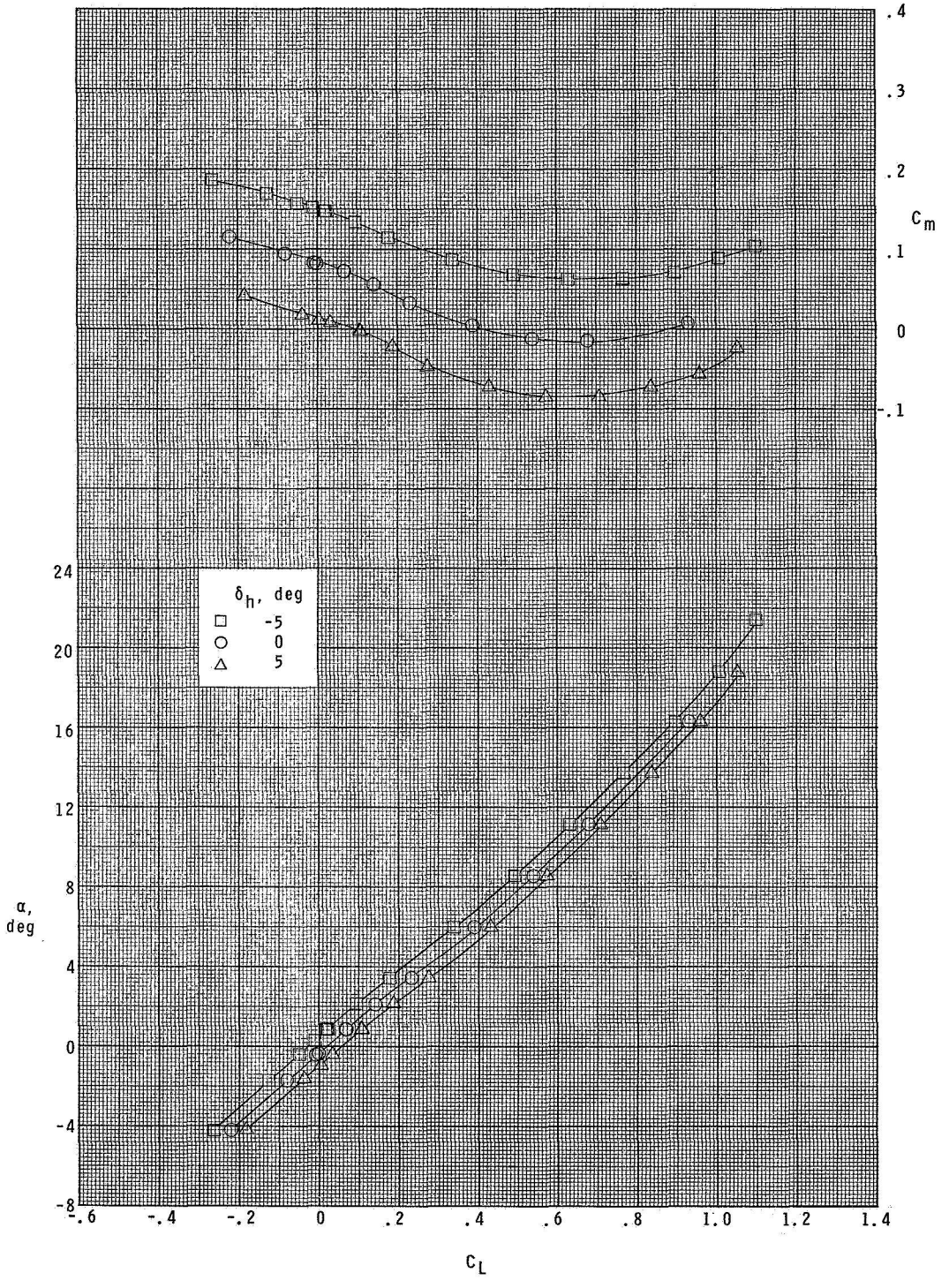
(a) M = 1.75.

Figure 6.- Longitudinal control effectiveness for $B_{11}X_{16}W_2H_9T_{12}V_{U5}Y_5N_{13}T_{13}$ (HRE and tanks on).



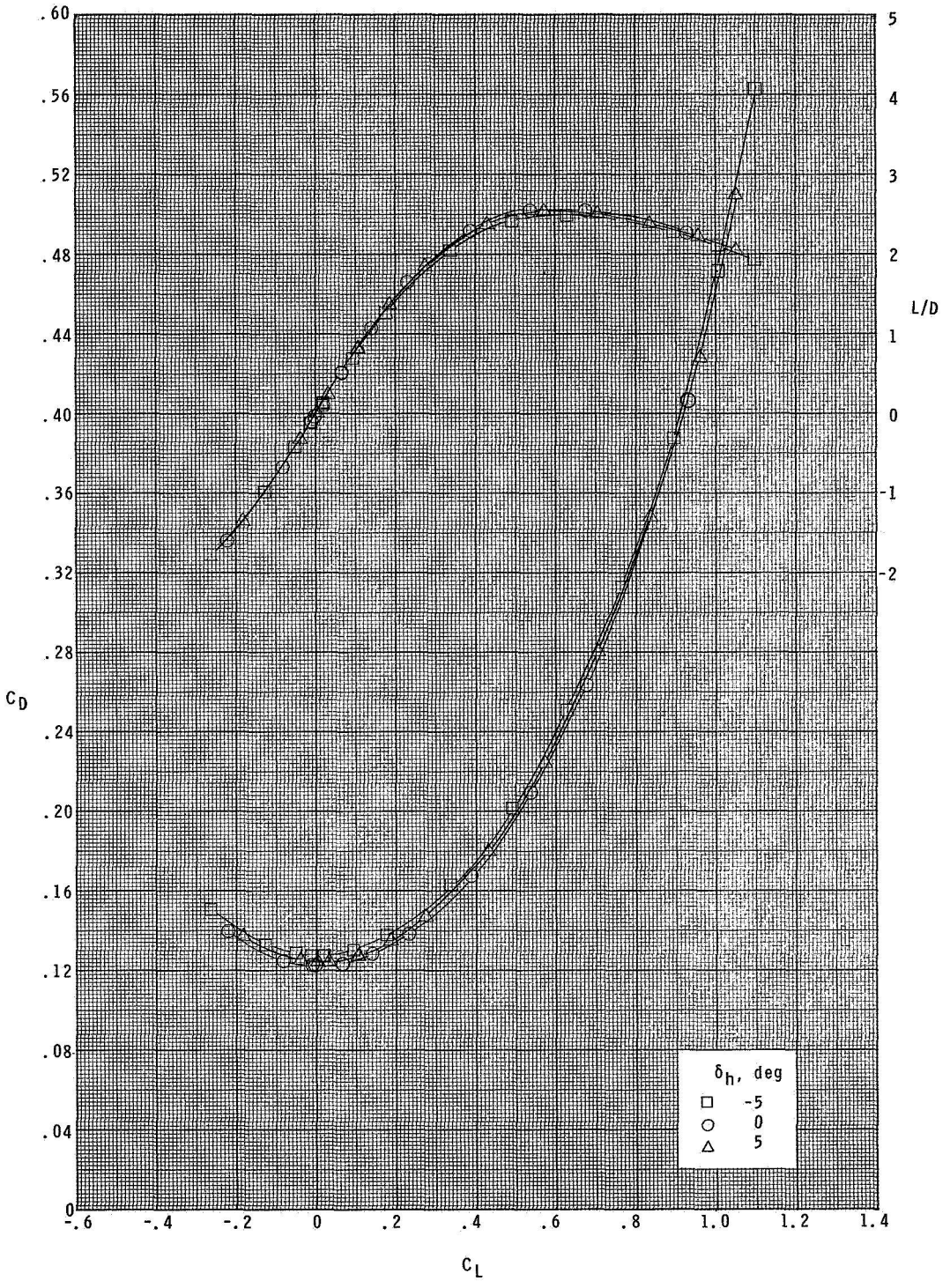
(a) Concluded.

Figure 6.- Continued.



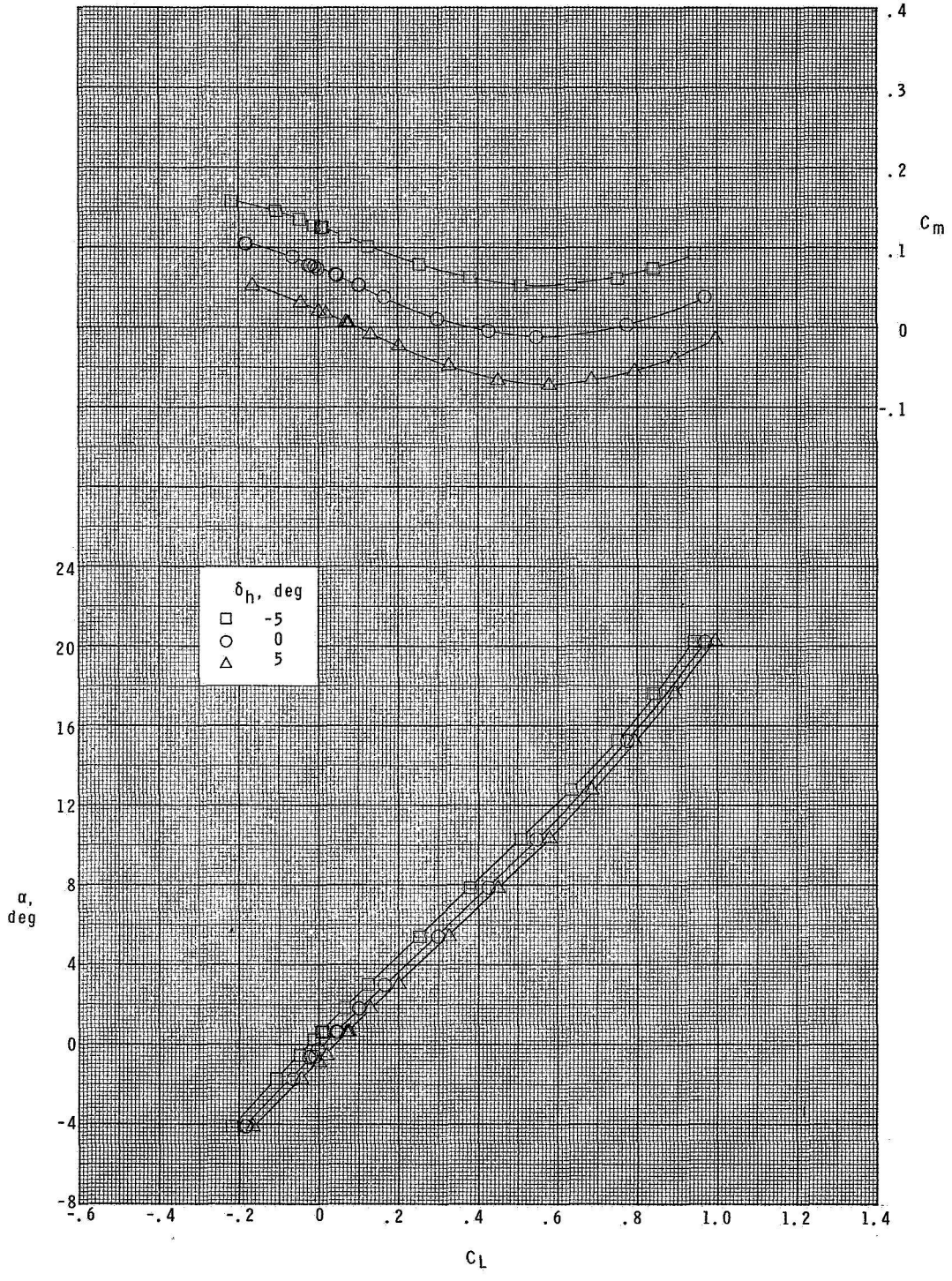
(b) M = 2.00.

Figure 6.- Continued.



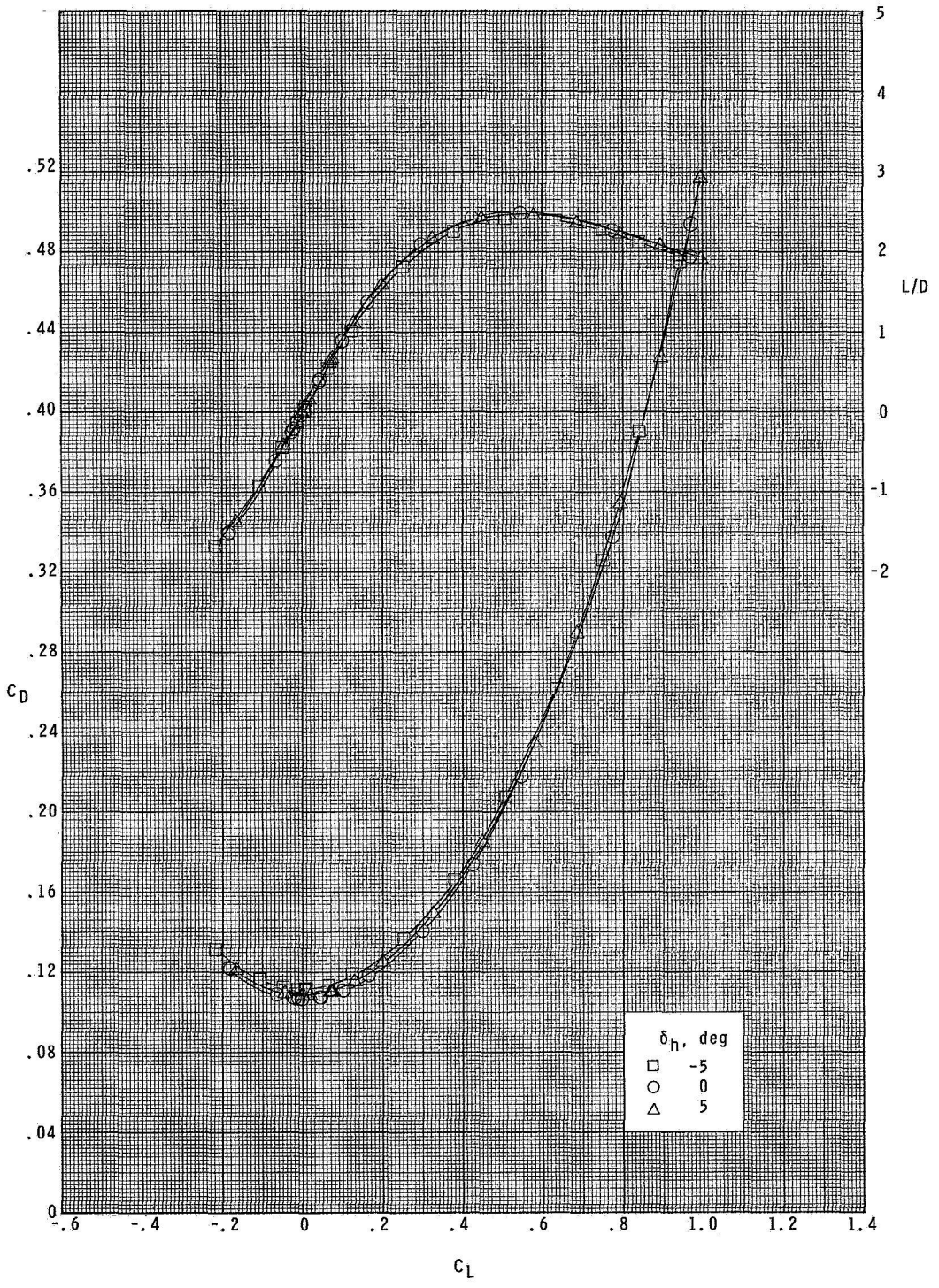
(b) Concluded.

Figure 6.- Continued.



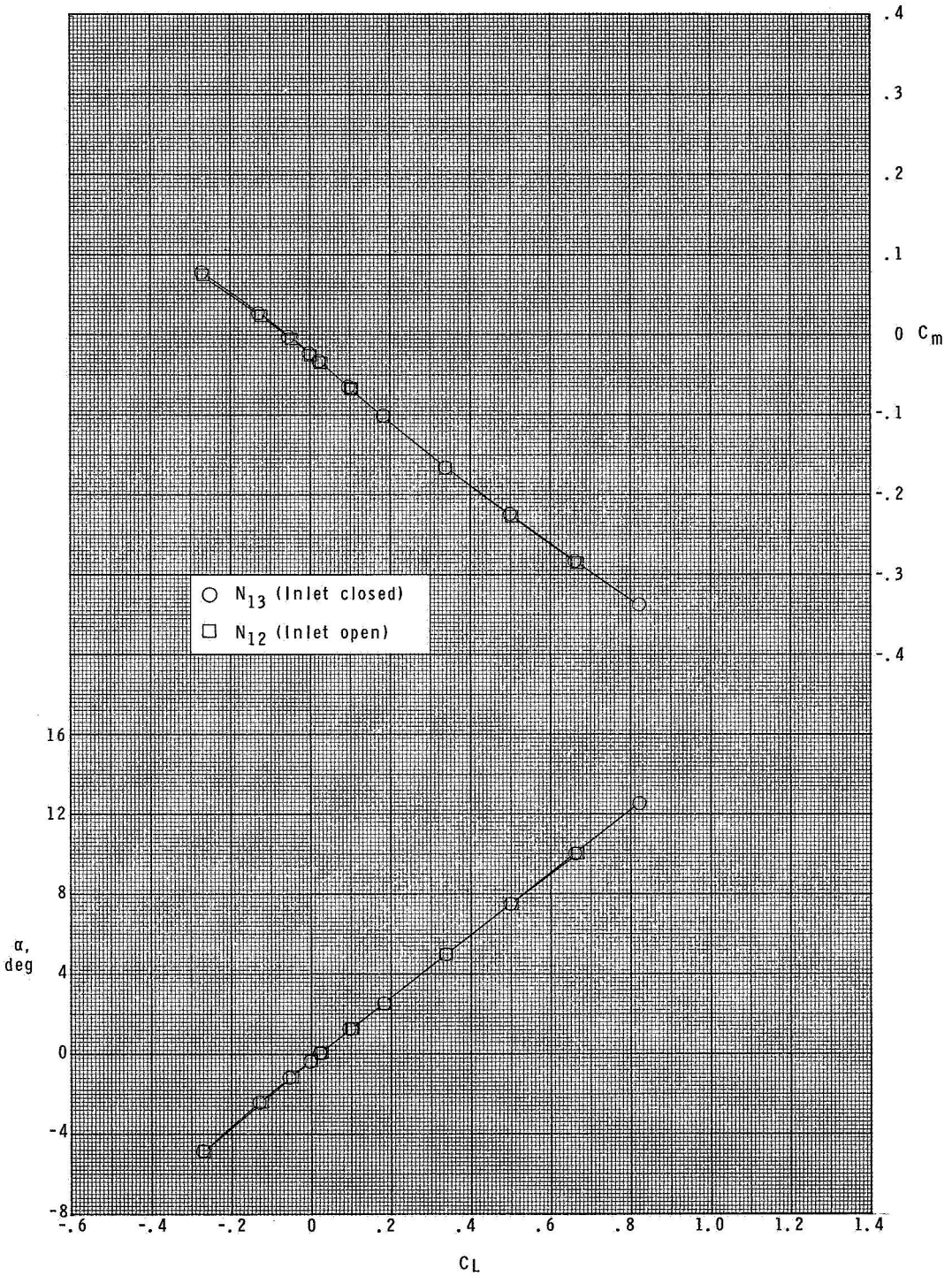
(c) M = 2.50.

Figure 6.- Continued.



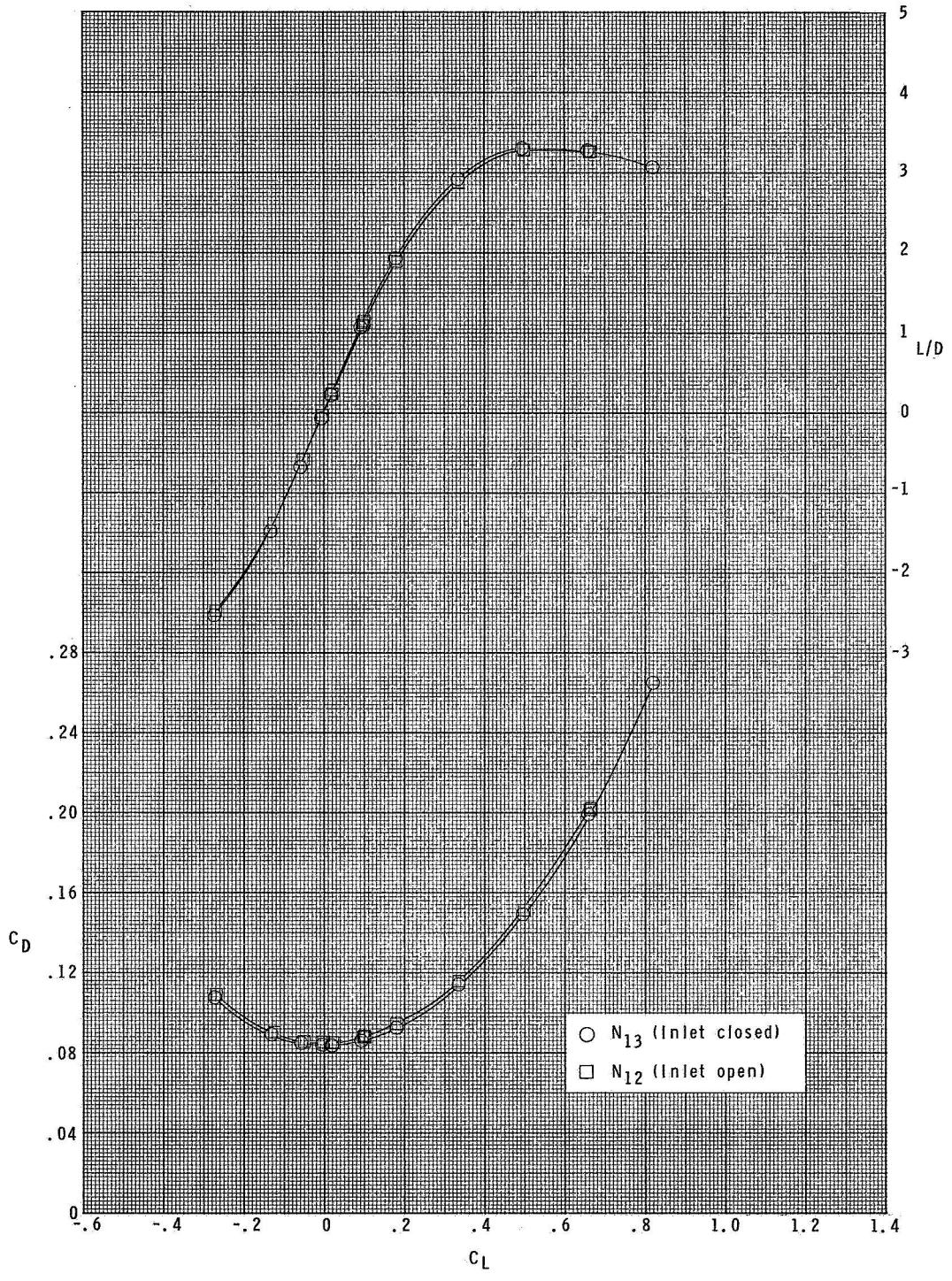
(c) Concluded.

Figure 6.- Concluded.



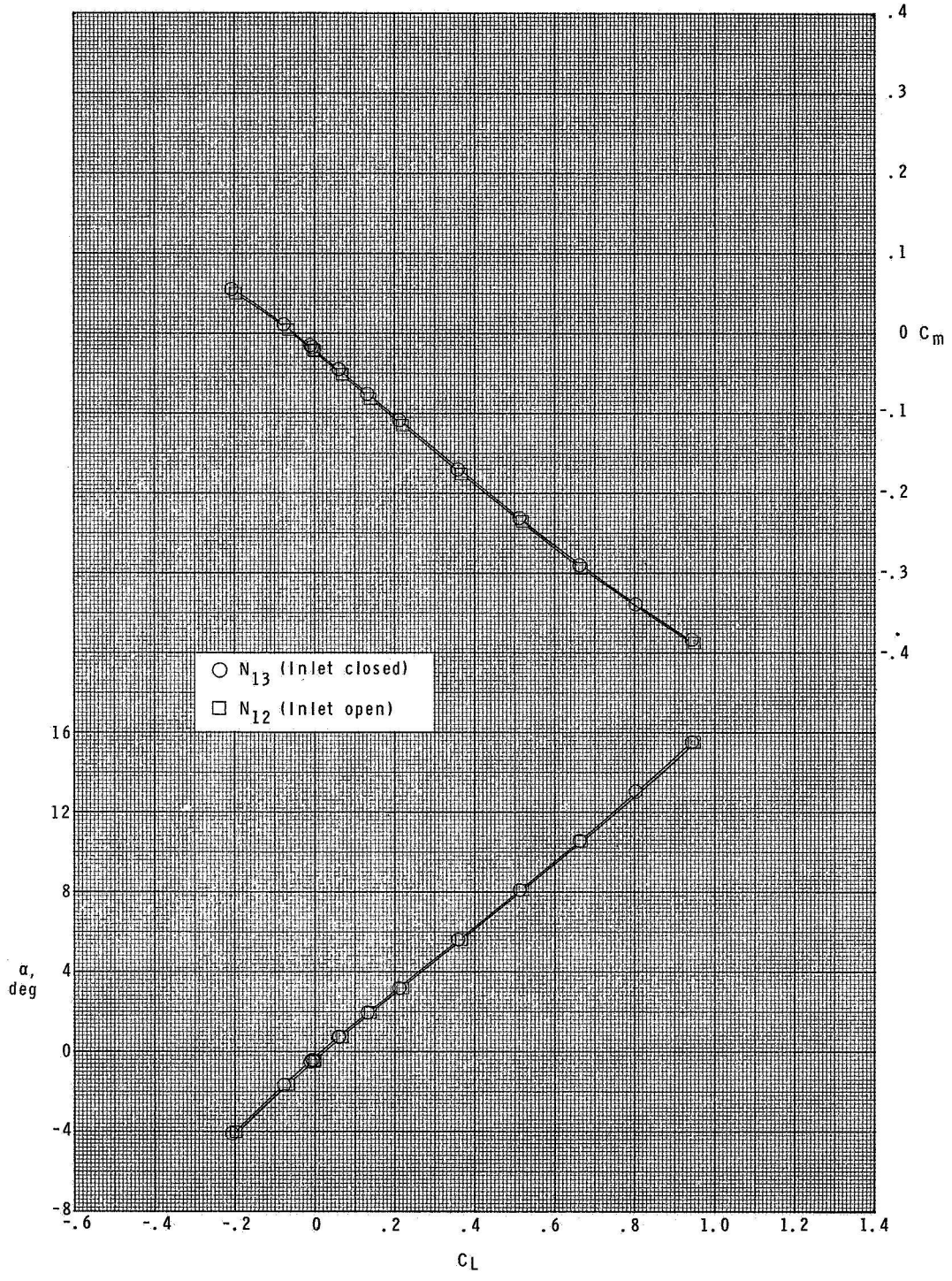
(a) M = 1.75.

Figure 7.- Effect of HRE spike position (no airflow) on longitudinal aerodynamic characteristics for $B_{11}X_{16}W_2H_9T_{12}V_{U5}Y_5$.



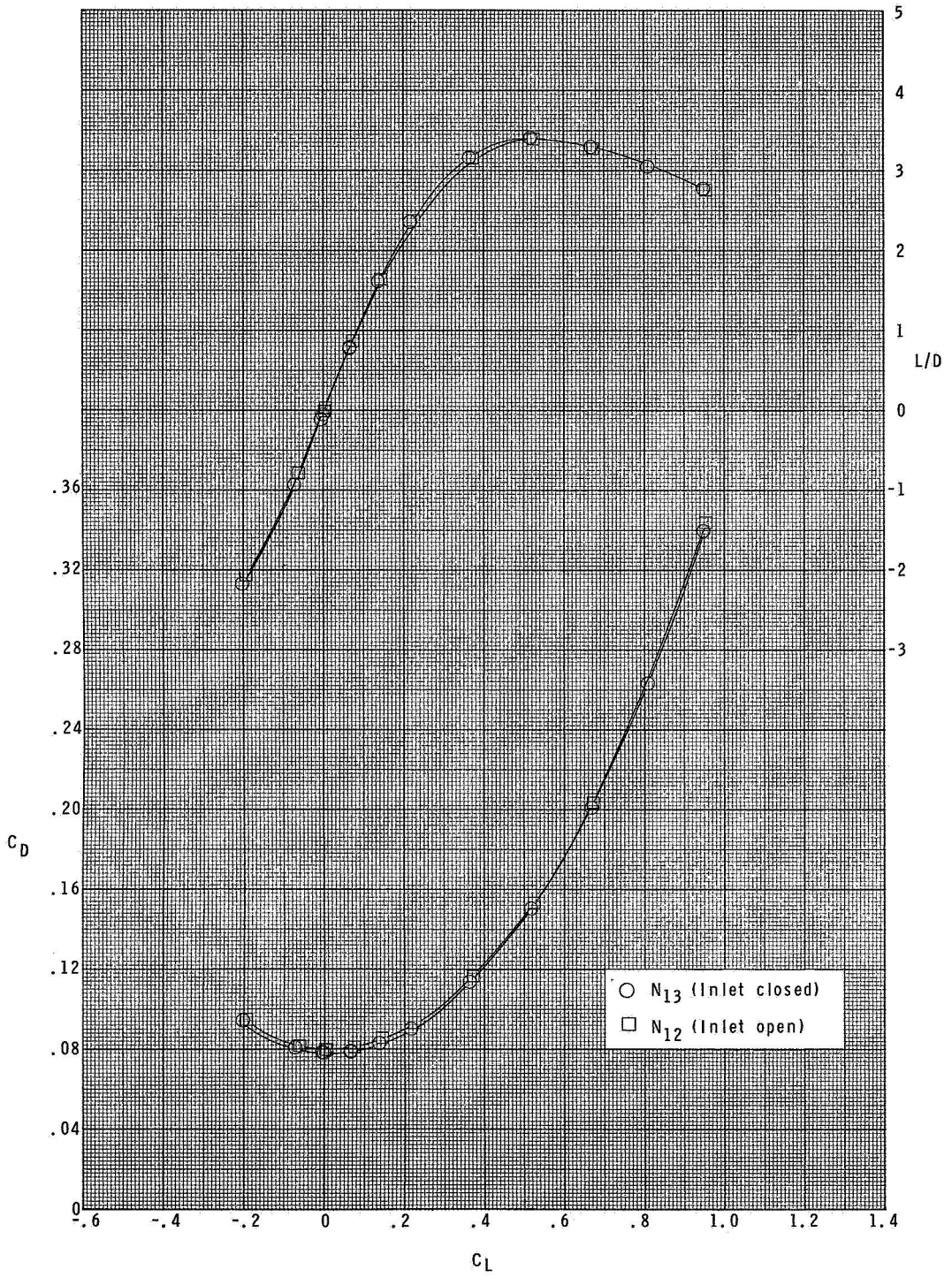
(a) Concluded.

Figure 7.- Continued.



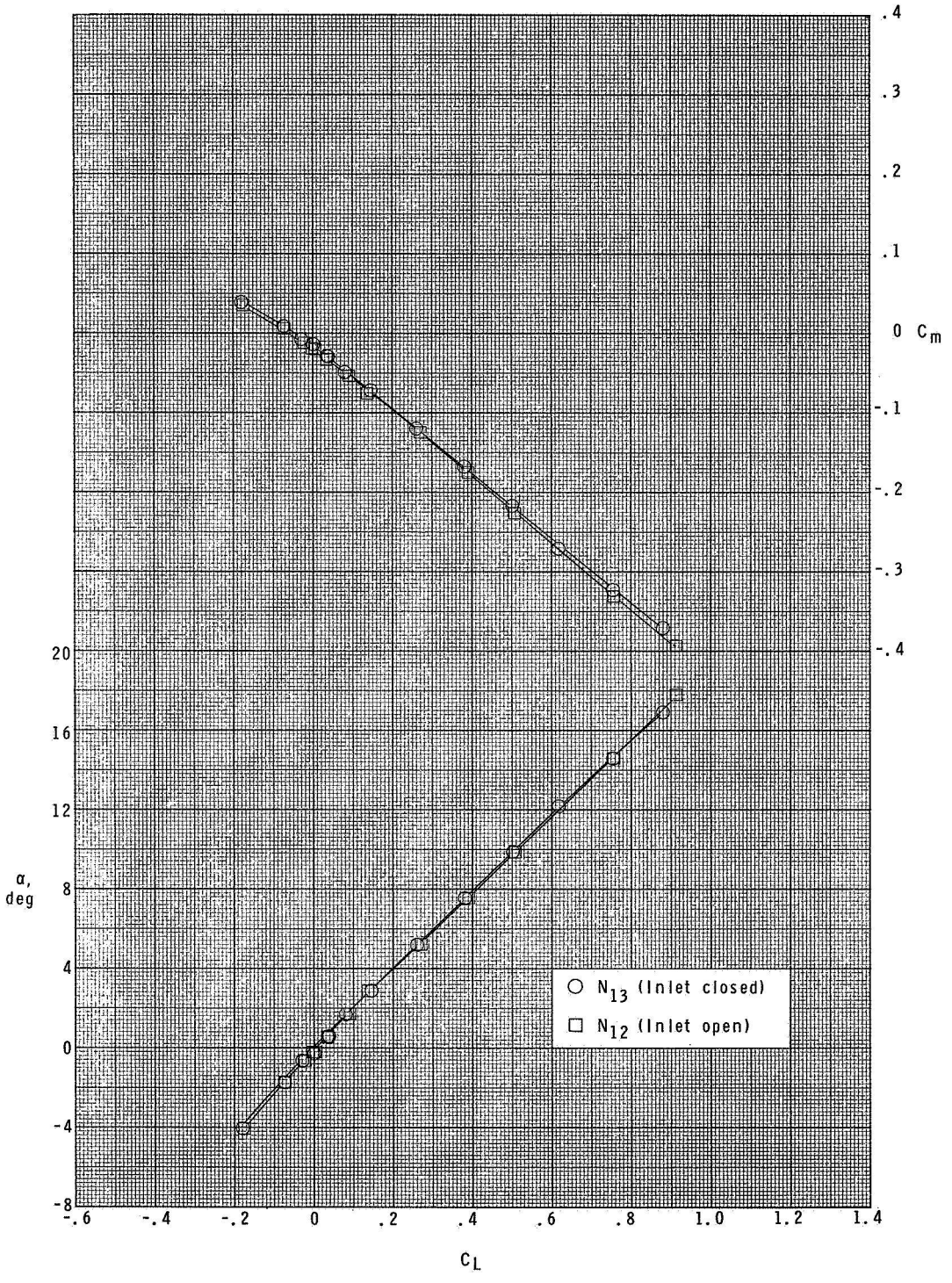
(b) M = 2.00.

Figure 7.- Continued.



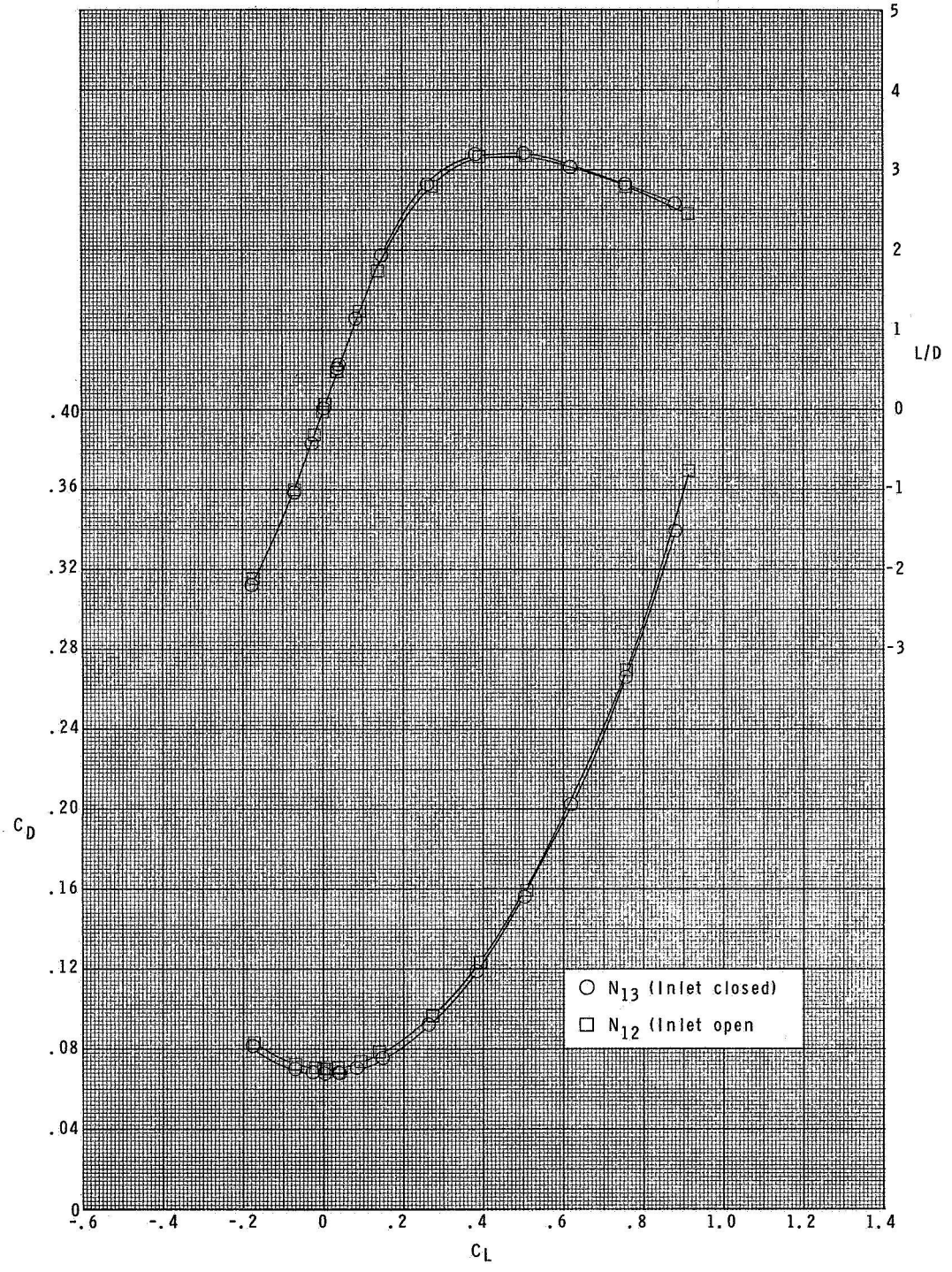
(b) Concluded.

Figure 7.- Continued.



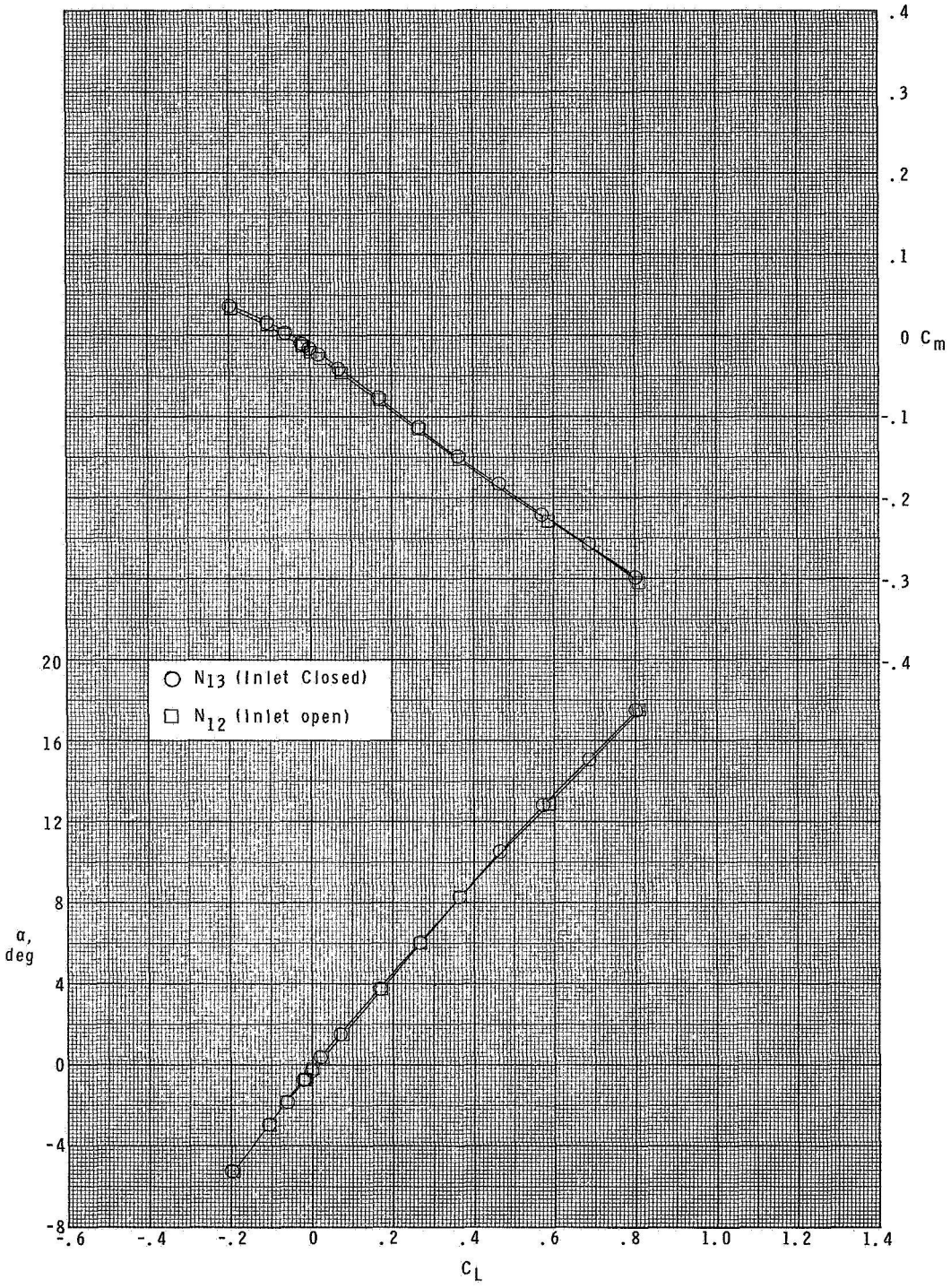
(c) M = 2.50.

Figure 7.- Continued.



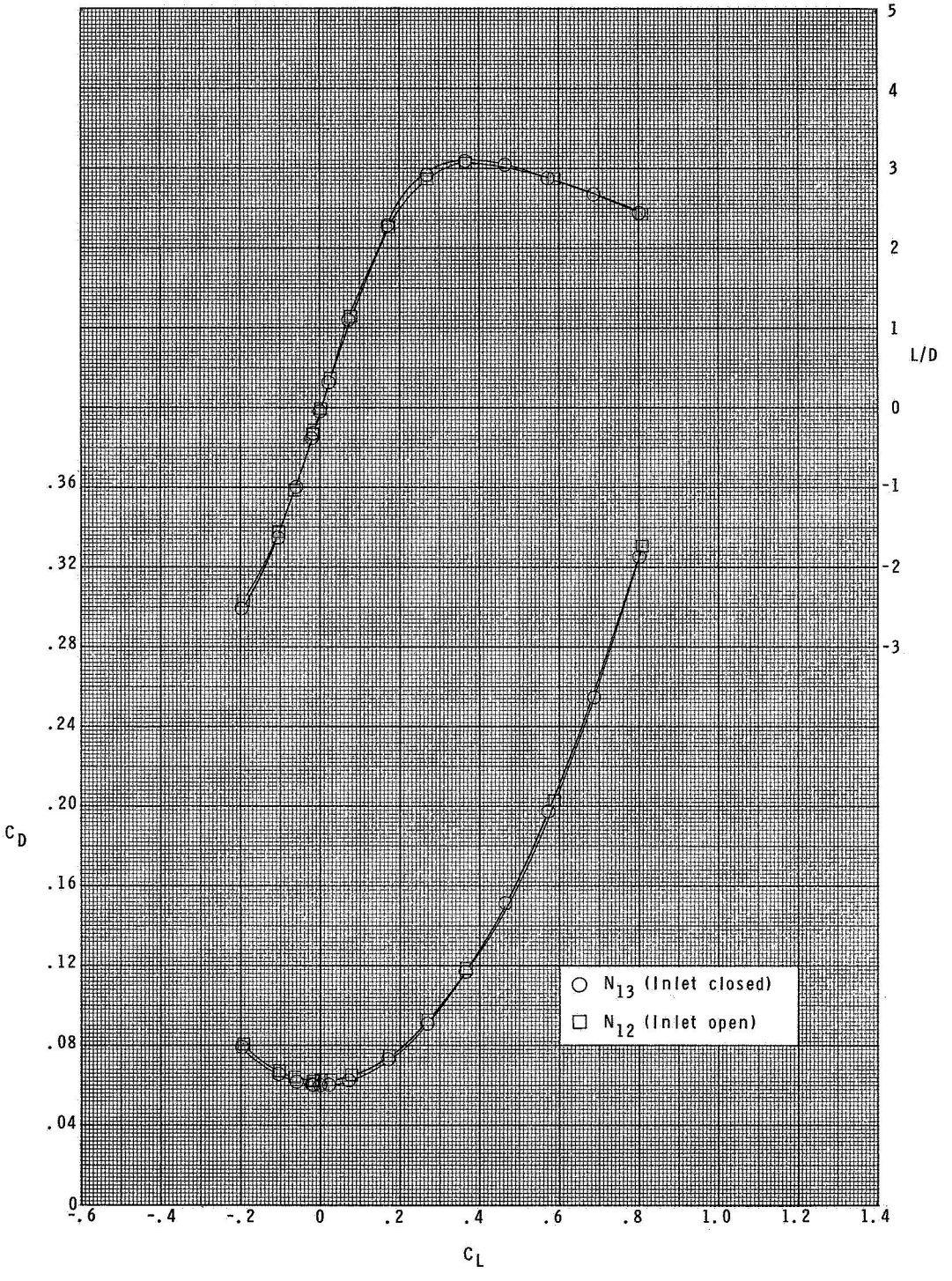
(c) Concluded.

Figure 7.- Continued.



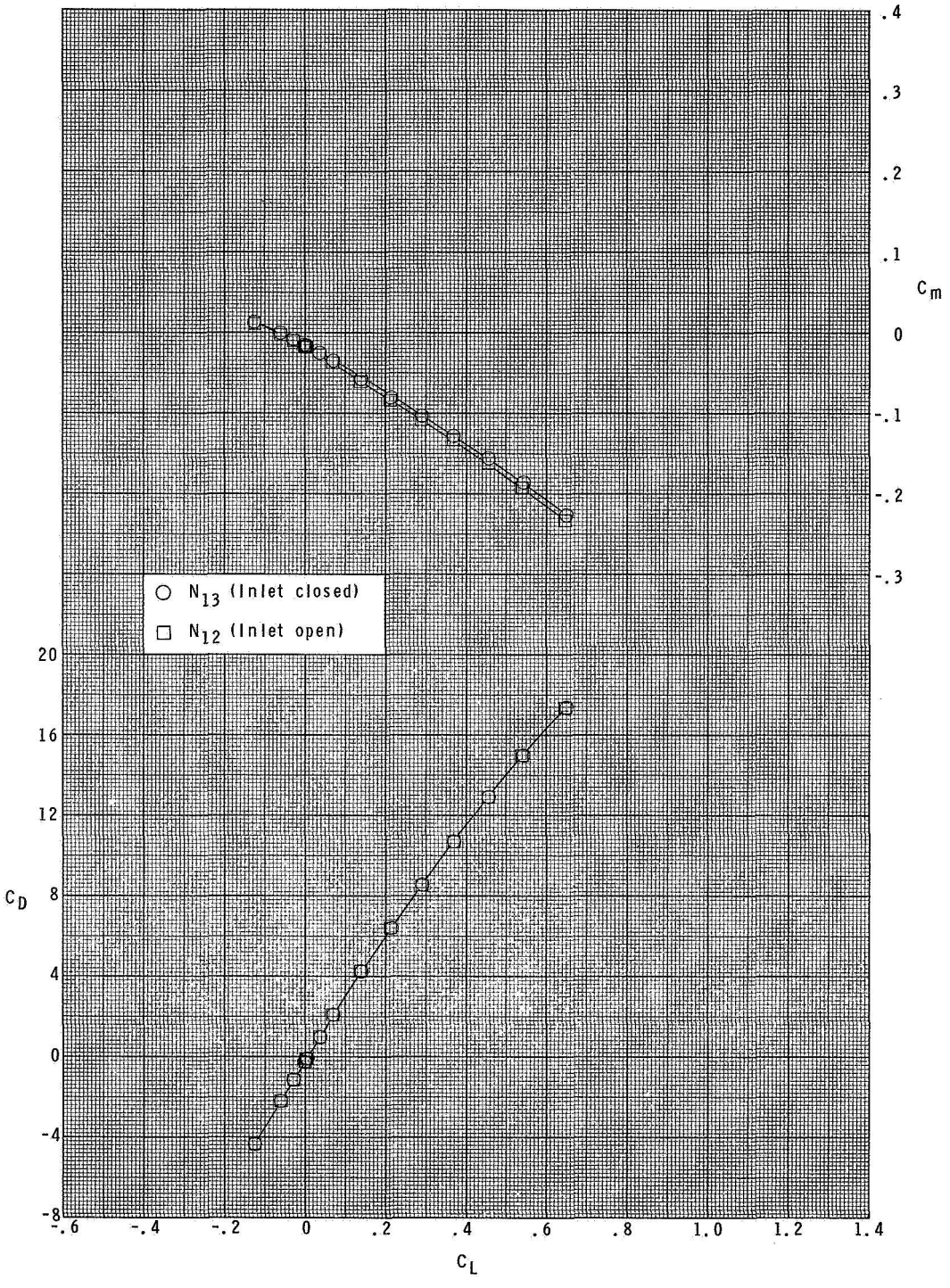
(d) M = 2.86.

Figure 7.- Continued.



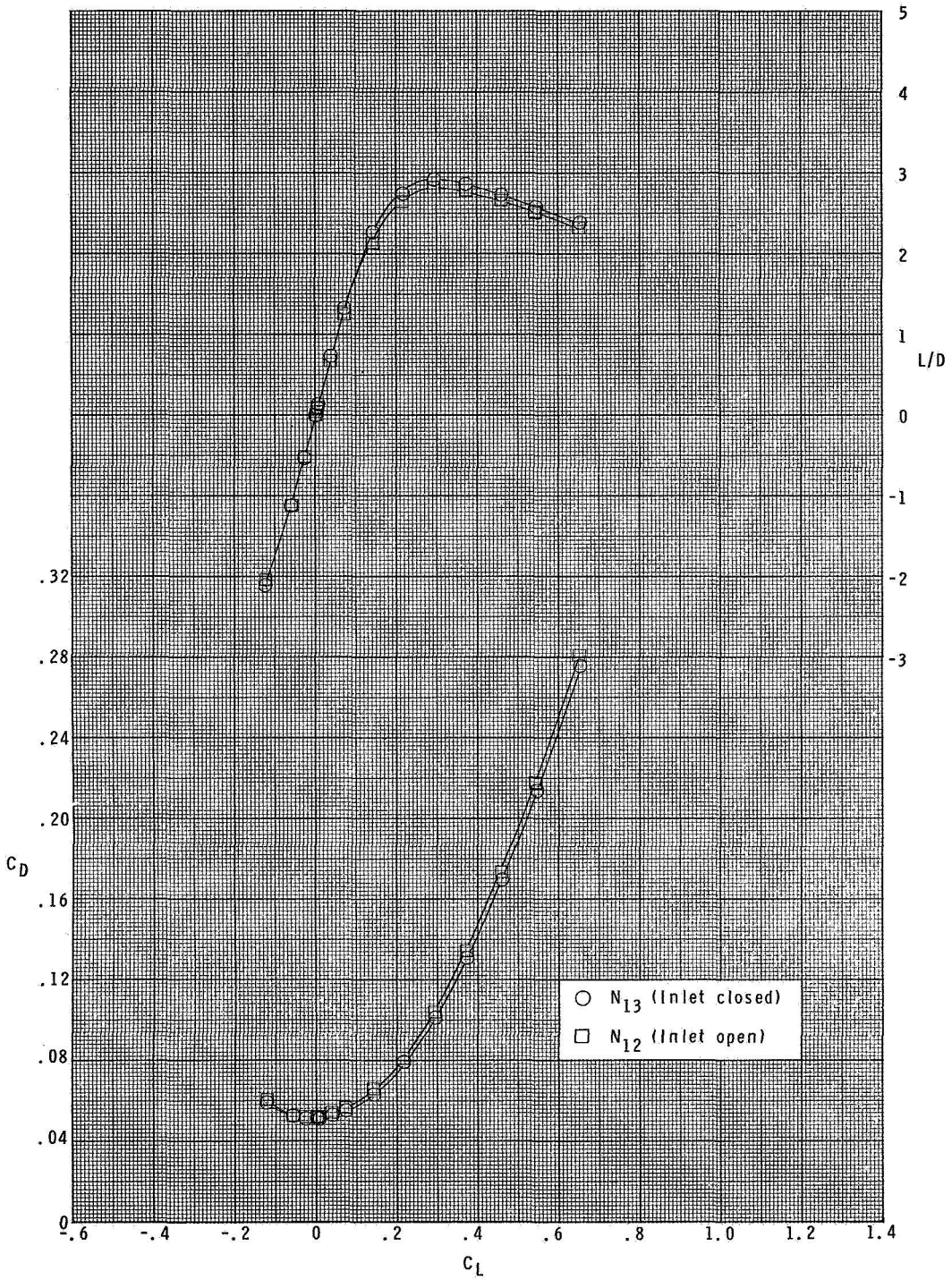
(d) Concluded.

Figure 7.- Continued.



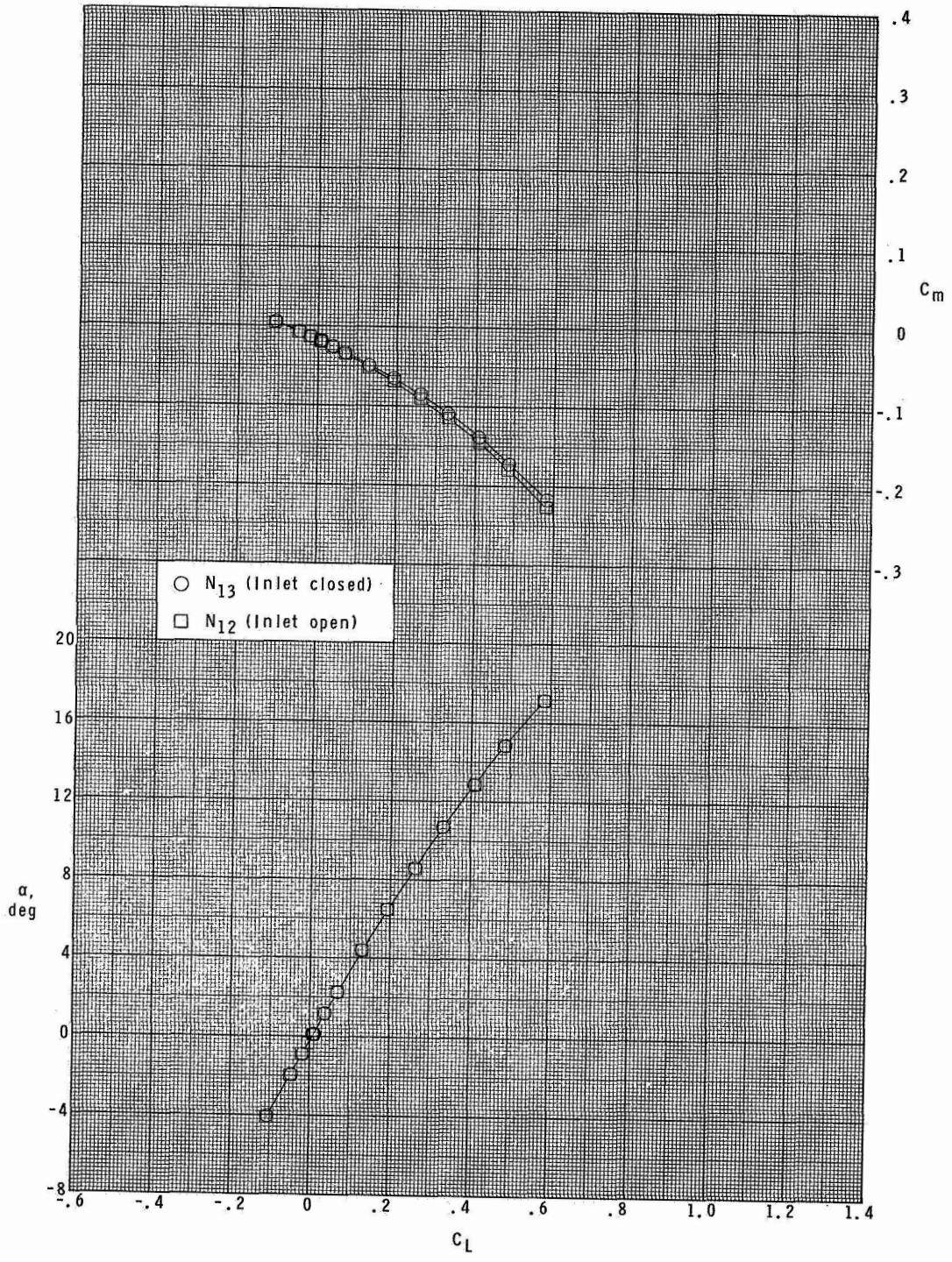
(e) M = 3.95.

Figure 7.- Continued.



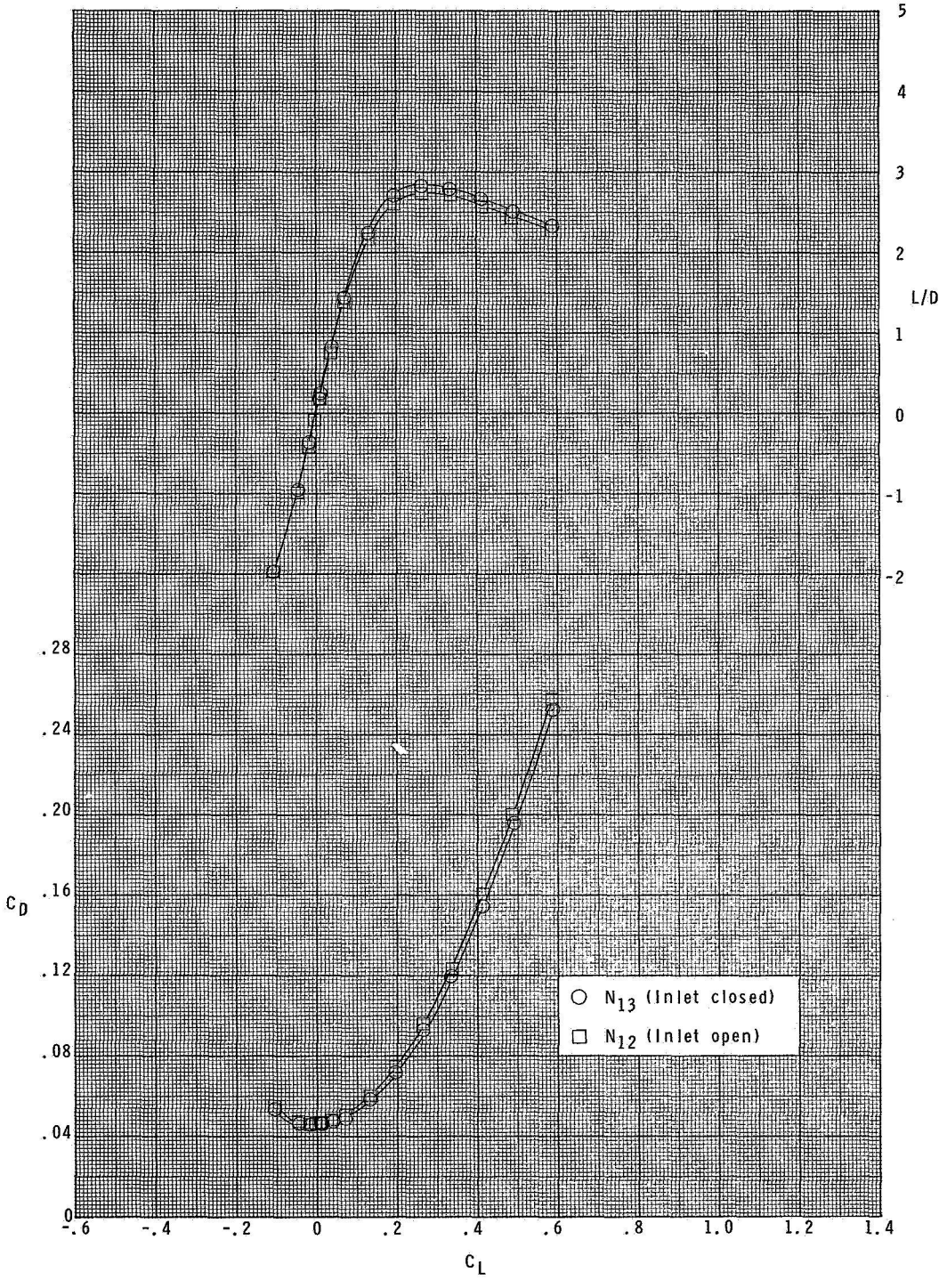
(e) Concluded.

Figure 7.- Continued.



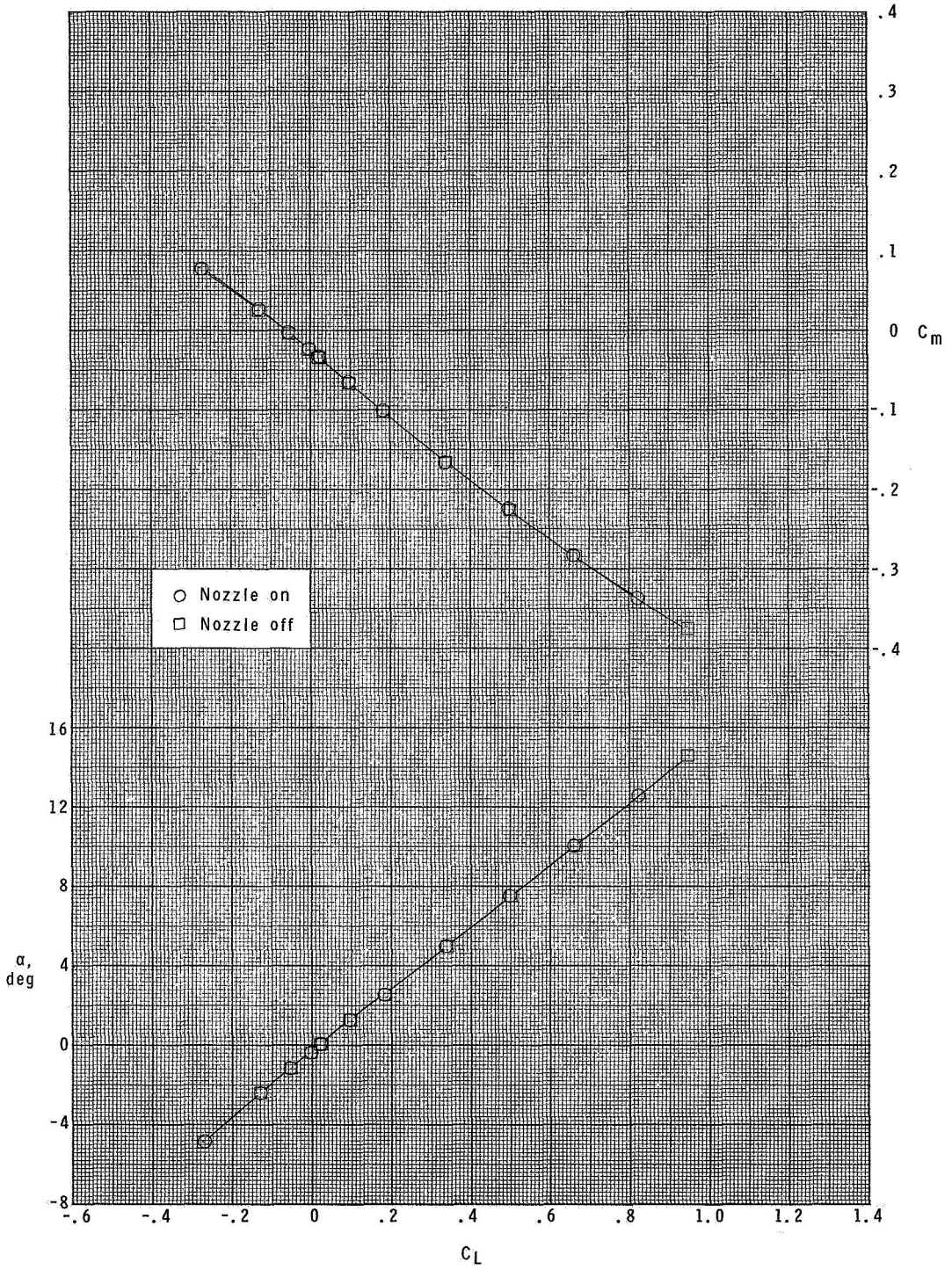
(f) M = 4.63.

Figure 7.- Continued.



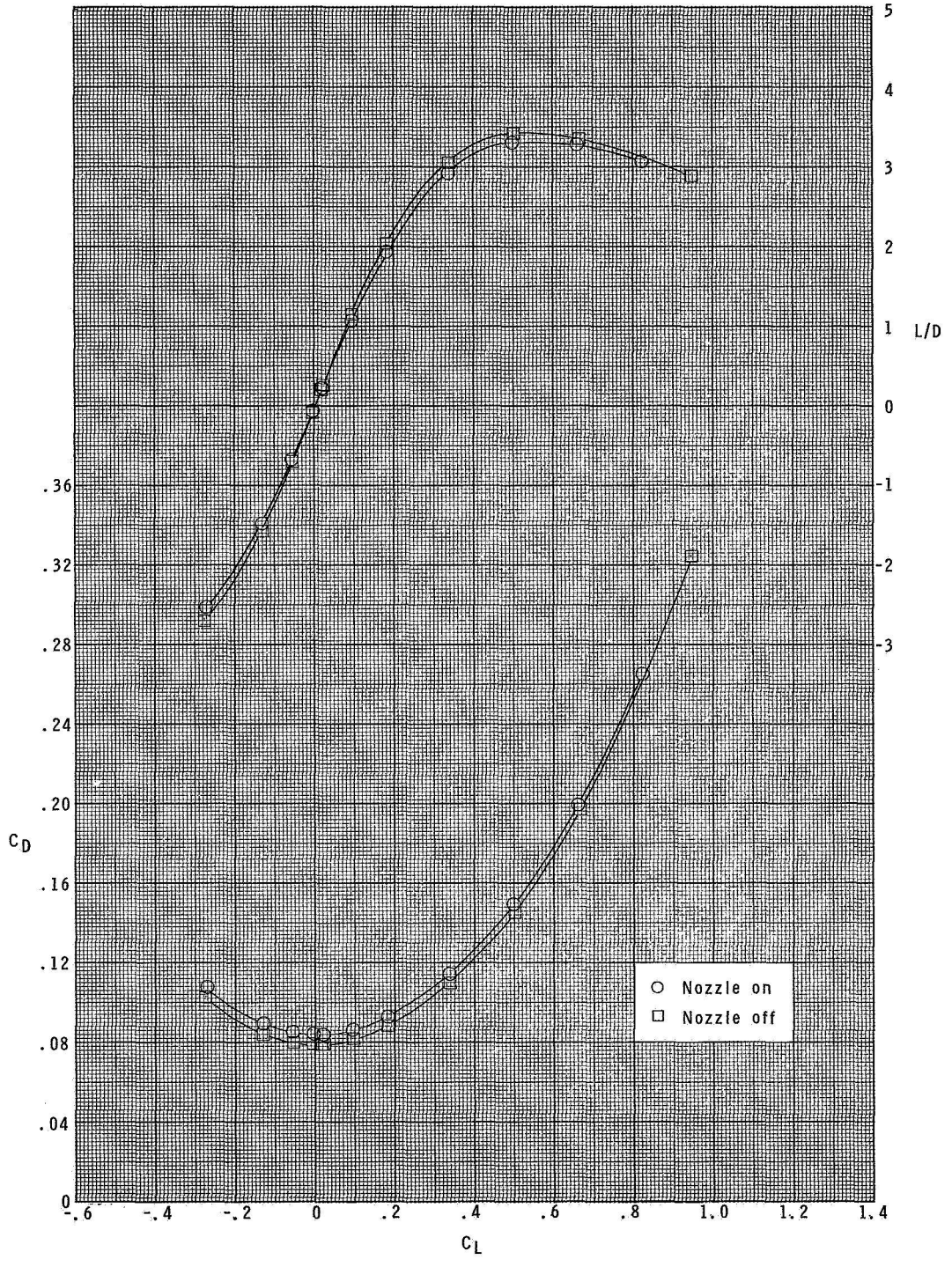
(f) Concluded.

Figure 7.- Concluded.



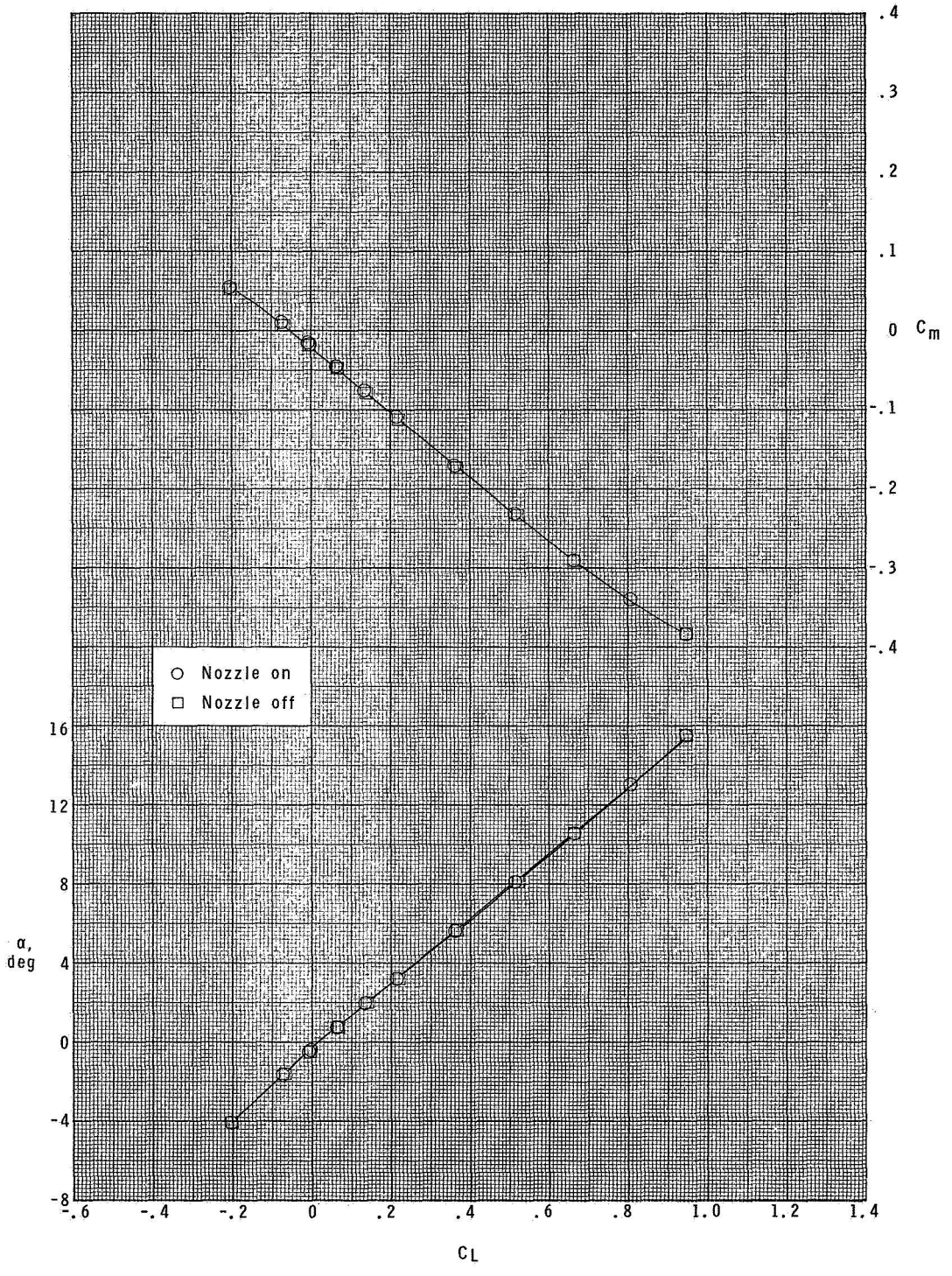
(a) M = 1.75.

Figure 8.- Effect of fuselage nozzle on longitudinal aerodynamic characteristics for $B_{11}X_{16}W_2H_9T_{12}V_{U5}Y_5N_{13}$.



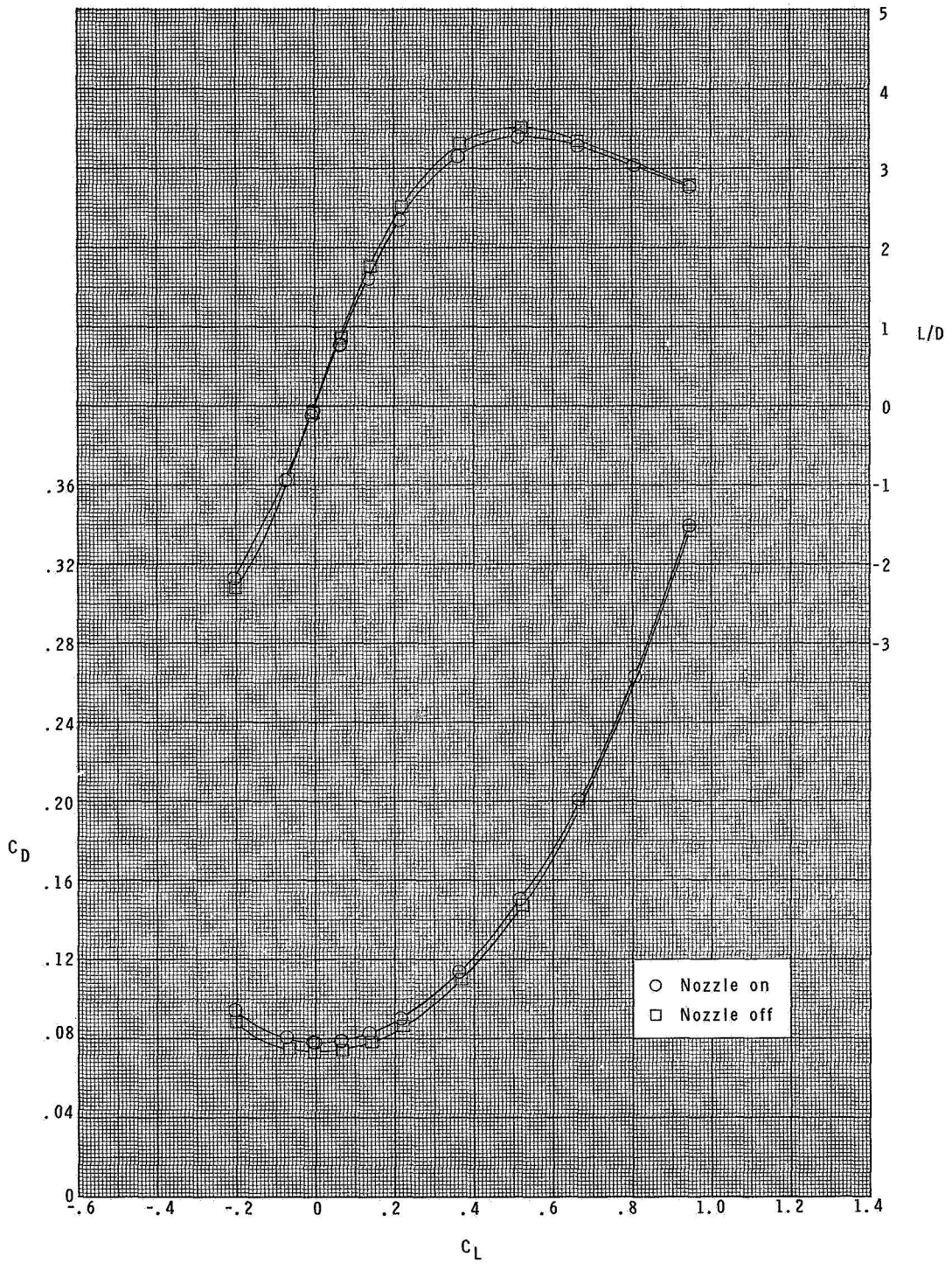
(a) Concluded.

Figure 8.- Continued.



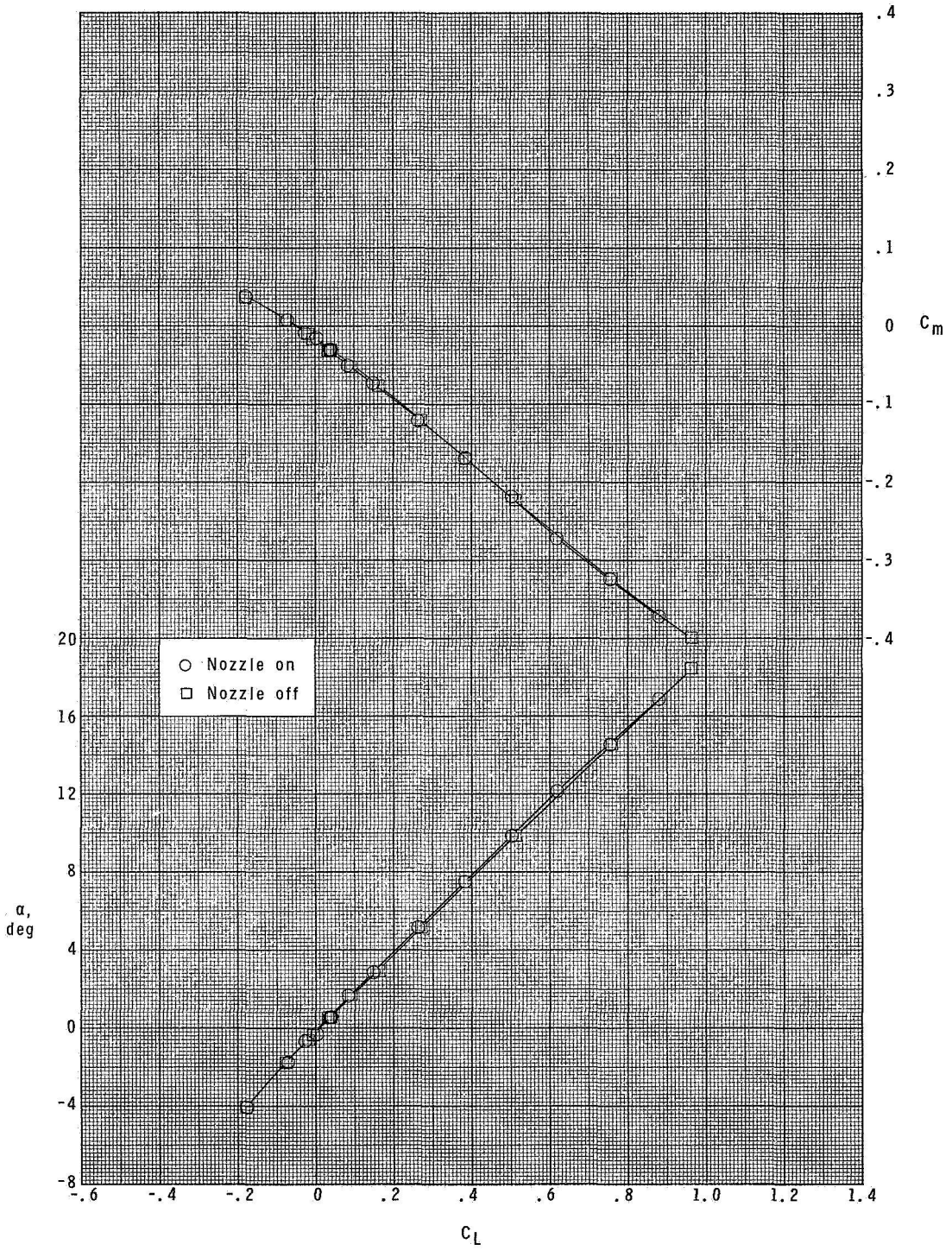
(b) M = 2.00.

Figure 8.- Continued.



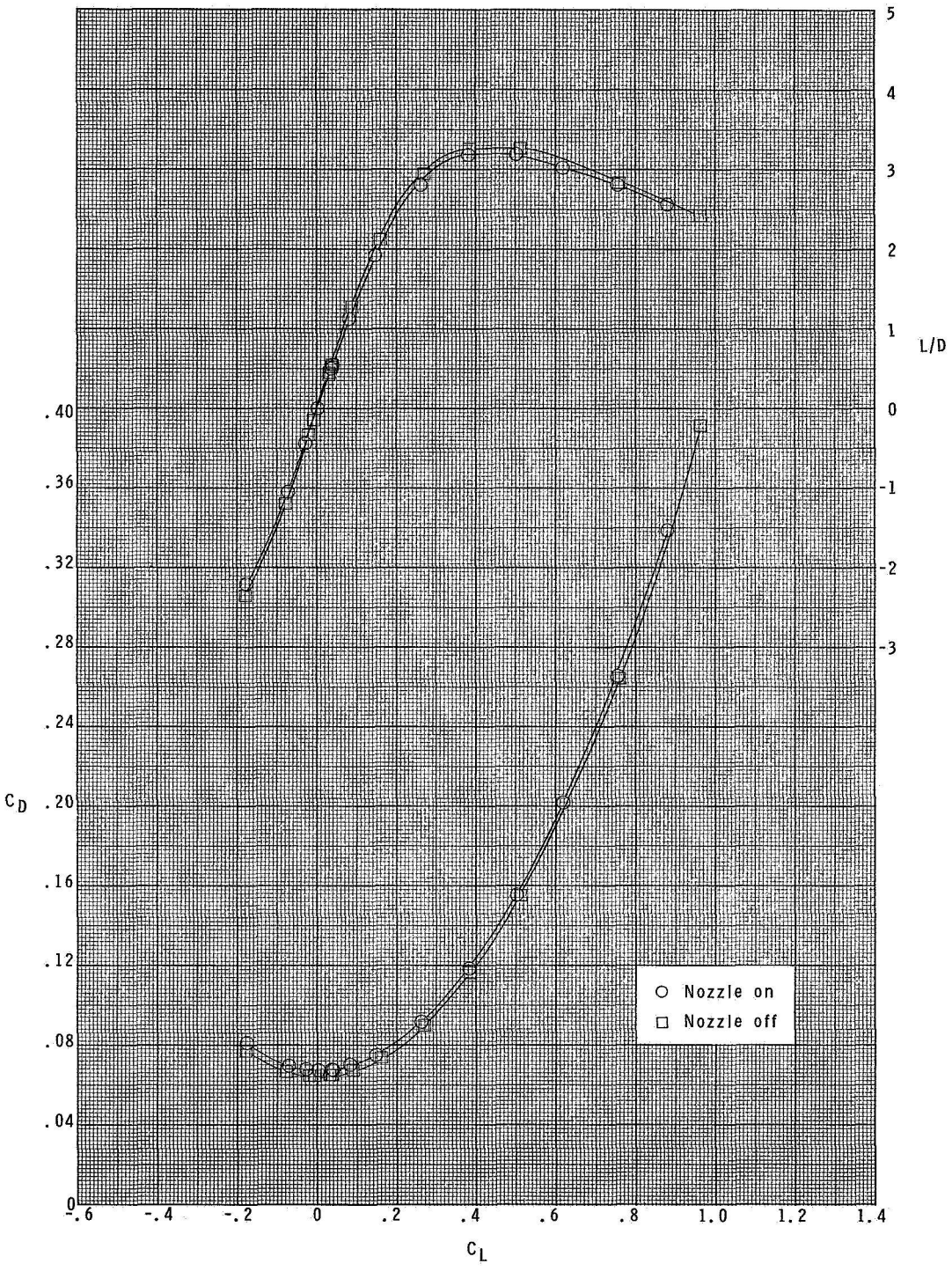
(b) Concluded.

Figure 8.- Continued.



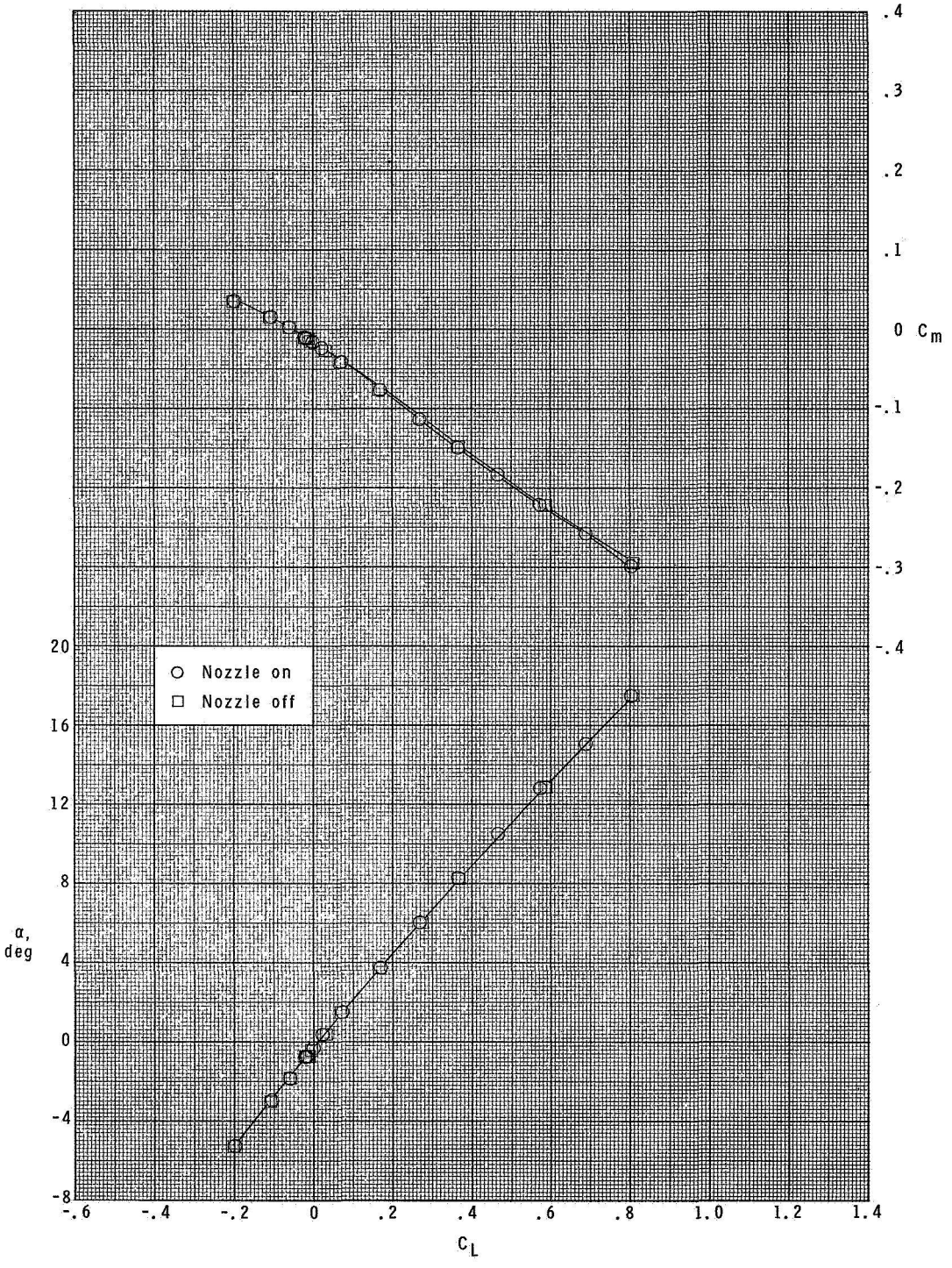
(c) M = 2.50.

Figure 8.- Continued.



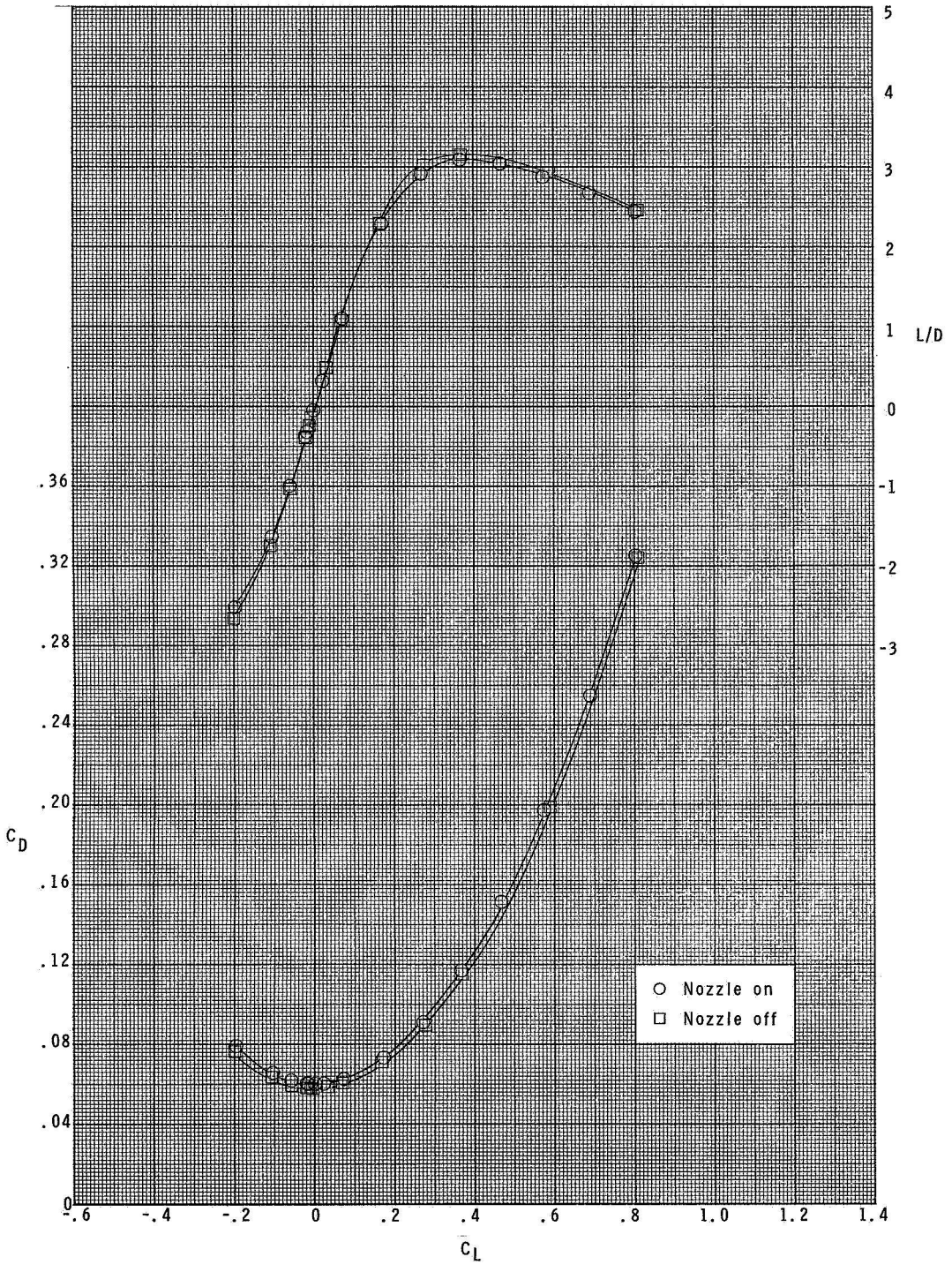
(c) Concluded.

Figure 8.- Continued.



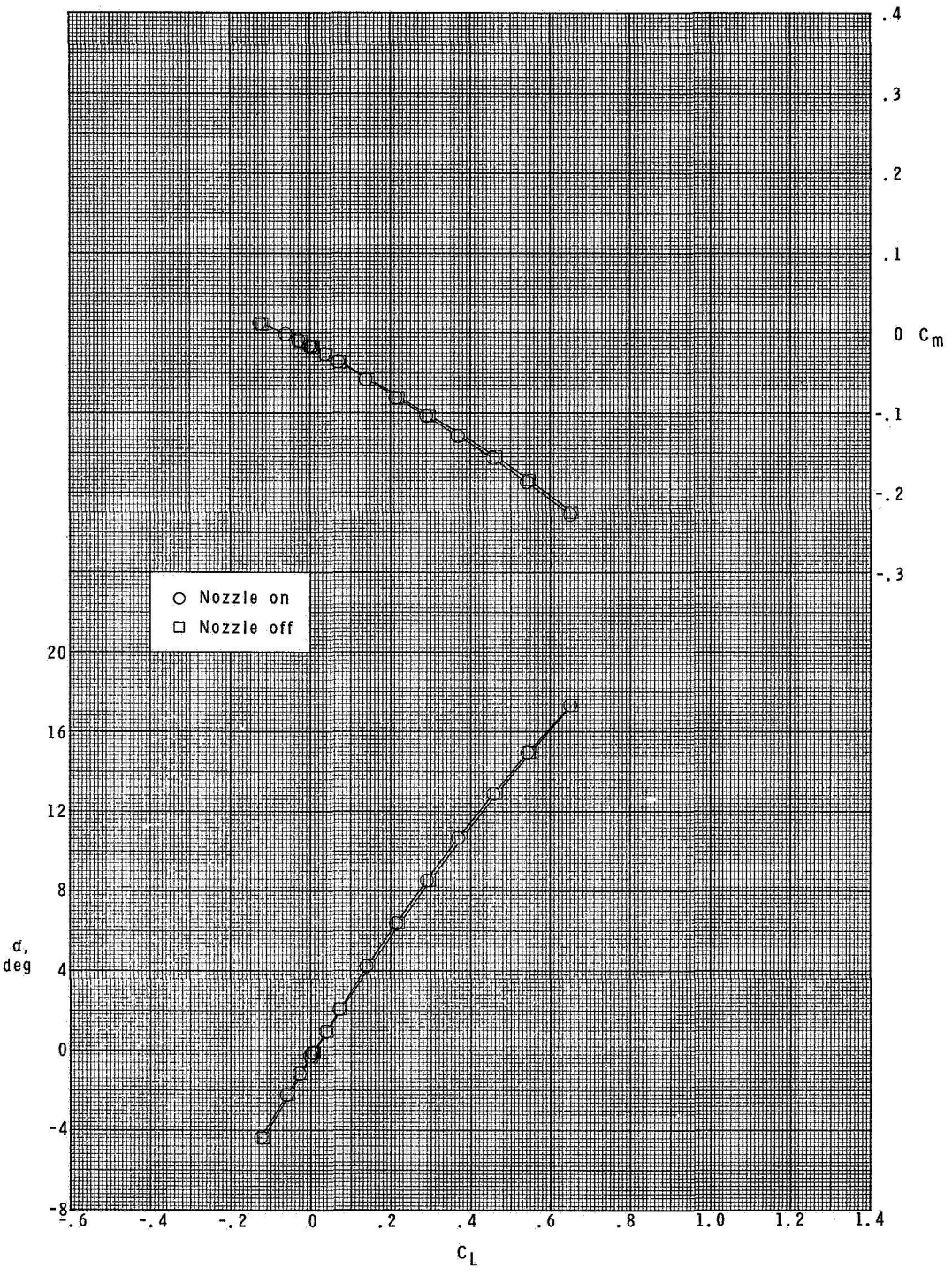
(d) M = 2.86.

Figure 8.- Continued.



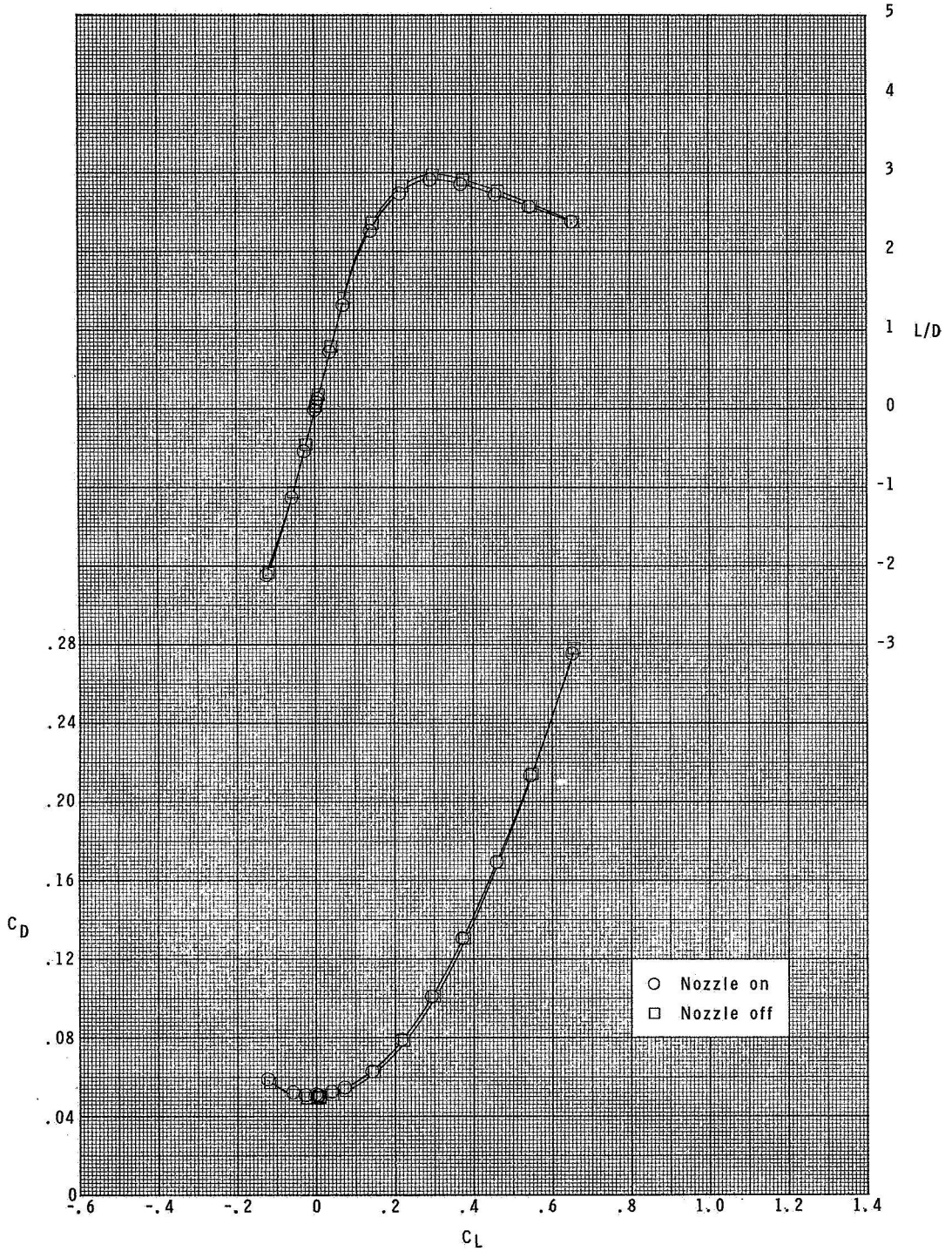
(d) Concluded.

Figure 8.- Continued.



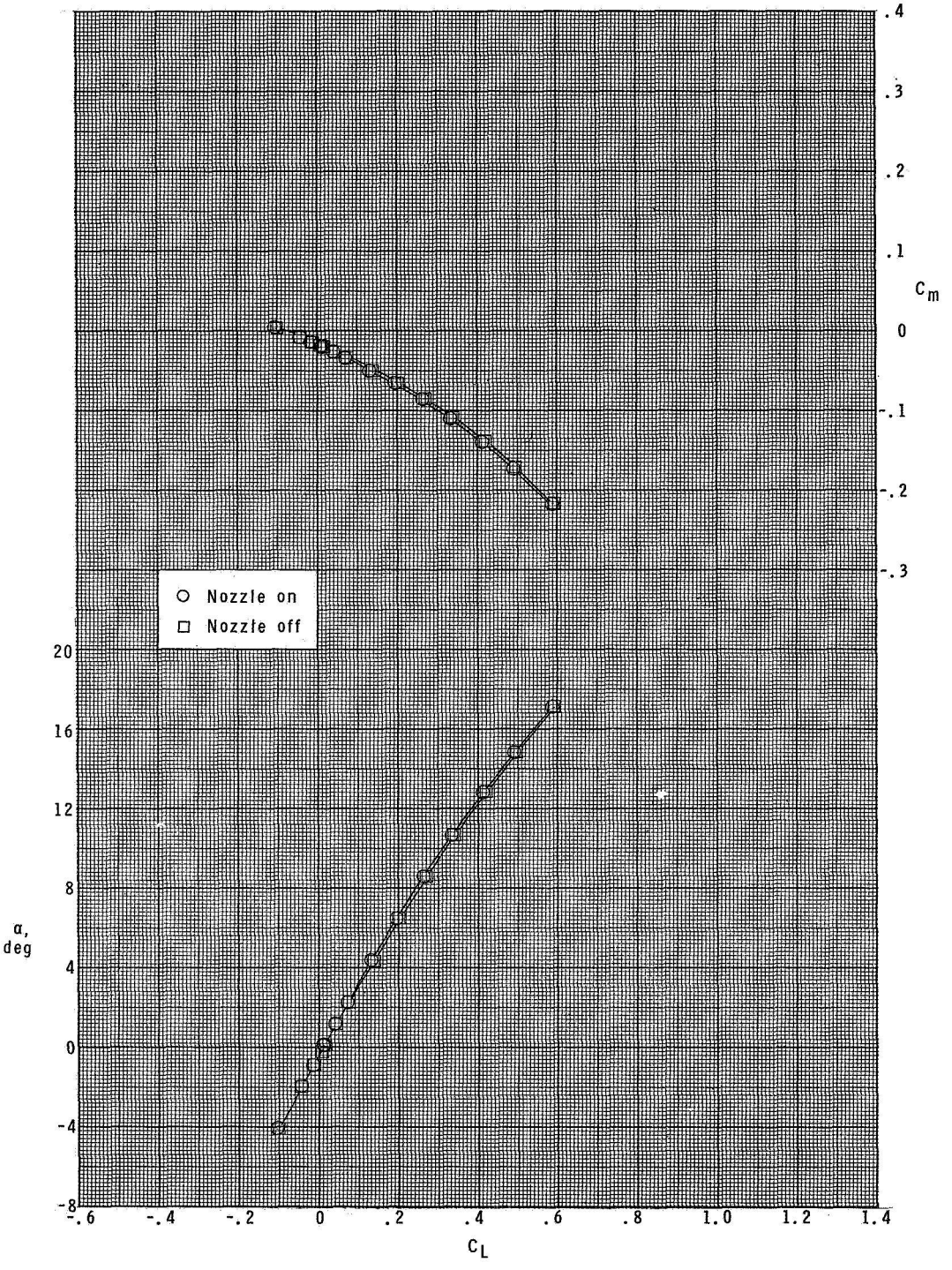
(e) M = 3.95.

Figure 8.- Continued.



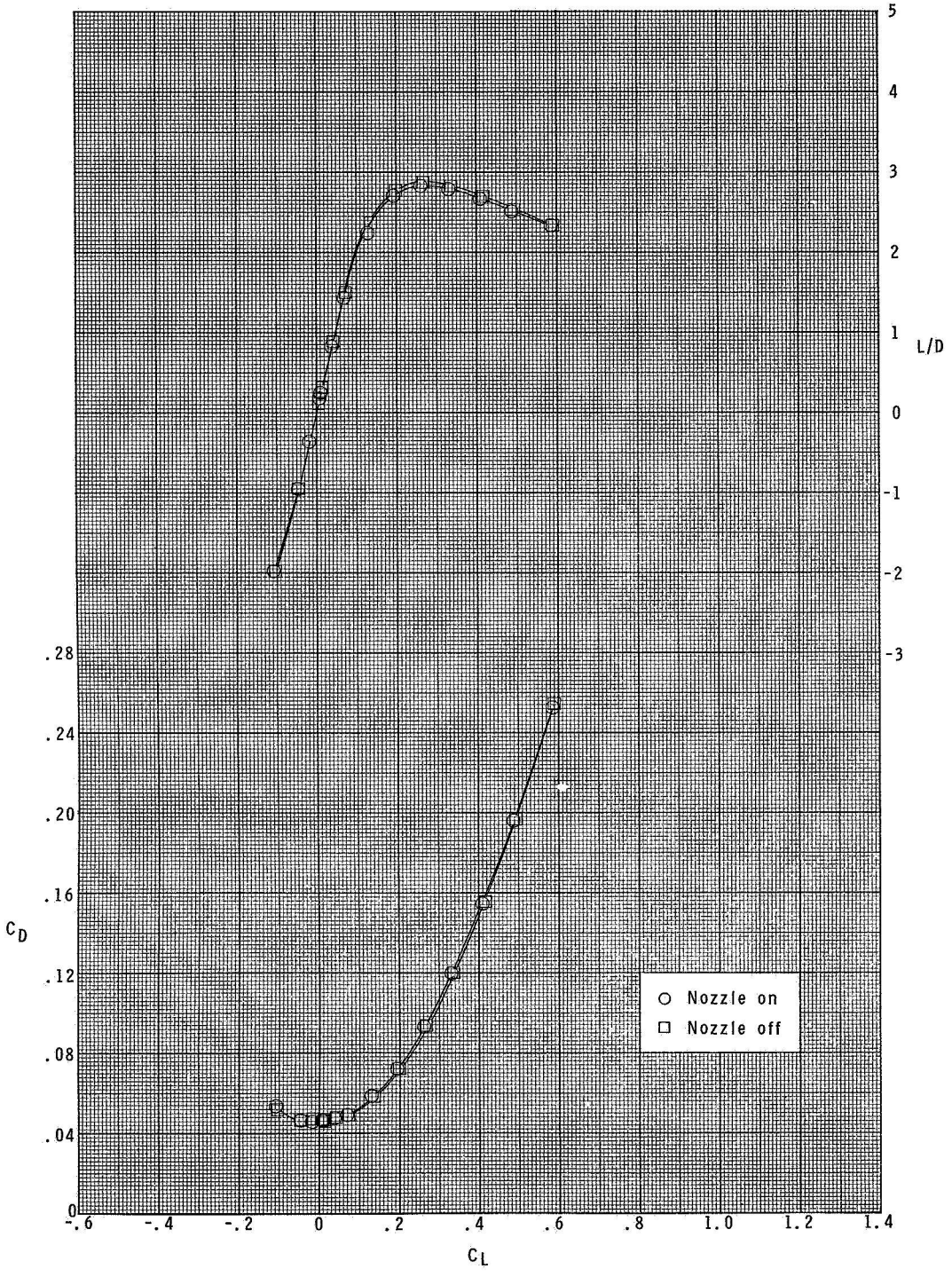
(e) Concluded.

Figure 8.- Continued.



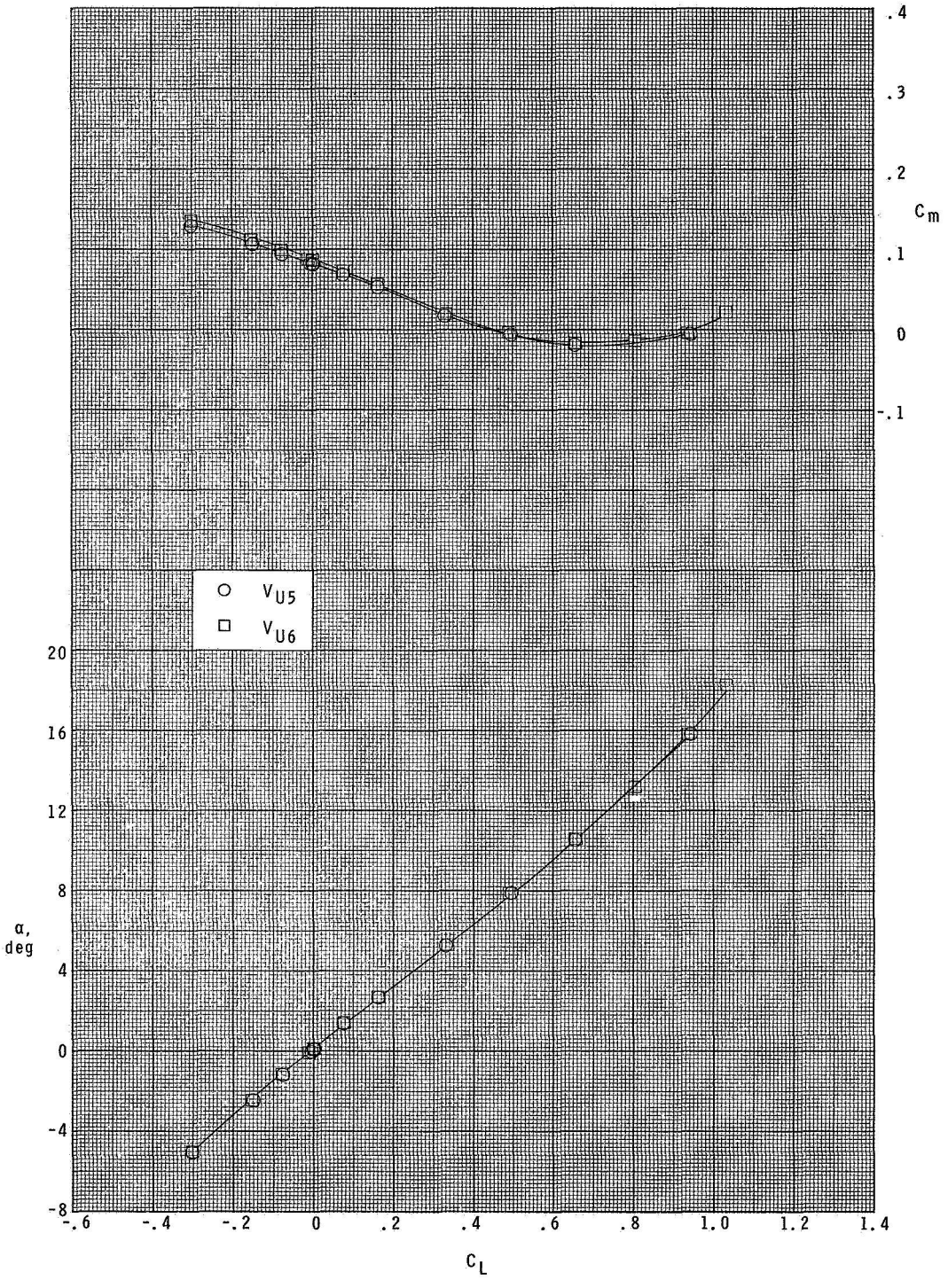
(f) M = 4.63.

Figure 8.- Continued.



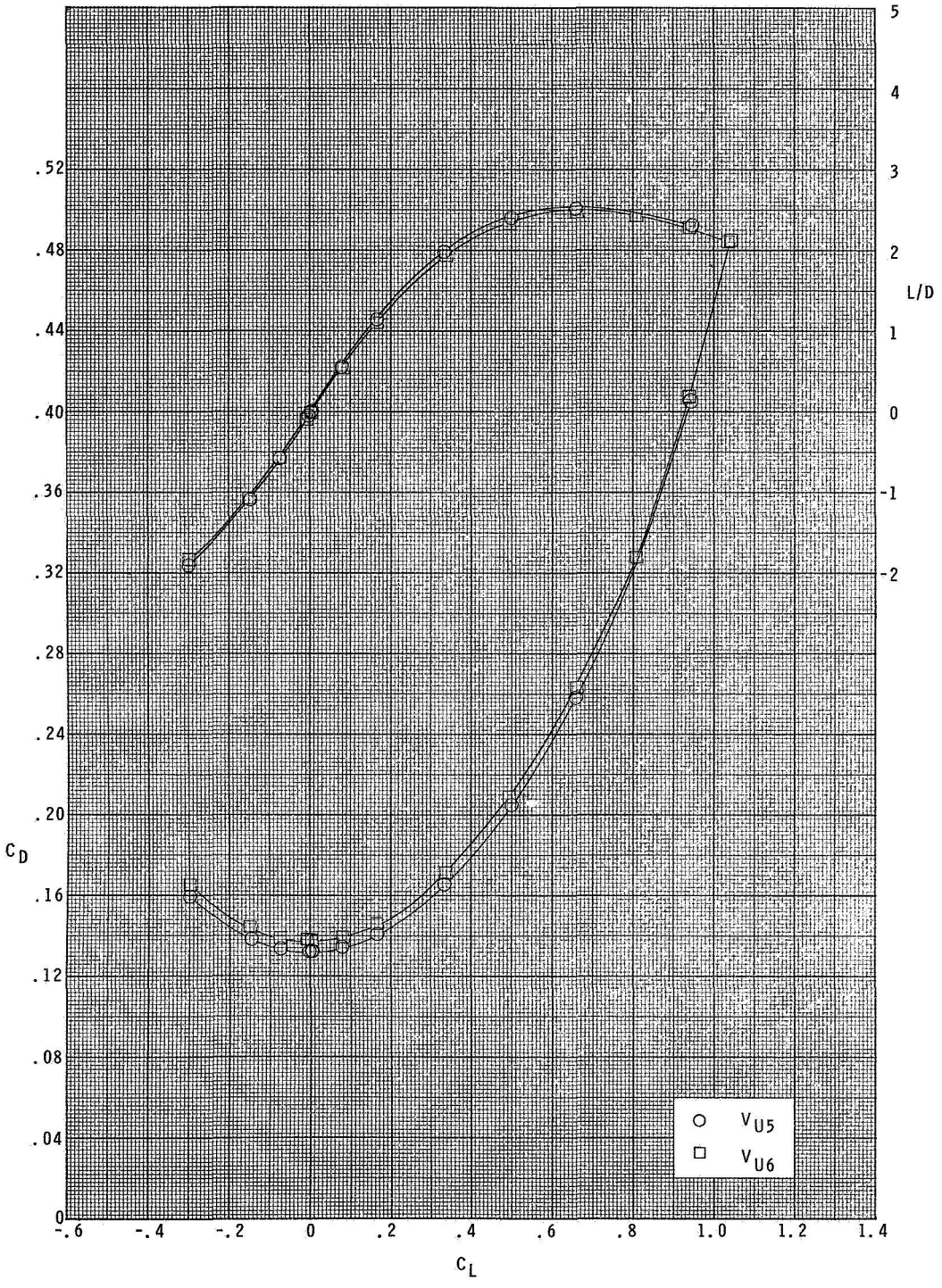
(f) Concluded.

Figure 8.- Concluded.



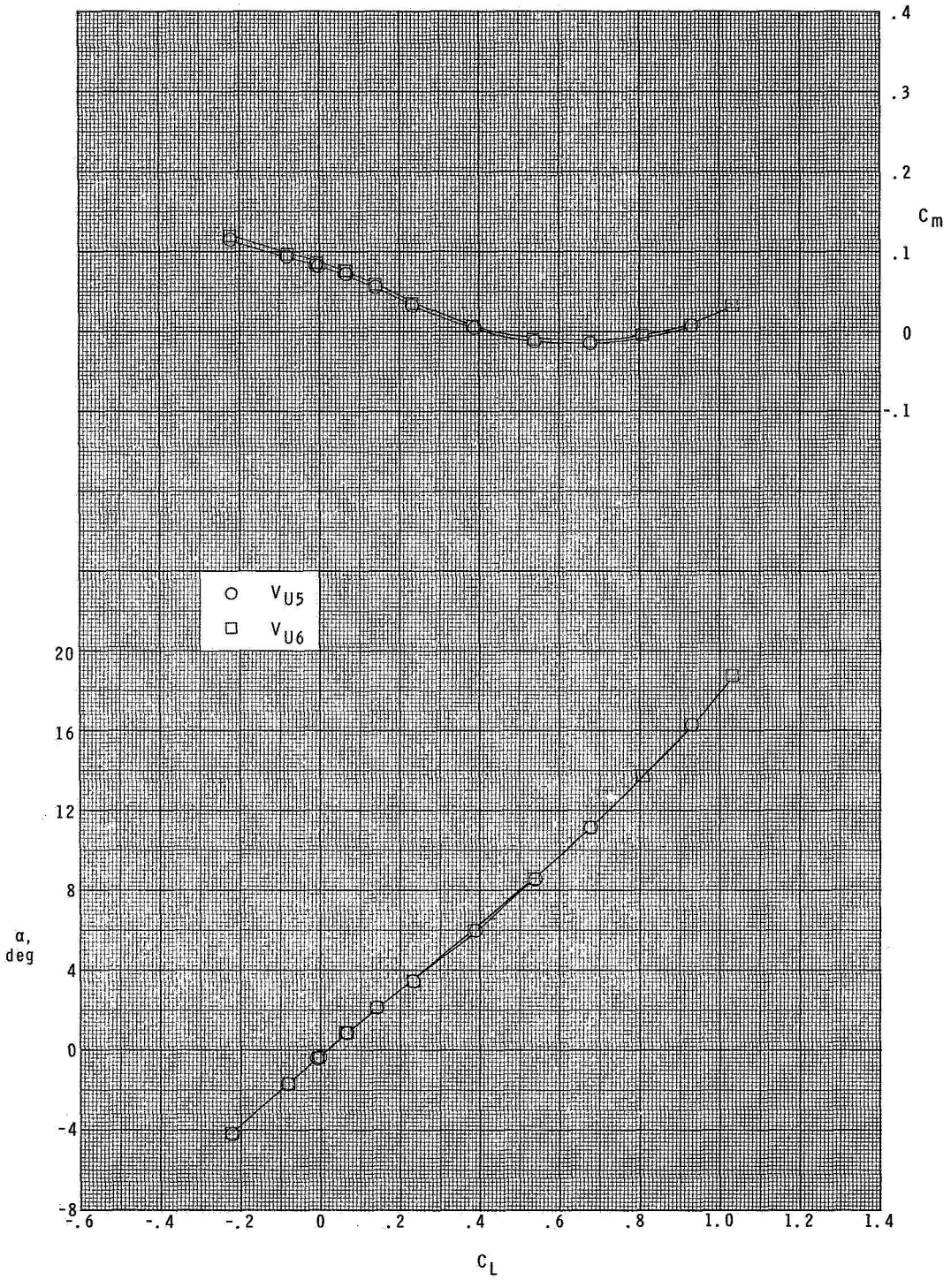
(a) M = 1.75.

Figure 9.- Effect of extended vertical tail on longitudinal aerodynamic characteristics for $B_{11}X_{16}W_2H_9T_{12}Y_5N_{13}T_{13}$ (HRE and tanks on).



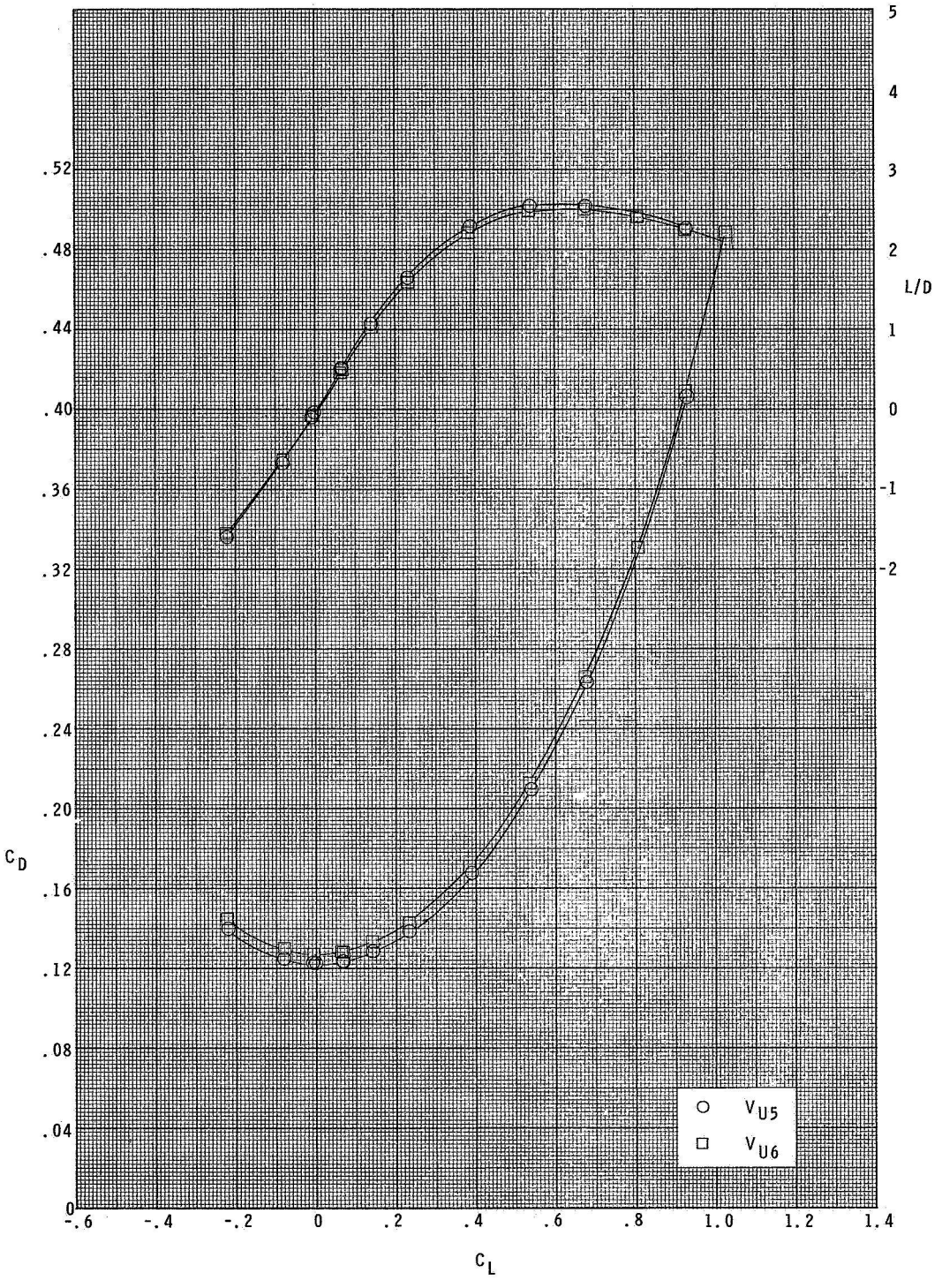
(a) Concluded.

Figure 9.- Continued.



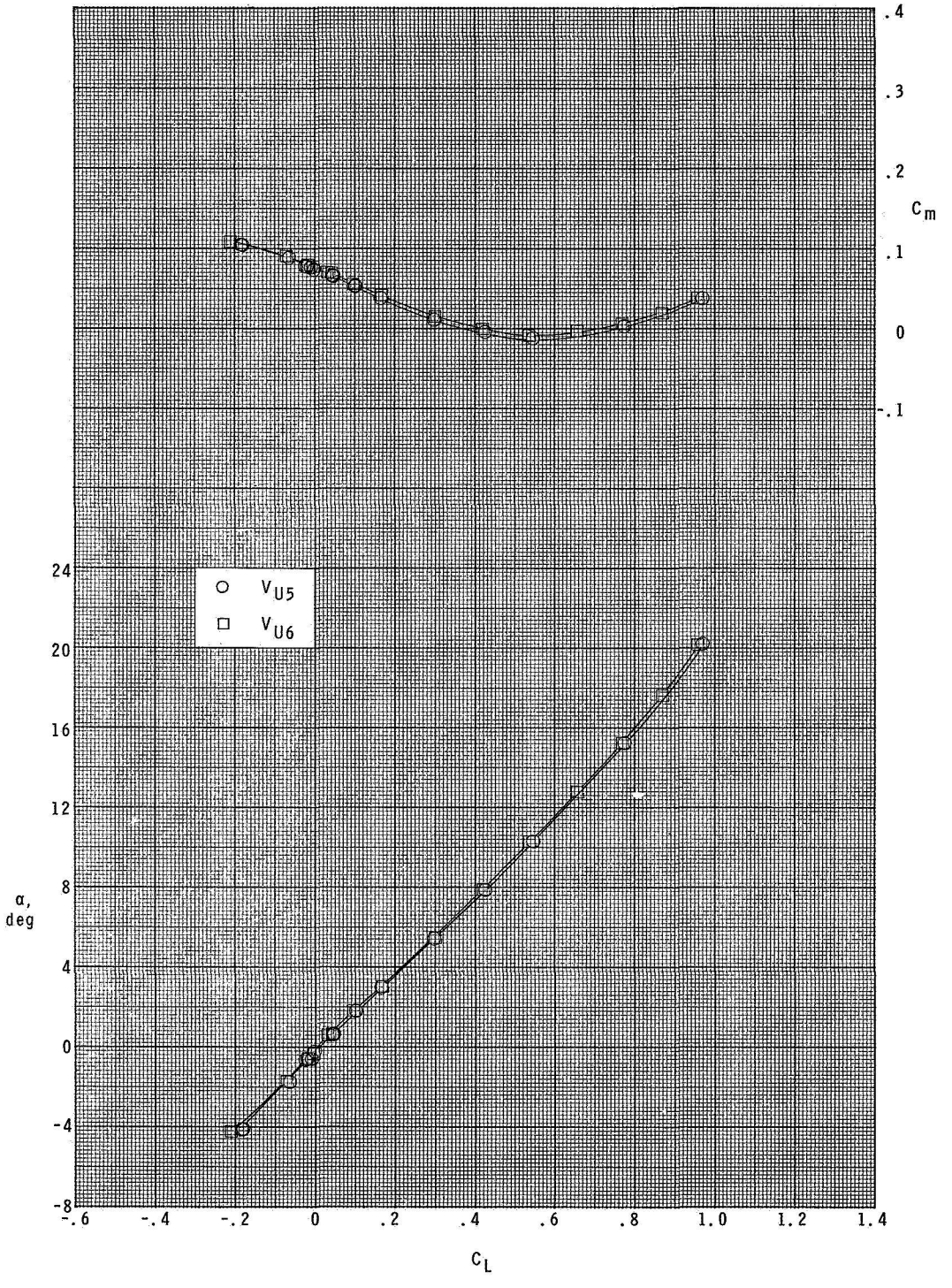
(b) M = 2.00.

Figure 9.- Continued.



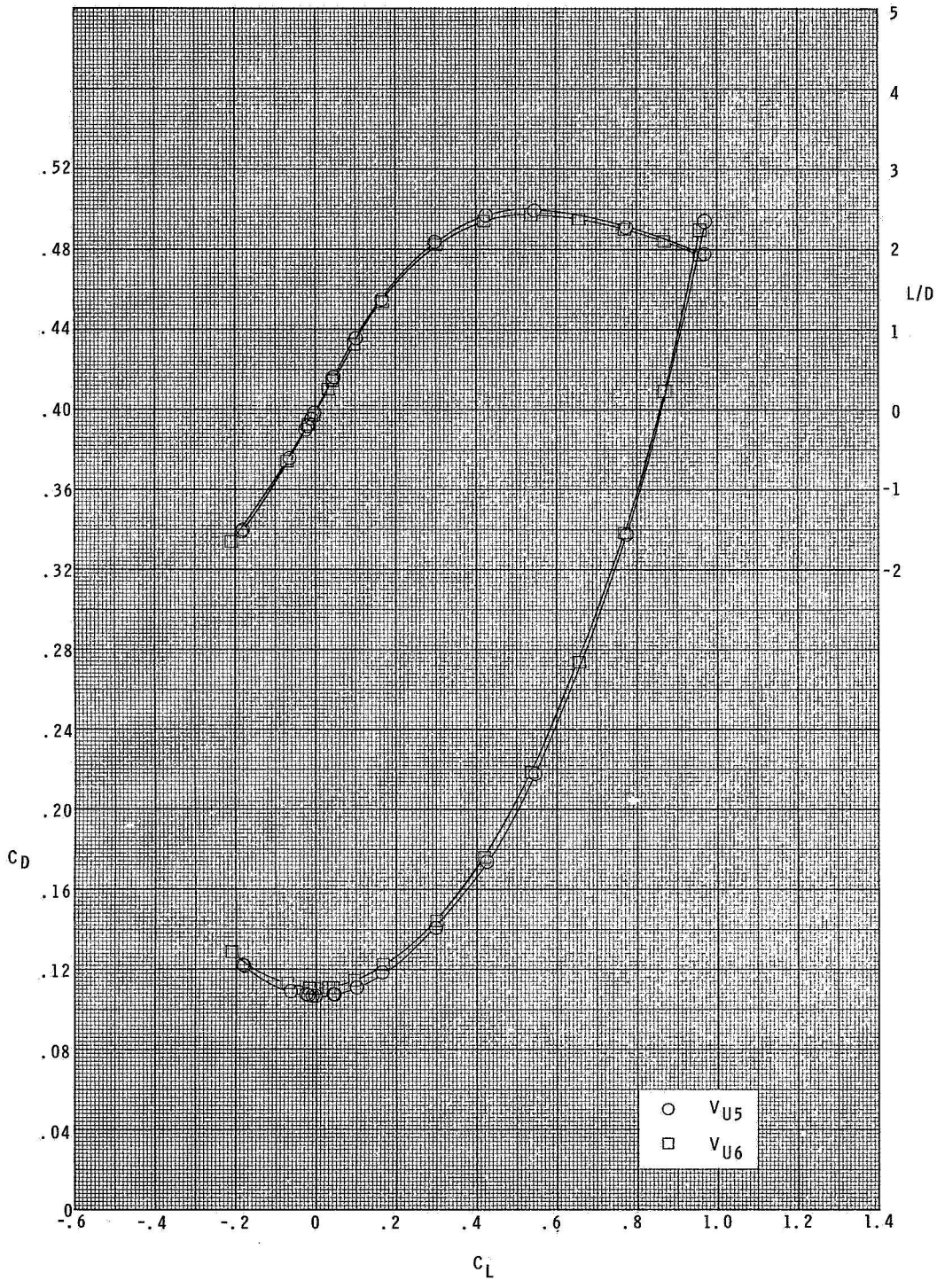
(b) Concluded.

Figure 9.- Continued.



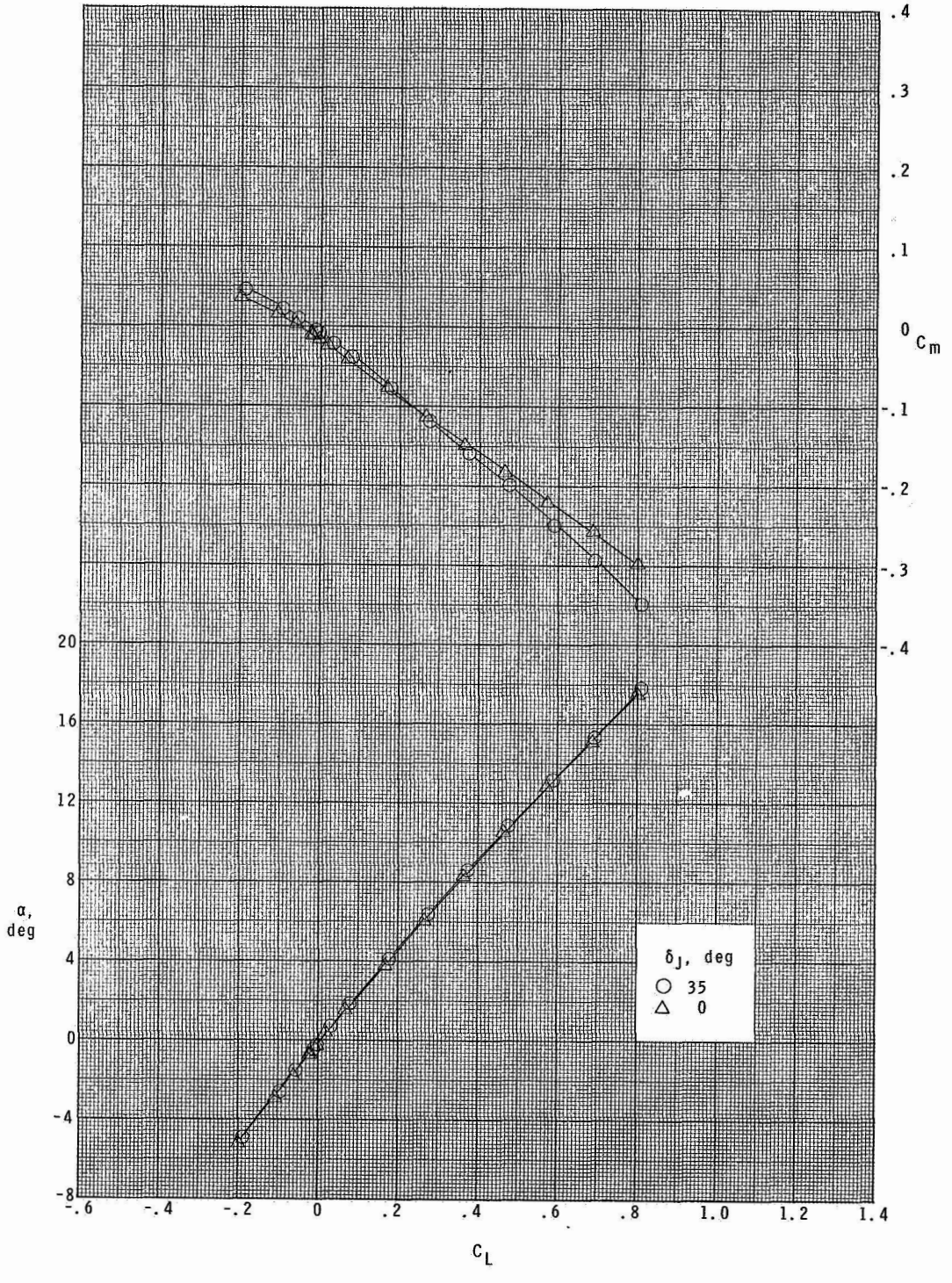
(c) M = 2.50.

Figure 9.- Continued.



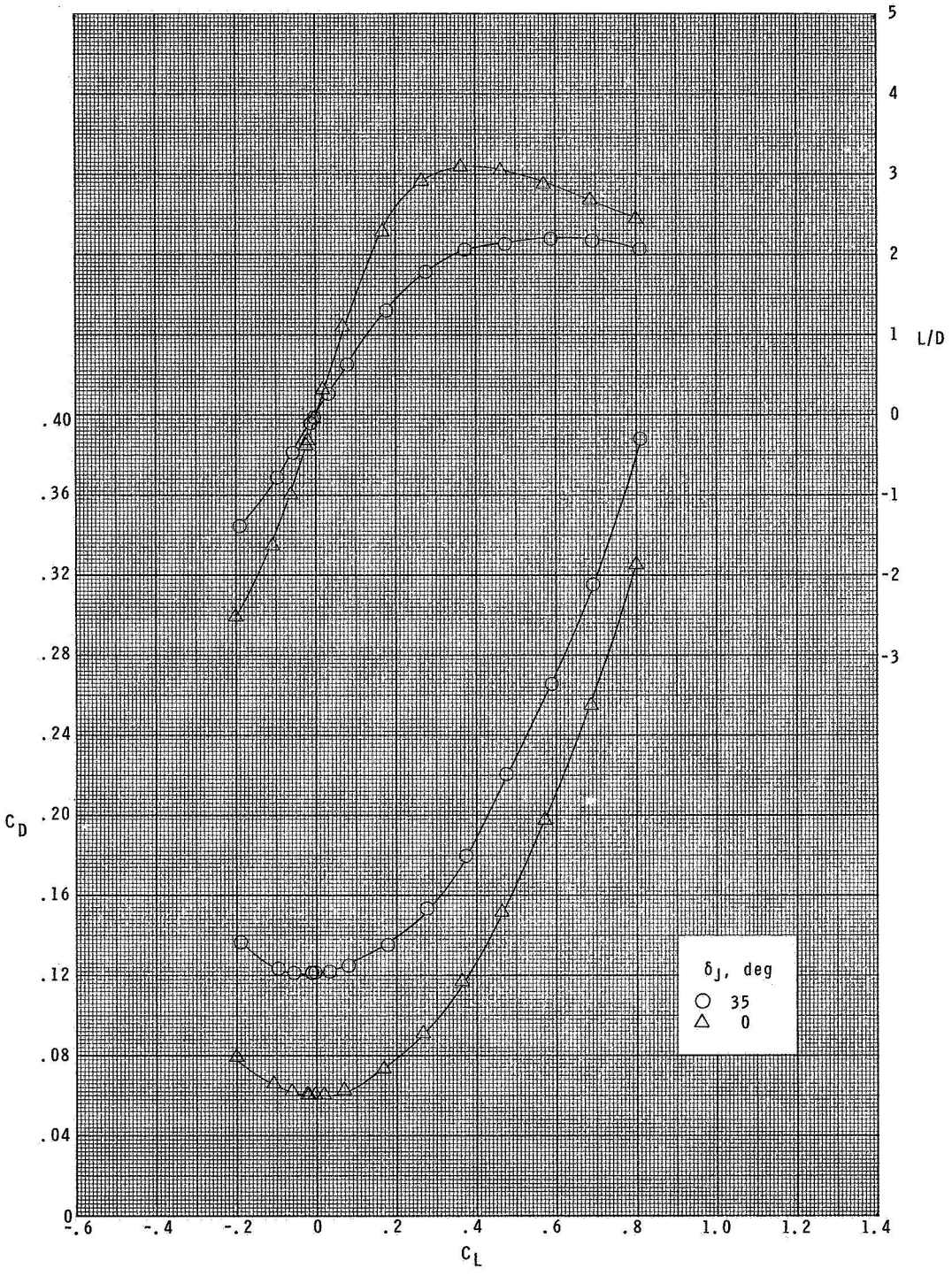
(c) Concluded.

Figure 9.- Concluded.



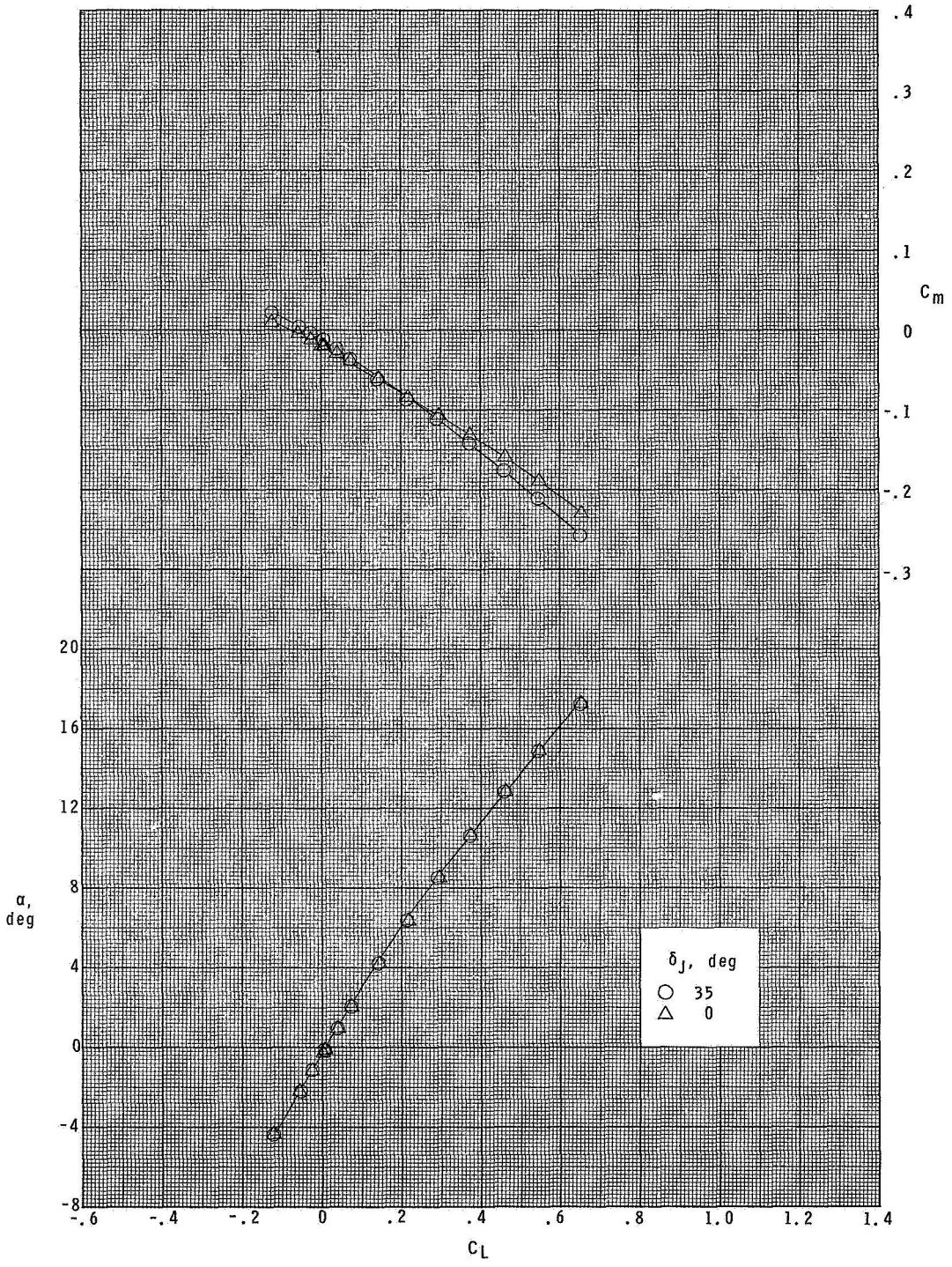
(a) M = 2.86.

Figure 10.- Effect of speed-brake deflection on longitudinal control for $B_{11}X_{16}W_2H_9T_{12}V_{U5}Y_5N_{13}$ (HRE on) with $\delta_h = 0^0$.



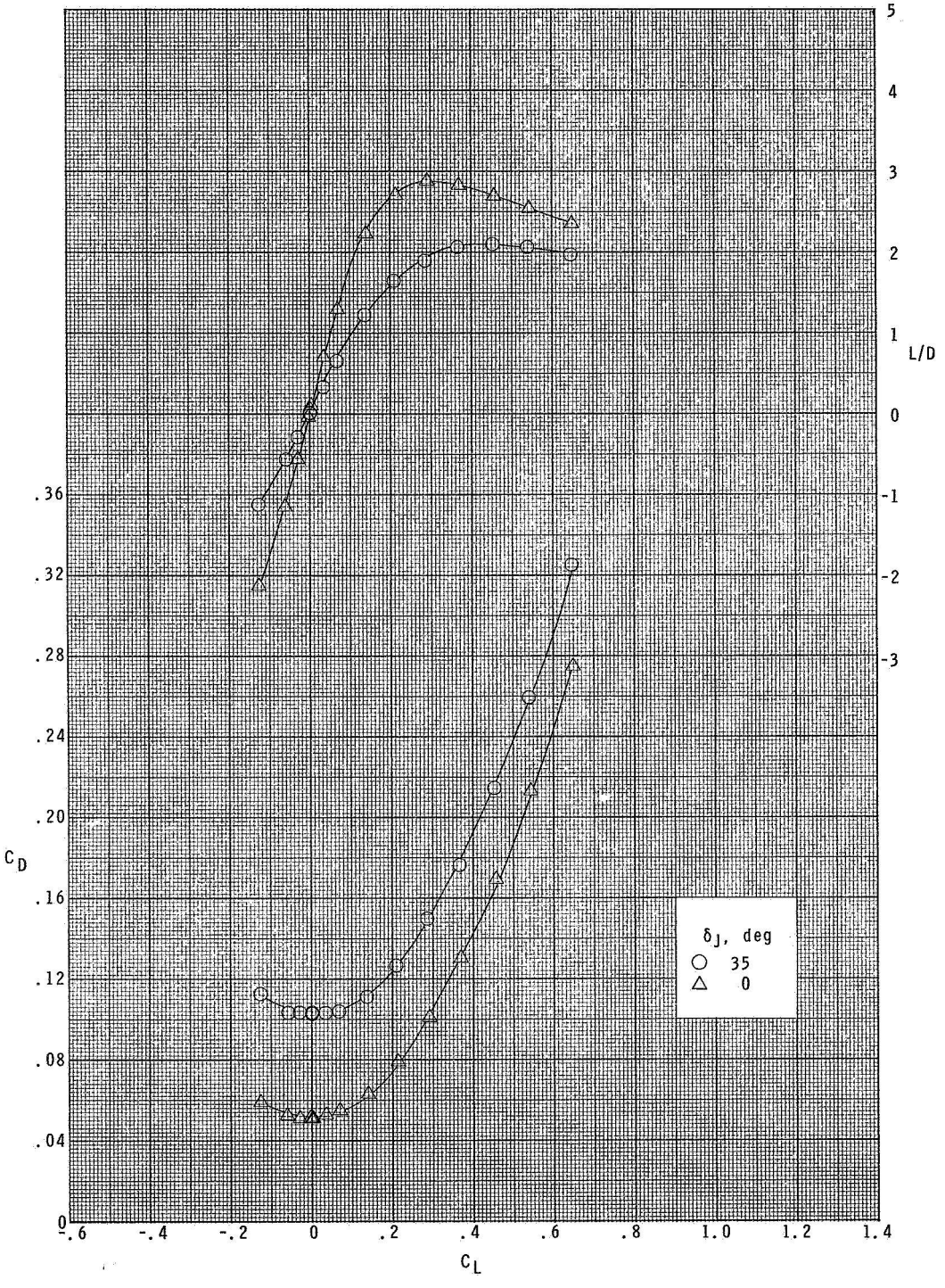
(a) Concluded.

Figure 10.- Continued.



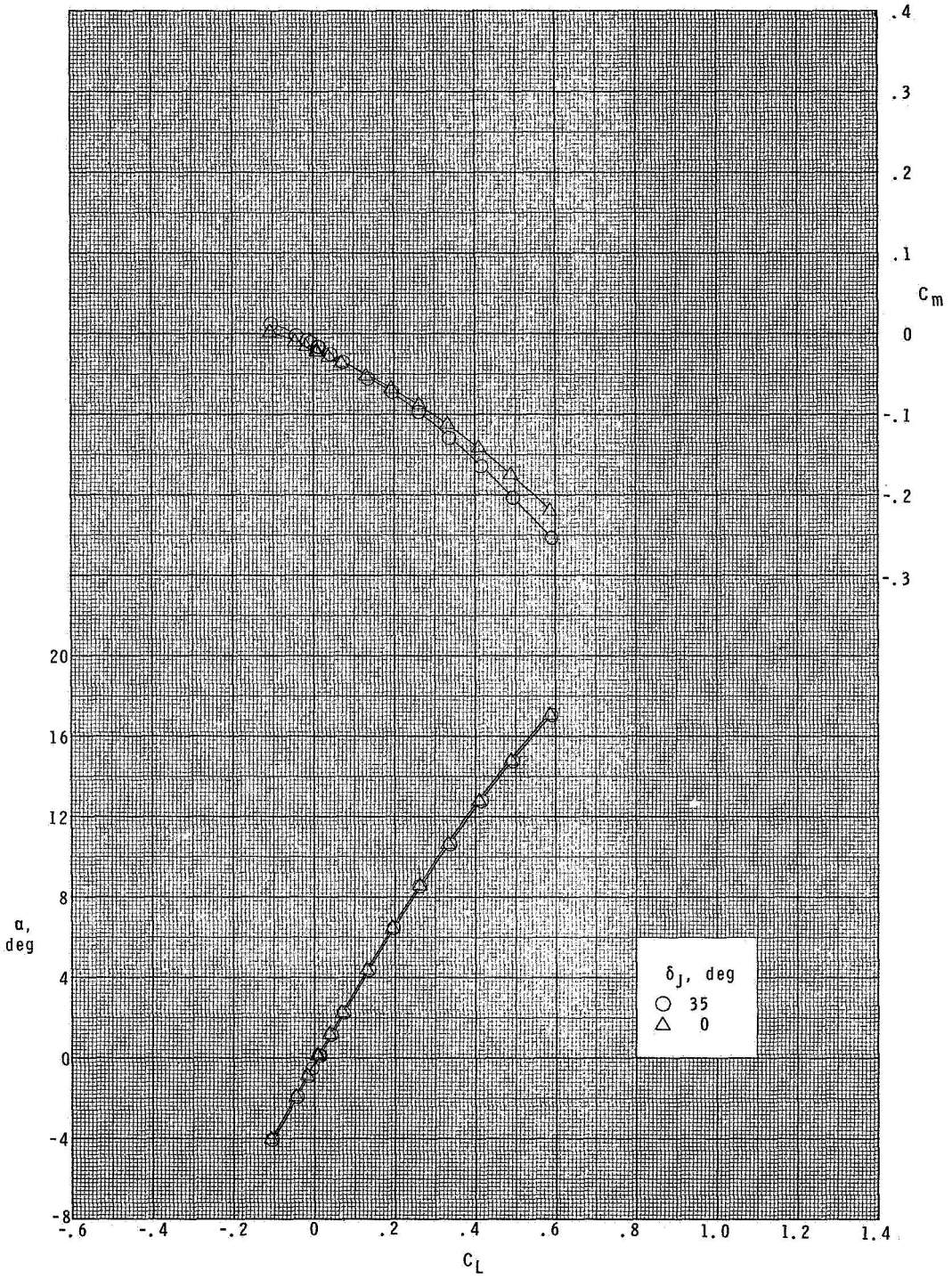
(b) M = 3.95.

Figure 10.- Continued.



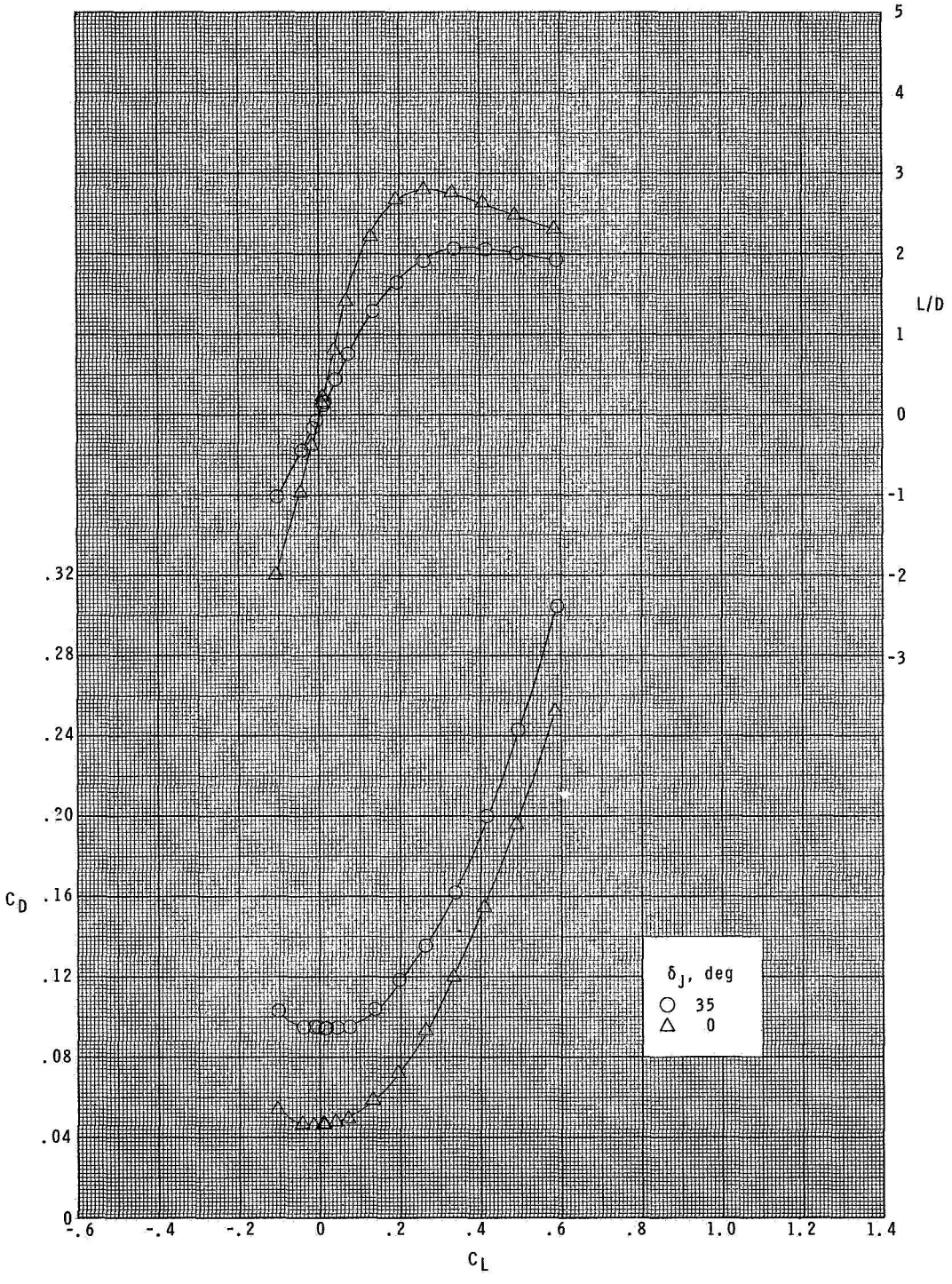
(b) Concluded.

Figure 10.- Continued.



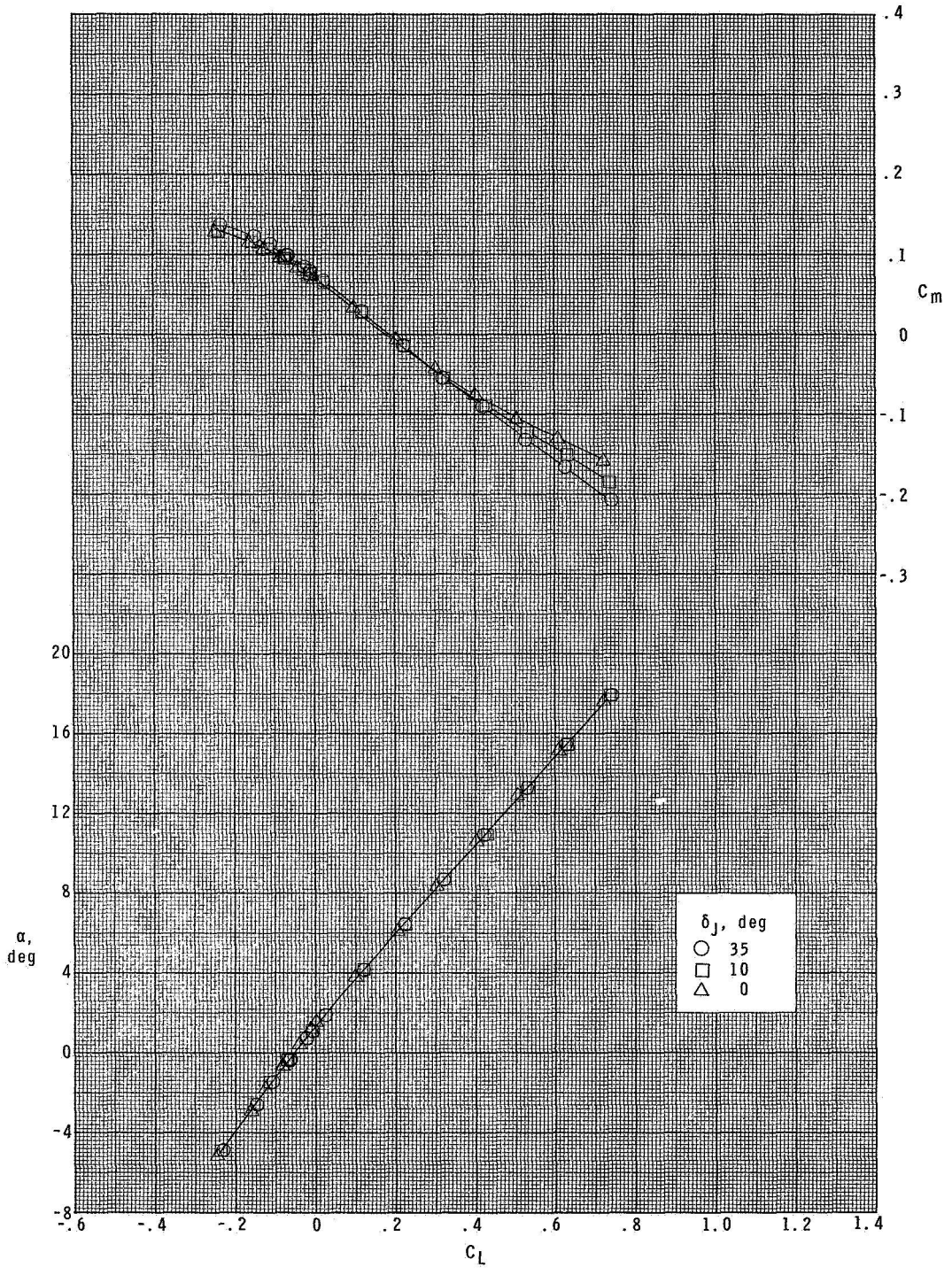
(c) M = 4.63.

Figure 10.- Continued.



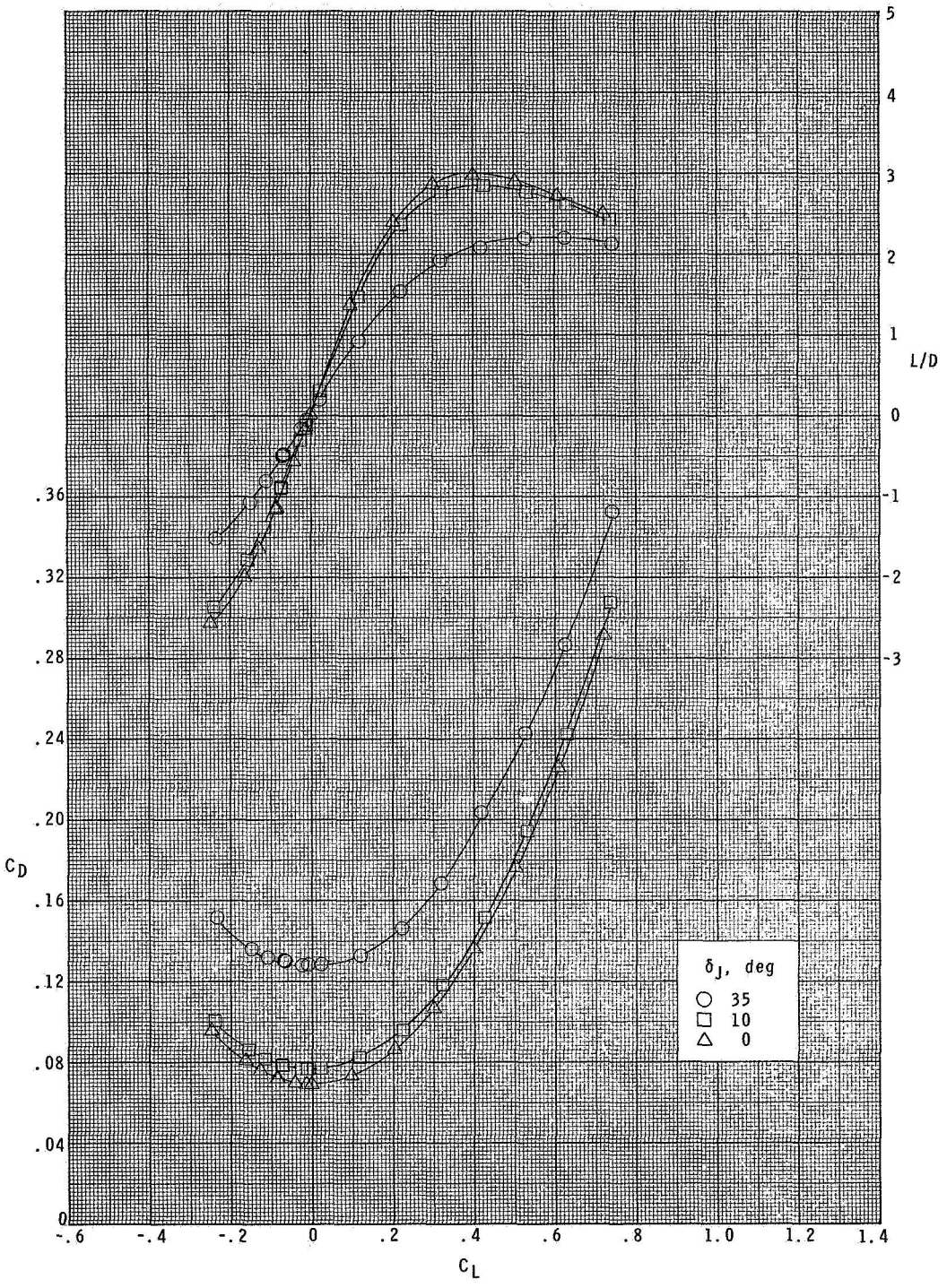
(c) Concluded.

Figure 10.- Concluded.



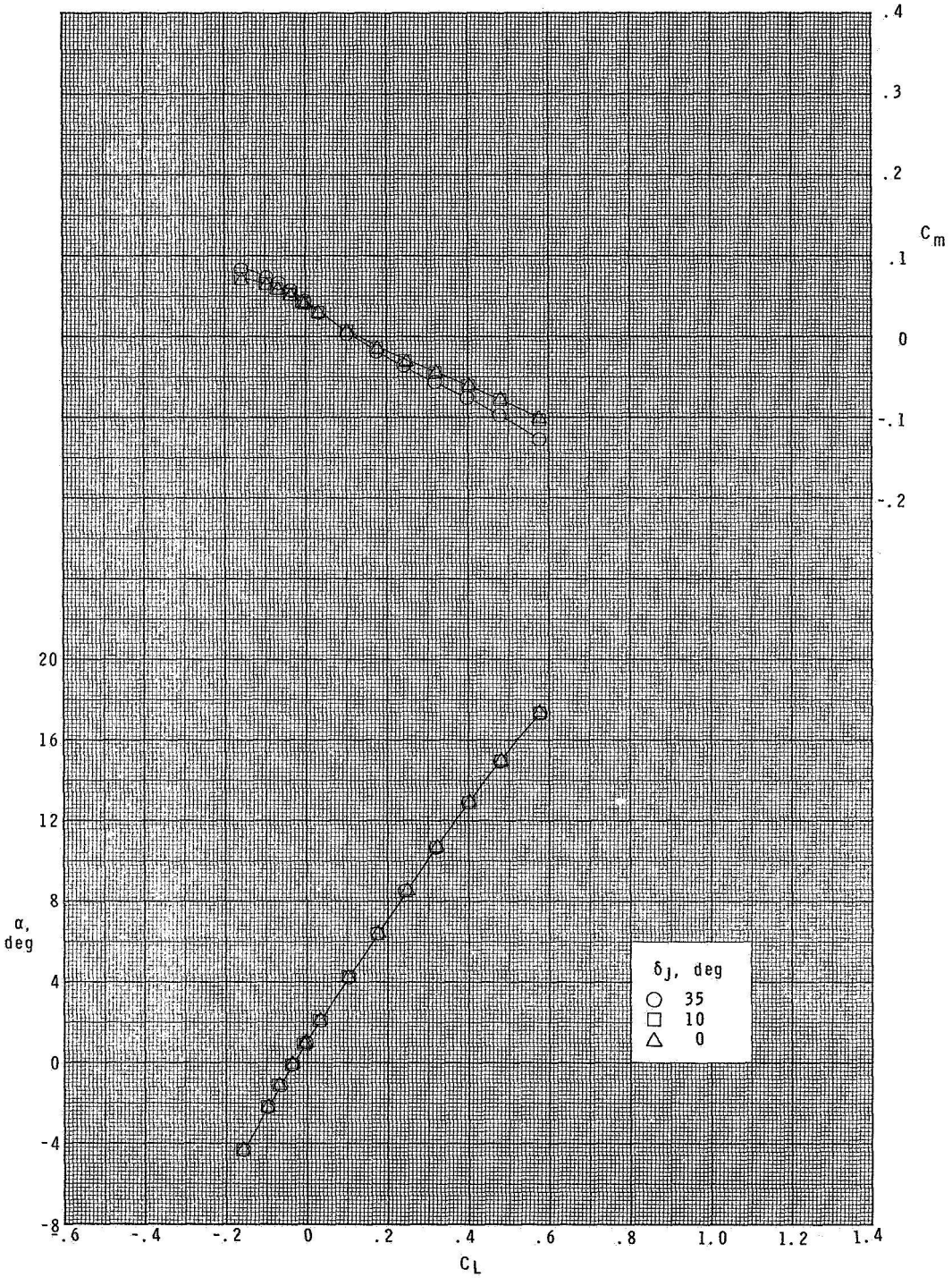
(a) M = 2.86.

Figure 11.- Effect of speed-brake deflection on longitudinal control for $B_{11}X_{16}W_2H_9T_{12}V_{U5}Y_5N_{13}$ (HRE on) with $\delta_h = -10^0$.



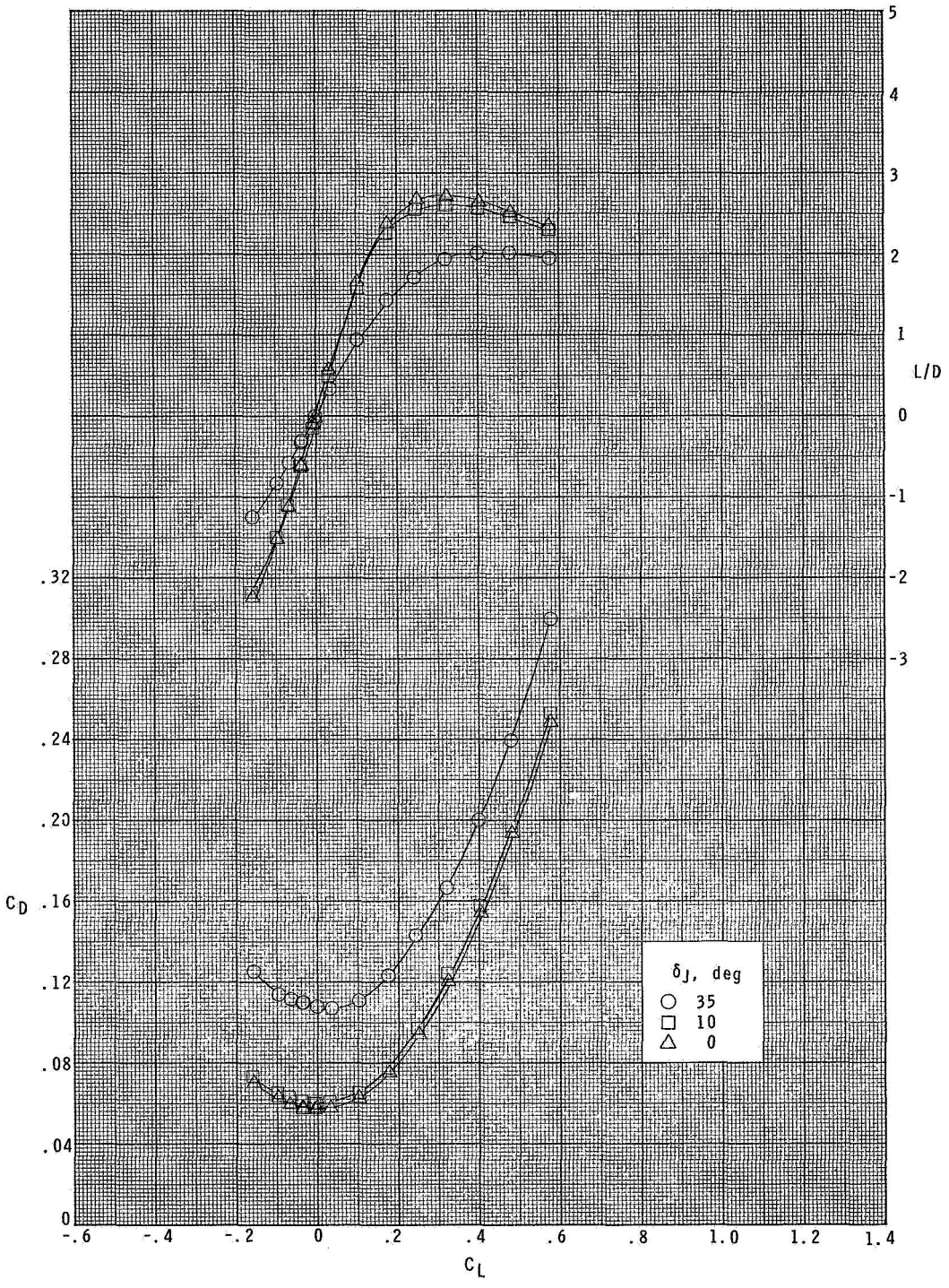
(a) Concluded.

Figure 11.- Continued.



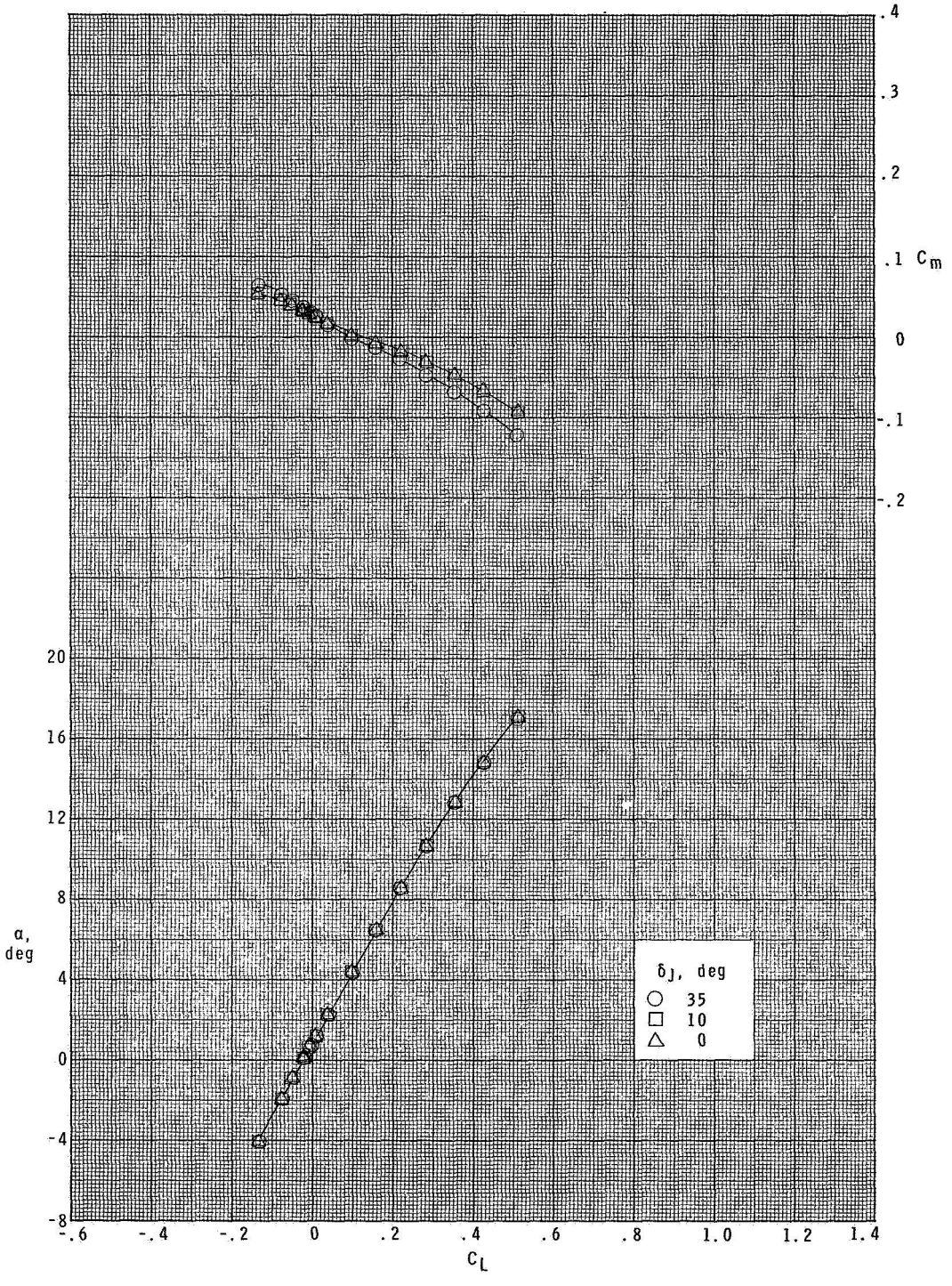
(b) M = 3.95.

Figure 11.- Continued.



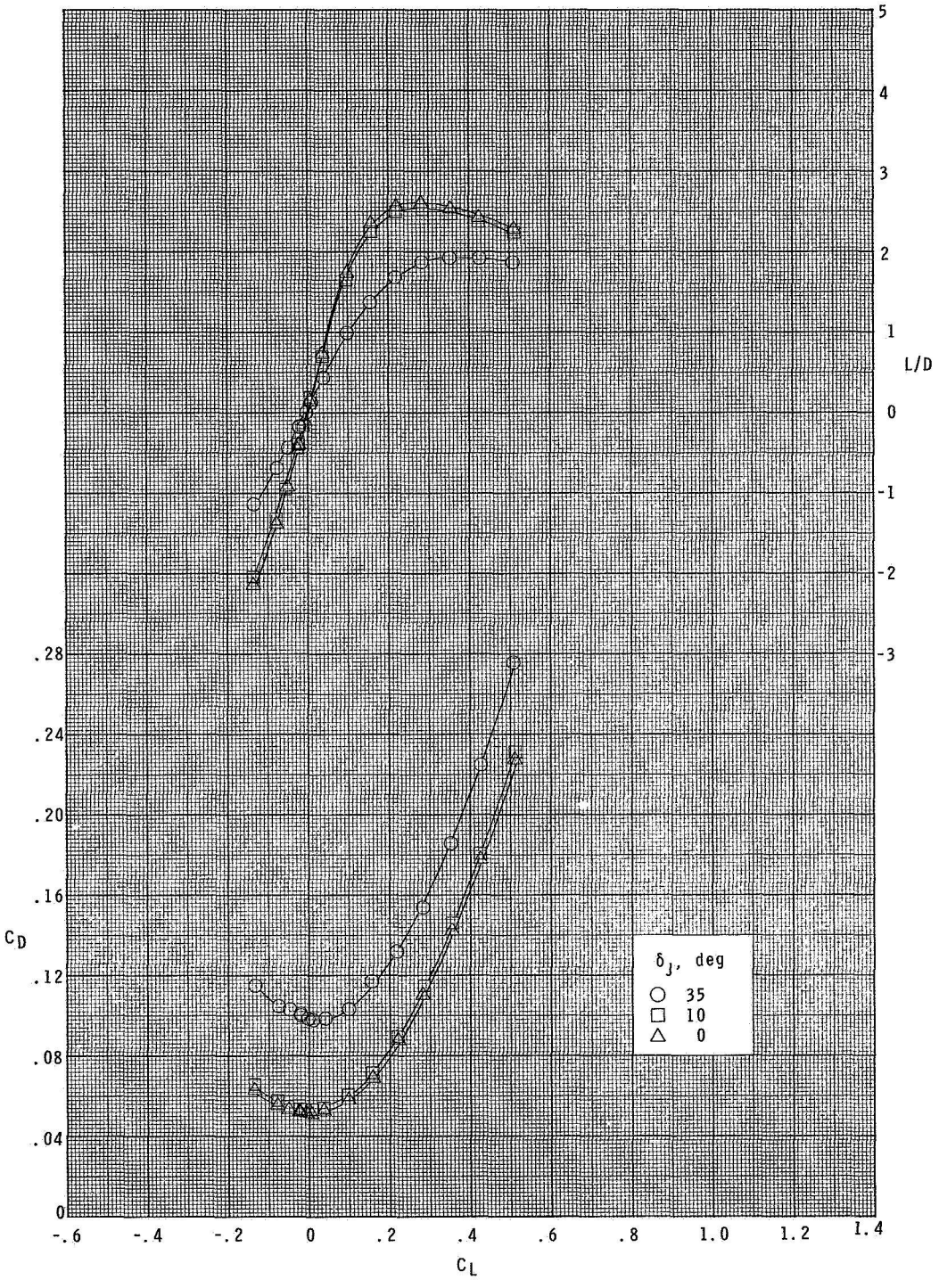
(b) Concluded.

Figure 11.- Continued.



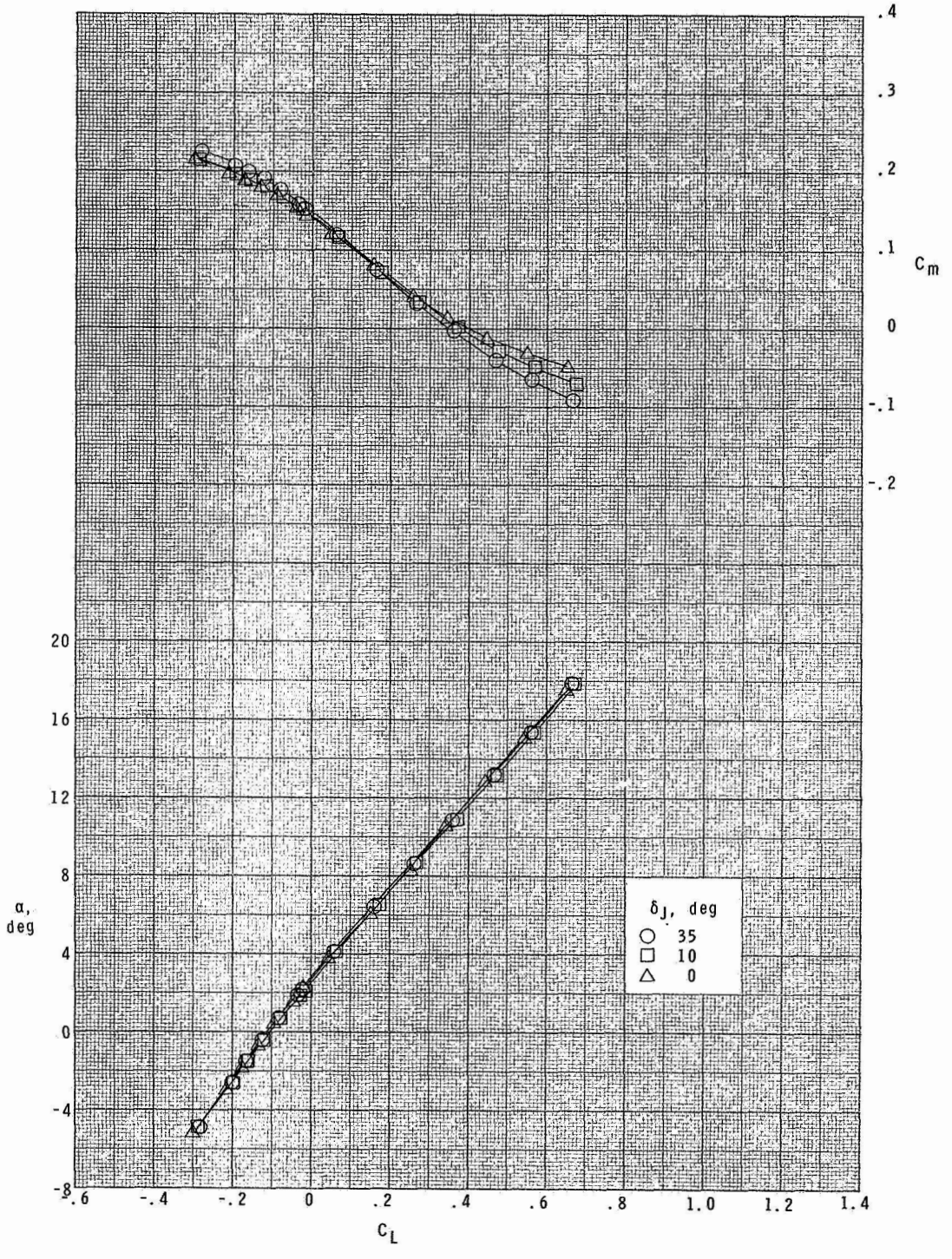
(c) M = 4.63.

Figure 11.- Continued.



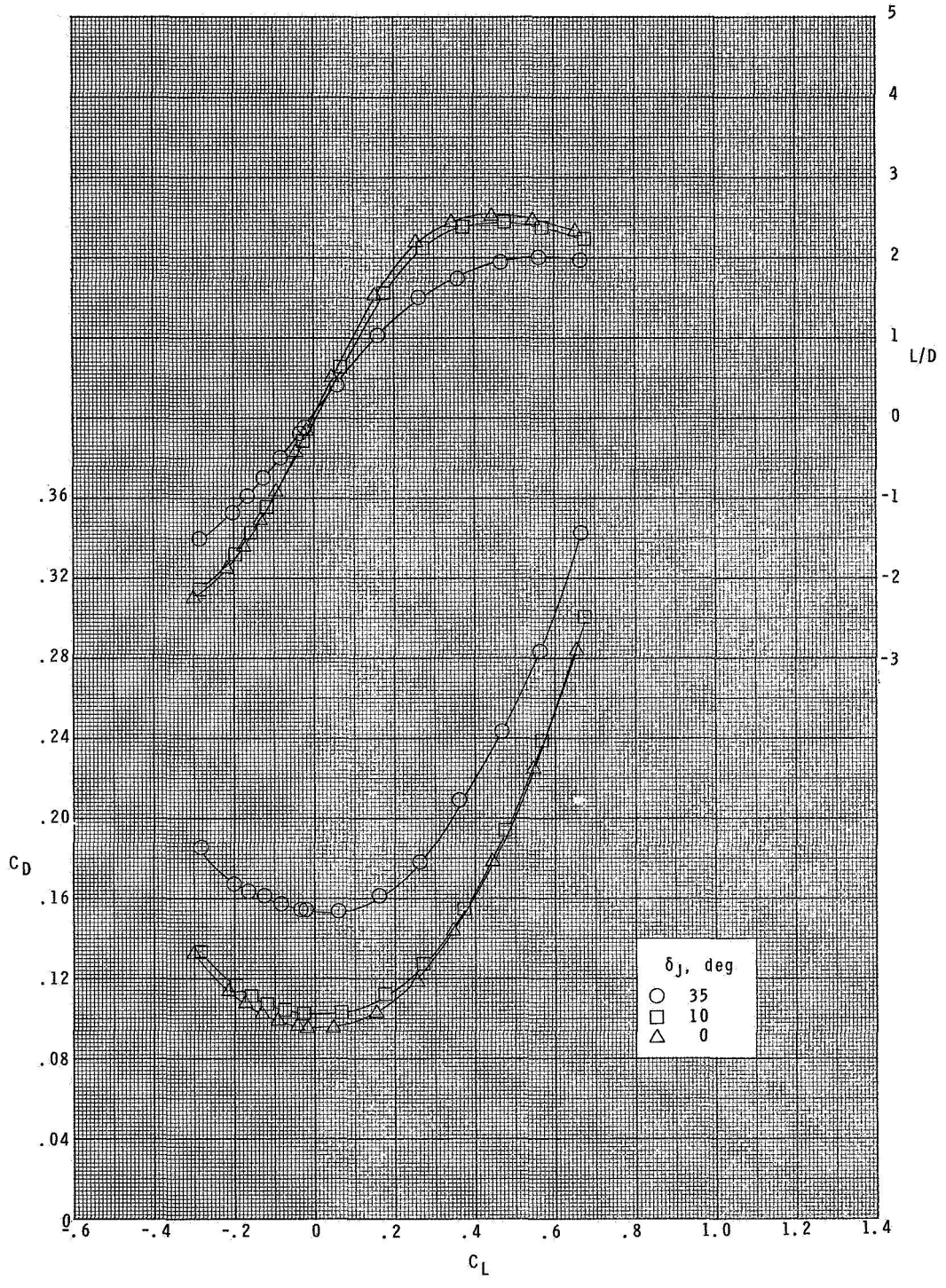
(c) Concluded.

Figure 11.- Concluded.



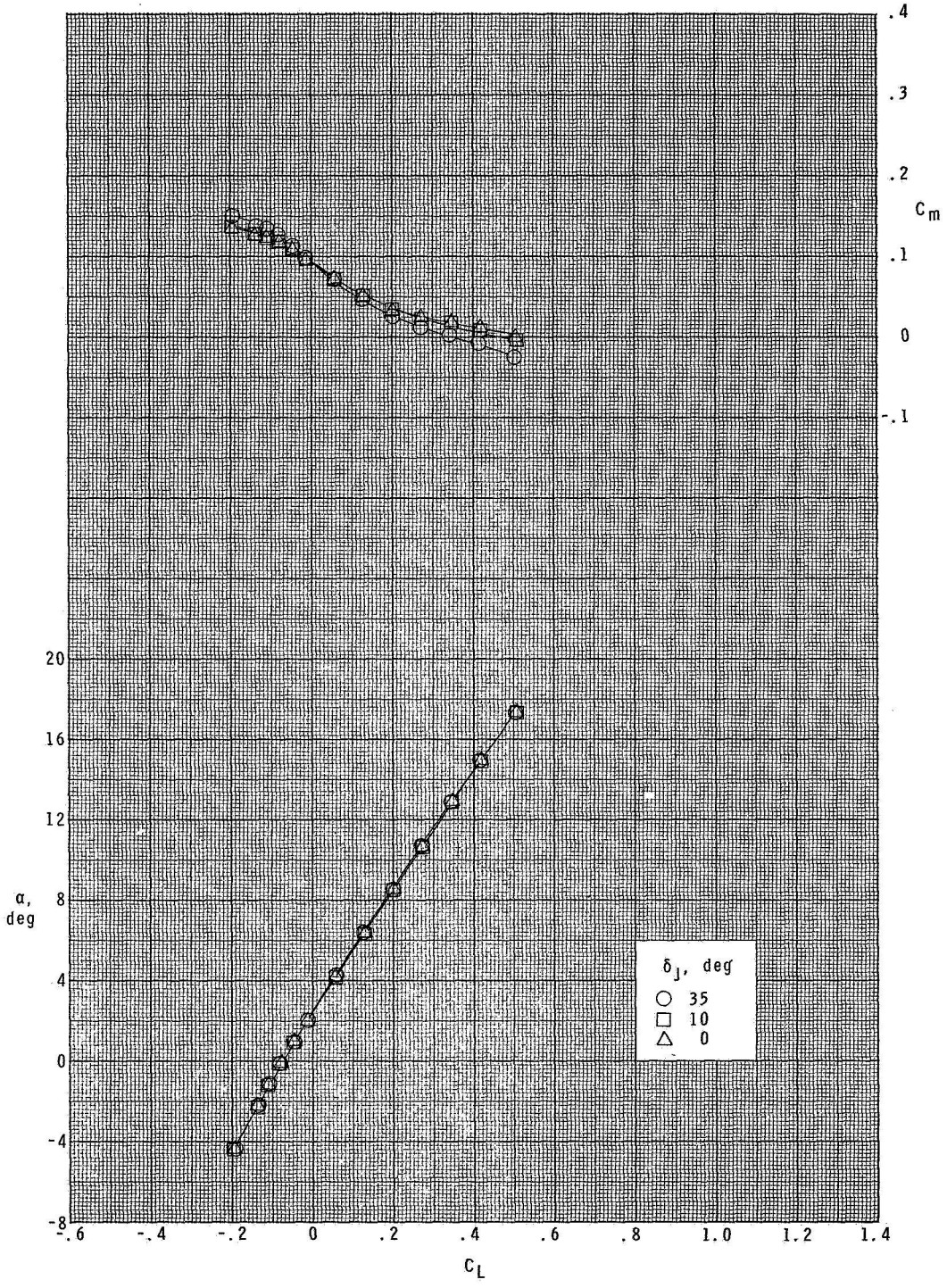
(a) M = 2.86.

Figure 12.- Effect of speed-brake deflection on longitudinal control for $B_{11}X_{16}W_2H_9T_{12}V_{U5}Y_5N_{13}$ (HRE on) with $\delta_h = -20^o$.



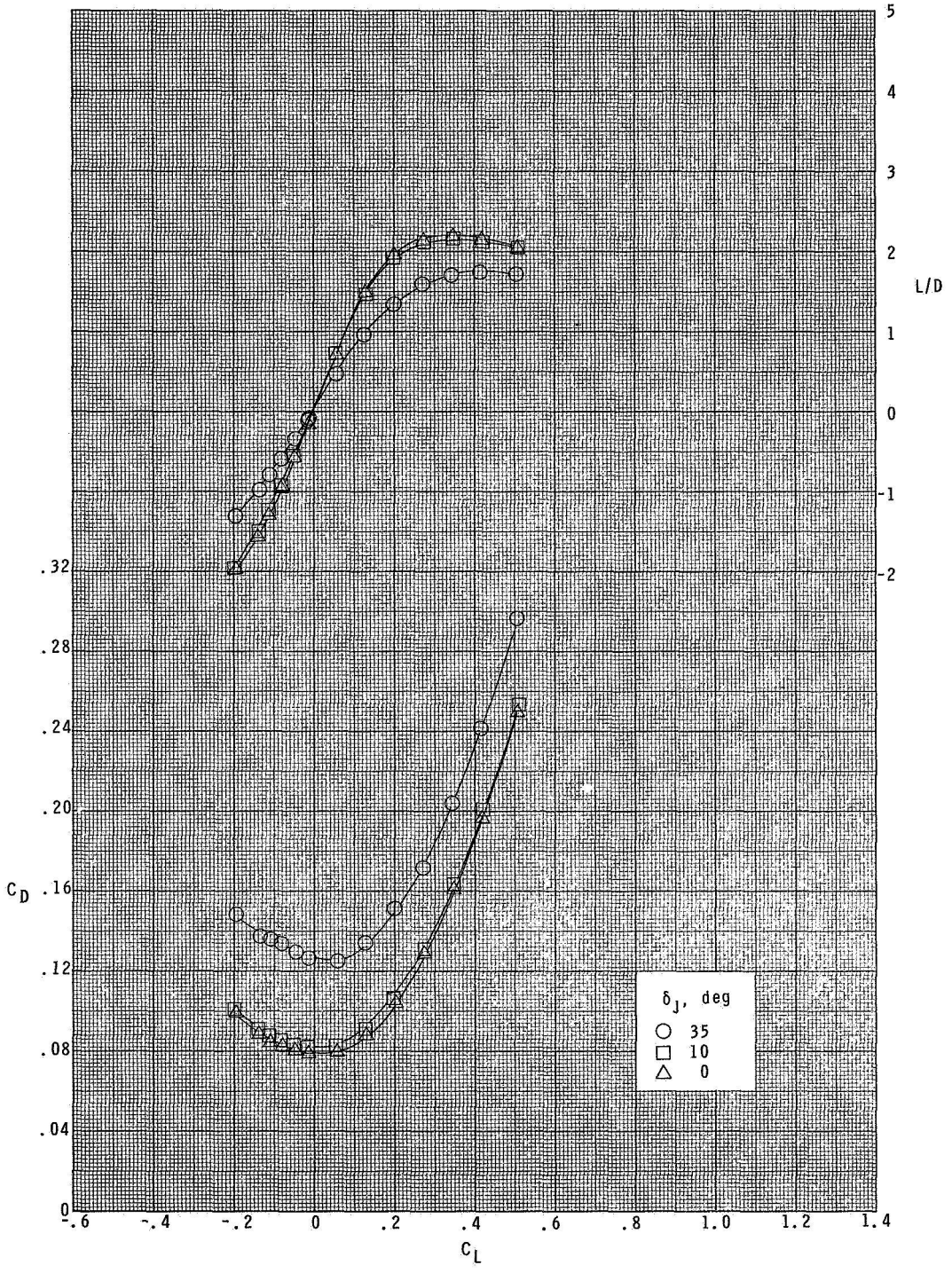
(a) Concluded.

Figure 12.- Continued.



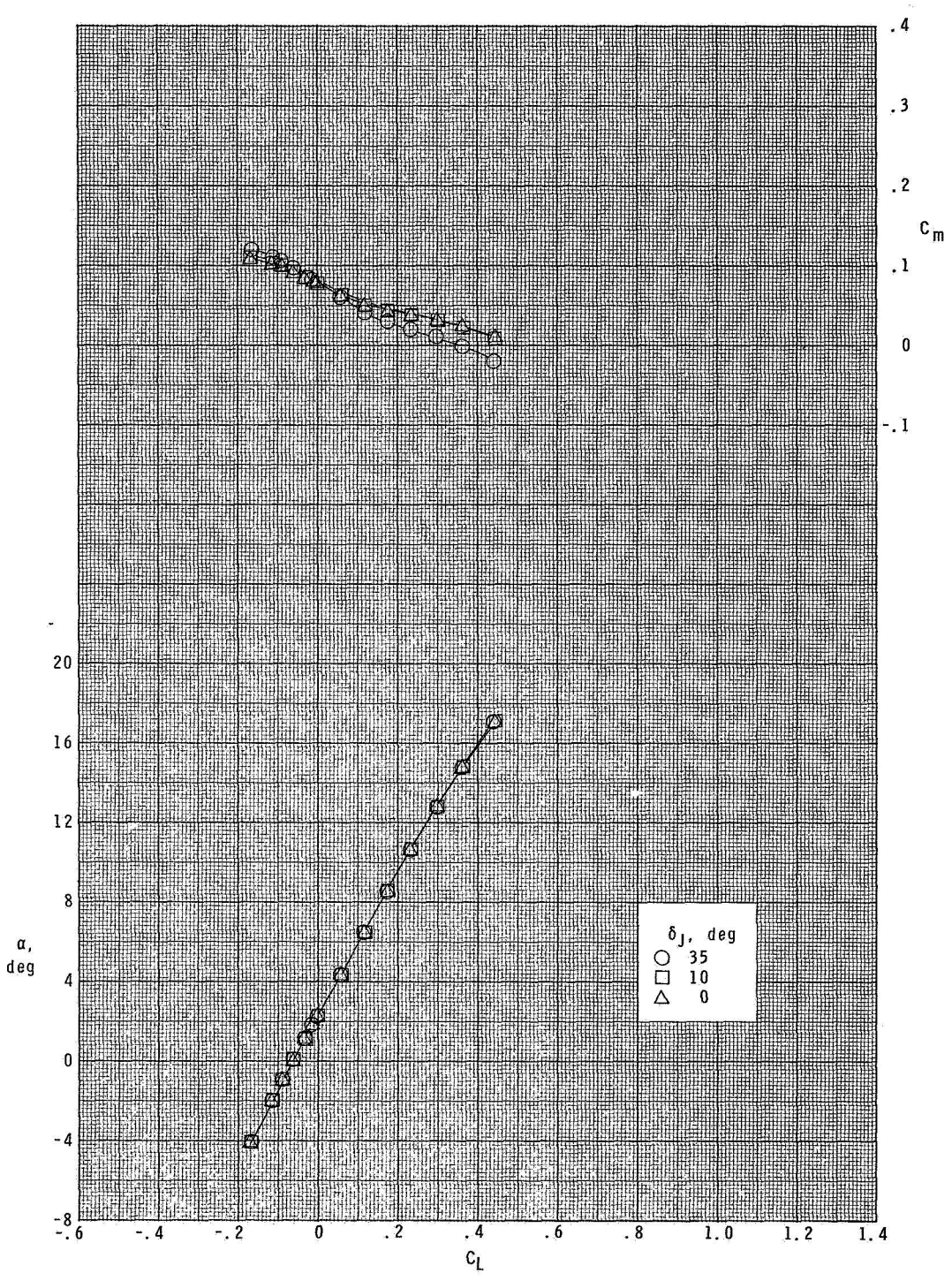
(b) M = 3.95.

Figure 12.- Continued.



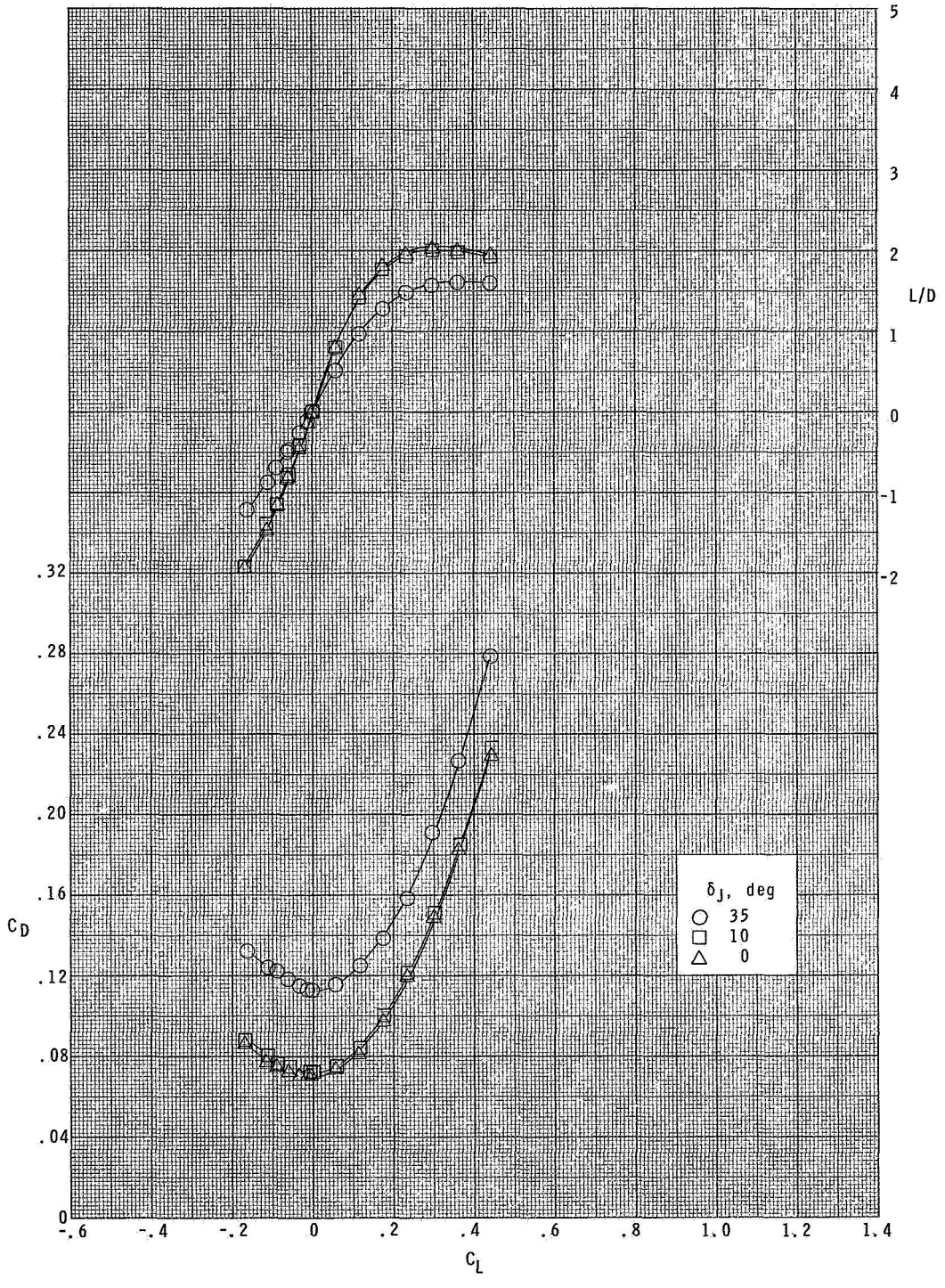
(b) Concluded.

Figure 12.- Continued.



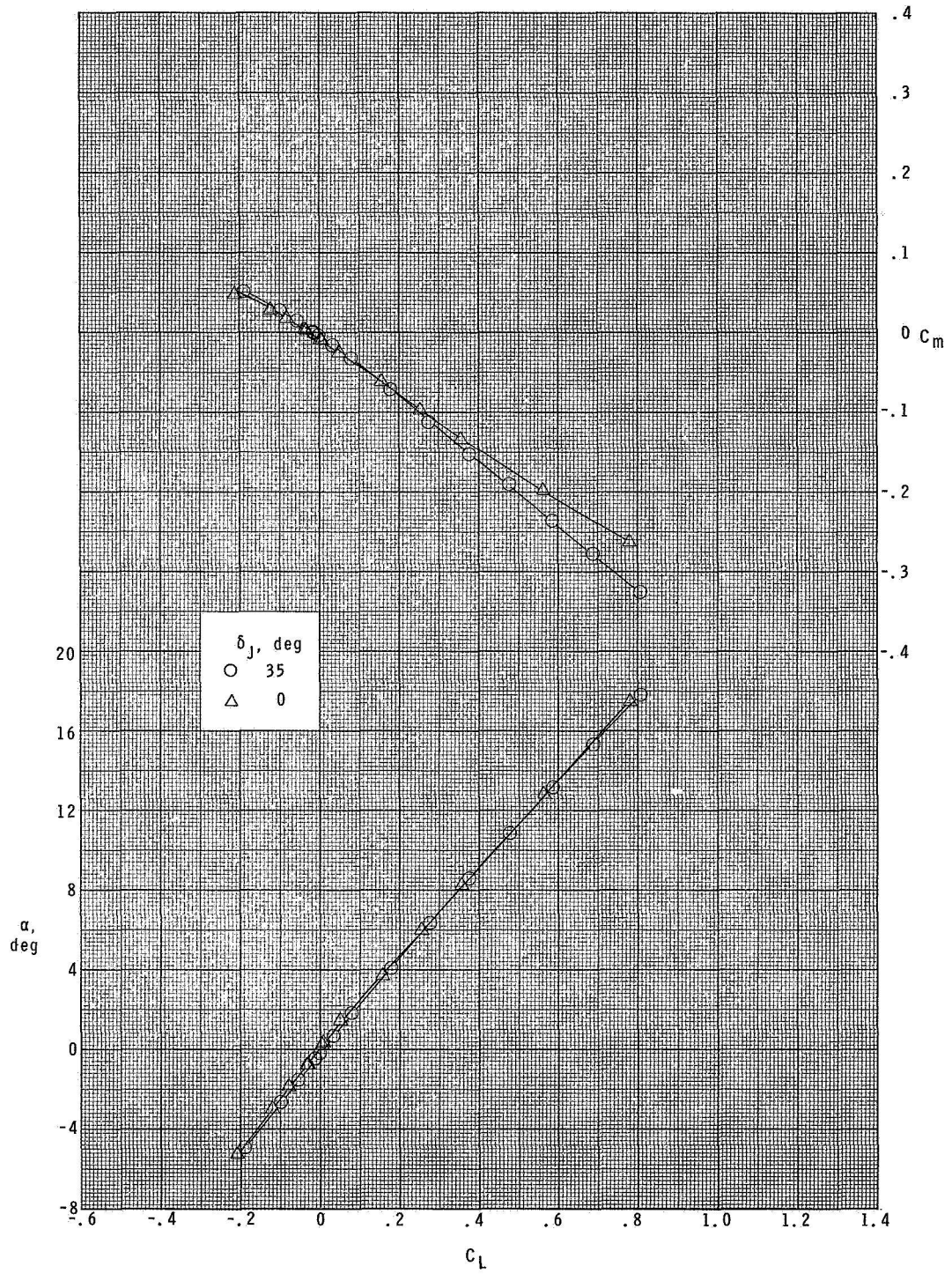
(c) M = 4.63.

Figure 12.- Continued.



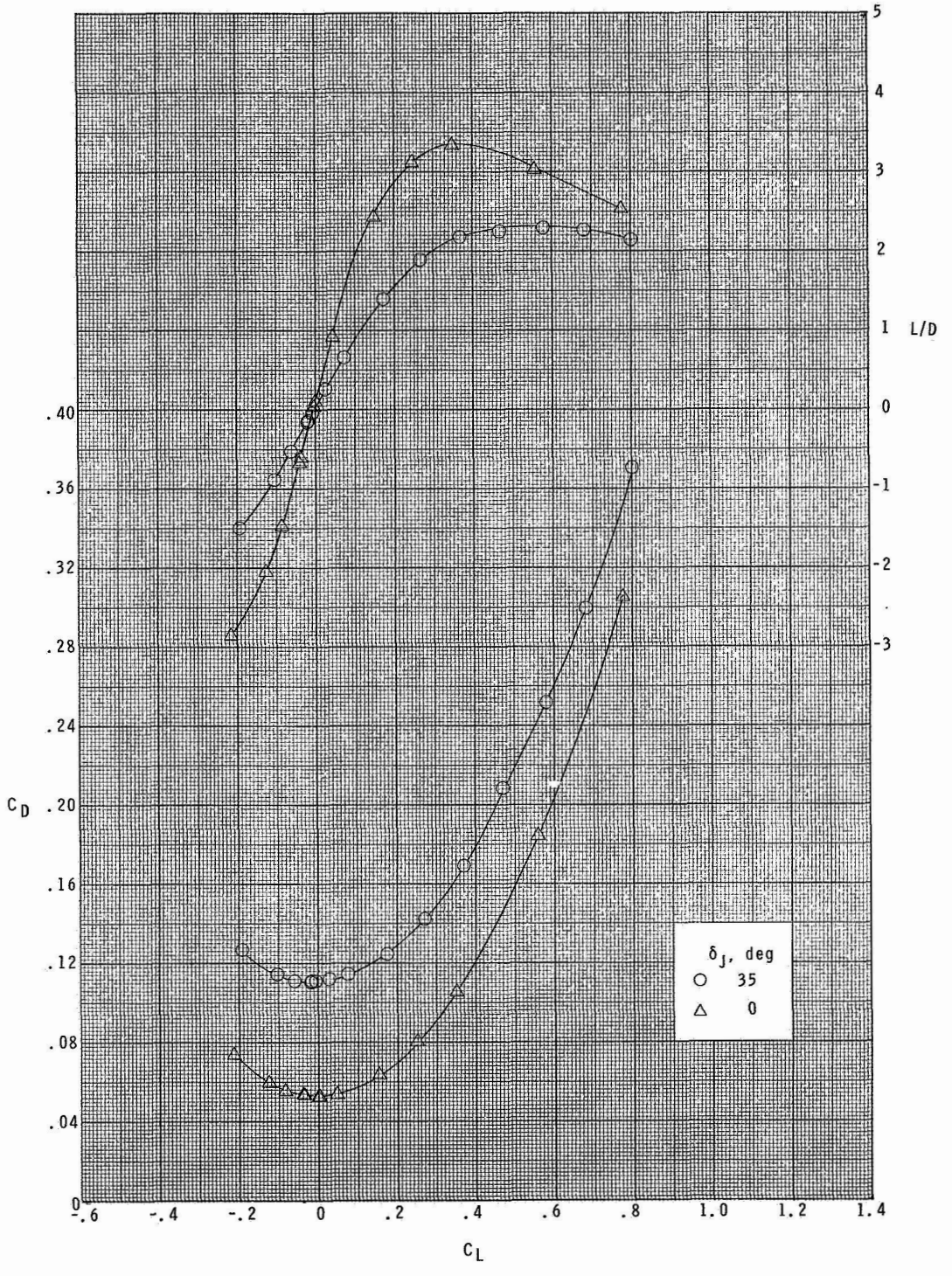
(c) Concluded.

Figure 12.- Concluded.



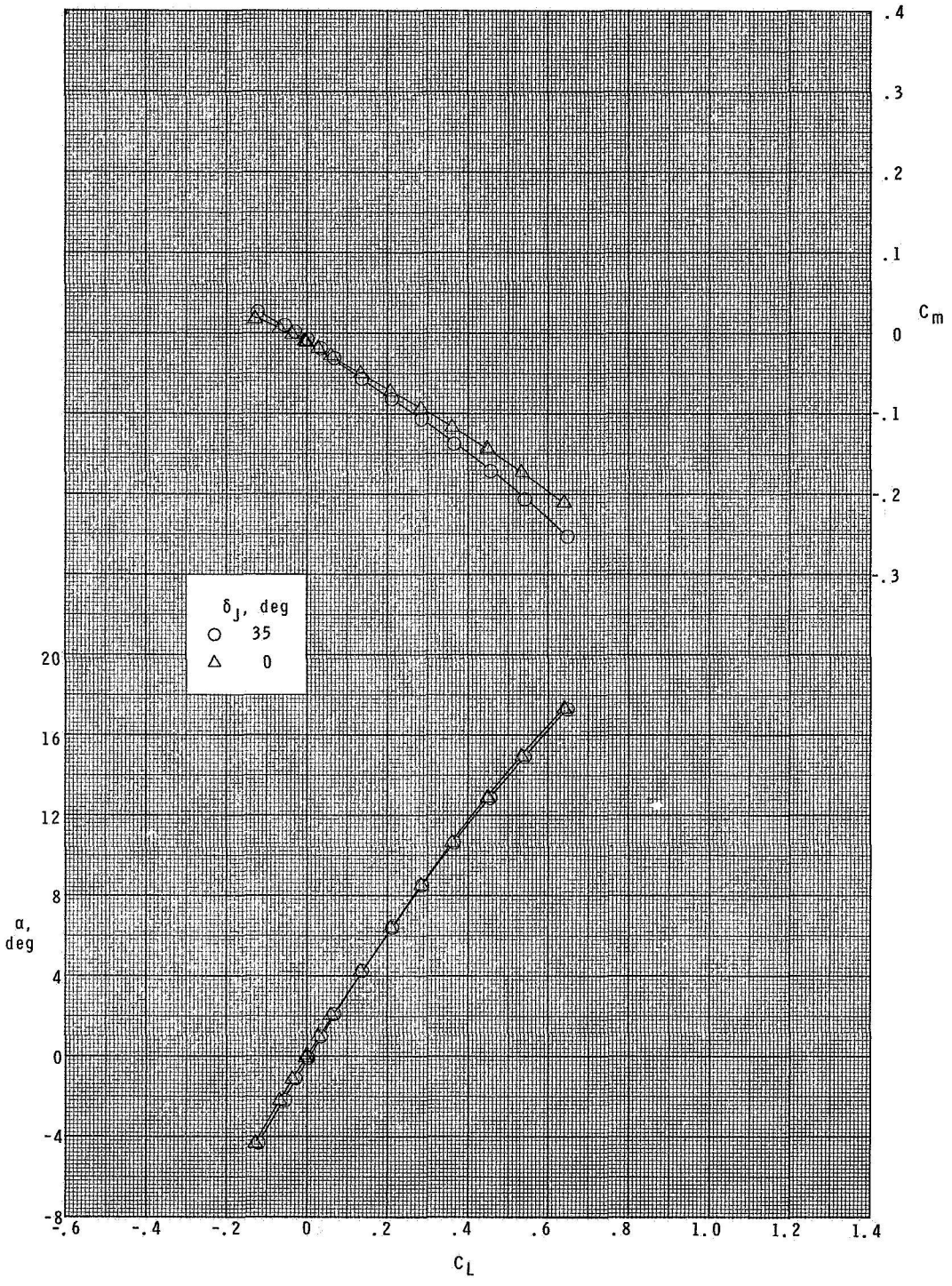
(a) M = 2.86.

Figure 13.- Effect of speed-brake deflection on longitudinal control for $B_{11}X_{16}W_2H_9T_{12}V_{U5}Y_5$ (HRE off) with $\delta_h = 0^o$.



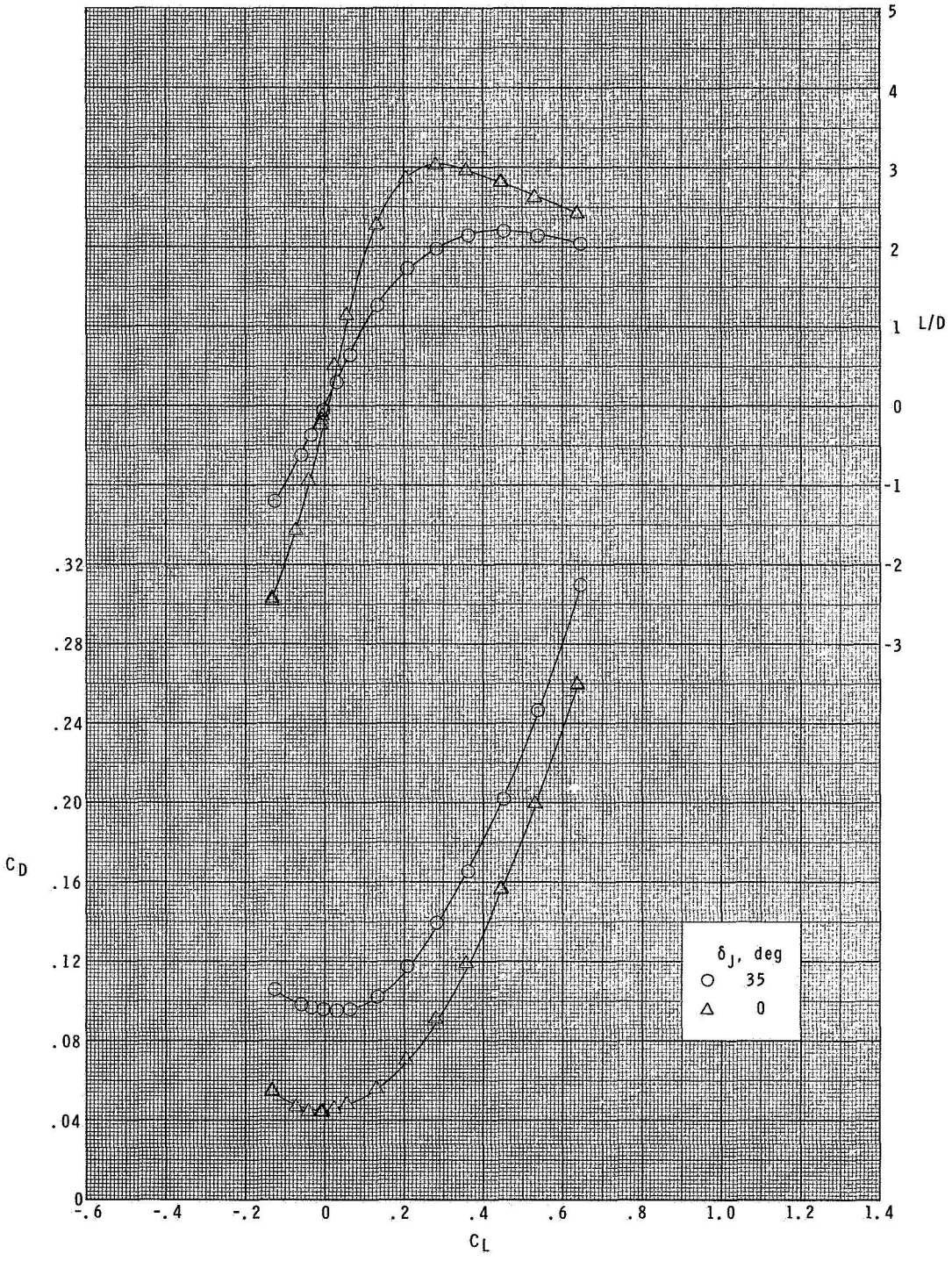
(a) Concluded.

Figure 13.- Continued.



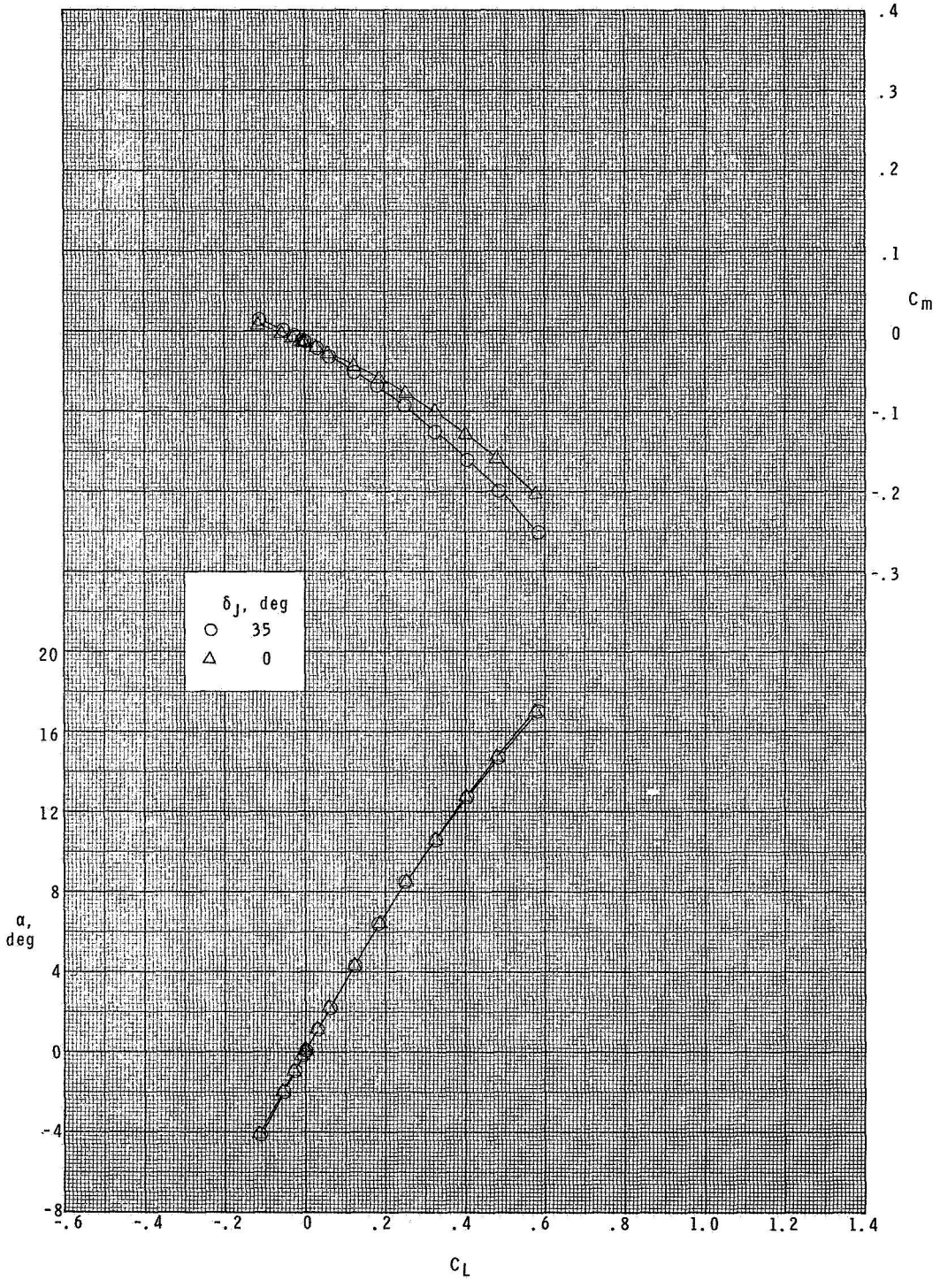
(b) M = 3.95.

Figure 13.- Continued.



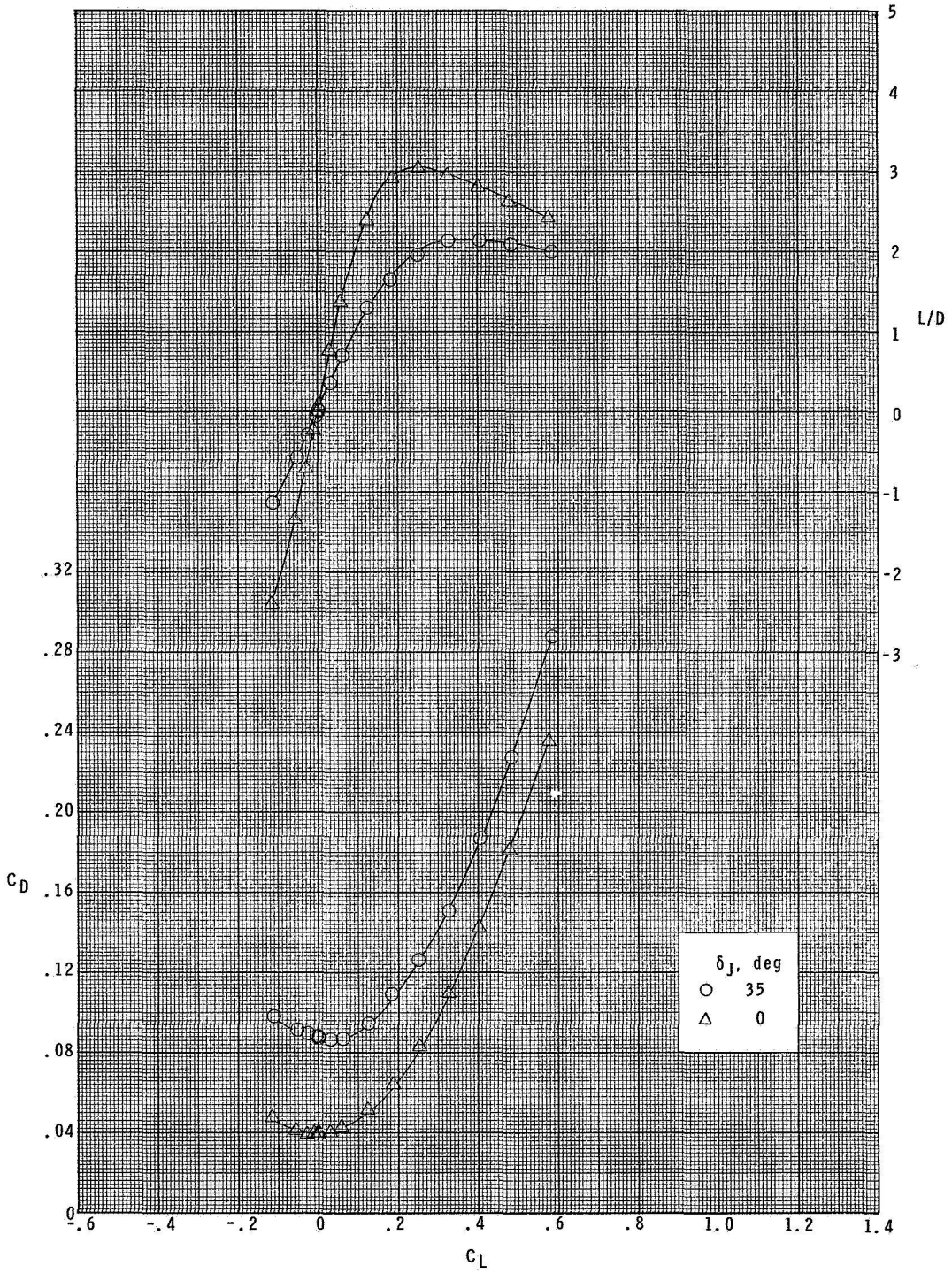
(b) Concluded.

Figure 13.- Continued.



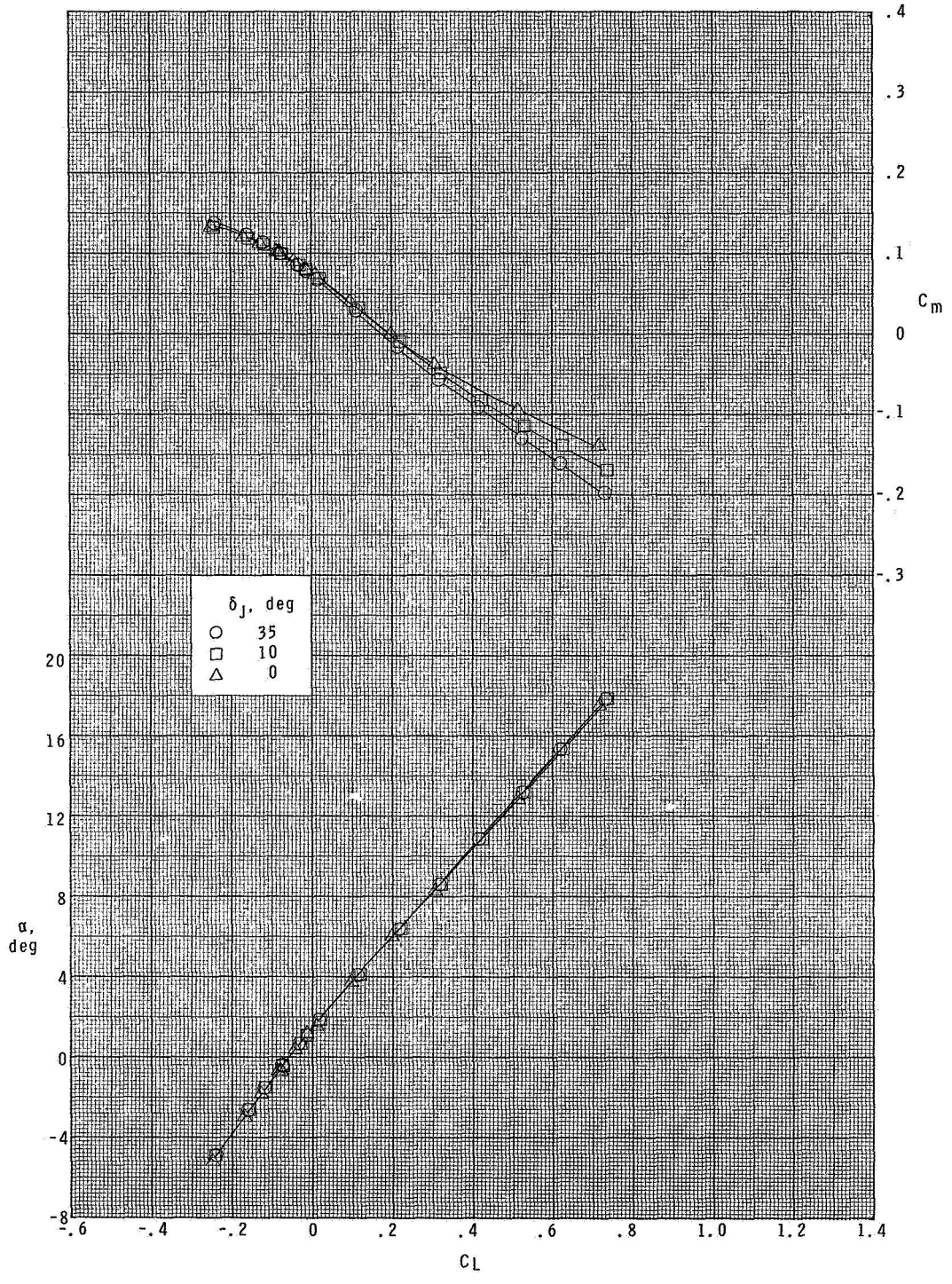
(c) M = 4.63.

Figure 13.- Continued.



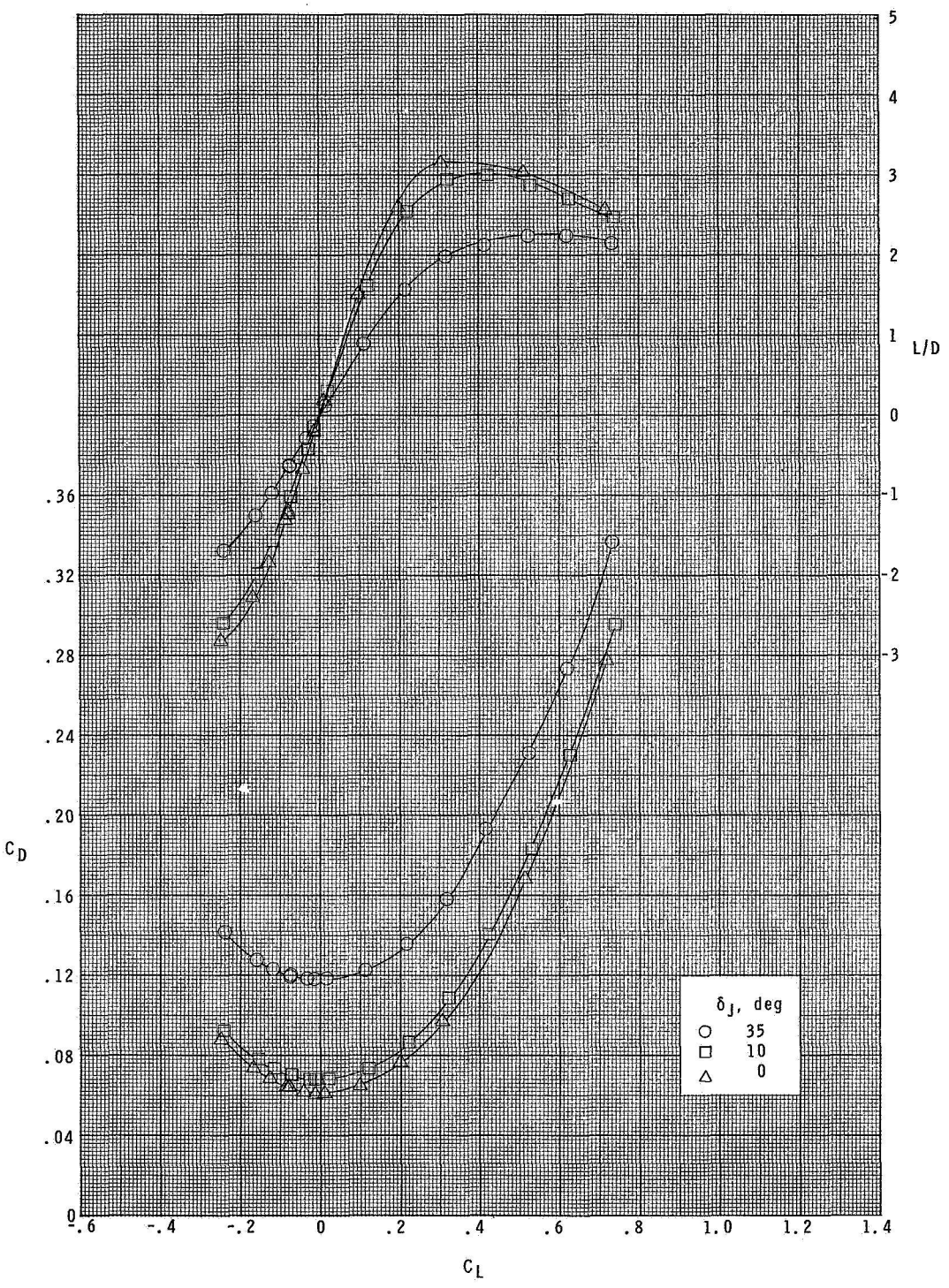
(c) Concluded.

Figure 13.- Concluded.



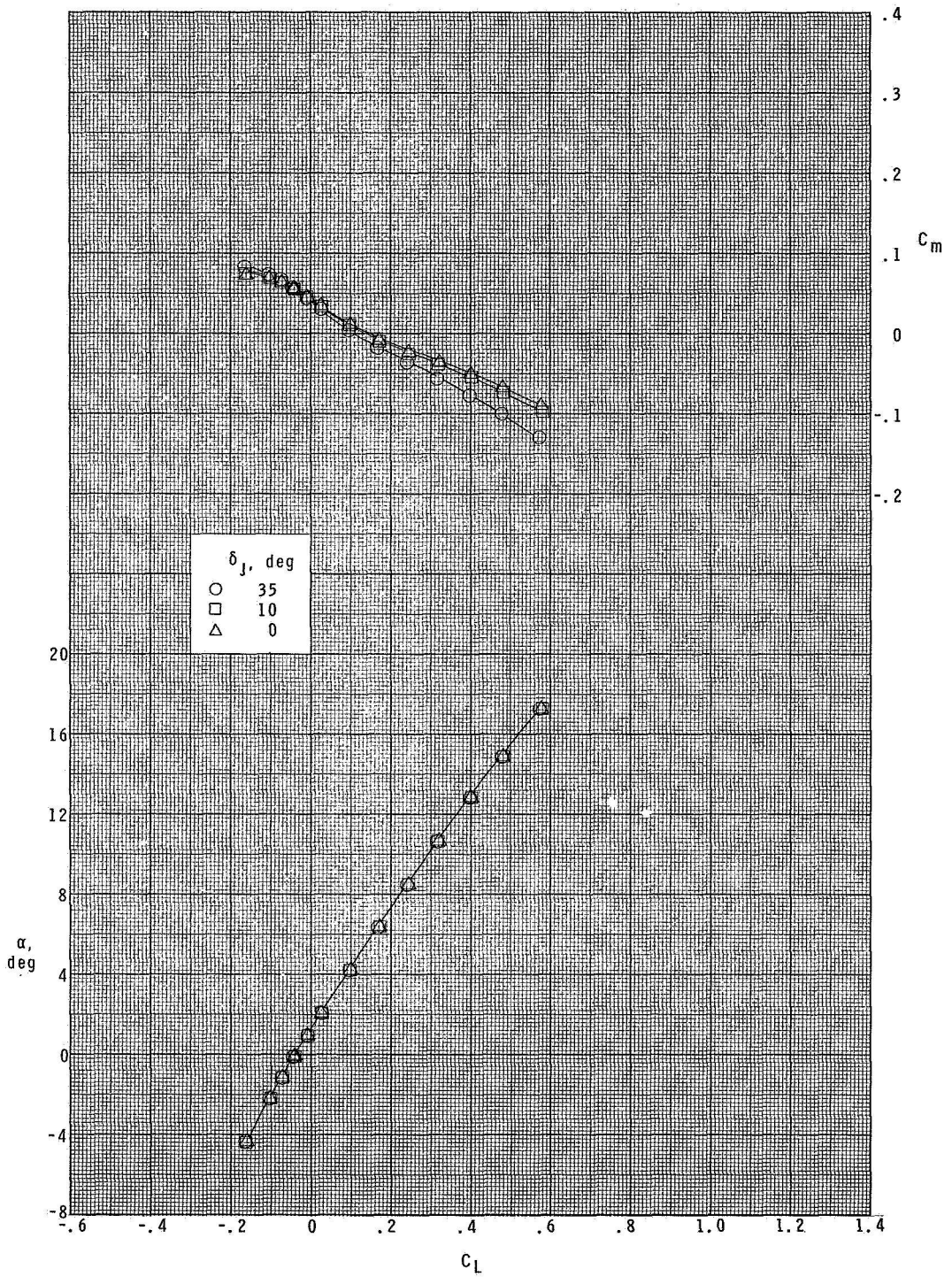
(a) M = 2.86.

Figure 14.- Effect of speed-brake deflection on longitudinal control for $B_{11}X_{16}W_2H_9T_{12}V_{U5}Y_5$ (HRE off) with $\delta_h = -10^o$.



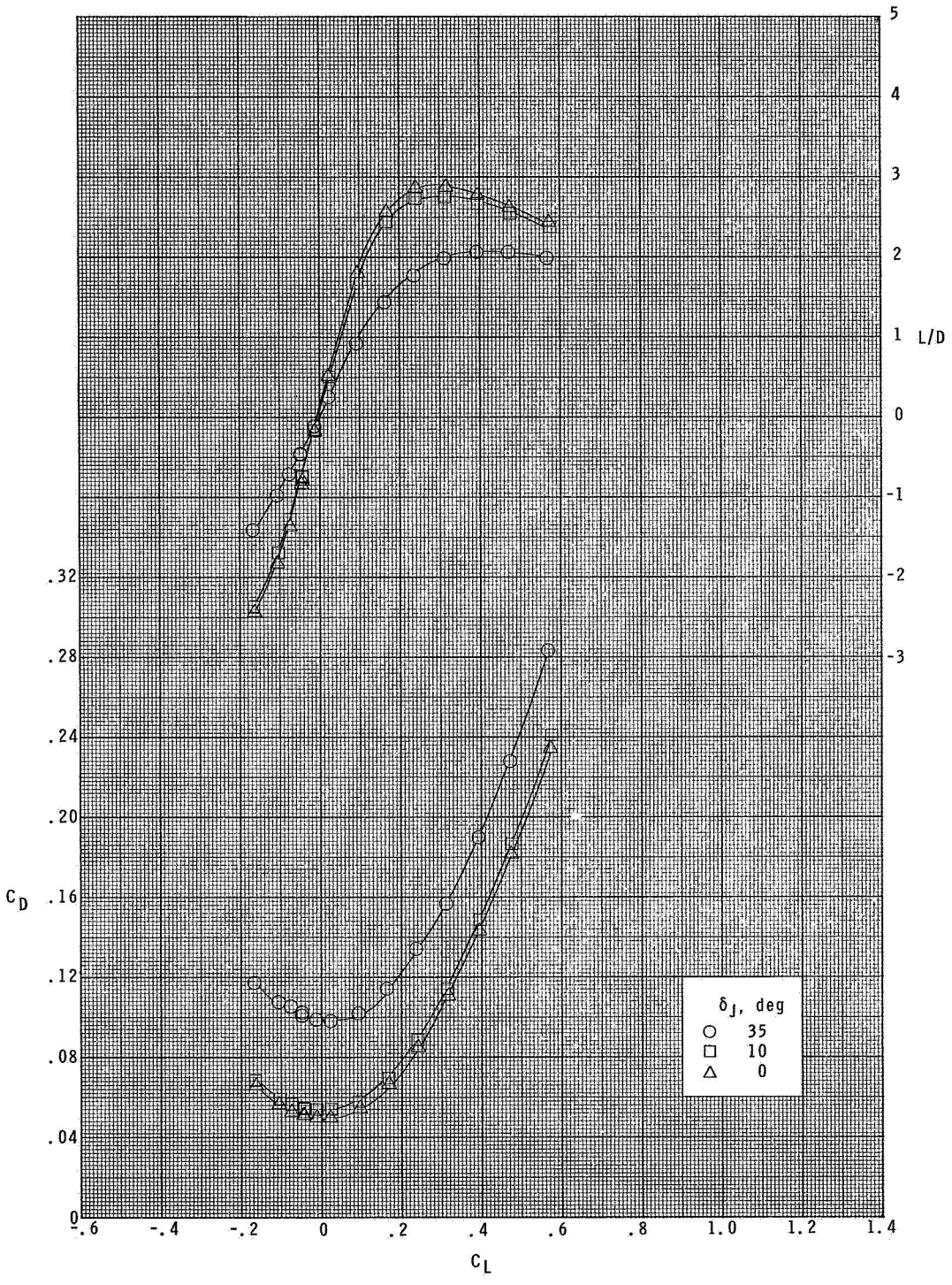
(a) Concluded.

Figure 14.- Continued.



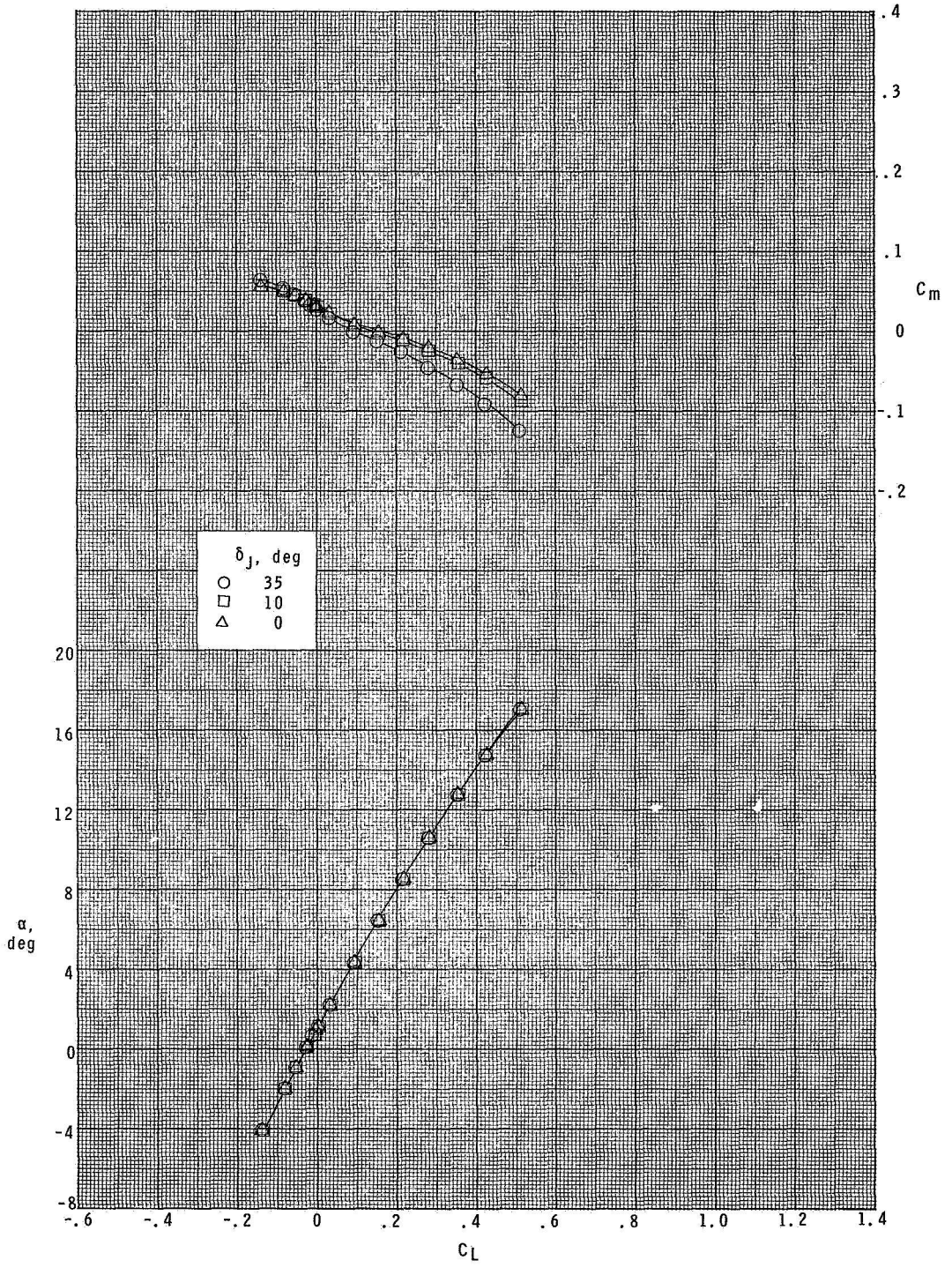
(b) M = 3.95.

Figure 14.- Continued.



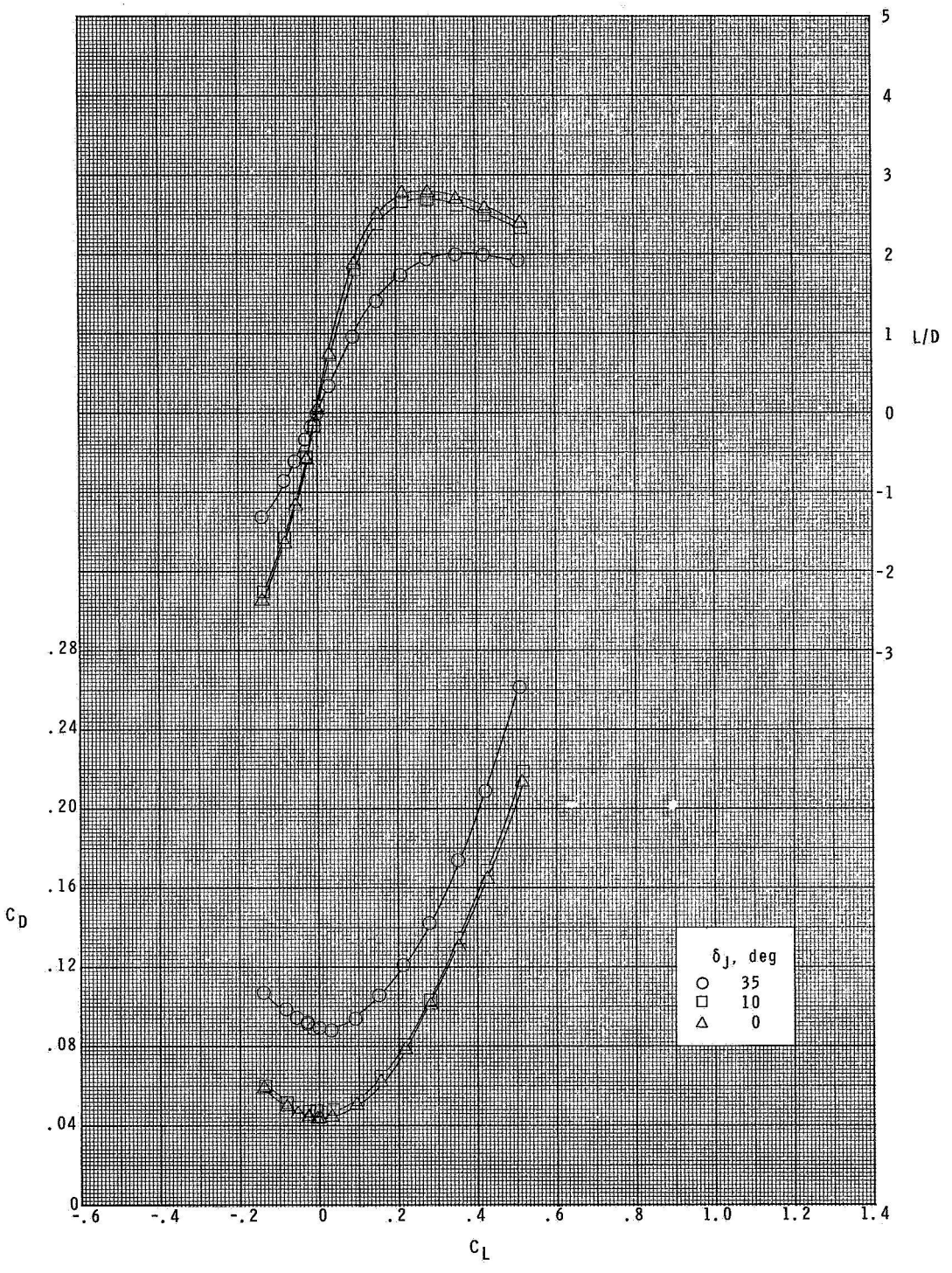
(b) Concluded.

Figure 14.- Continued.



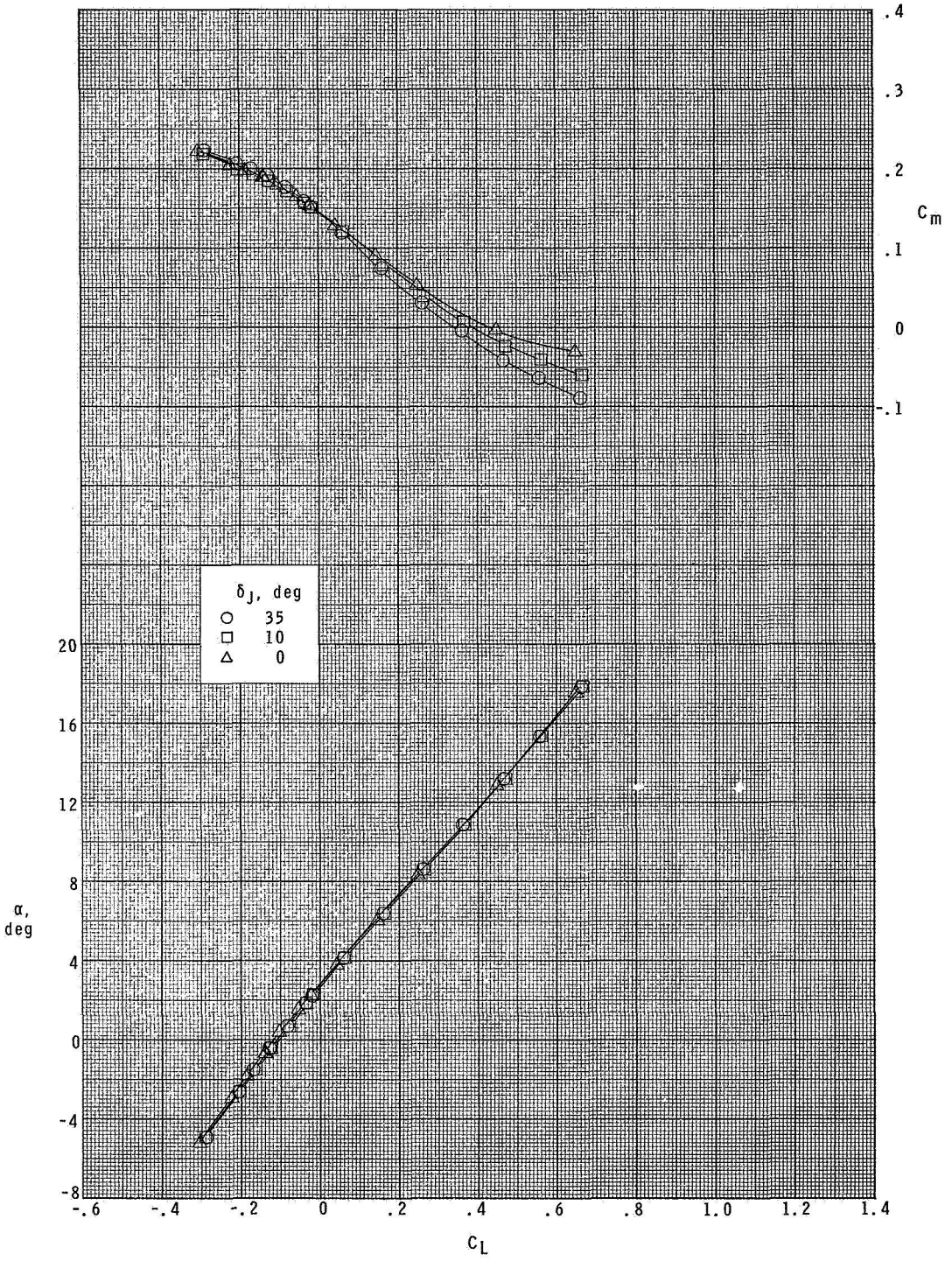
(c) M = 4.63.

Figure 14.- Continued.



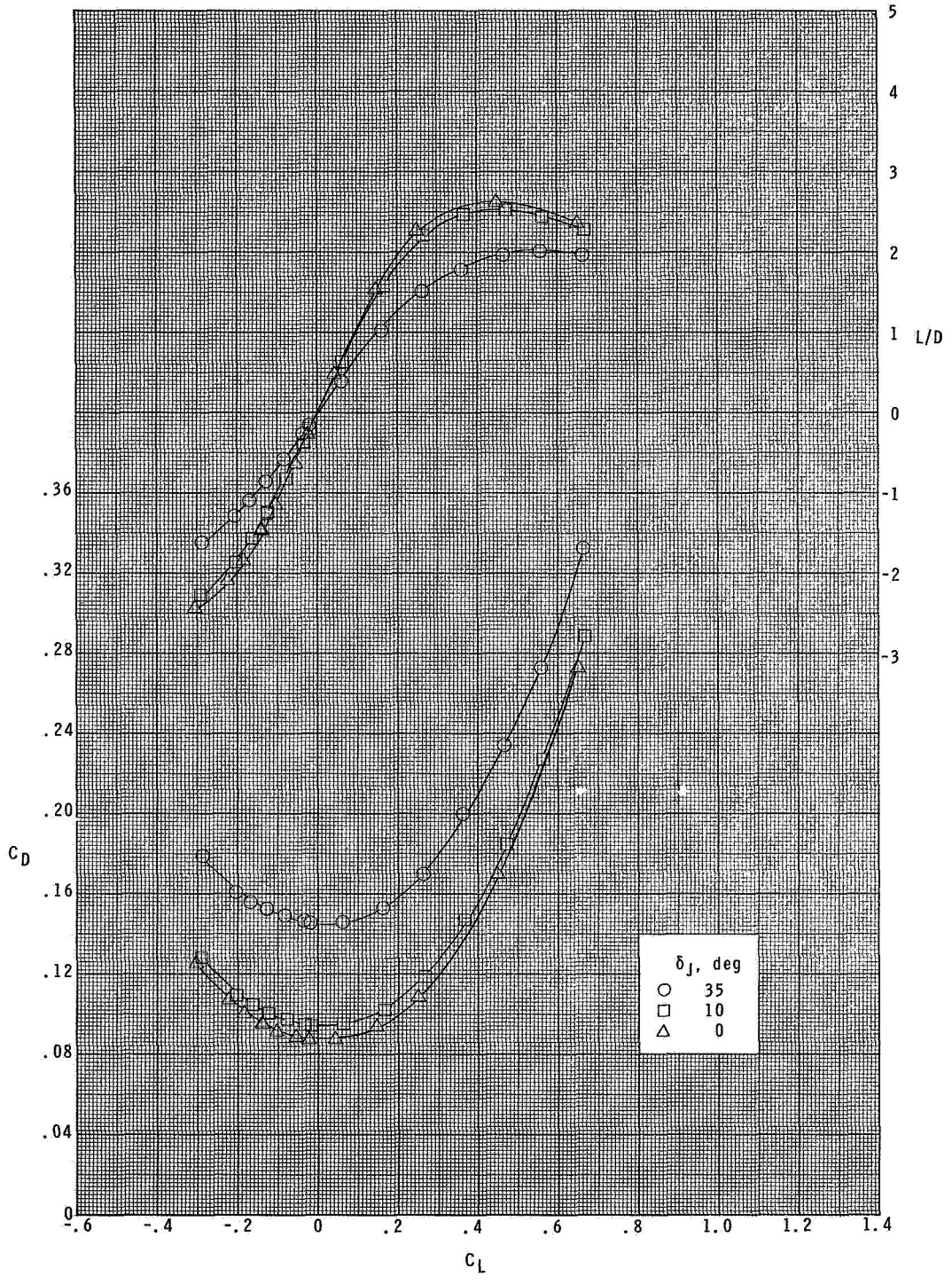
(c) Concluded.

Figure 14.- Concluded.



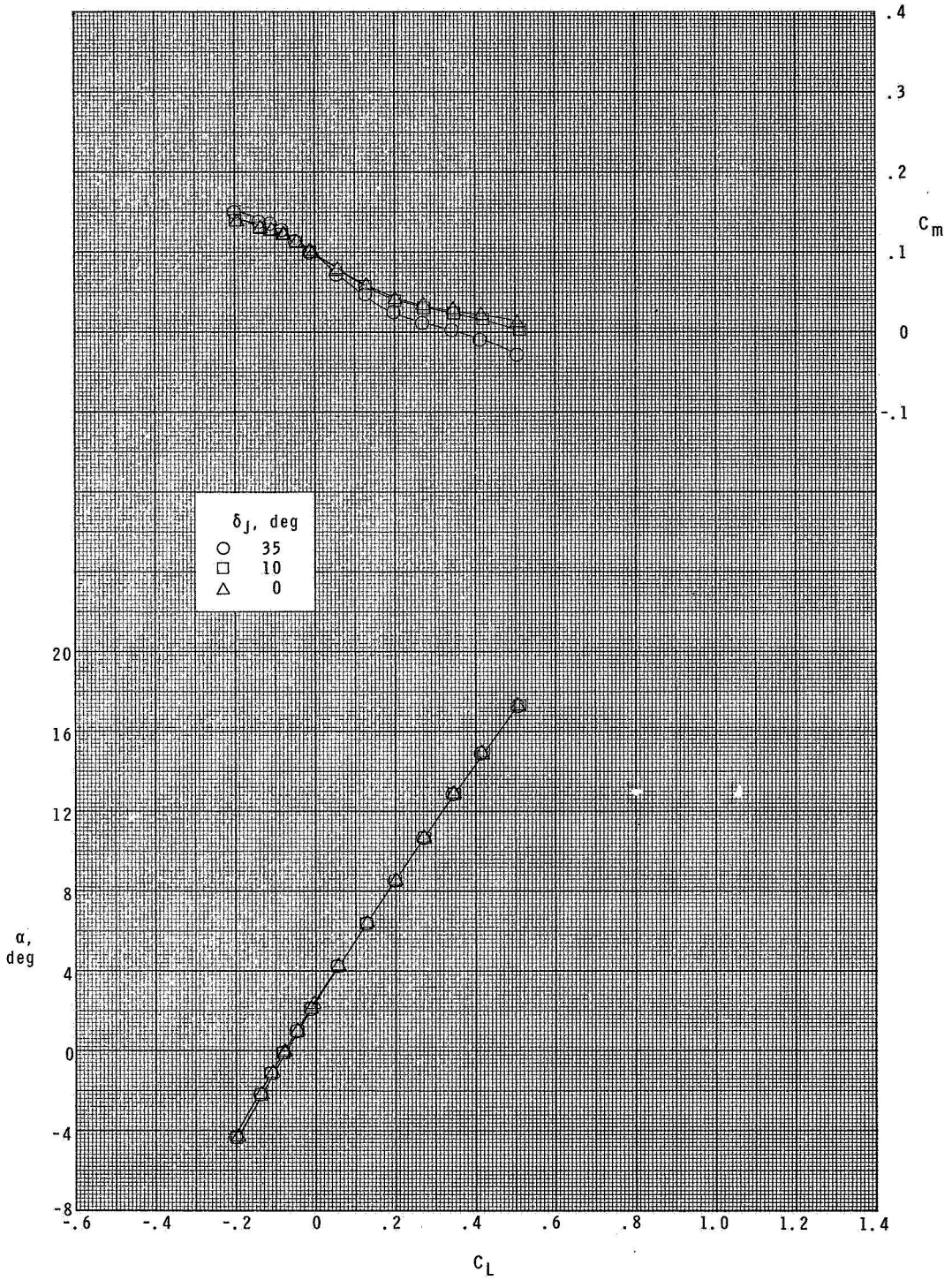
(a) M = 2.86.

Figure 15.- Effect of speed-brake deflection on longitudinal control for $B_{11}X_{16}W_2H_9T_{12}V_{U5}Y_5$ (HRE off) with $\delta_h = -20^0$.



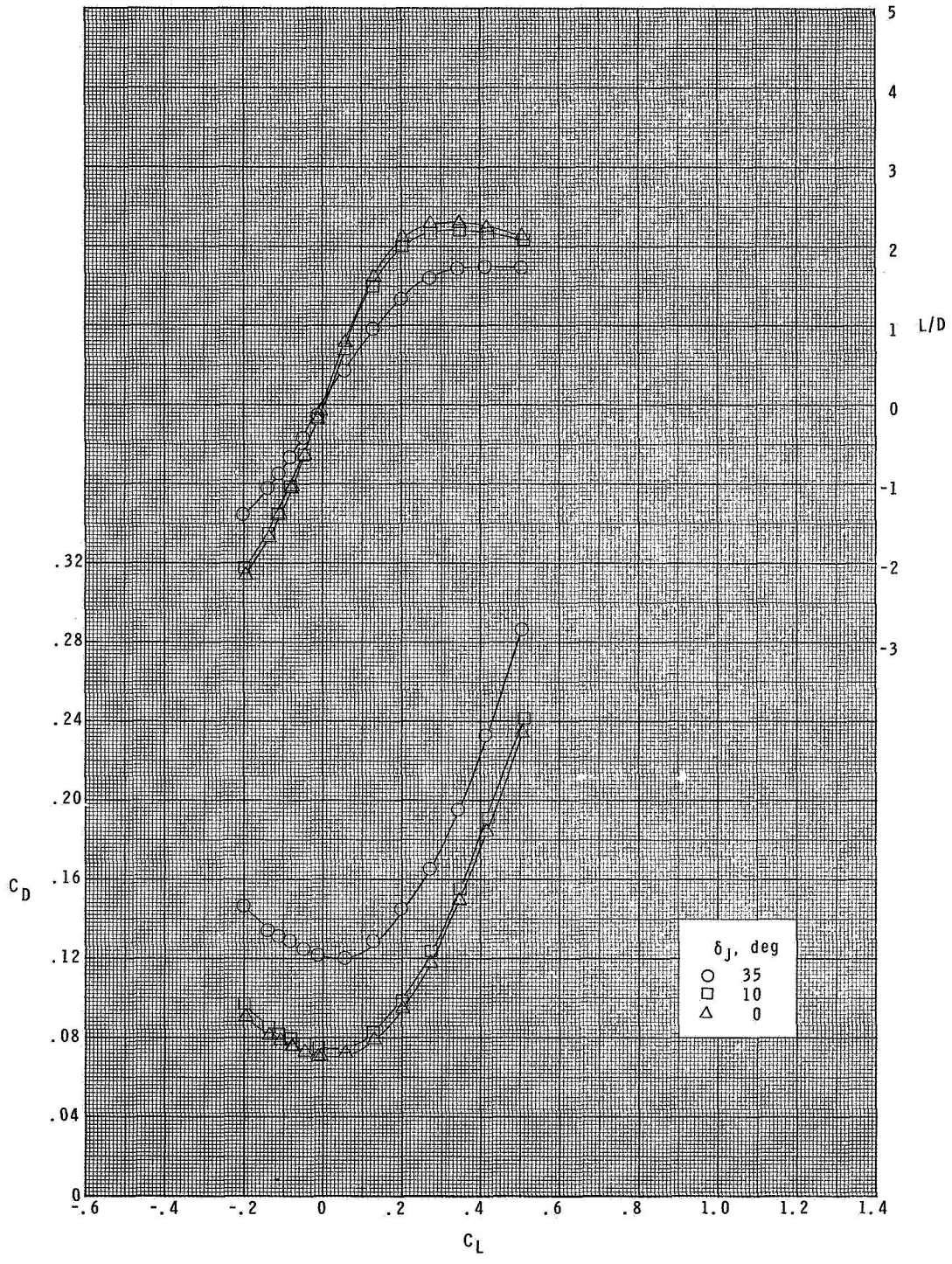
(a) Concluded.

Figure 15.- Continued.



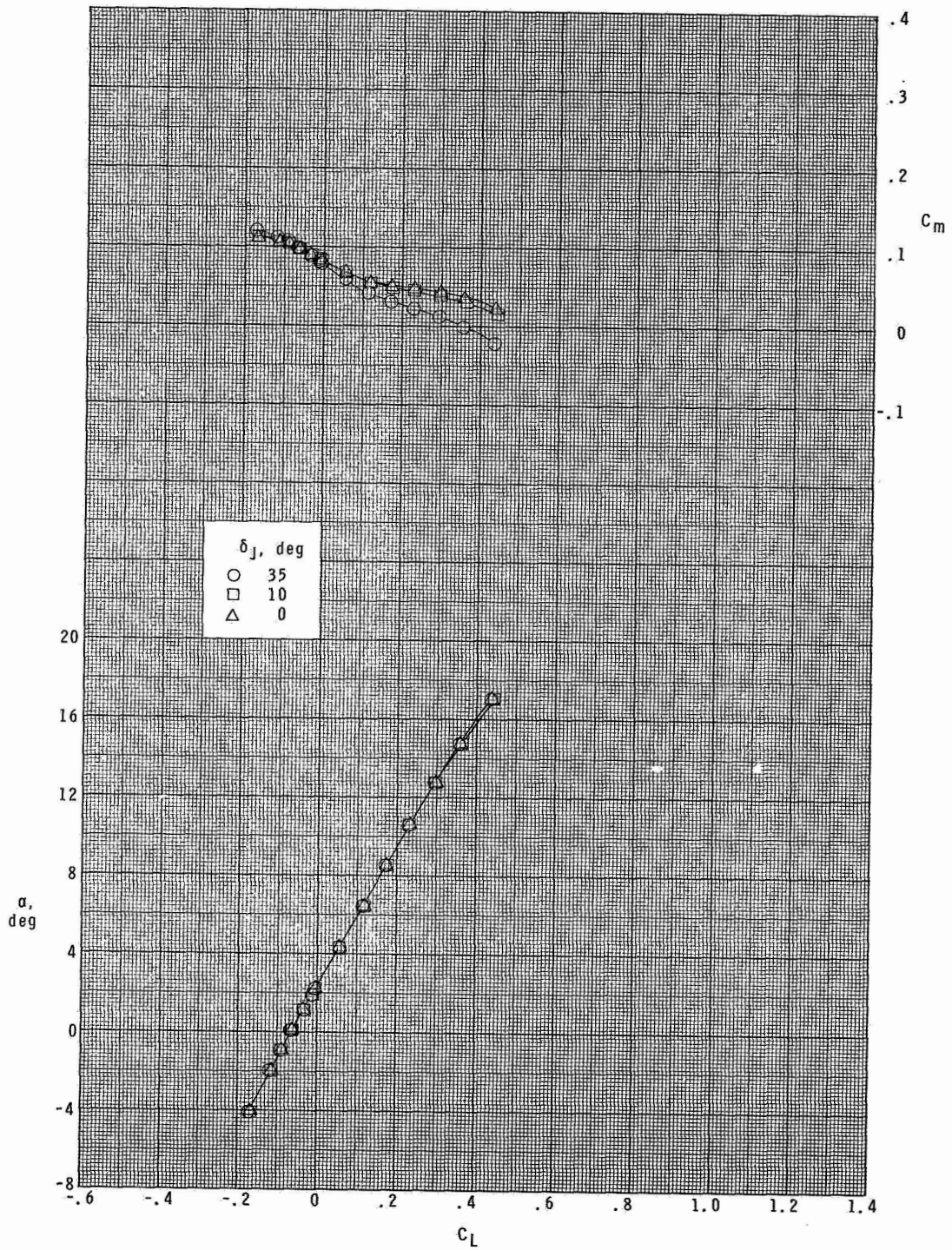
(b) M = 3.95.

Figure 15.- Continued.



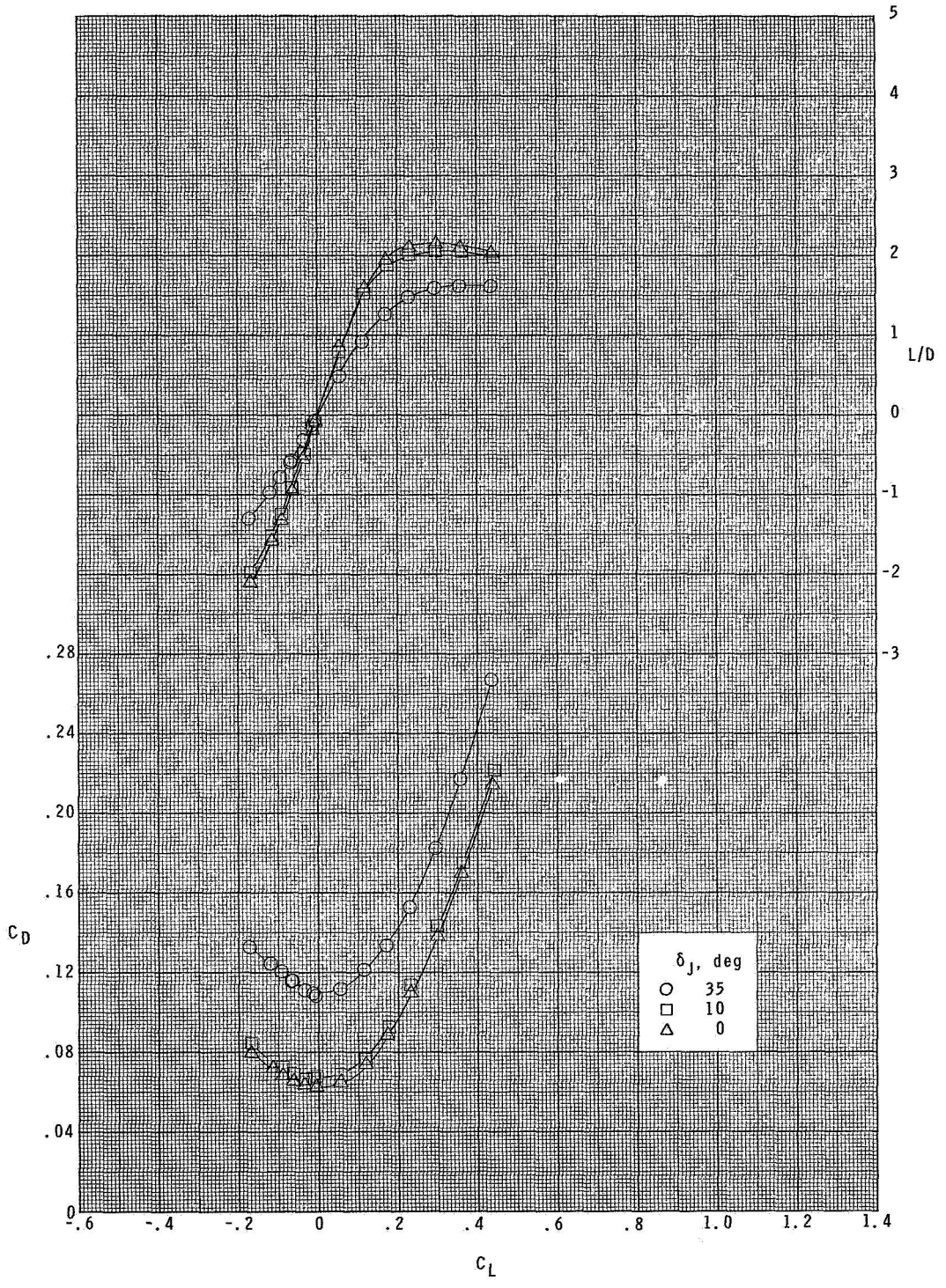
(b) Concluded.

Figure 15.- Continued.



(c) M = 4.63.

Figure 15.- Continued.



(c) Concluded.

Figure 15.- Concluded.

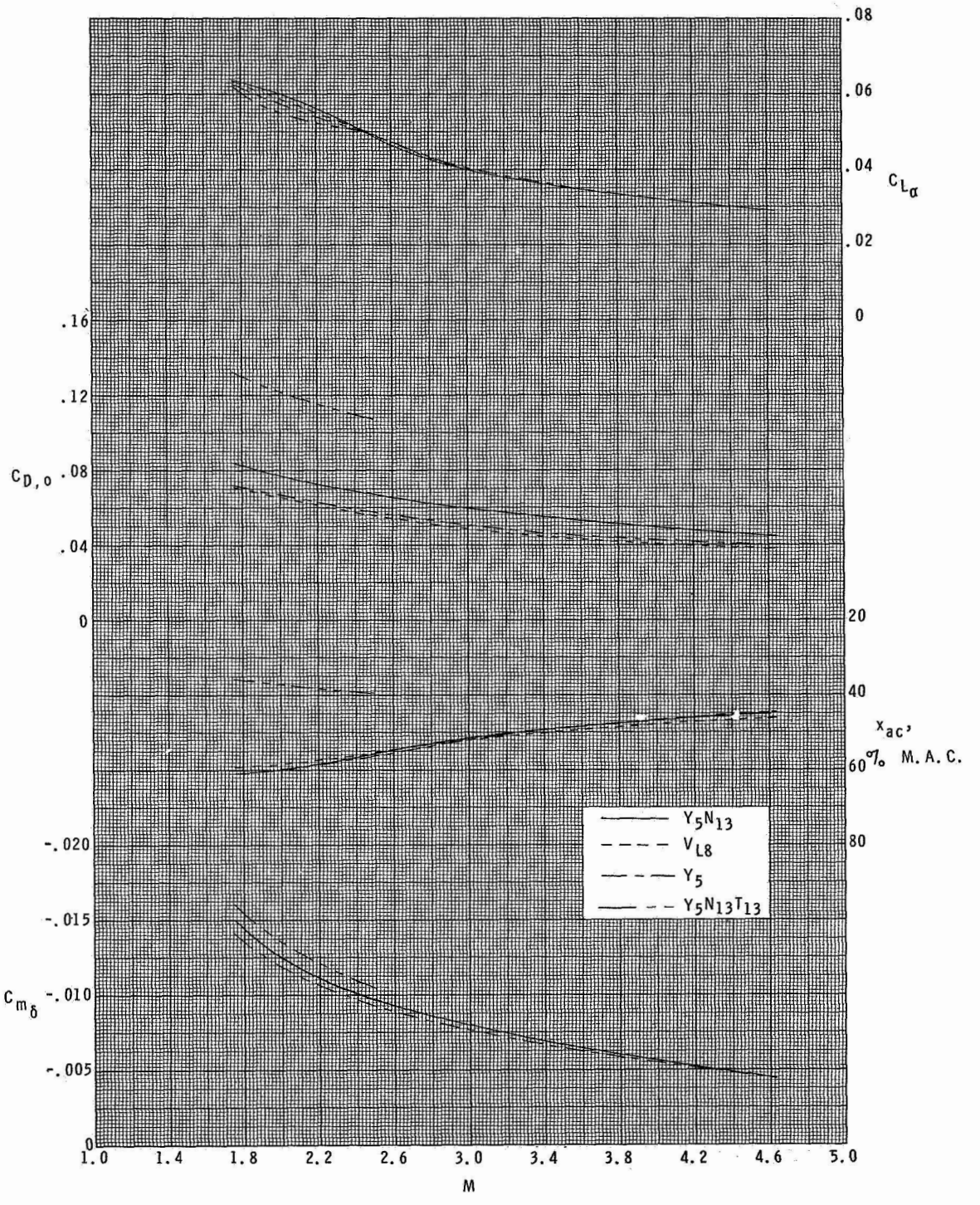
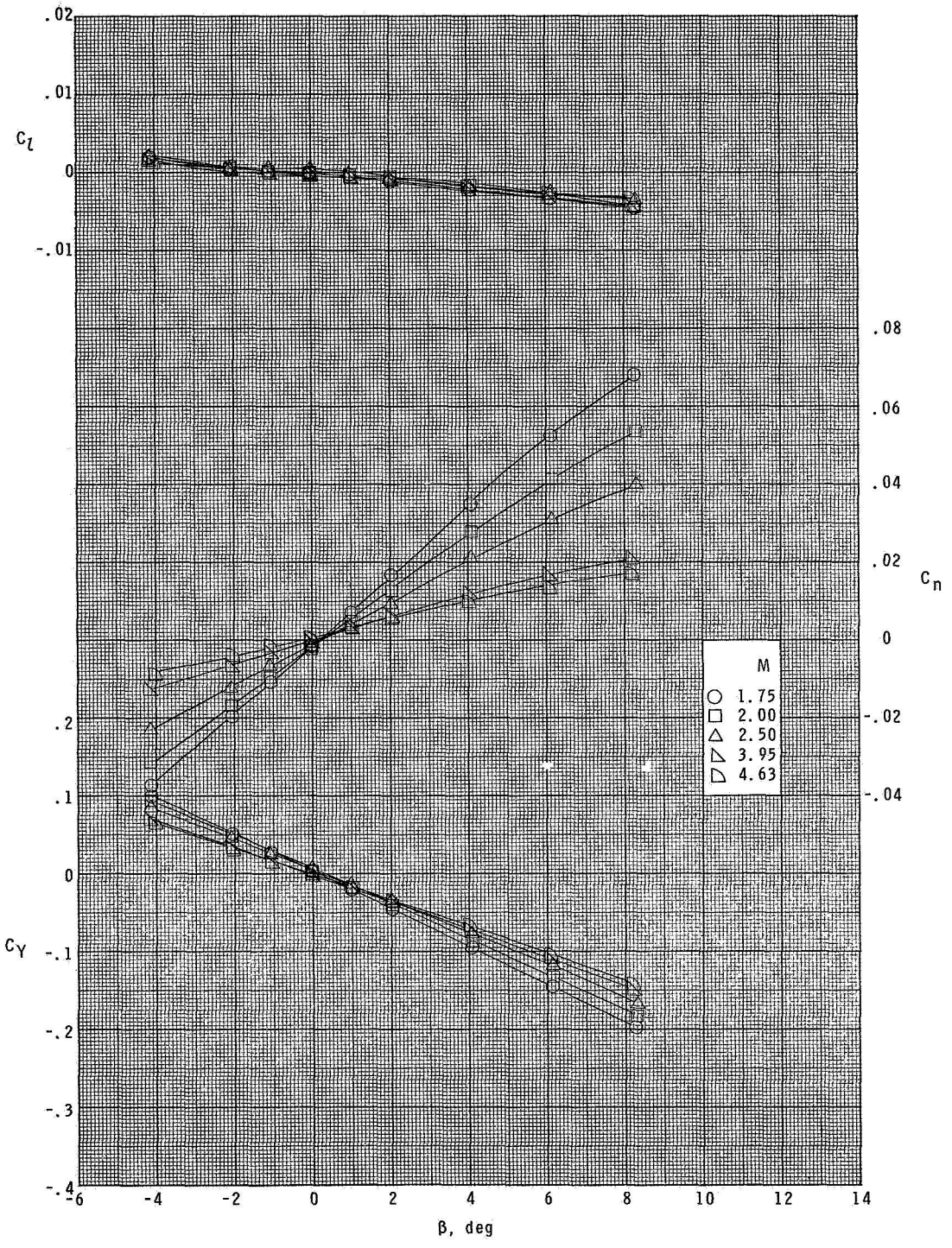
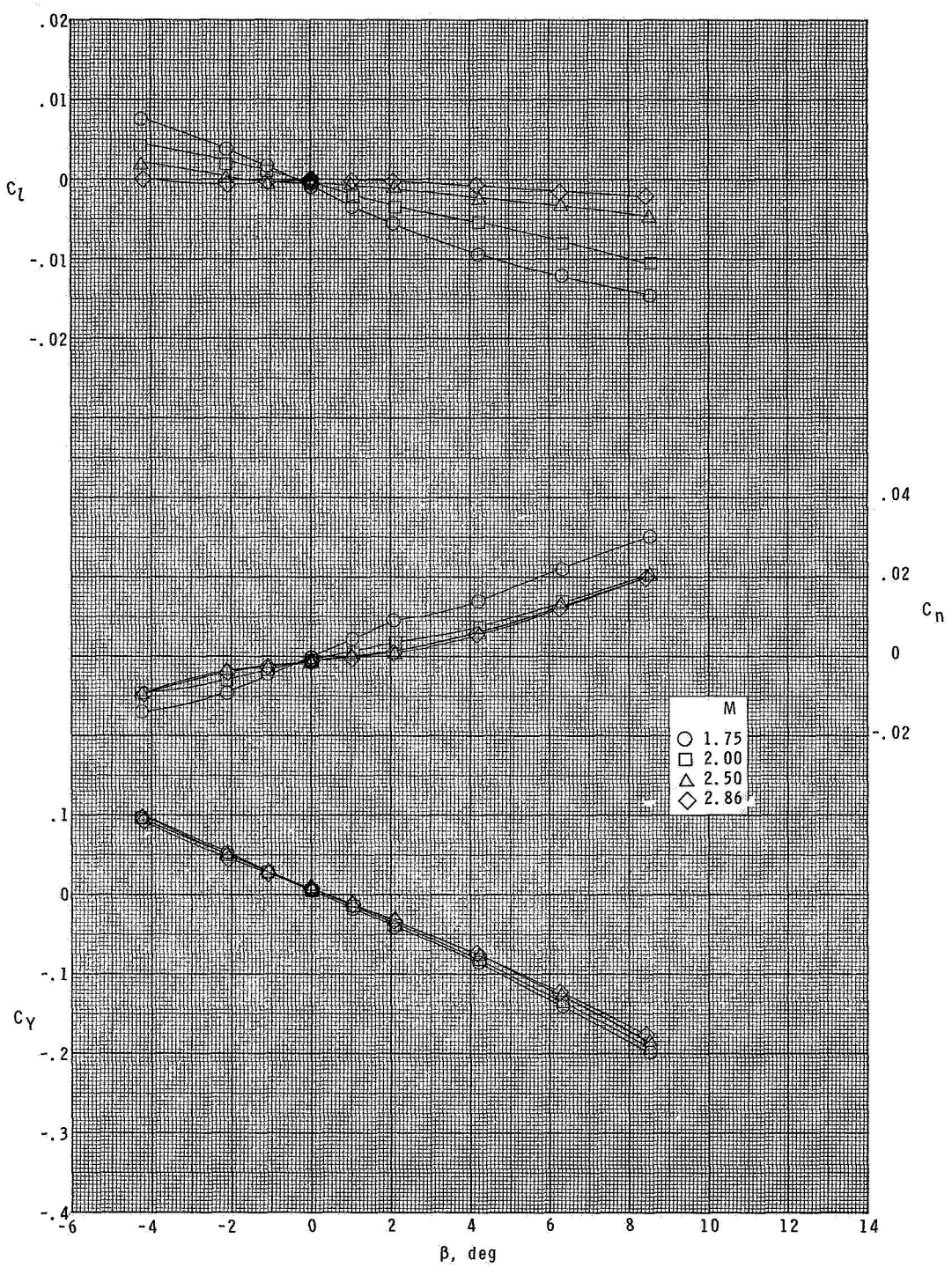


Figure 16.- Summary of longitudinal aerodynamic characteristics for $B_{11}X_{16}W_2H_9T_{12}V_{U5}$.



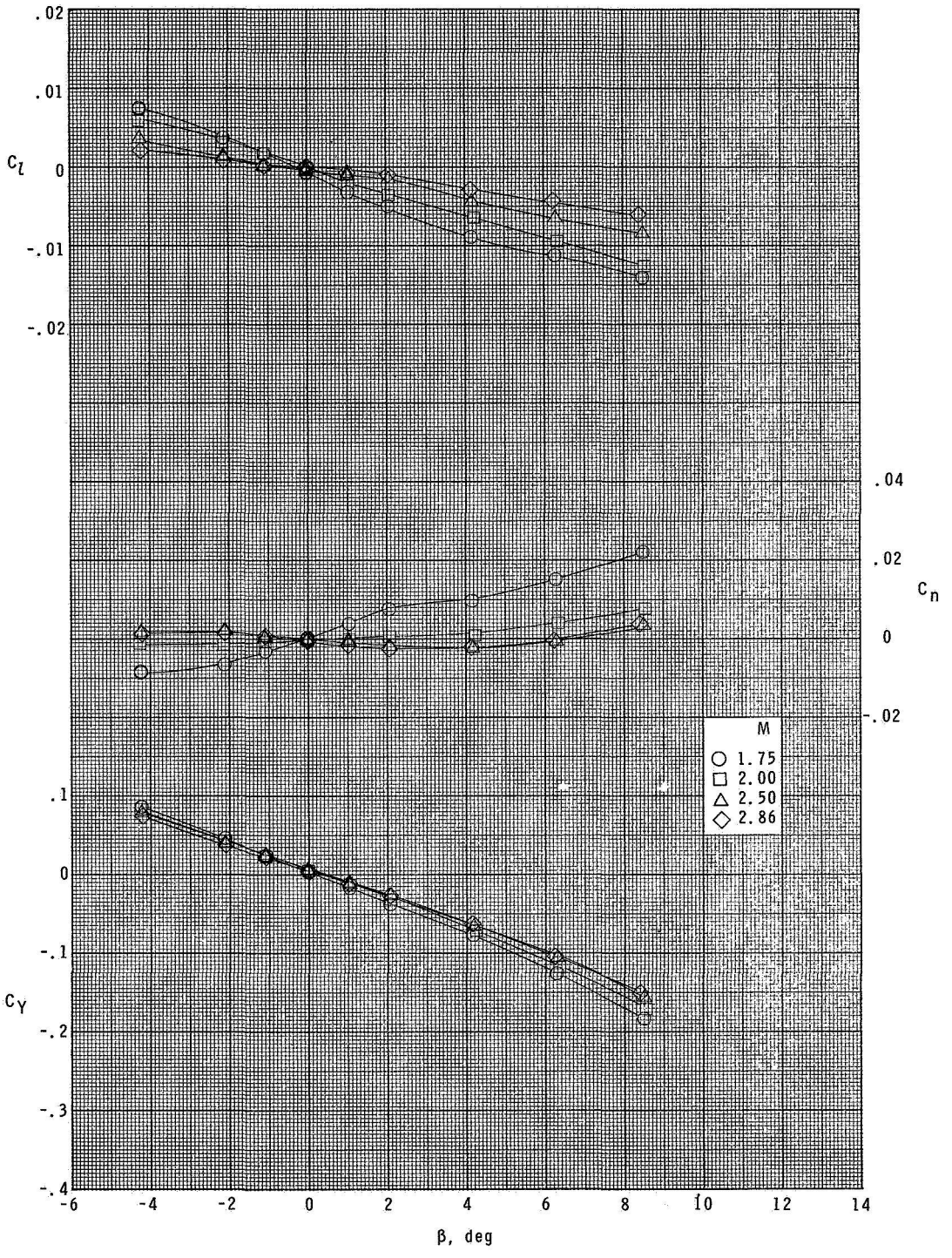
(a) N_{13}; $\delta_h = 0^0$; $\alpha \approx 0^0$.

Figure 17.- Variation of lateral aerodynamic coefficients with sideslip angle for $B_{11}X_{16}W_2H_9T_{12}V_{U5}Y_5$.



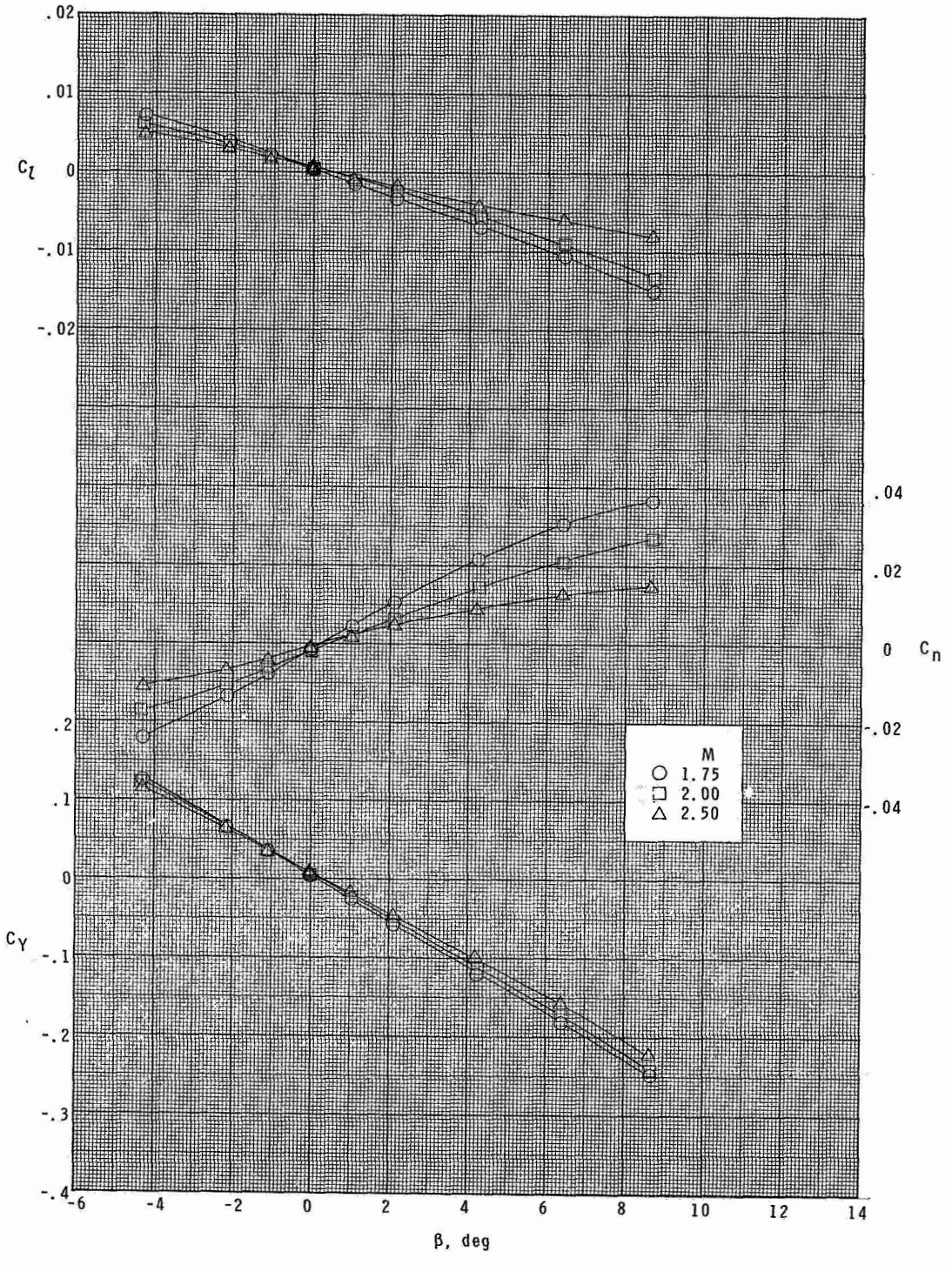
(b) N_{13}; $\delta_h = -20^0$; $\alpha \approx 10^0$.

Figure 17.- Continued.



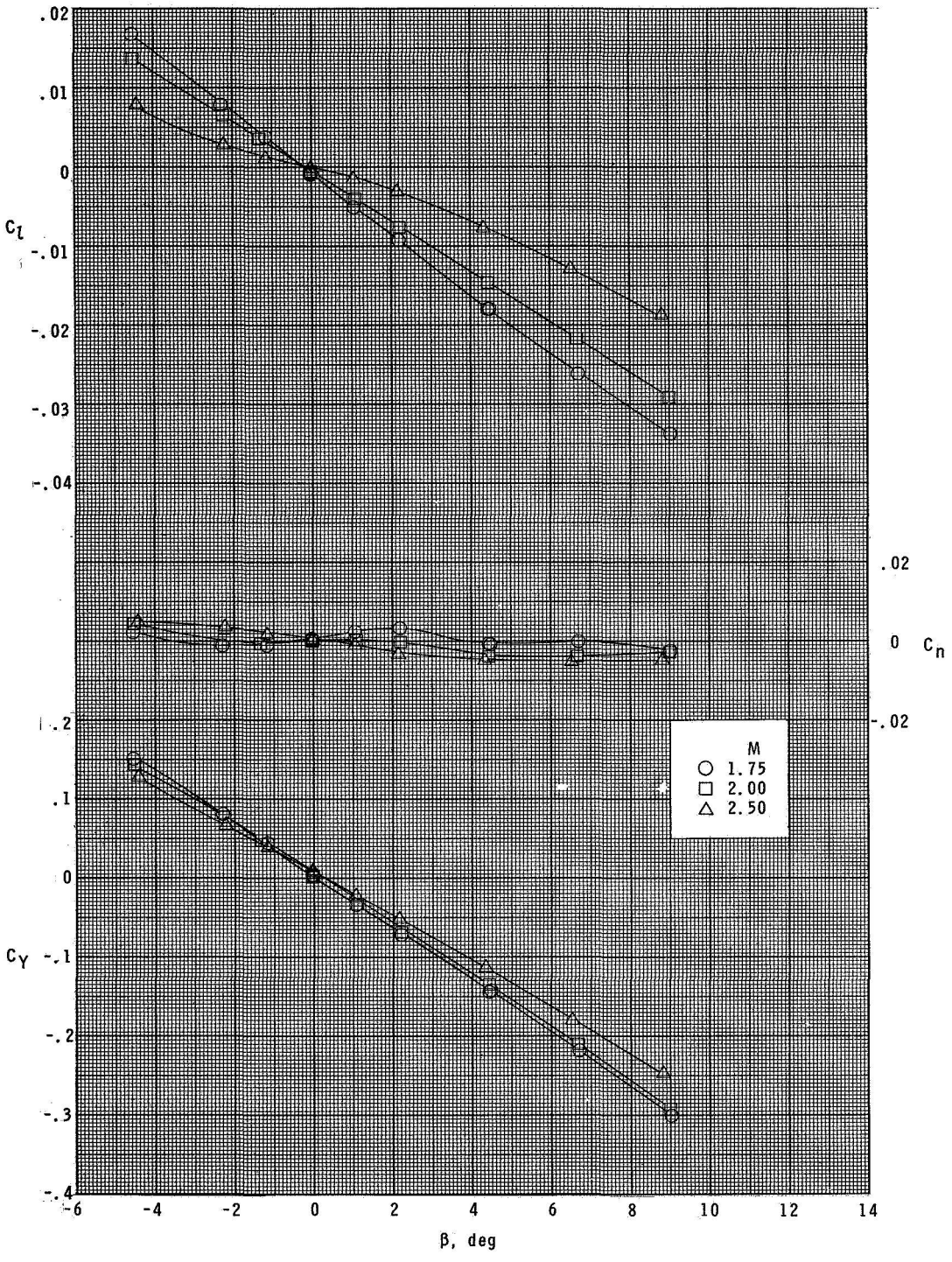
(c) HRE off; $\delta_h = -20^0$; $\alpha \approx 10^0$.

Figure 17.- Continued.



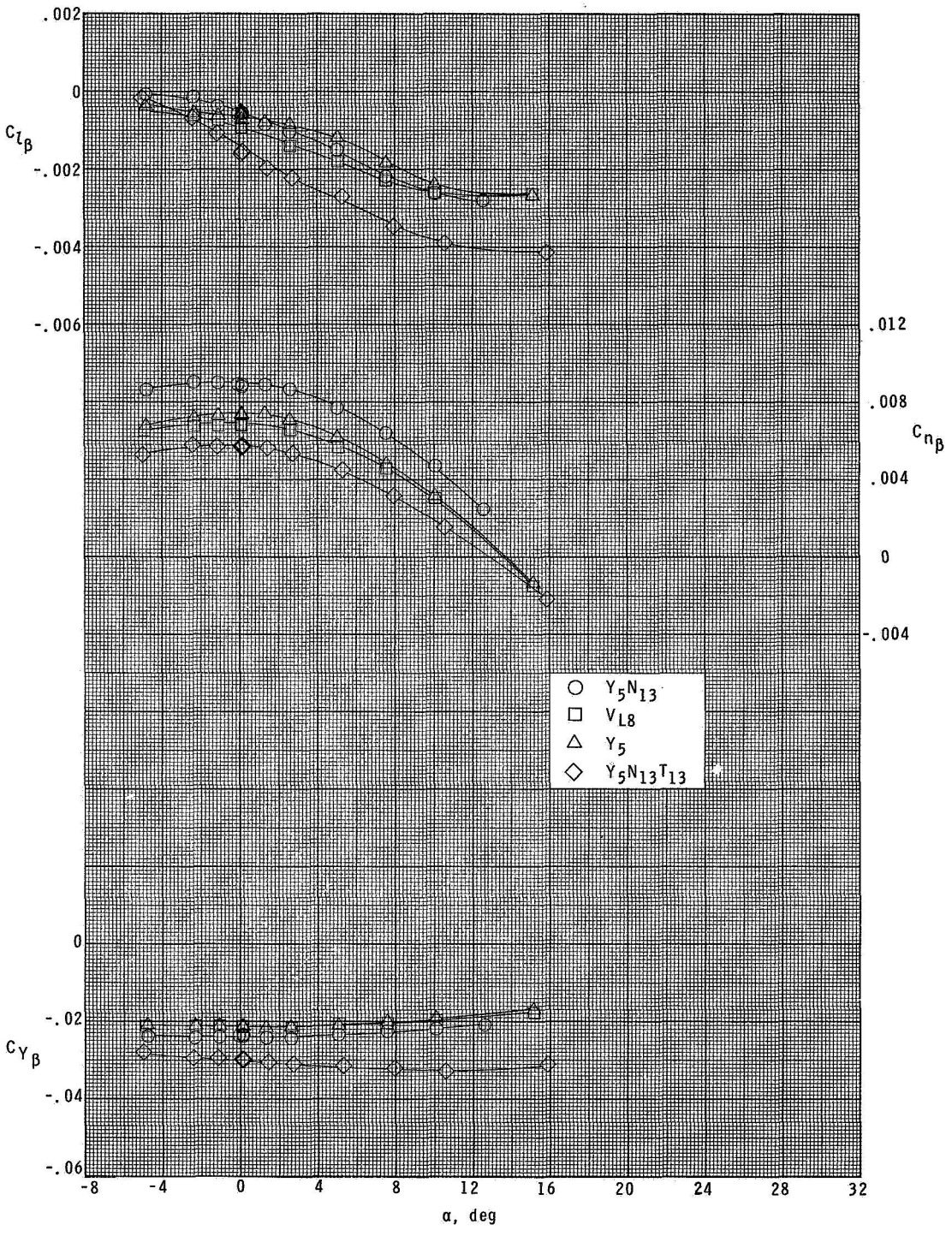
(d) $N_{13}T_{13}$ (tanks on); $\delta_h = 5^0$; $\alpha \approx 0^0$.

Figure 17.- Continued.



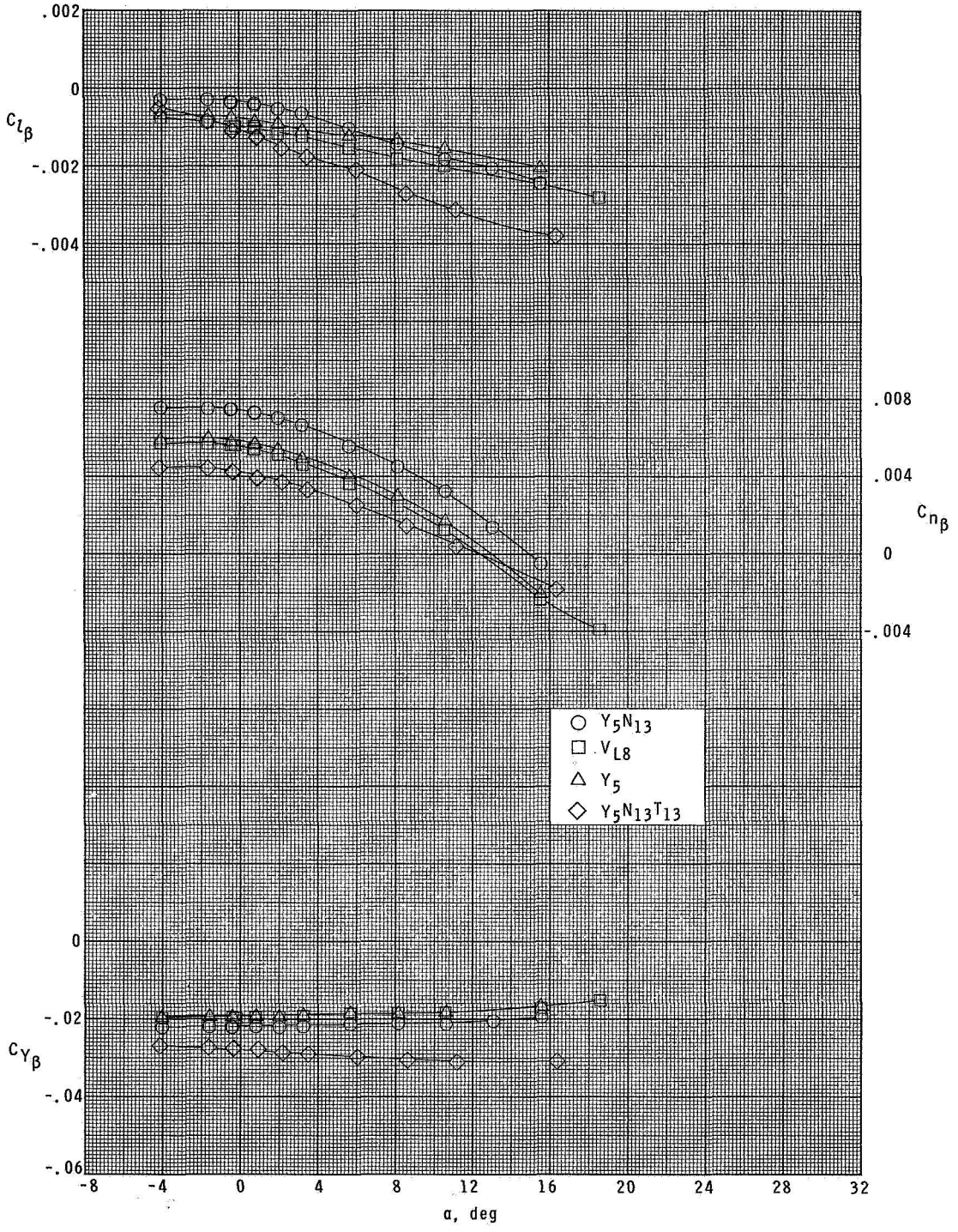
(e) $N_{13}T_{13}$ (tanks on); $\delta_h = -5^o$; $\alpha \approx 10^o$.

Figure 17.- Concluded.



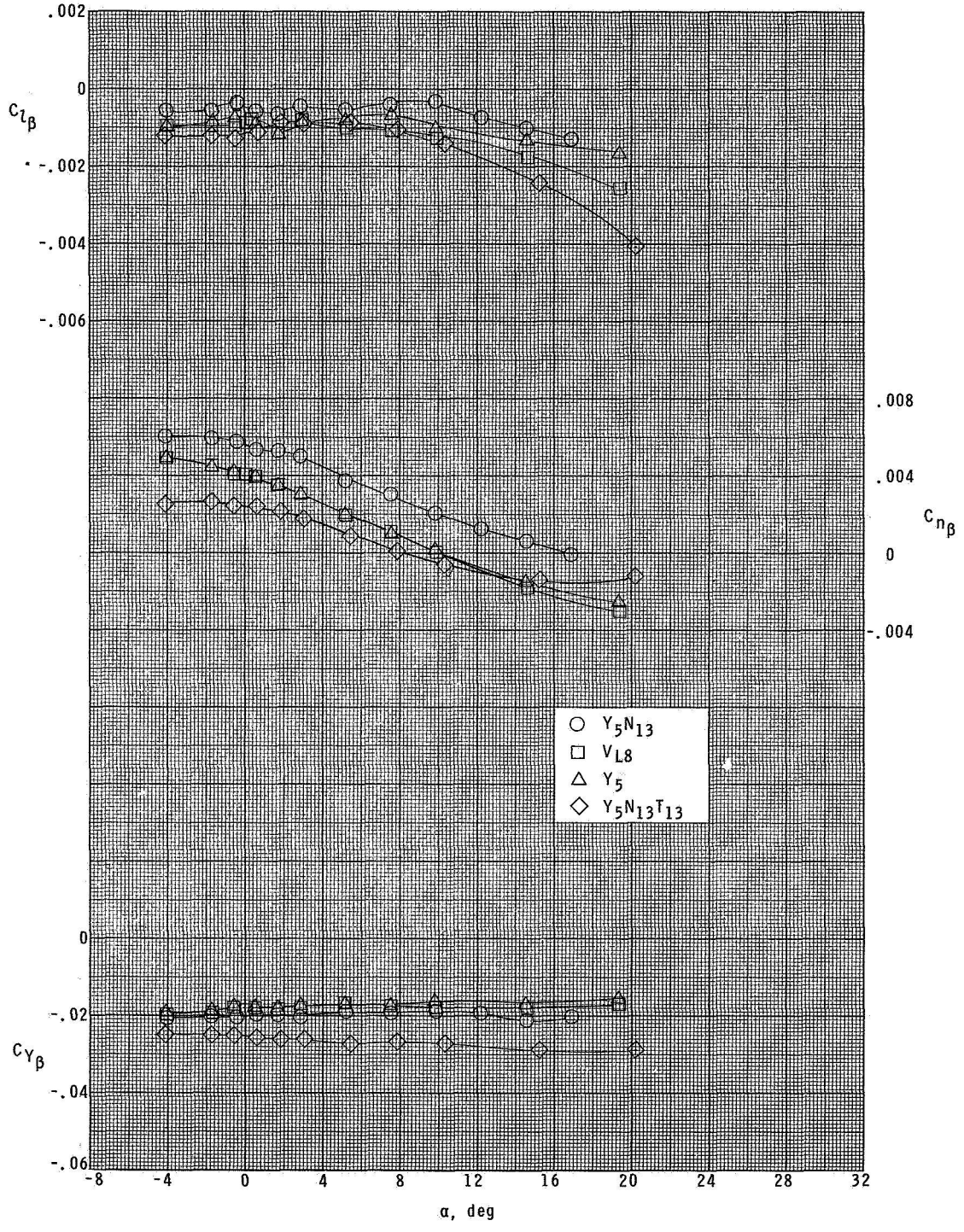
(a) M = 1.75.

Figure 18.- Effect of HRE components and fuel tanks on lateral stability parameters for $B_{11}X_{16}W_2H_9T_{12}V_{U5}$.



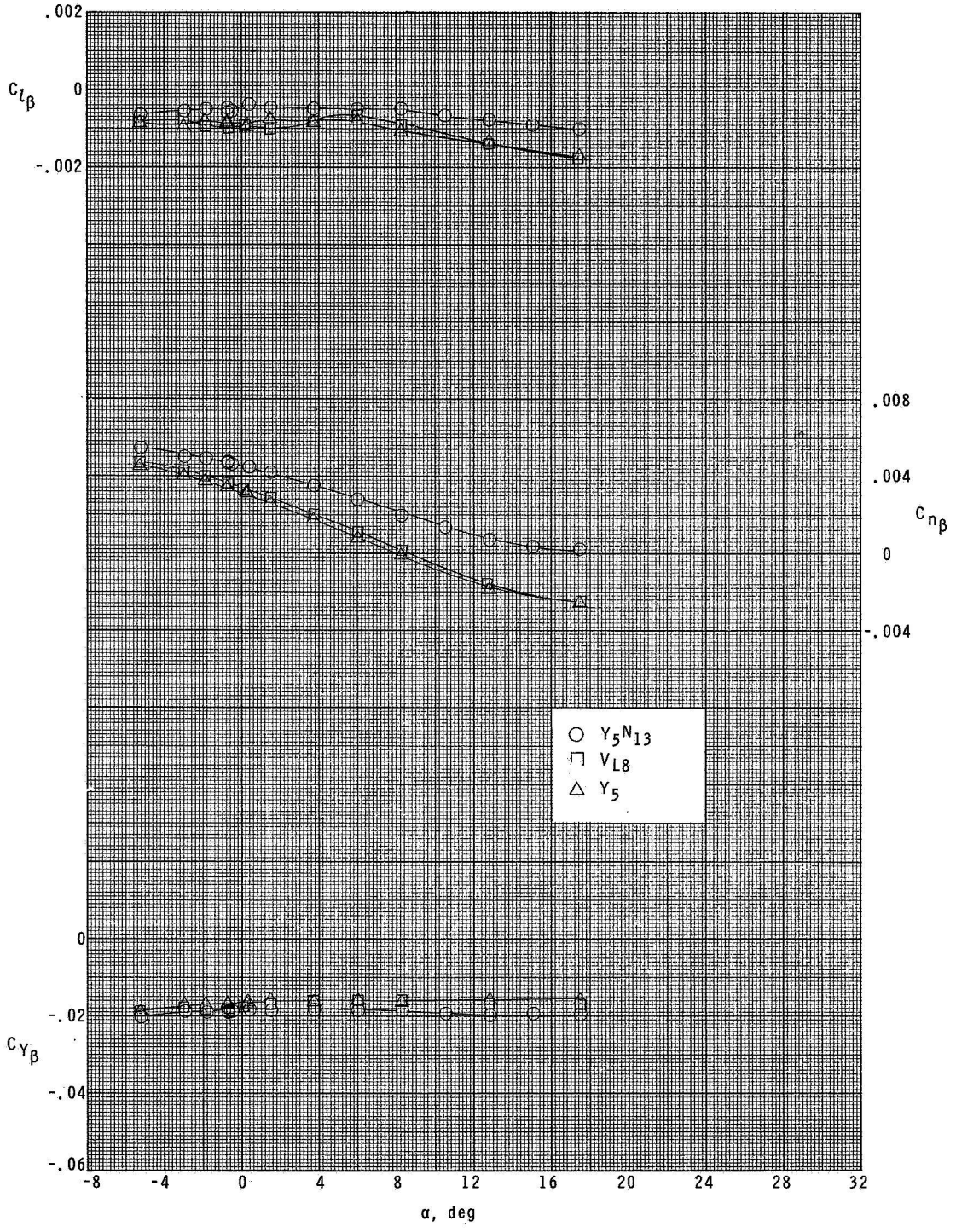
(b) M = 2.00.

Figure 18.- Continued.



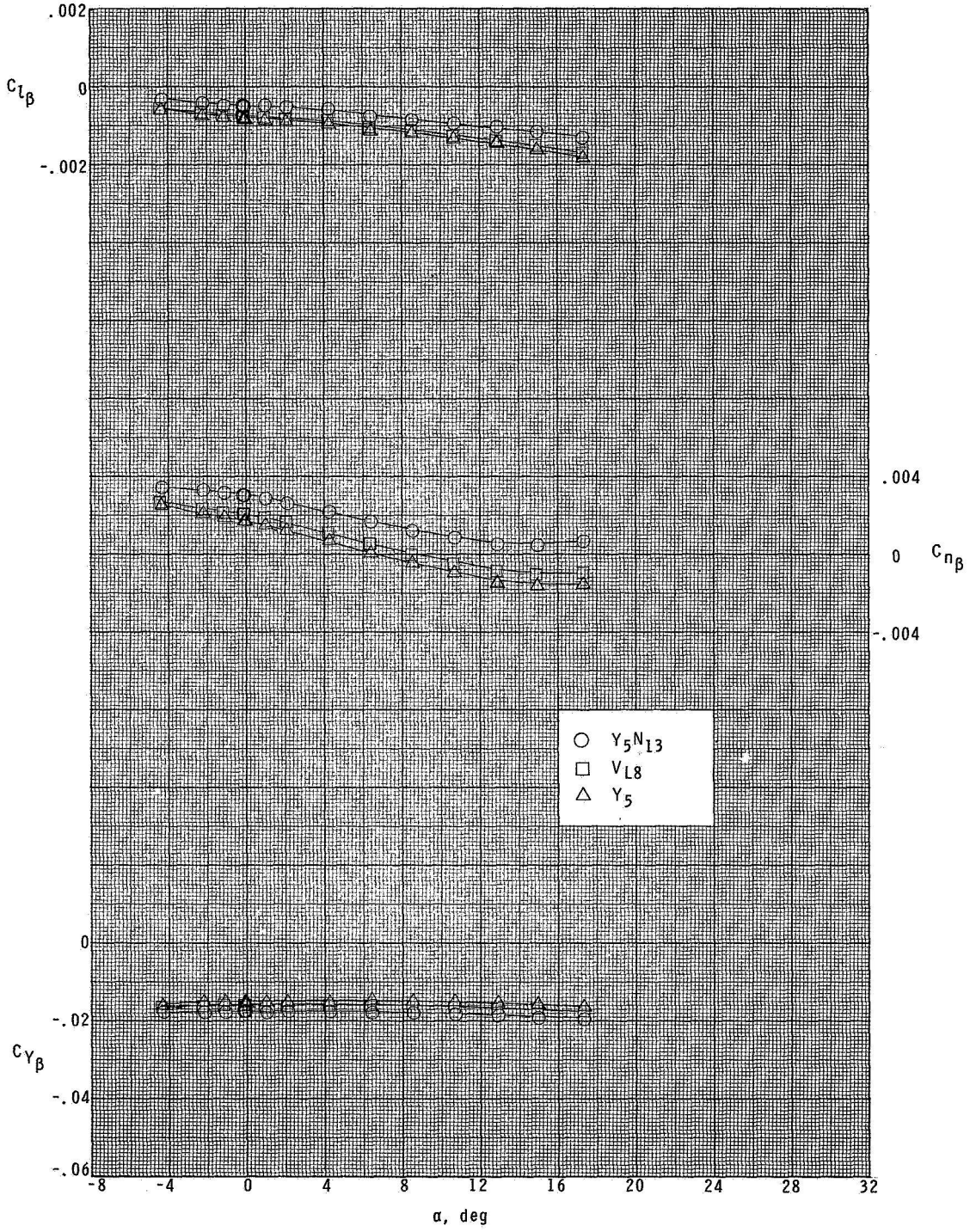
(c) M = 2.50.

Figure 18.- Continued.



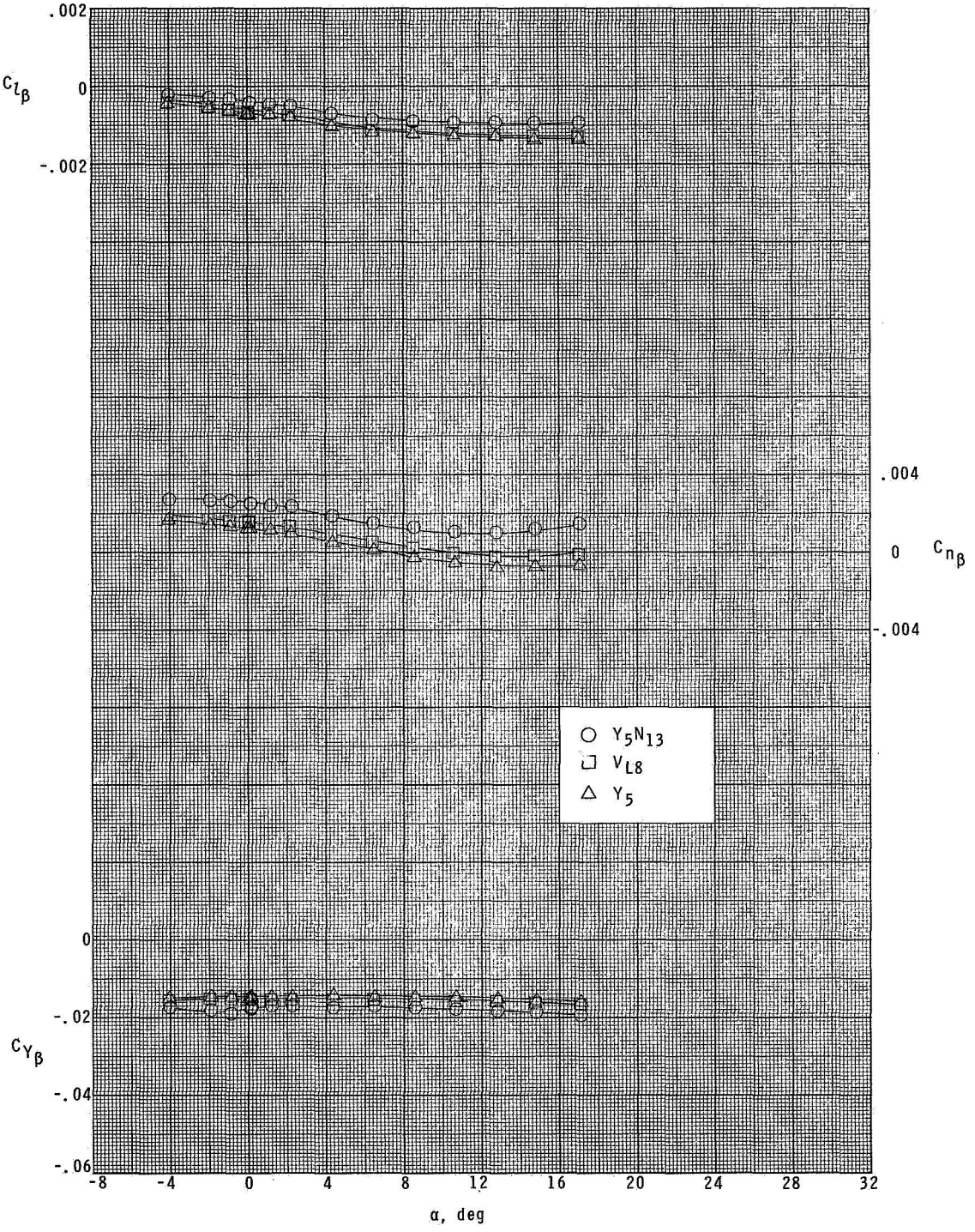
(d) M = 2.86.

Figure 18.- Continued.



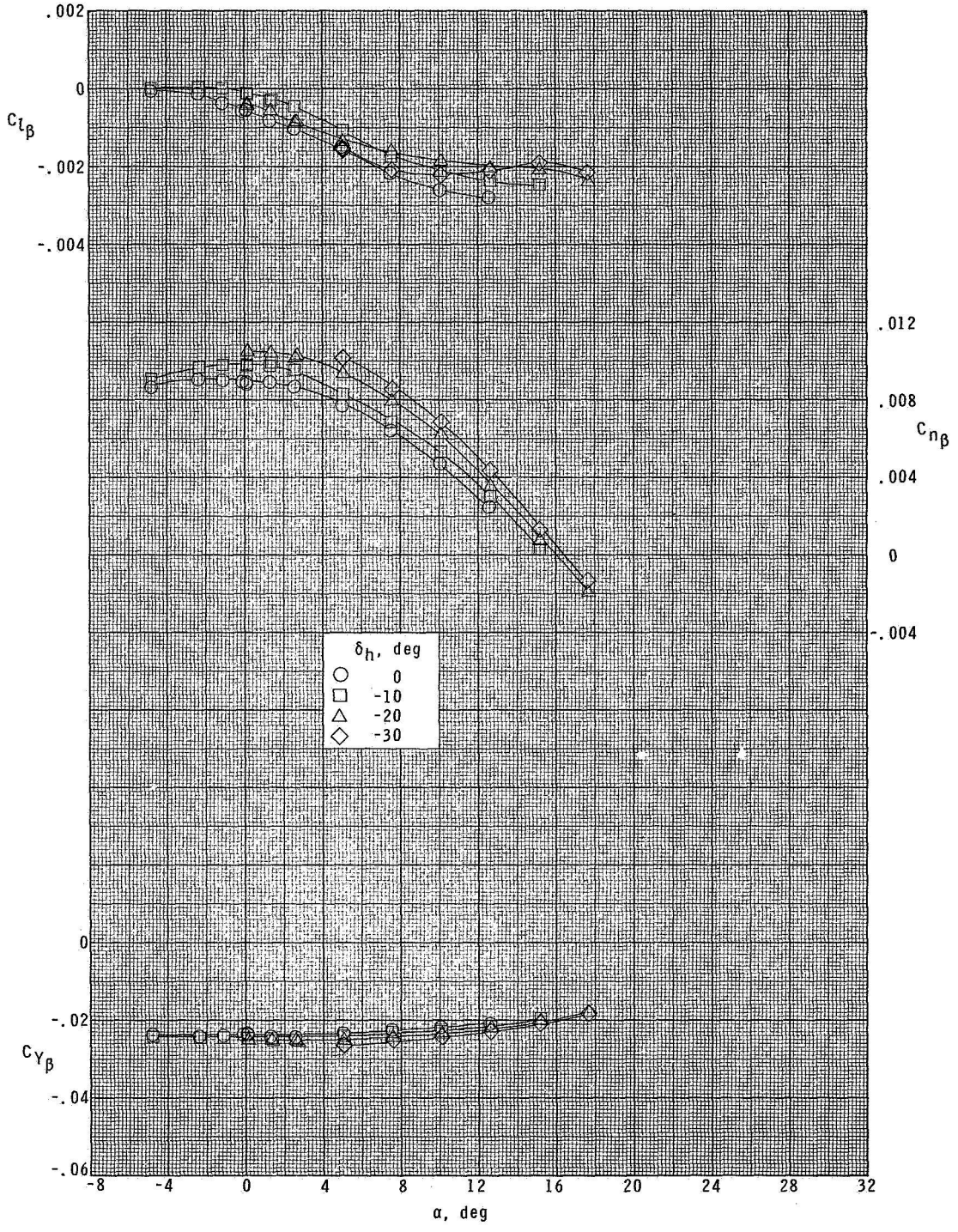
(e) M = 3.95.

Figure 18.- Continued.



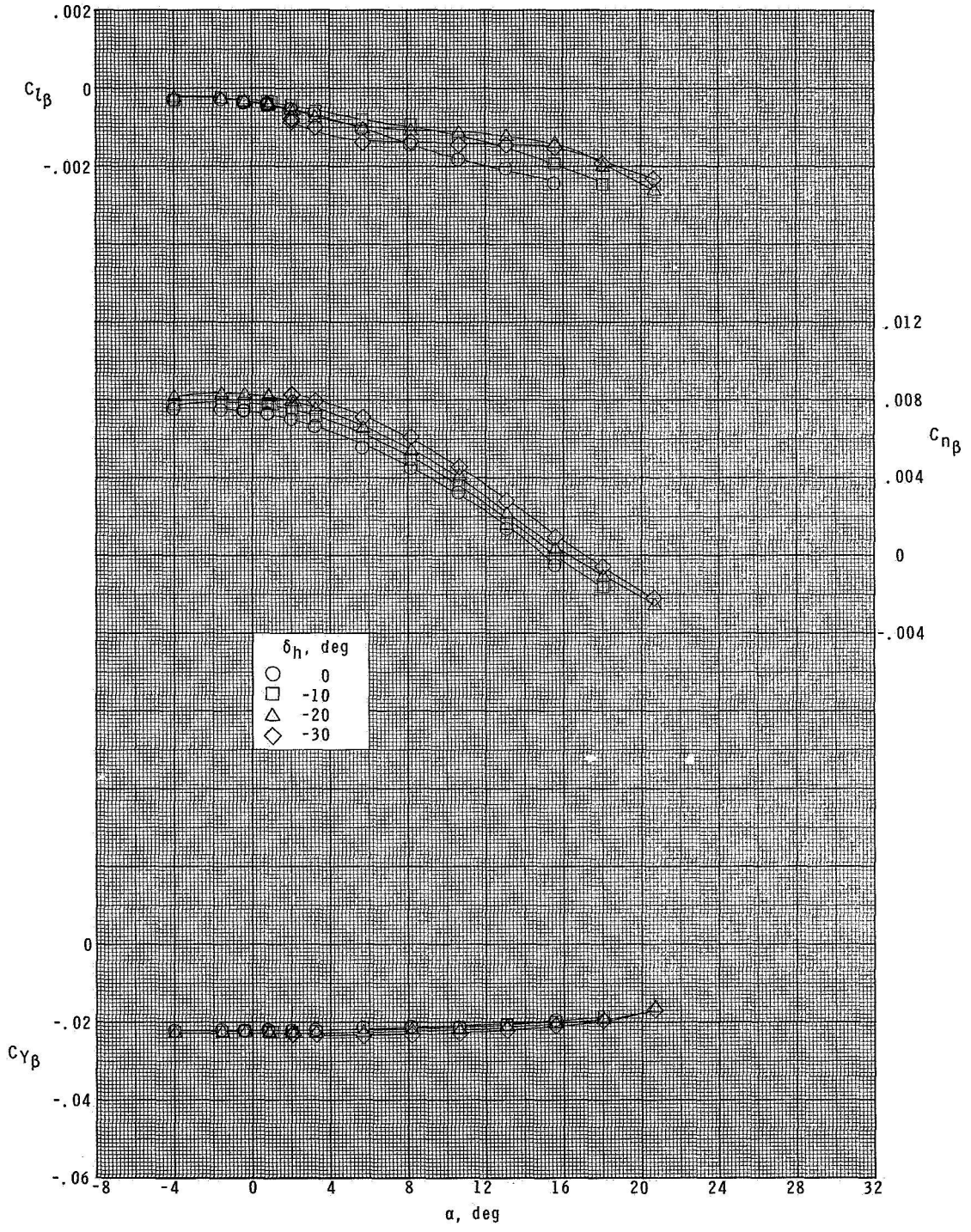
(f) M = 4.63.

Figure 18.- Concluded.



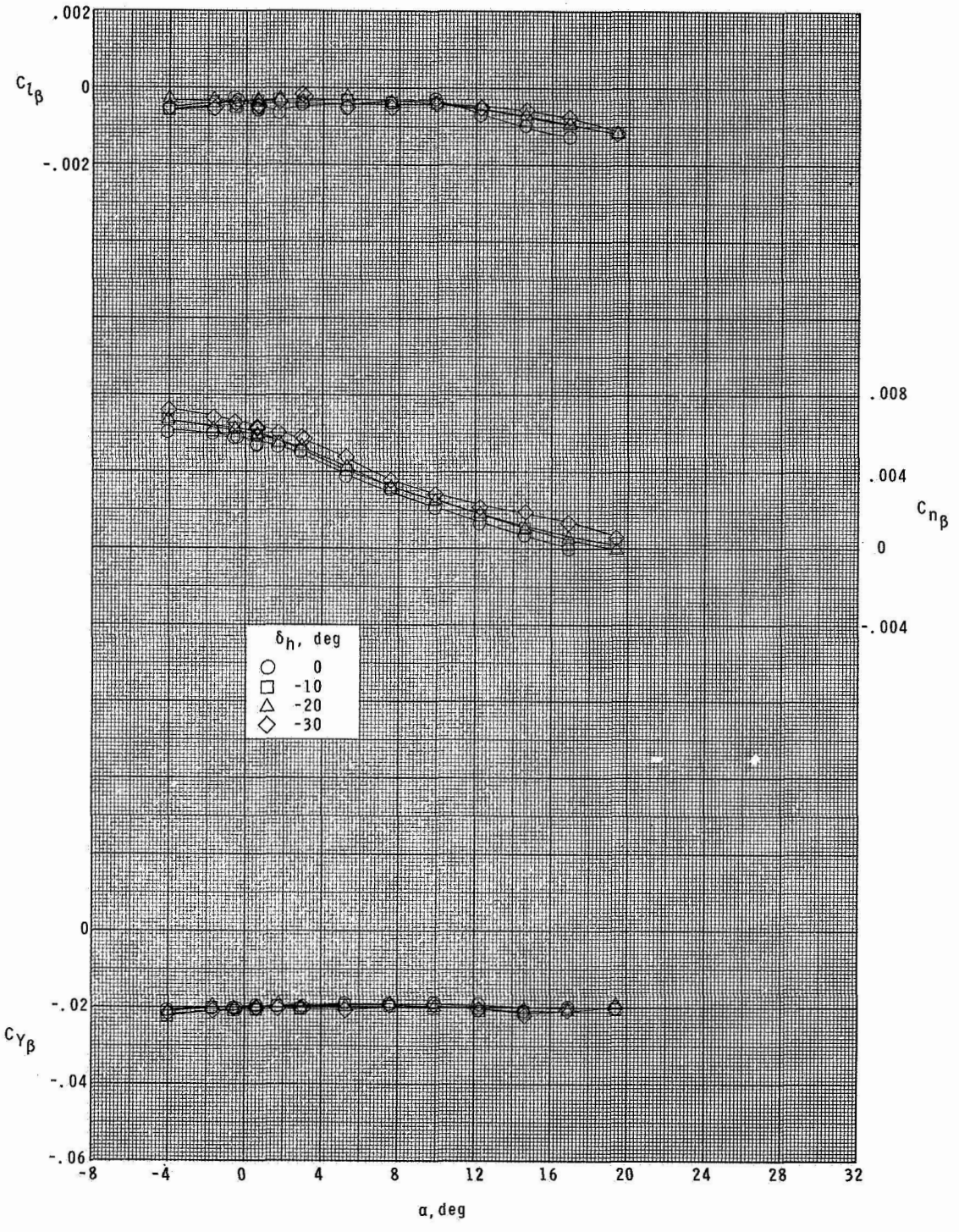
(a) M = 1.75.

Figure 19.- Effect of horizontal-tail deflection on lateral stability parameters for $B_{11}X_{16}W_2H_9T_{12}V_{U5}Y_5N_{13}$ (HRE on).



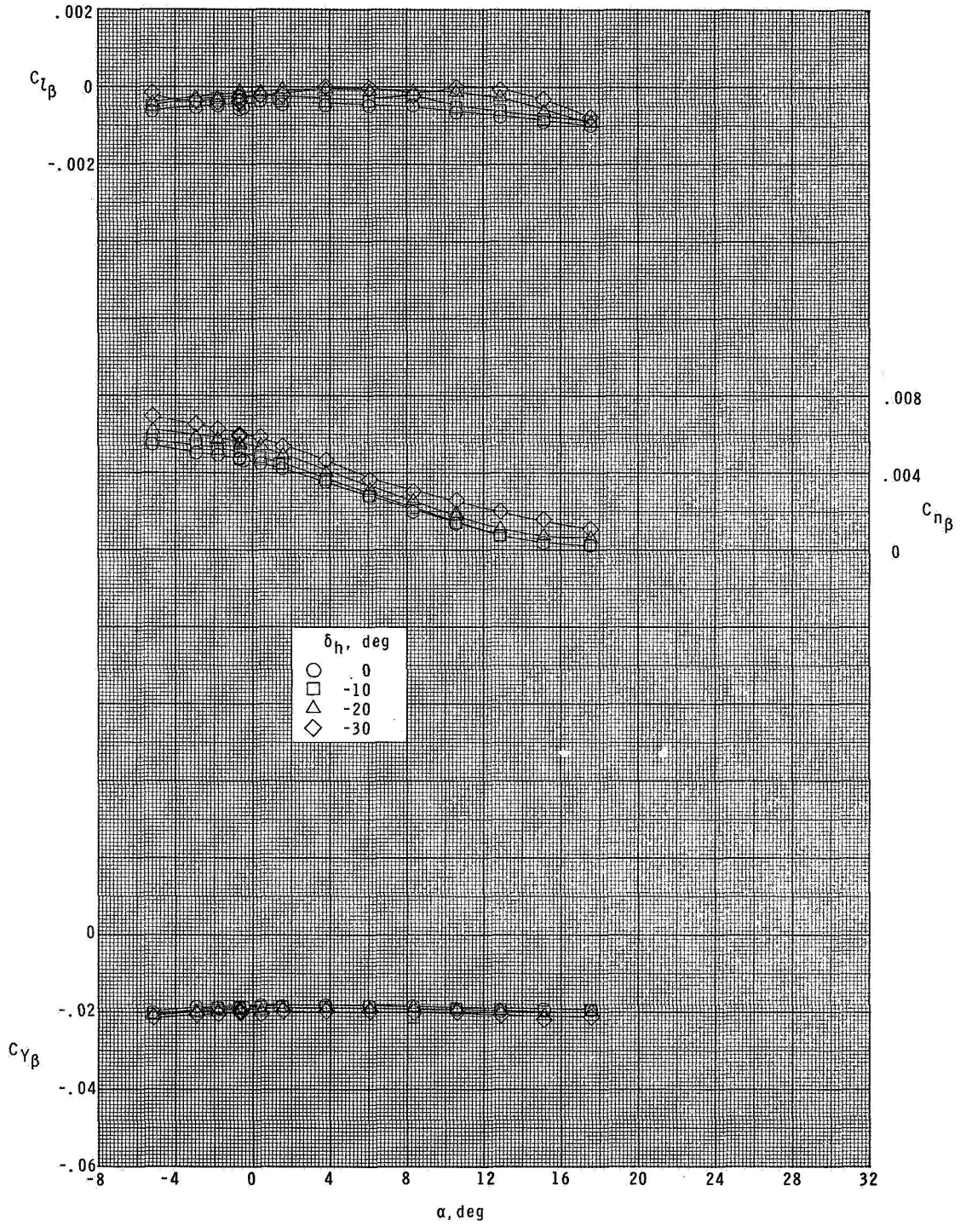
(b) M = 2.00.

Figure 19.- Continued.



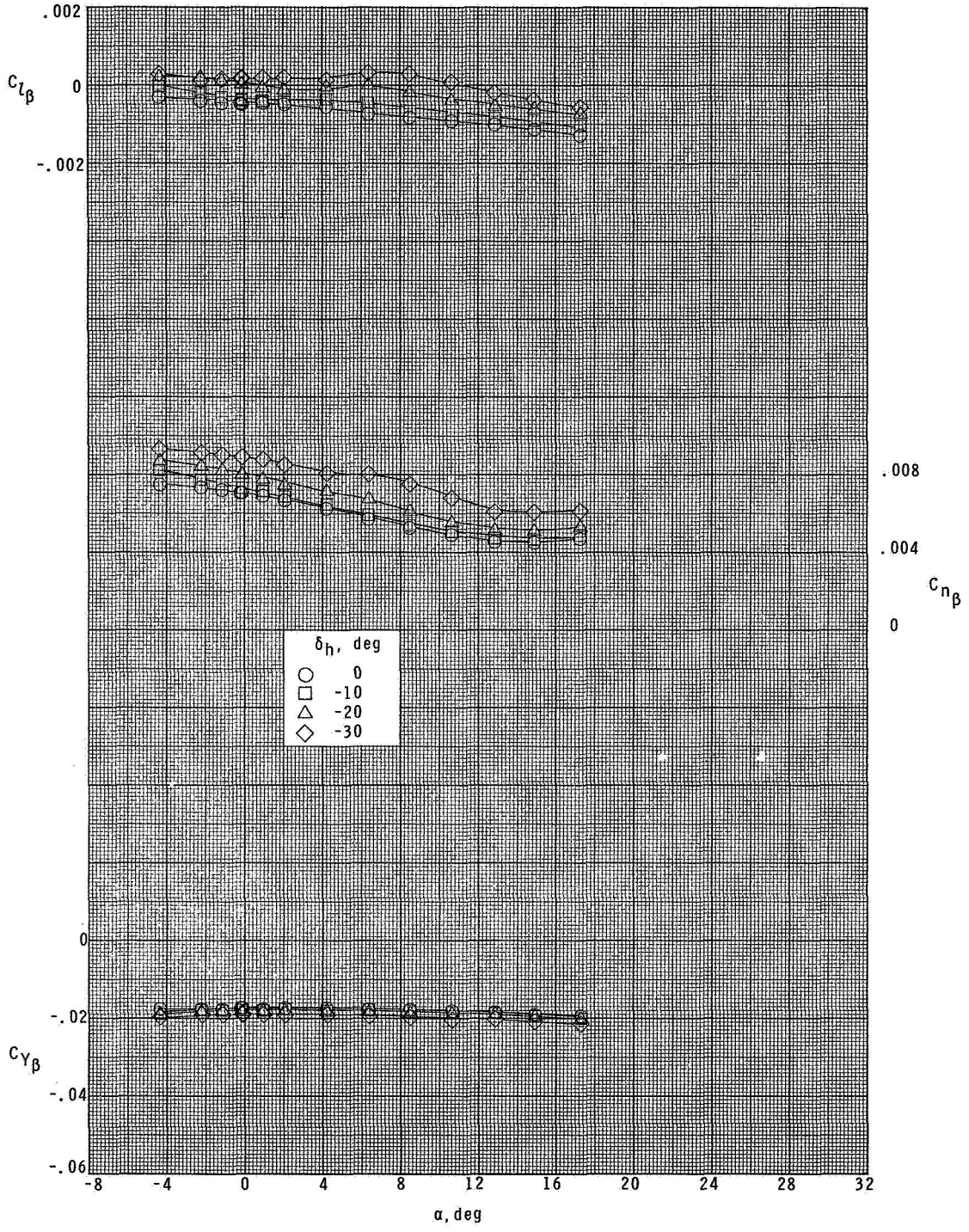
(c) M = 2.50.

Figure 19.- Continued.



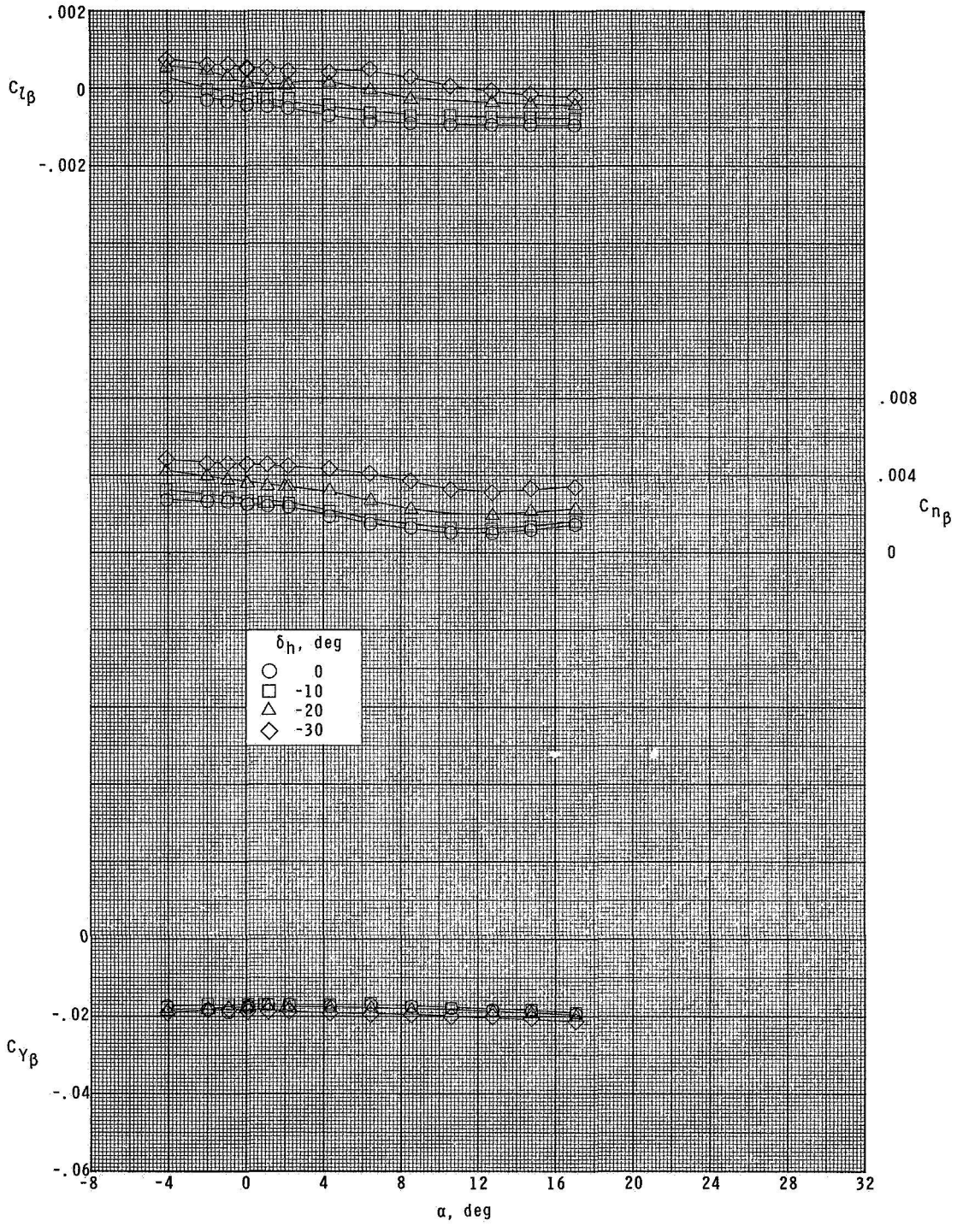
(d) M = 2.86.

Figure 19.- Continued.



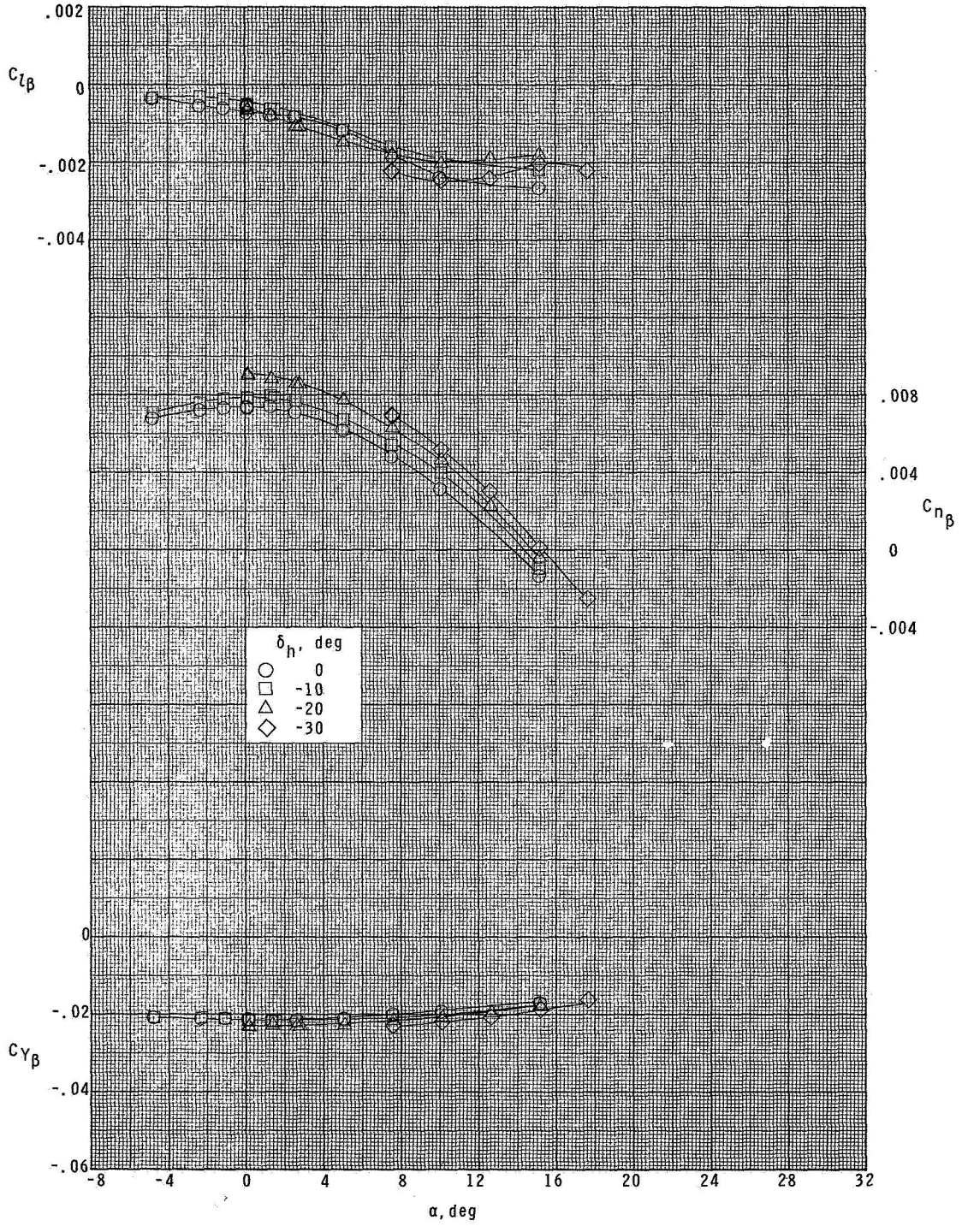
(e) M = 3.95.

Figure 19.- Continued.



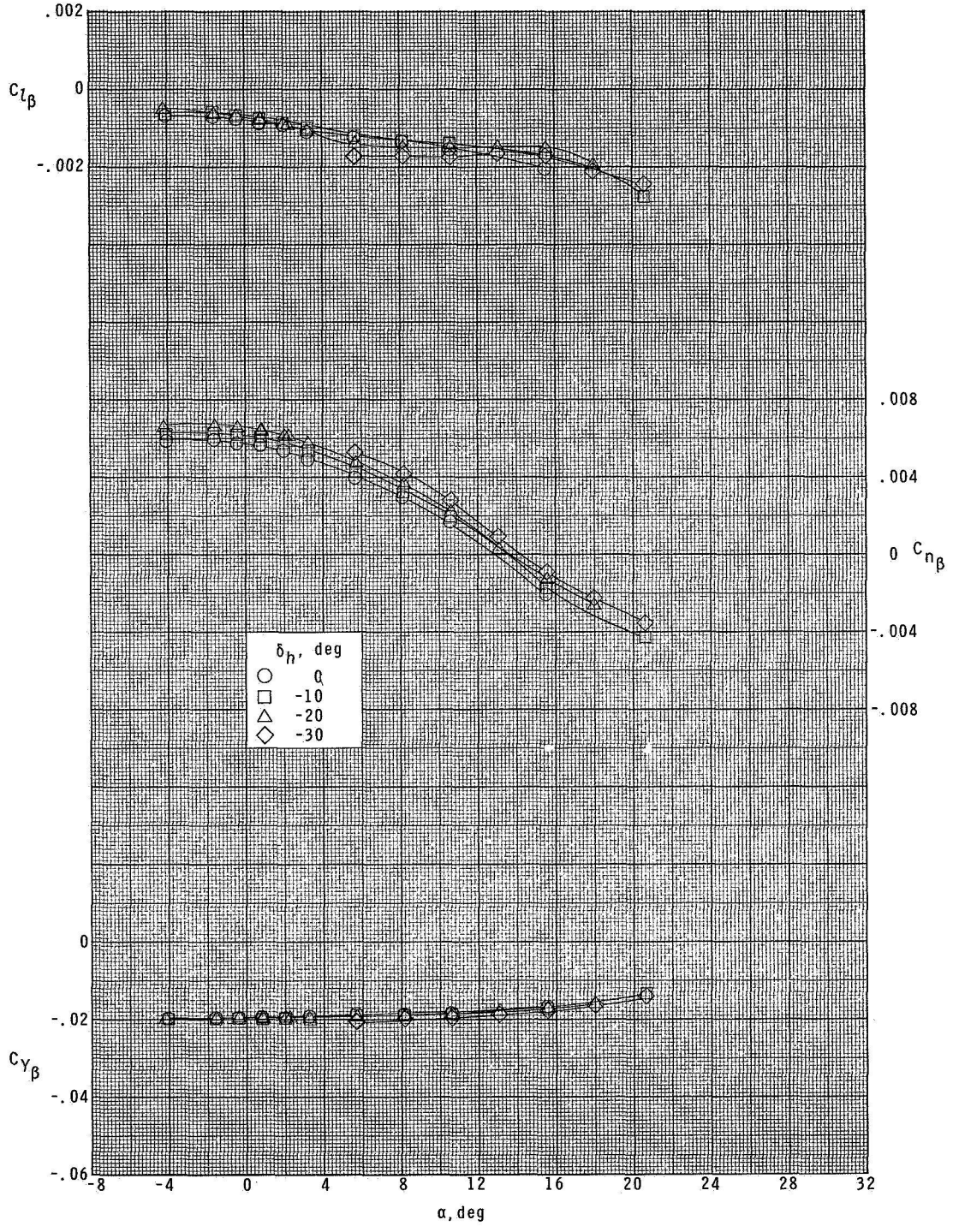
(f) M = 4.63.

Figure 19.- Concluded.



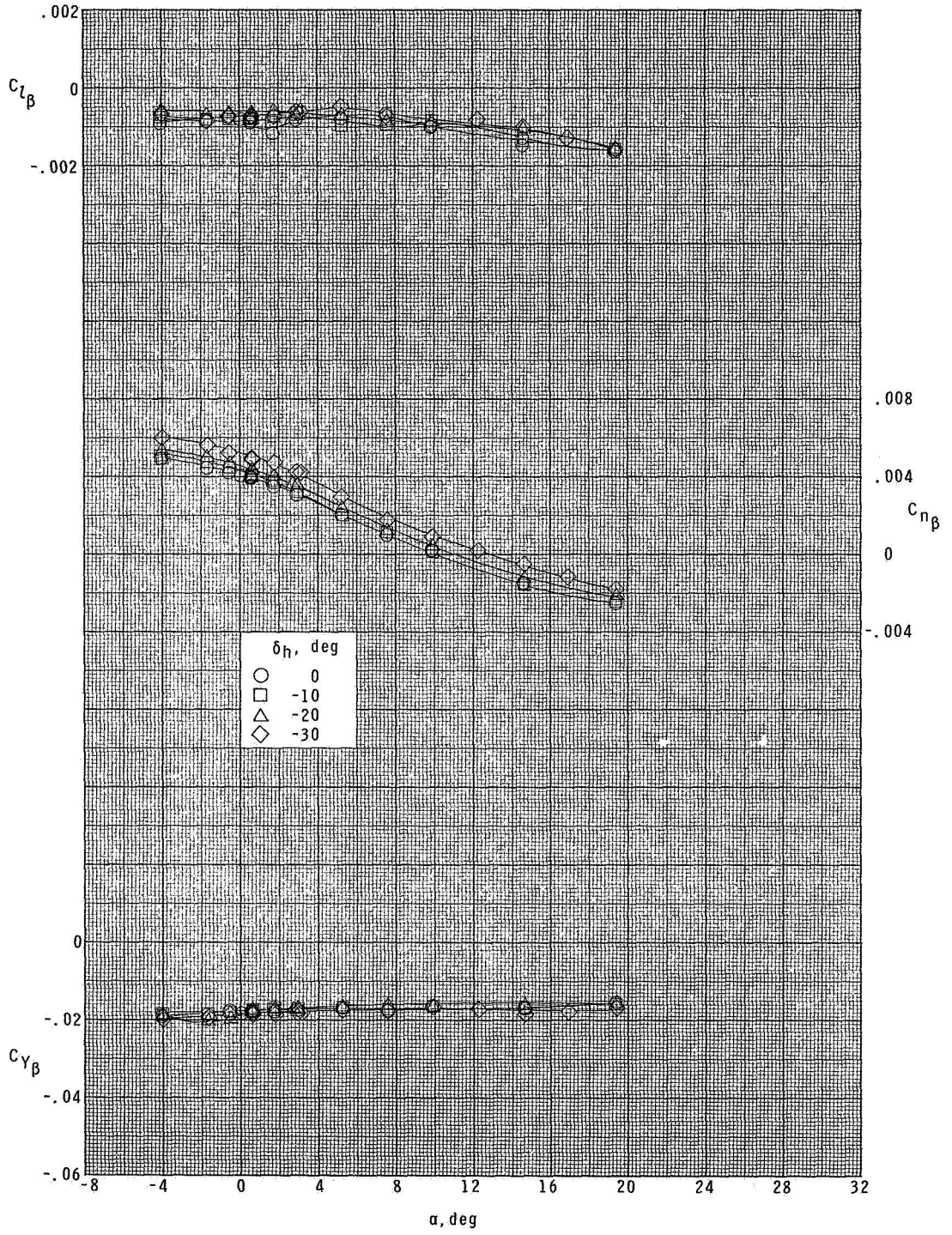
(a) M = 1.75.

Figure 20.- Effect of horizontal-tail deflection on lateral stability parameters for $B_{11}X_{16}W_2H_9T_{12}V_{U5}Y_5$ (HRE off).



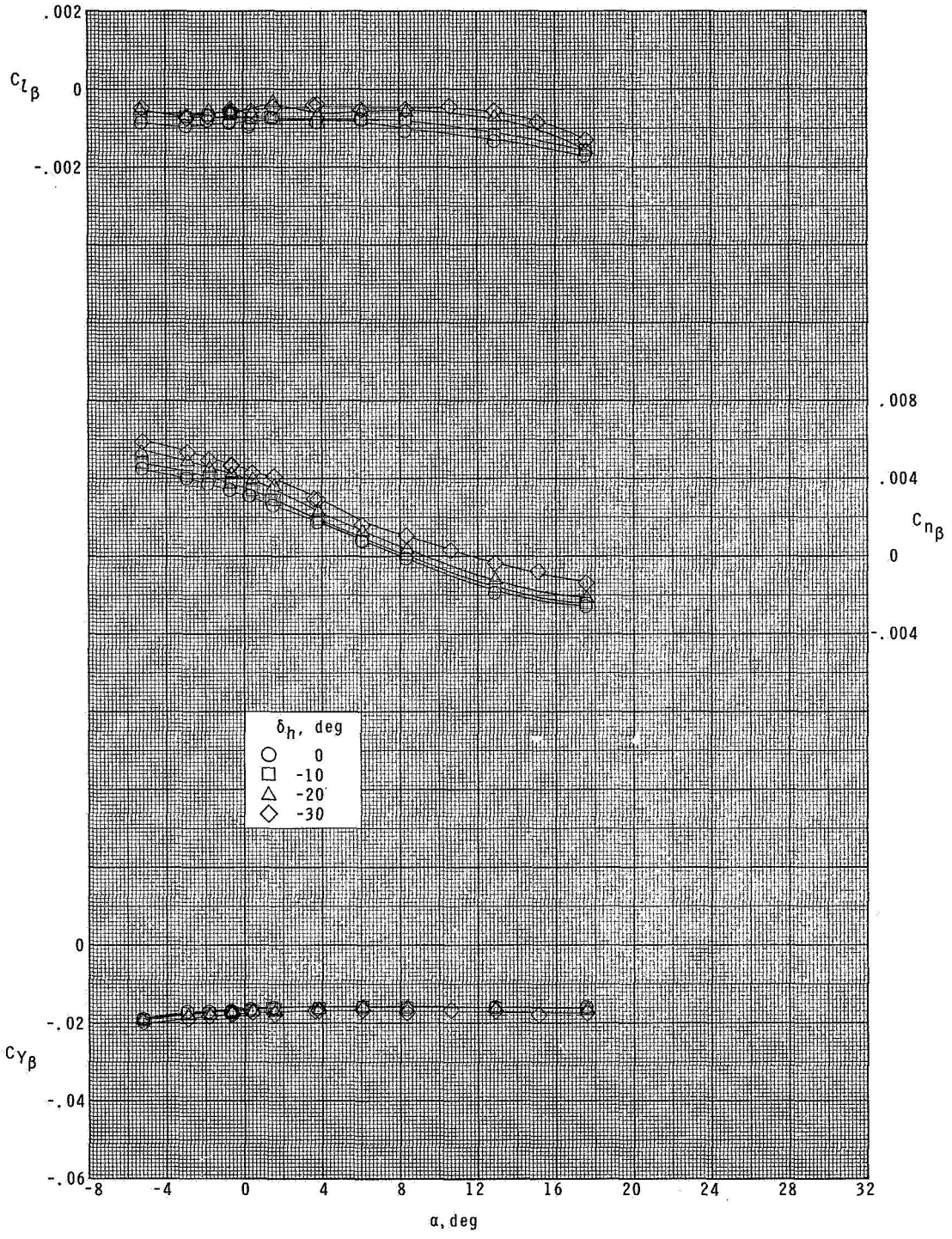
(b) M = 2.00.

Figure 20.- Continued.



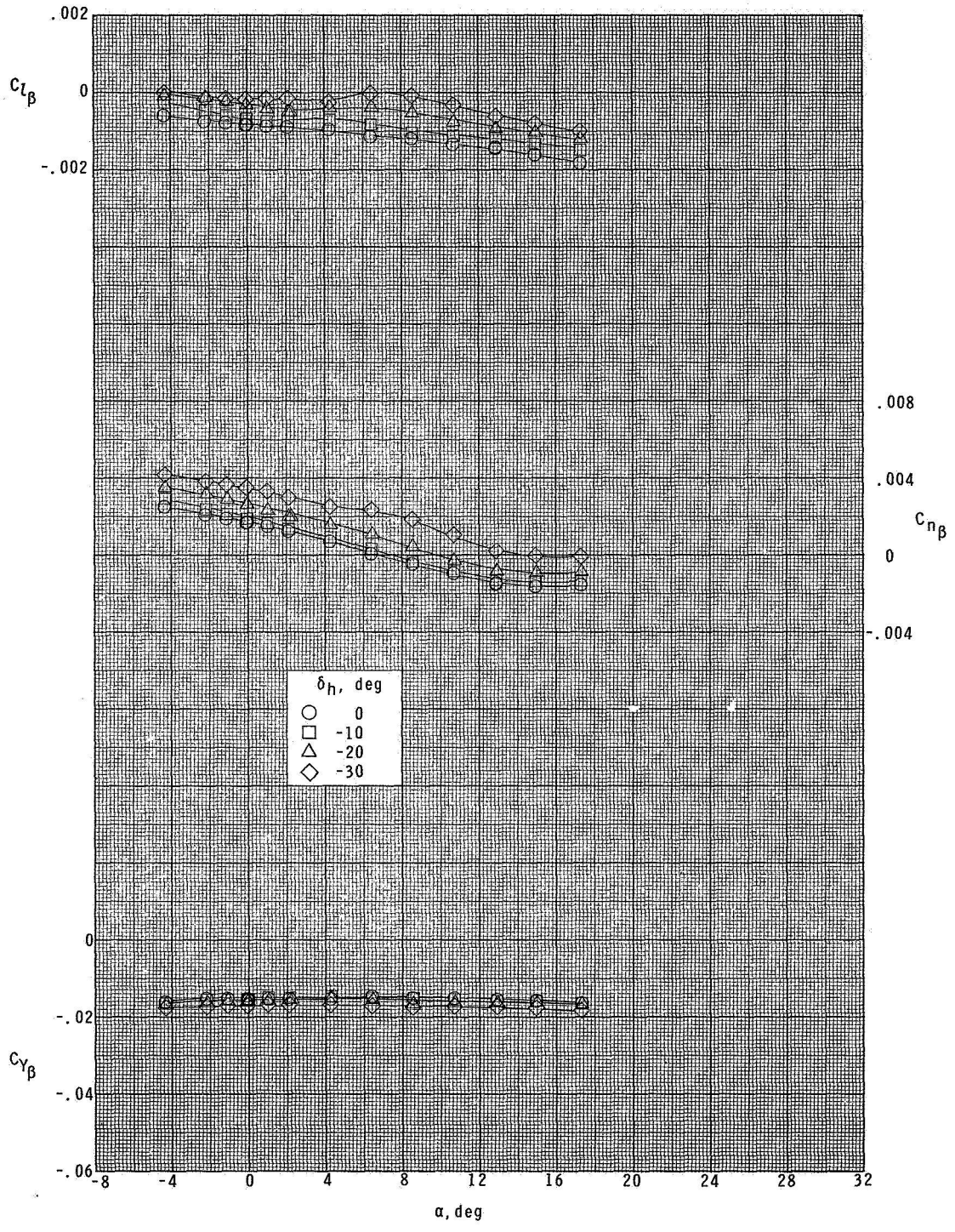
(c) M = 2.50.

Figure 20.- Continued.



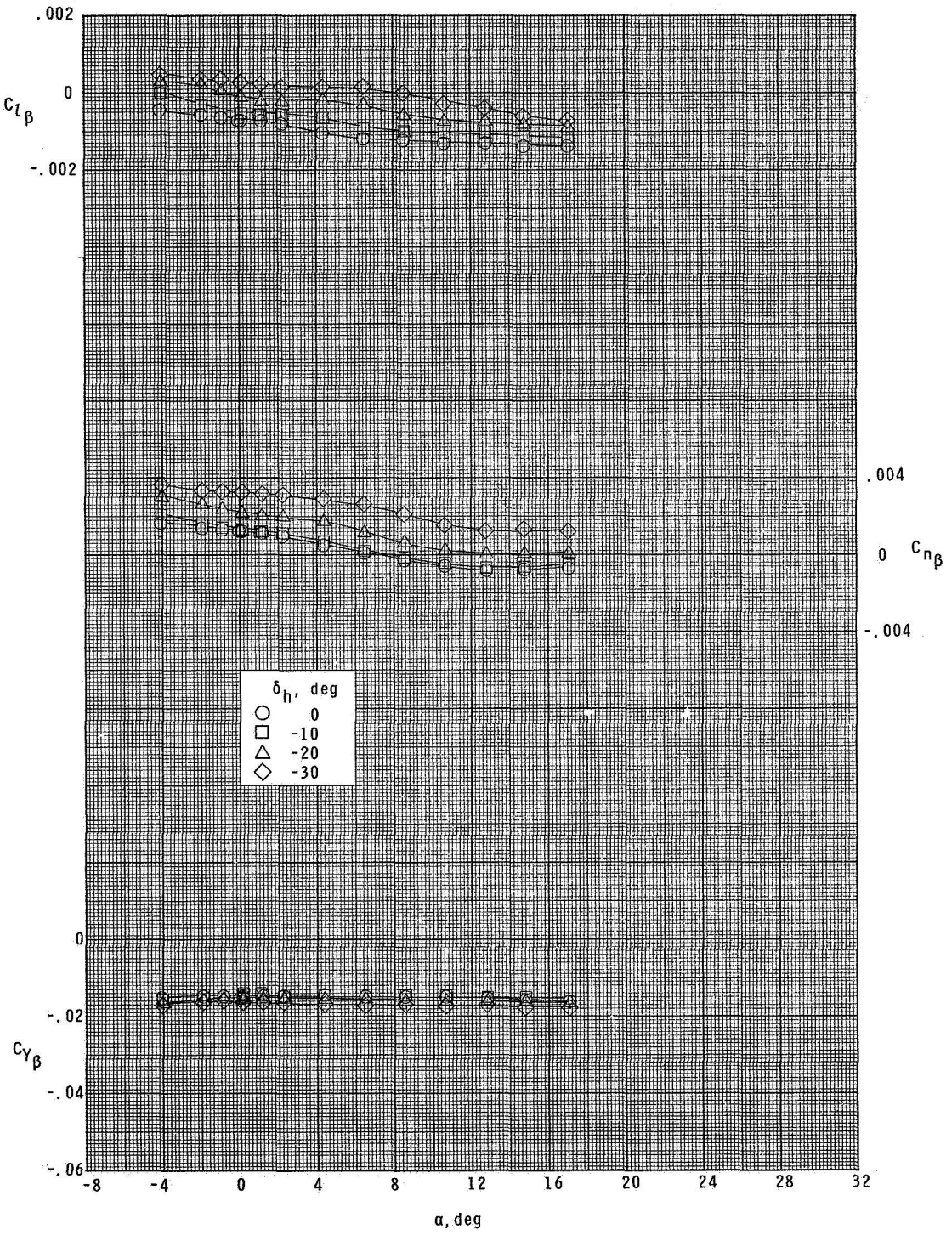
(d) M = 2.86.

Figure 20.- Continued.



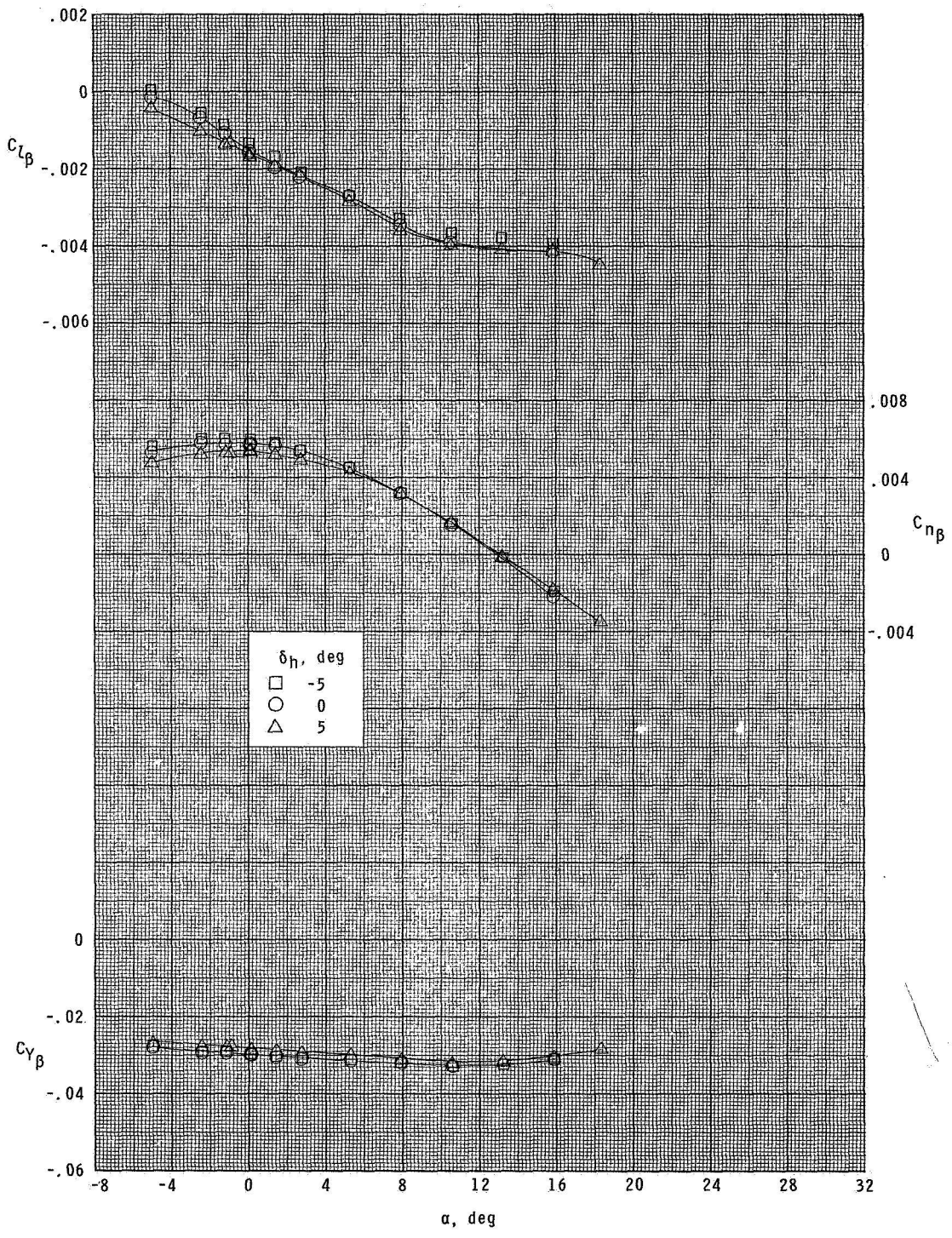
(e) M = 3.95.

Figure 20.- Continued.



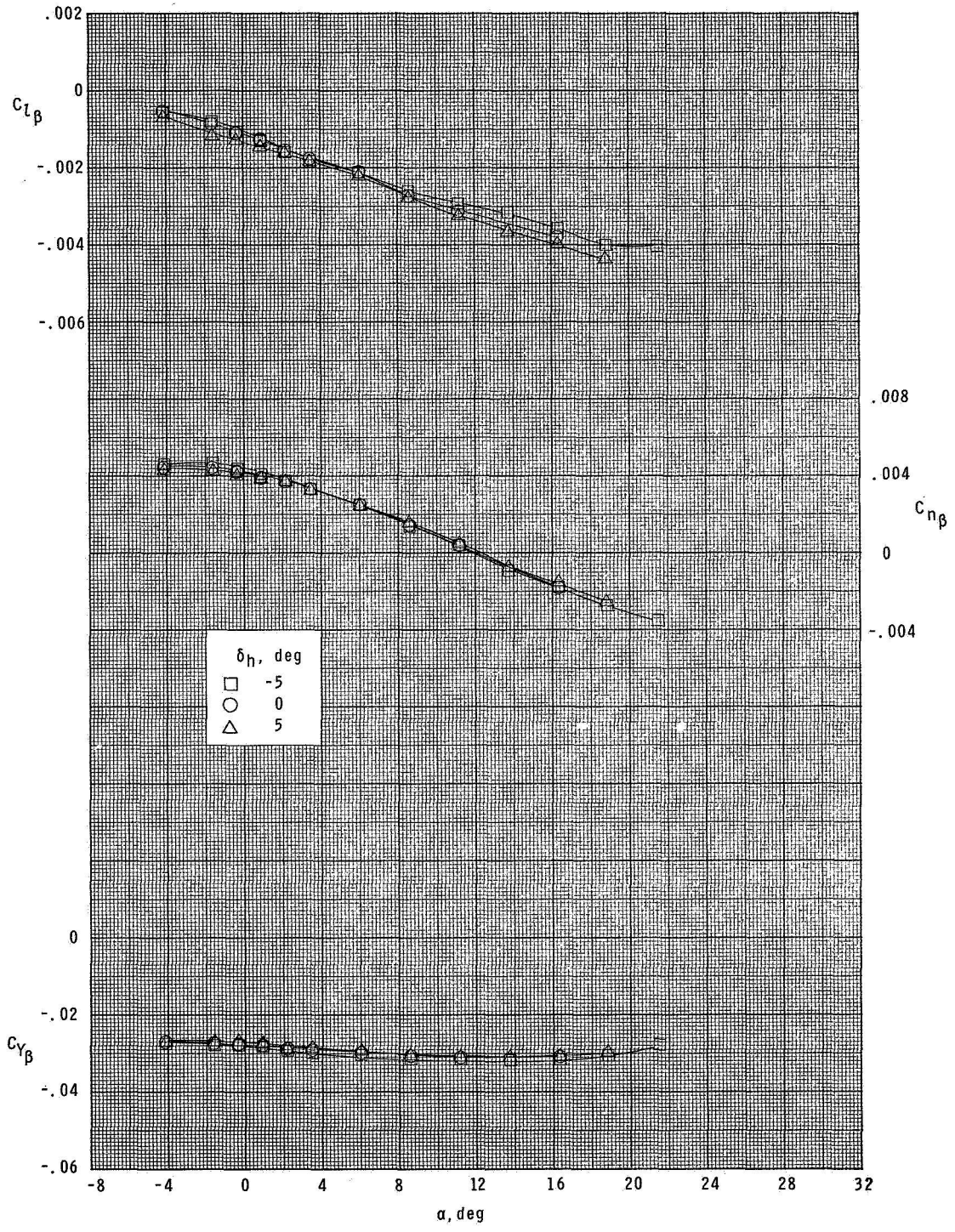
(f) M = 4.63.

Figure 20.- Concluded.



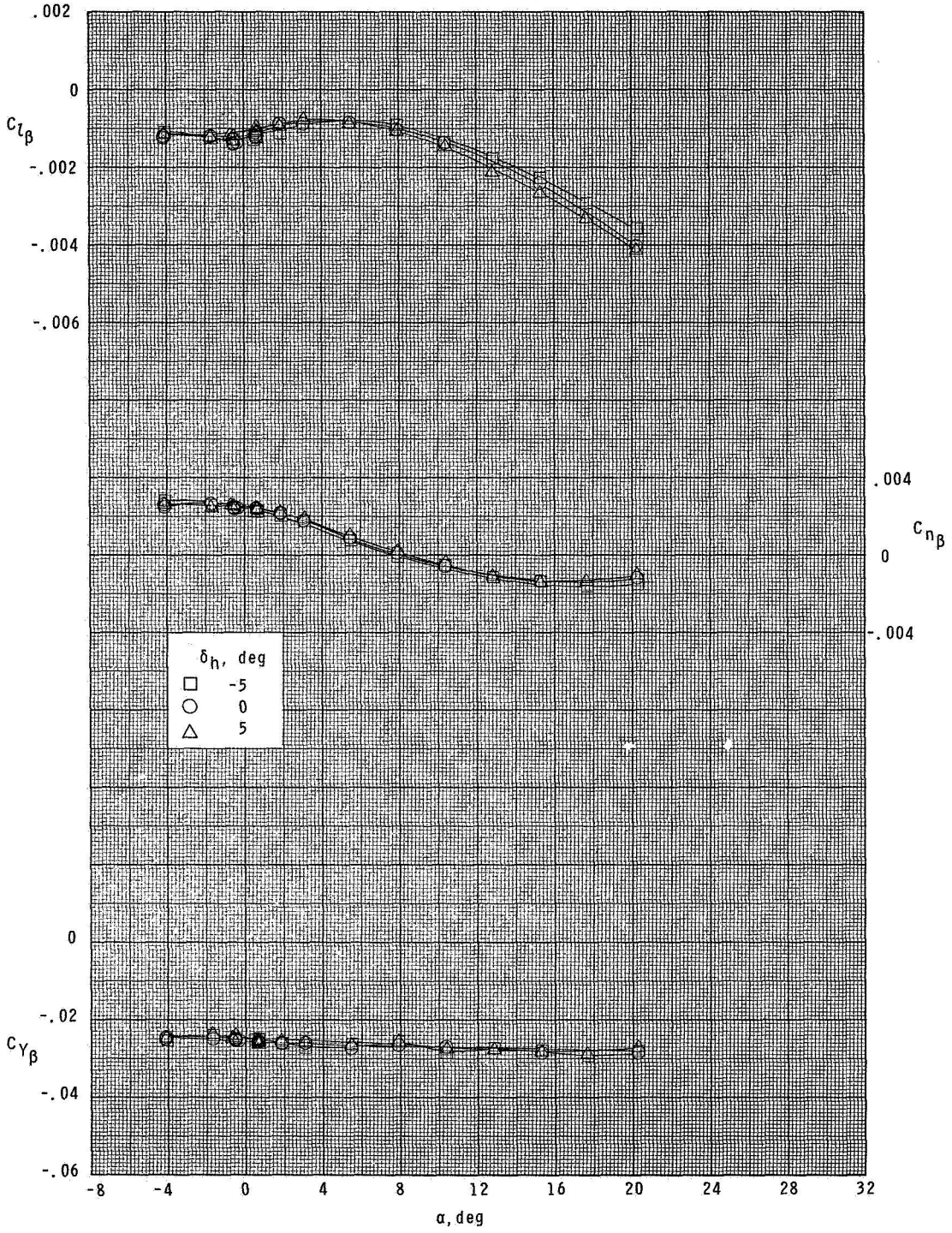
(a) M = 1.75.

Figure 21.- Effect of horizontal-tail deflection on lateral stability parameters for $B_{11}X_{16}W_2H_9T_{12}V_{U5}Y_5N_{13}T_{13}$ (HRE and tanks on).



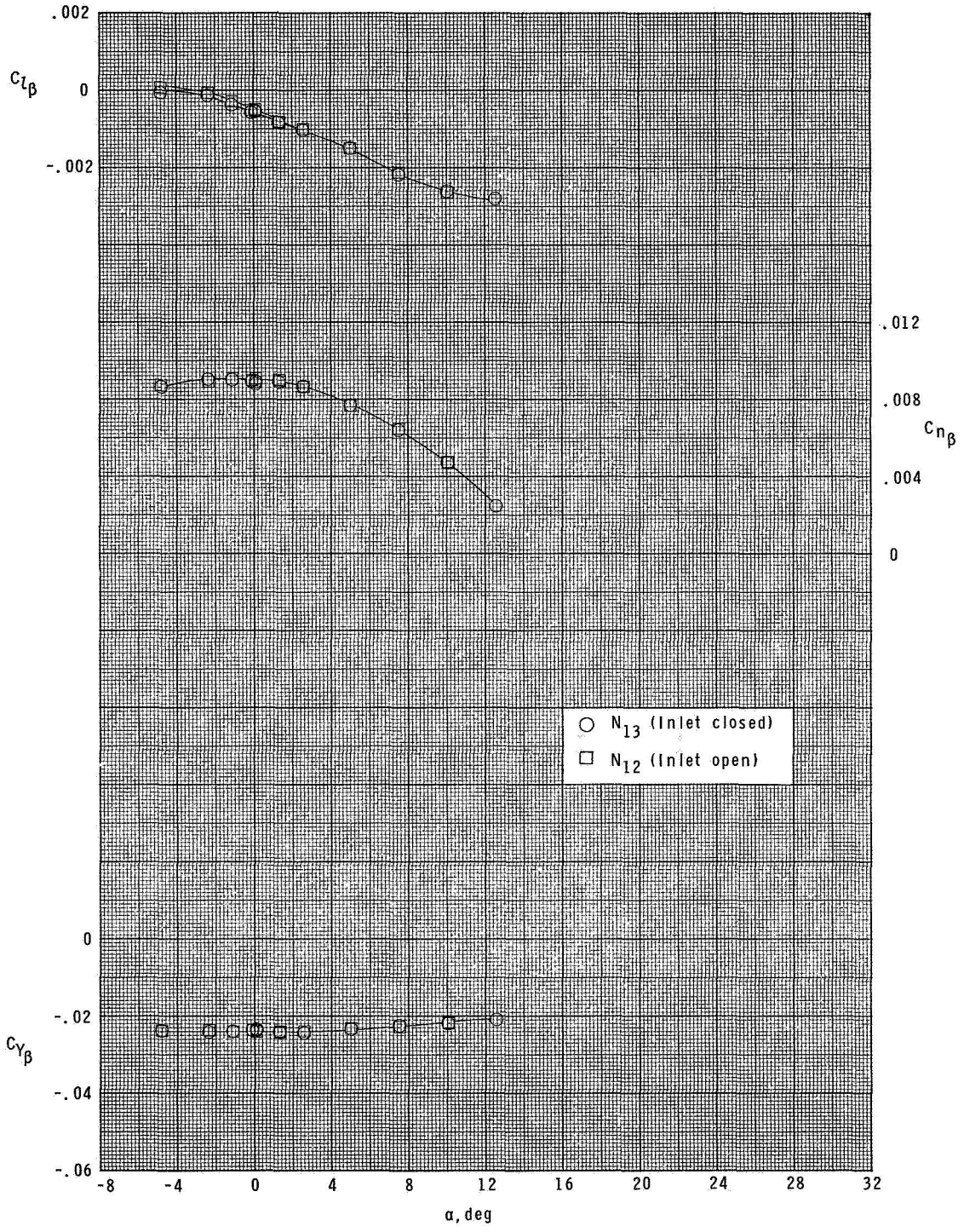
(b) M = 2.00.

Figure 21.- Continued.



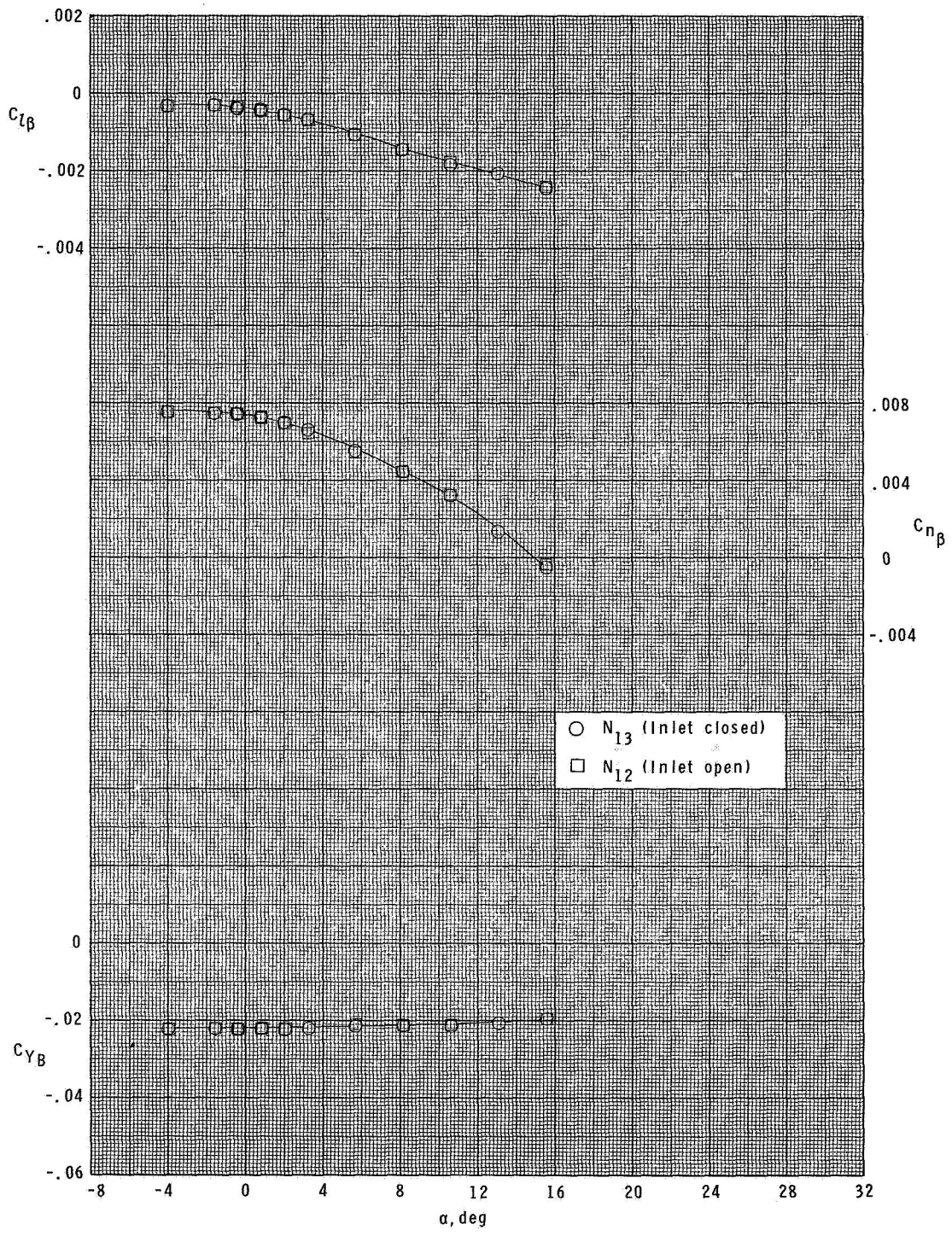
(c) M = 2.50.

Figure 21.- Concluded.



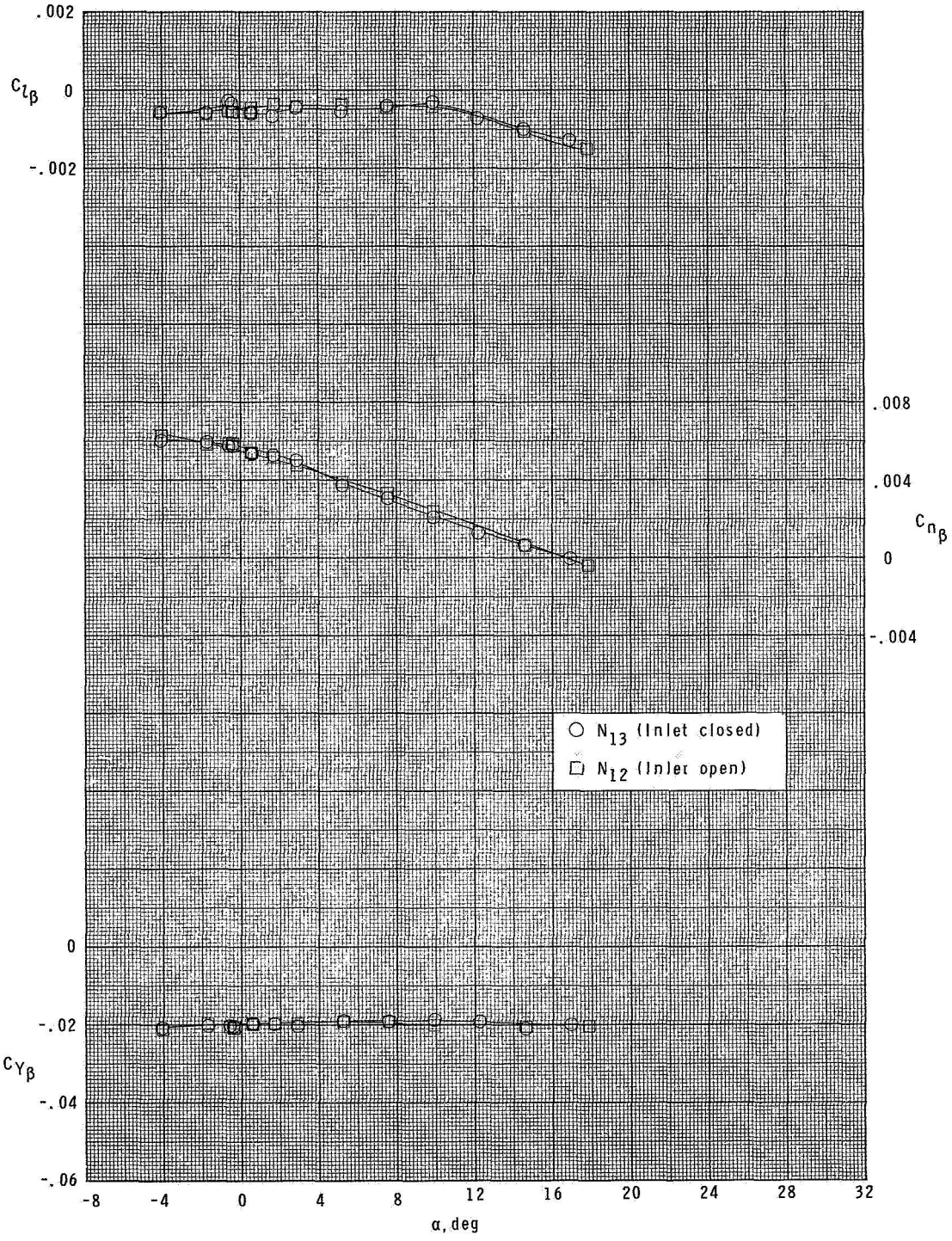
(a) M = 1.75.

Figure 22.- Effect of HRE spike position (no airflow) on lateral stability parameters for $B_{11}X_{16}W_2H_9T_{12}V_{U5}Y_5$.



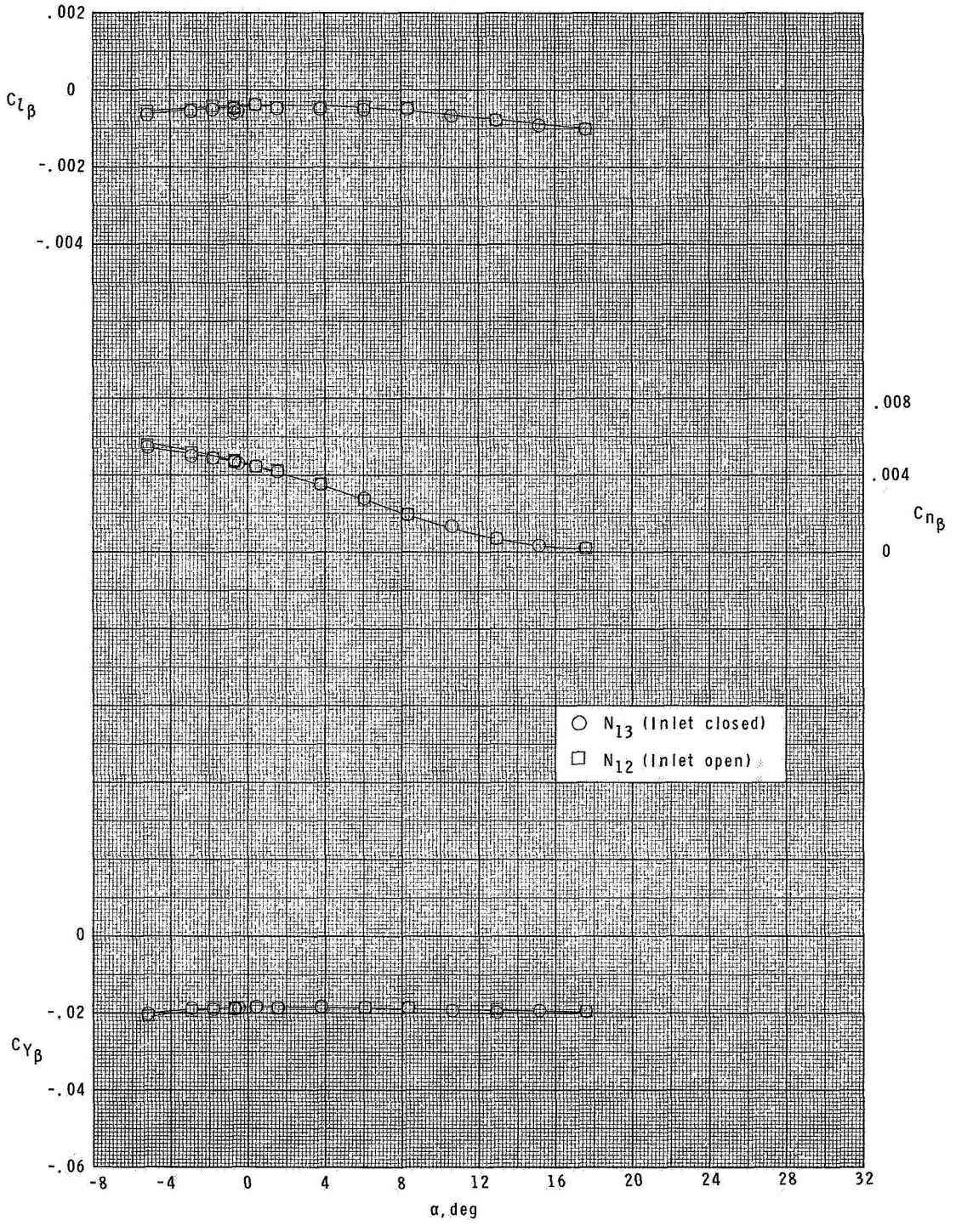
(b) M = 2.00.

Figure 22.- Continued.



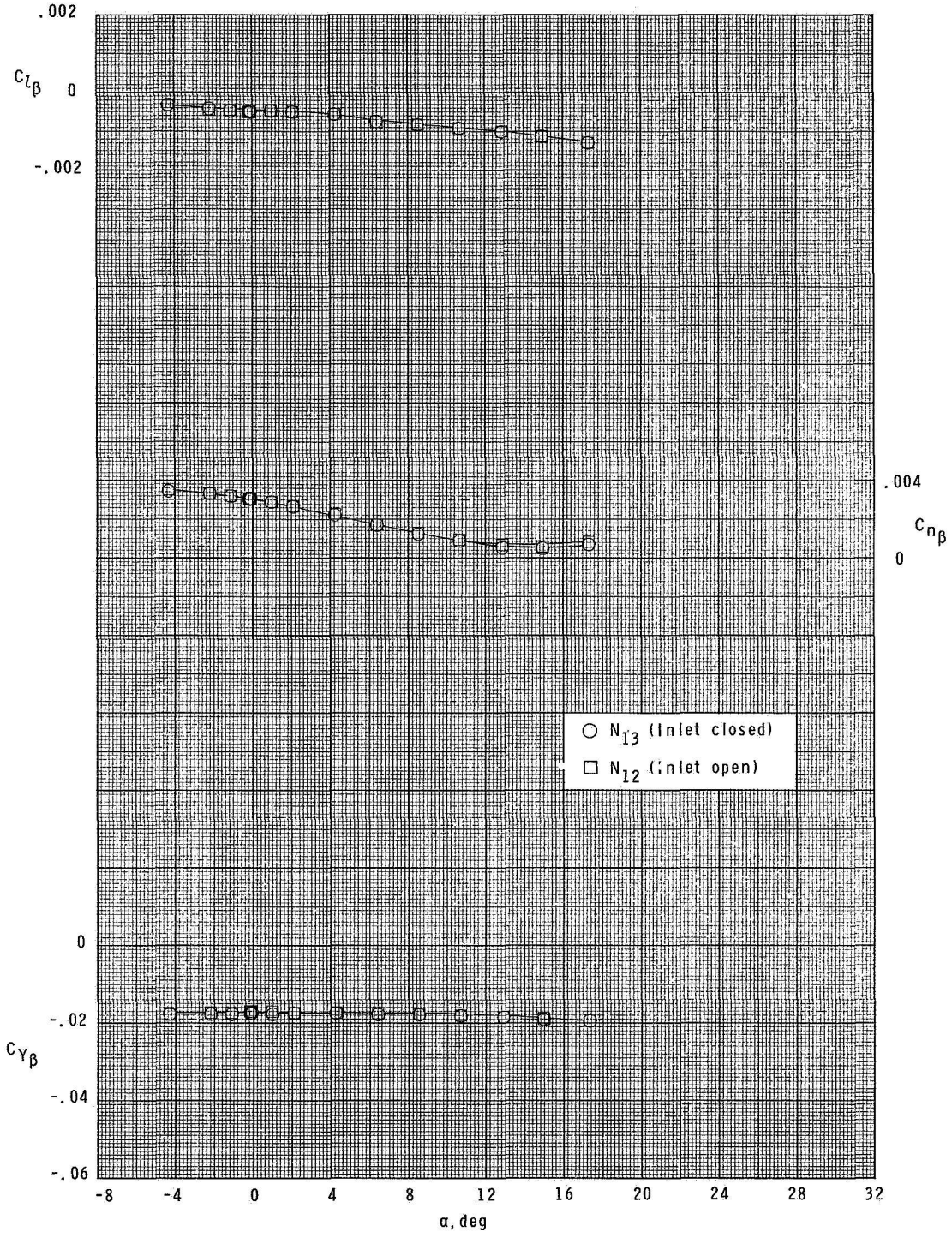
(c) M = 2.50.

Figure 22.- Continued.



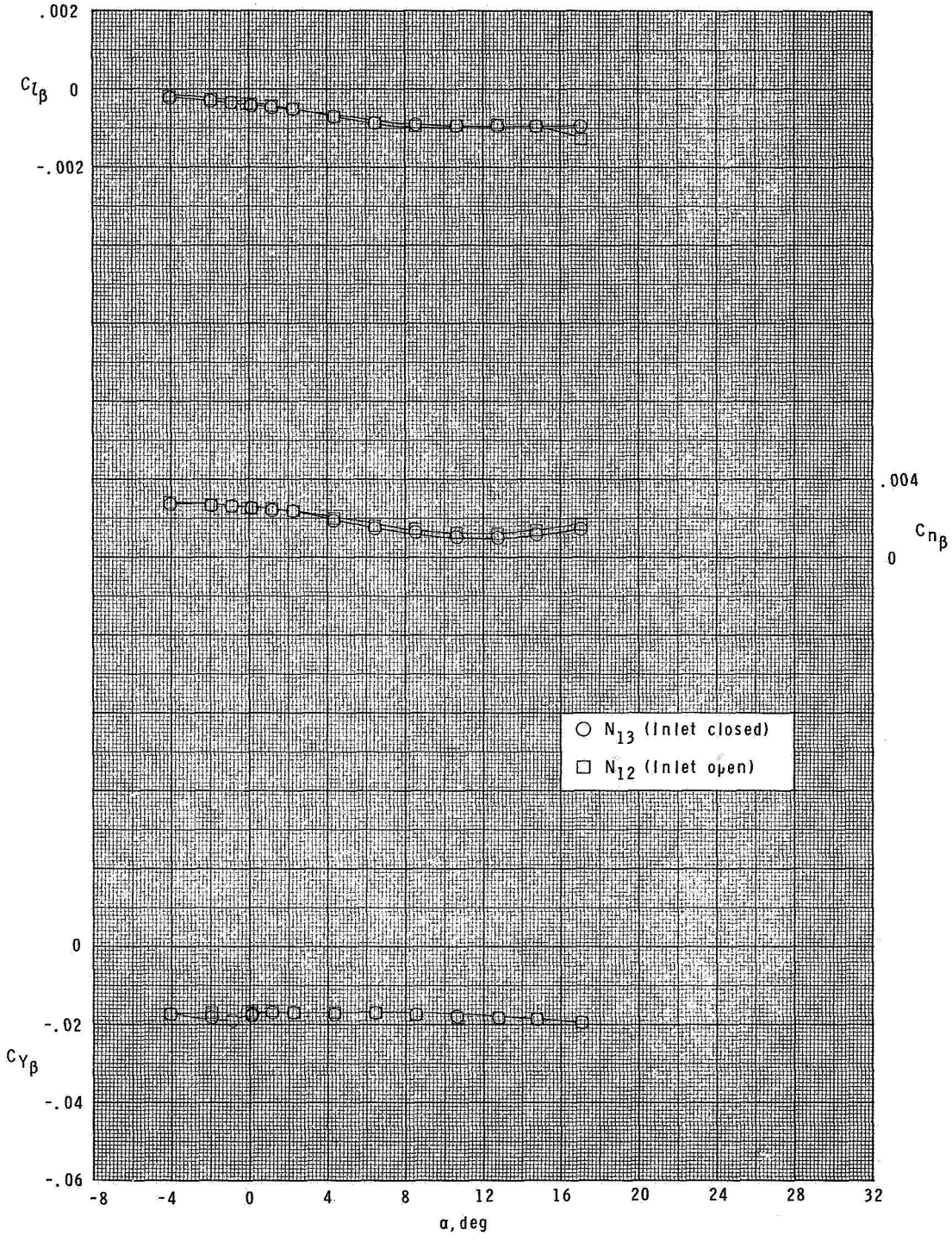
(d) M = 2.86.

Figure 22.- Continued.



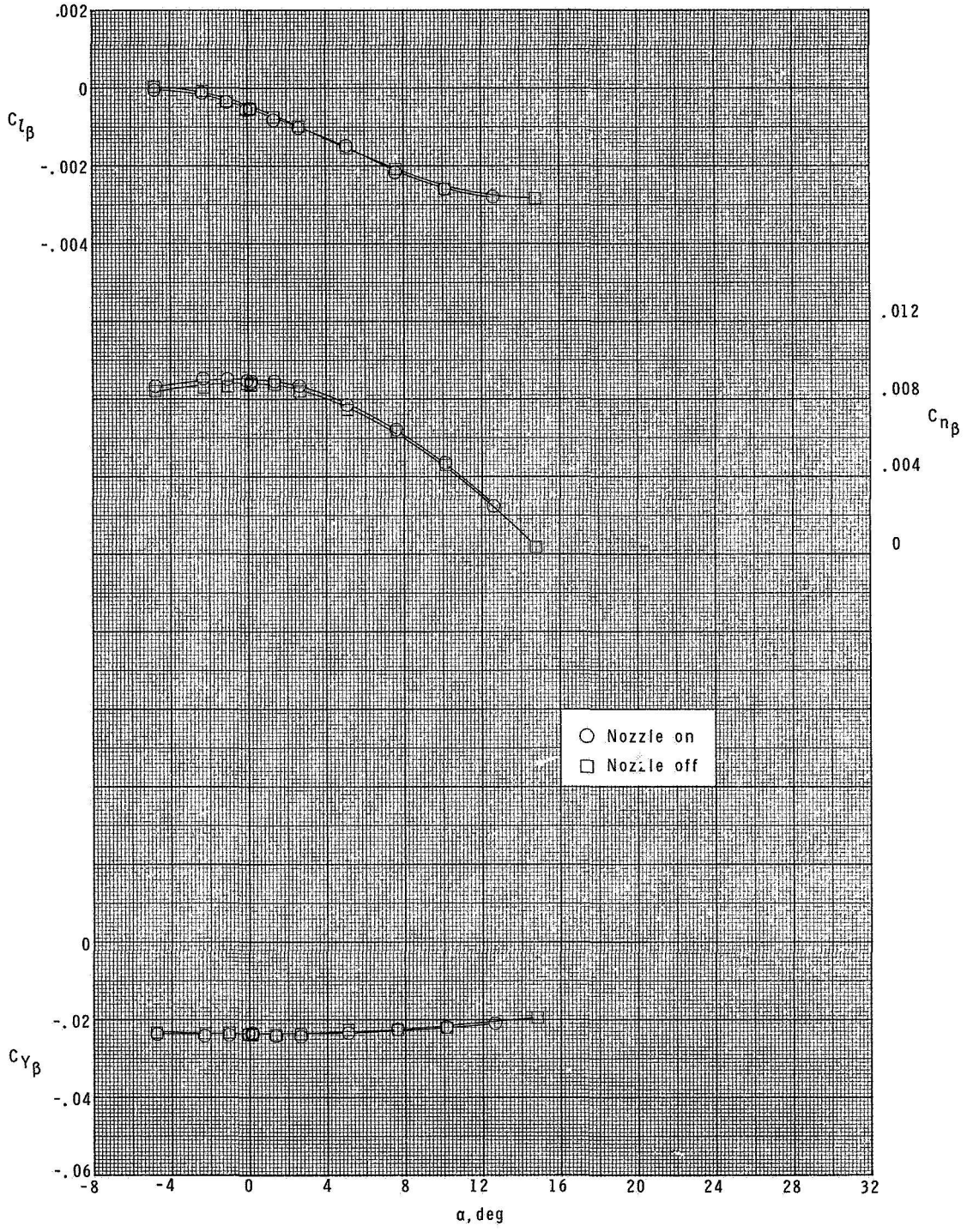
(e) M = 3.95.

Figure 22.- Continued.



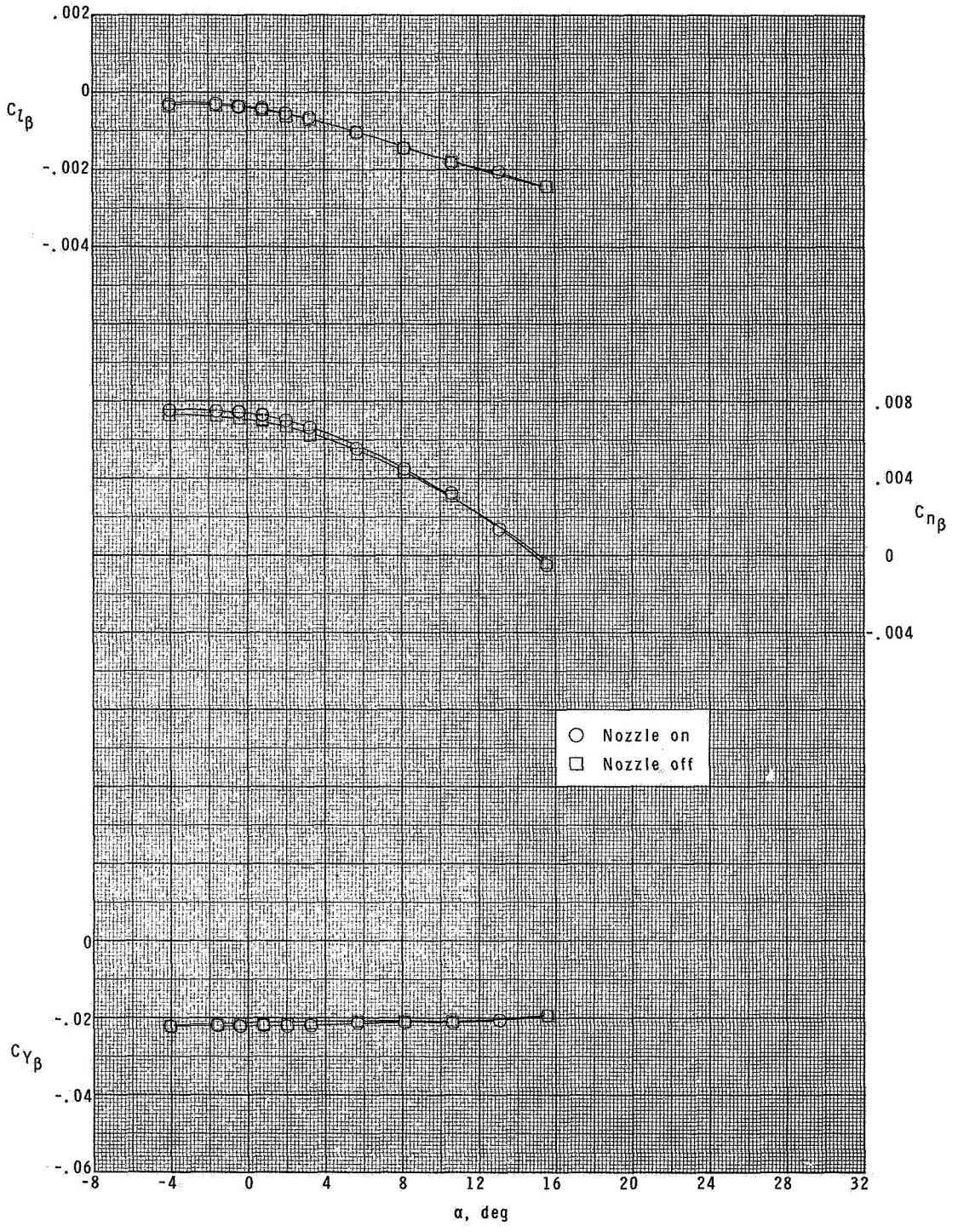
(f) M = 4.63.

Figure 22.- Concluded.



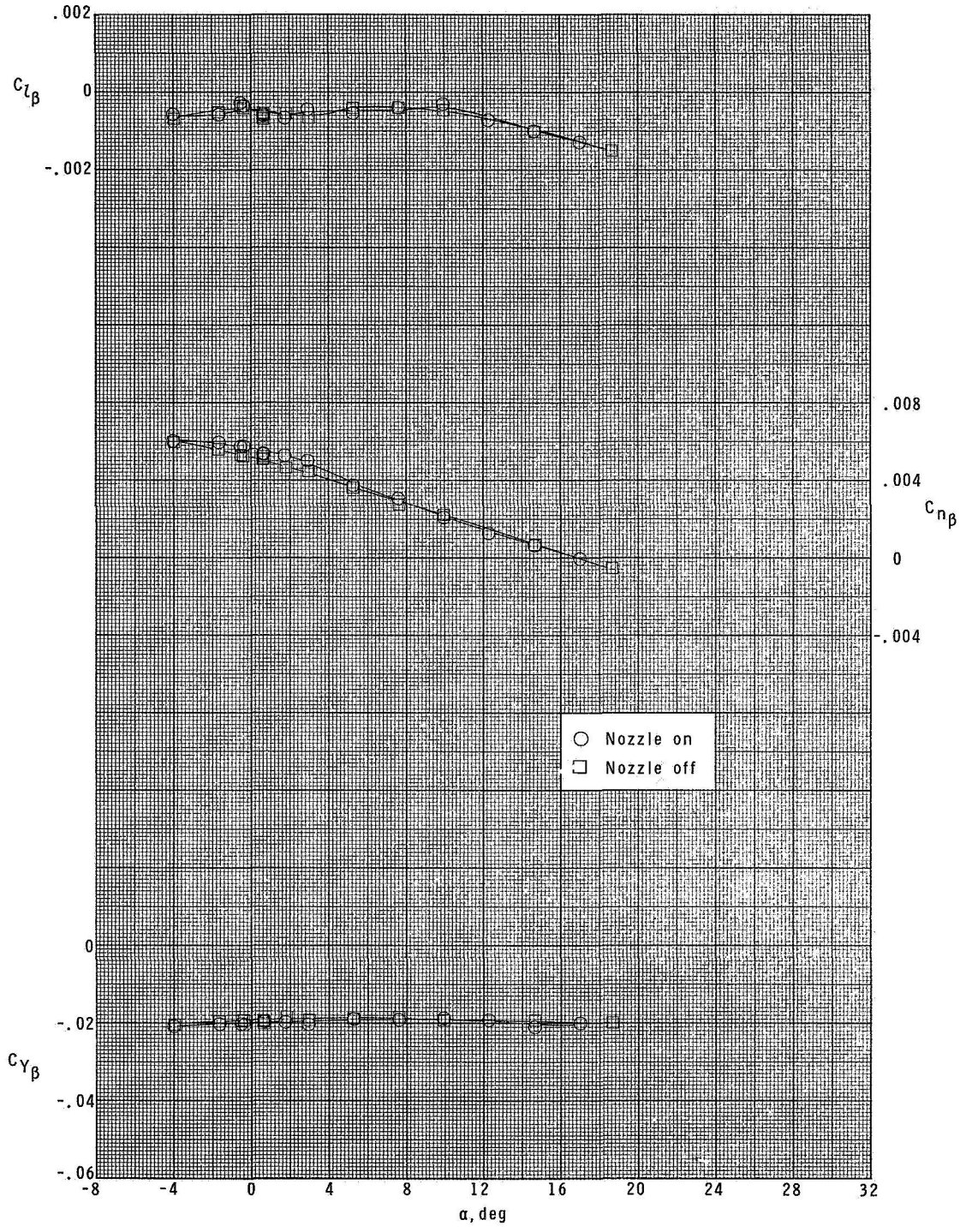
(a) M = 1.75.

Figure 23.- Effect of fuselage nozzle on lateral stability parameters for $B_{11}X_{16}W_2H_9T_{12}V_{U5}Y_5N_{13}$.



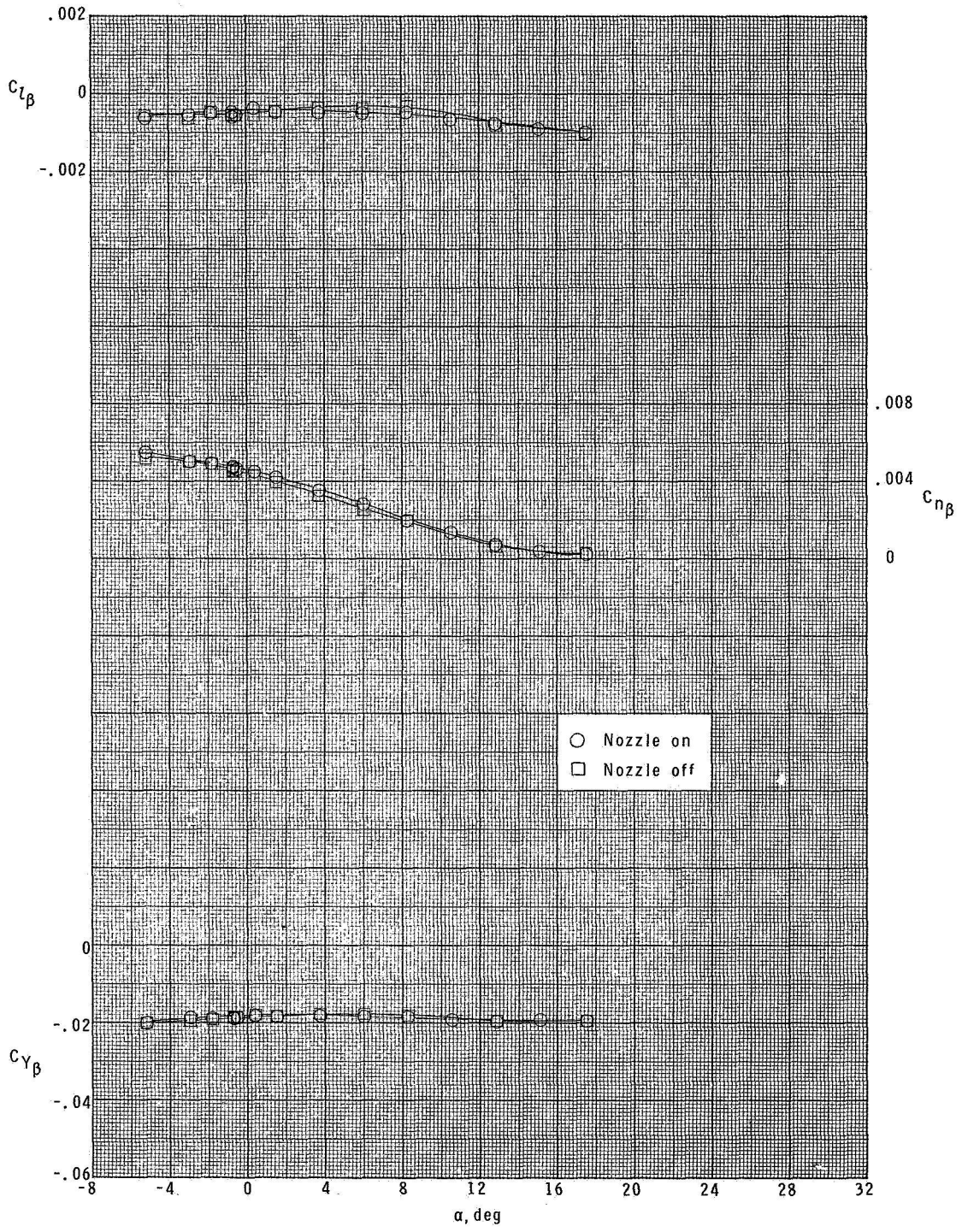
(b) M = 2.00.

Figure 23.- Continued.



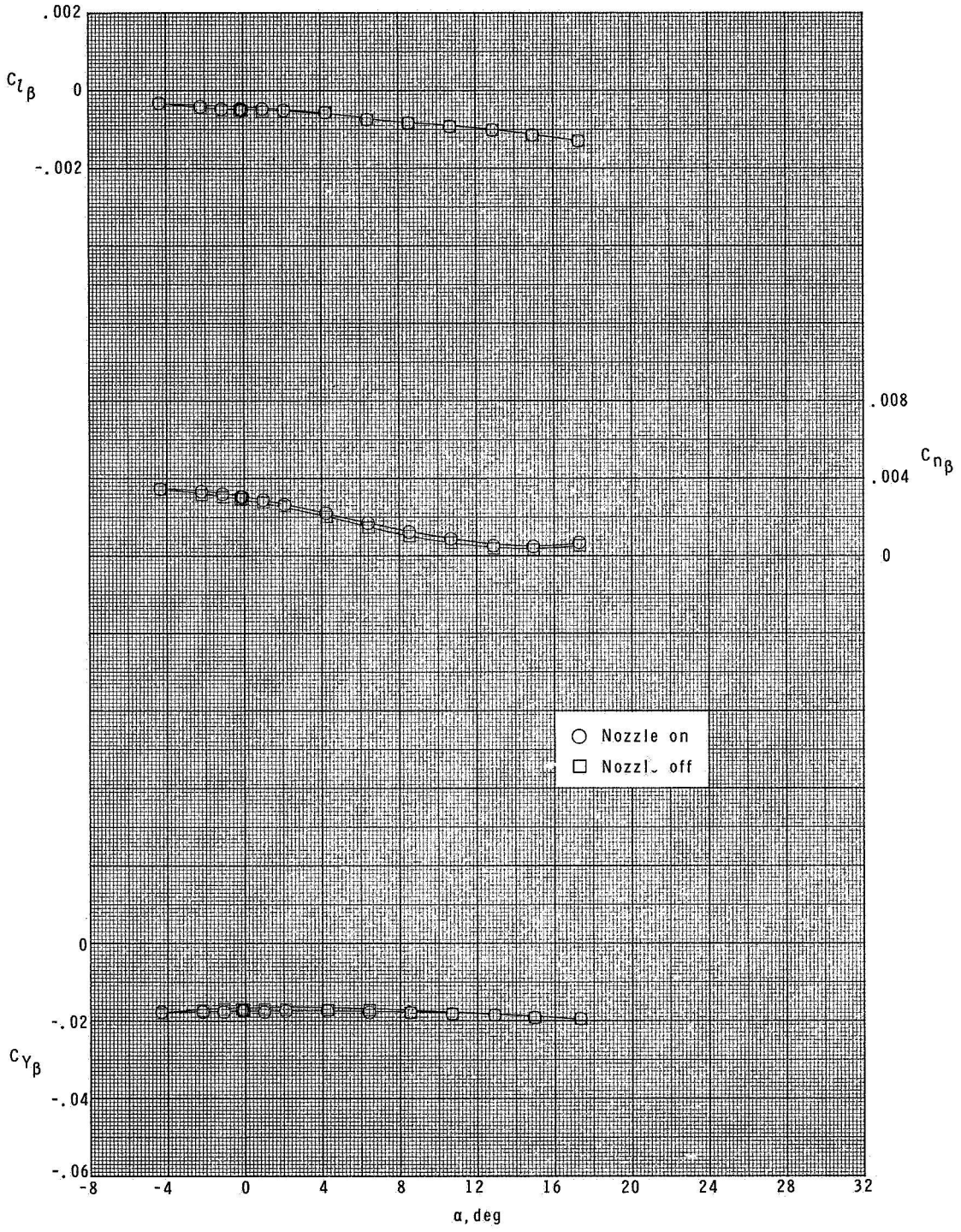
(c) M = 2.50.

Figure 23.- Continued.



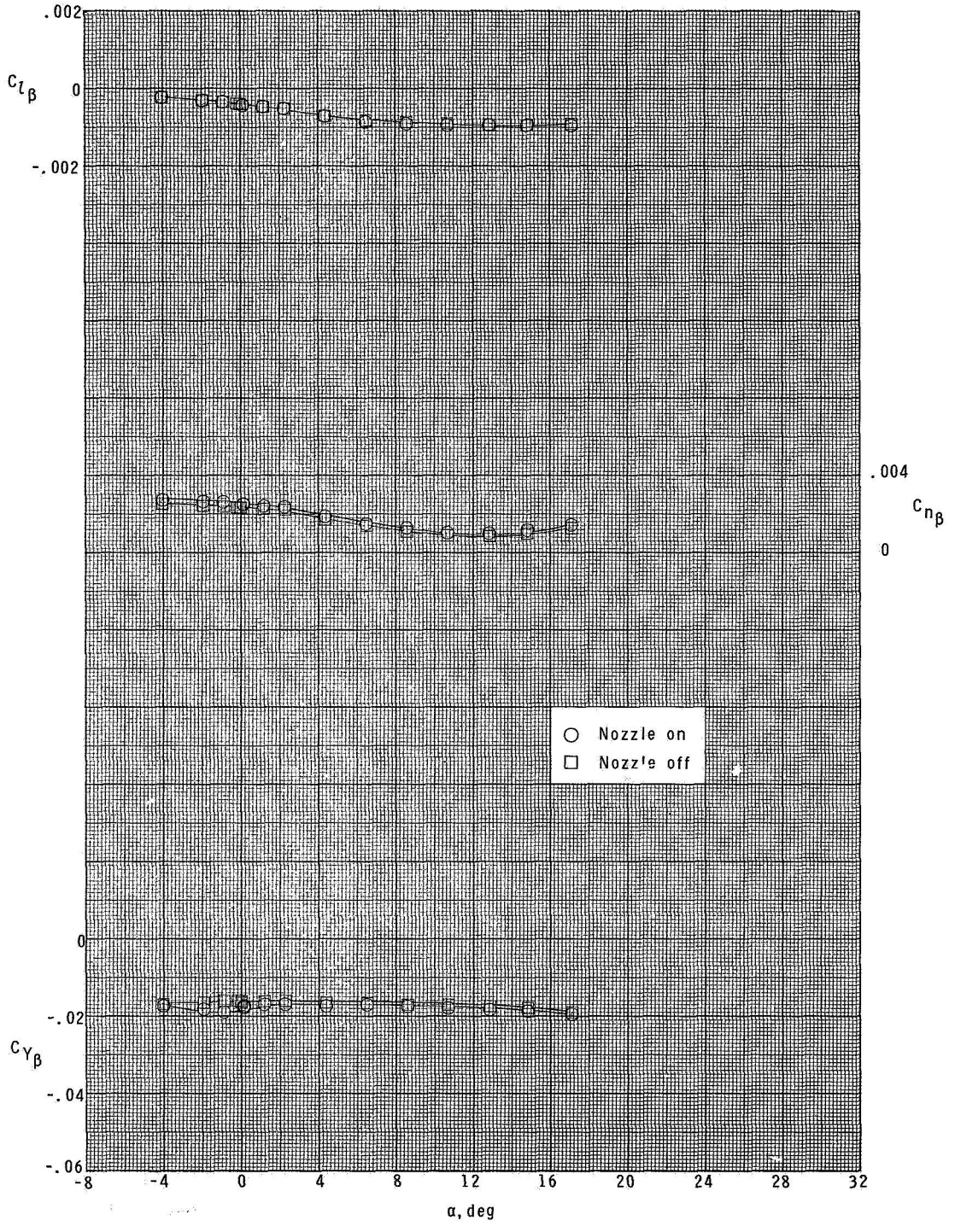
(d) M = 2.86.

Figure 23.- Continued.



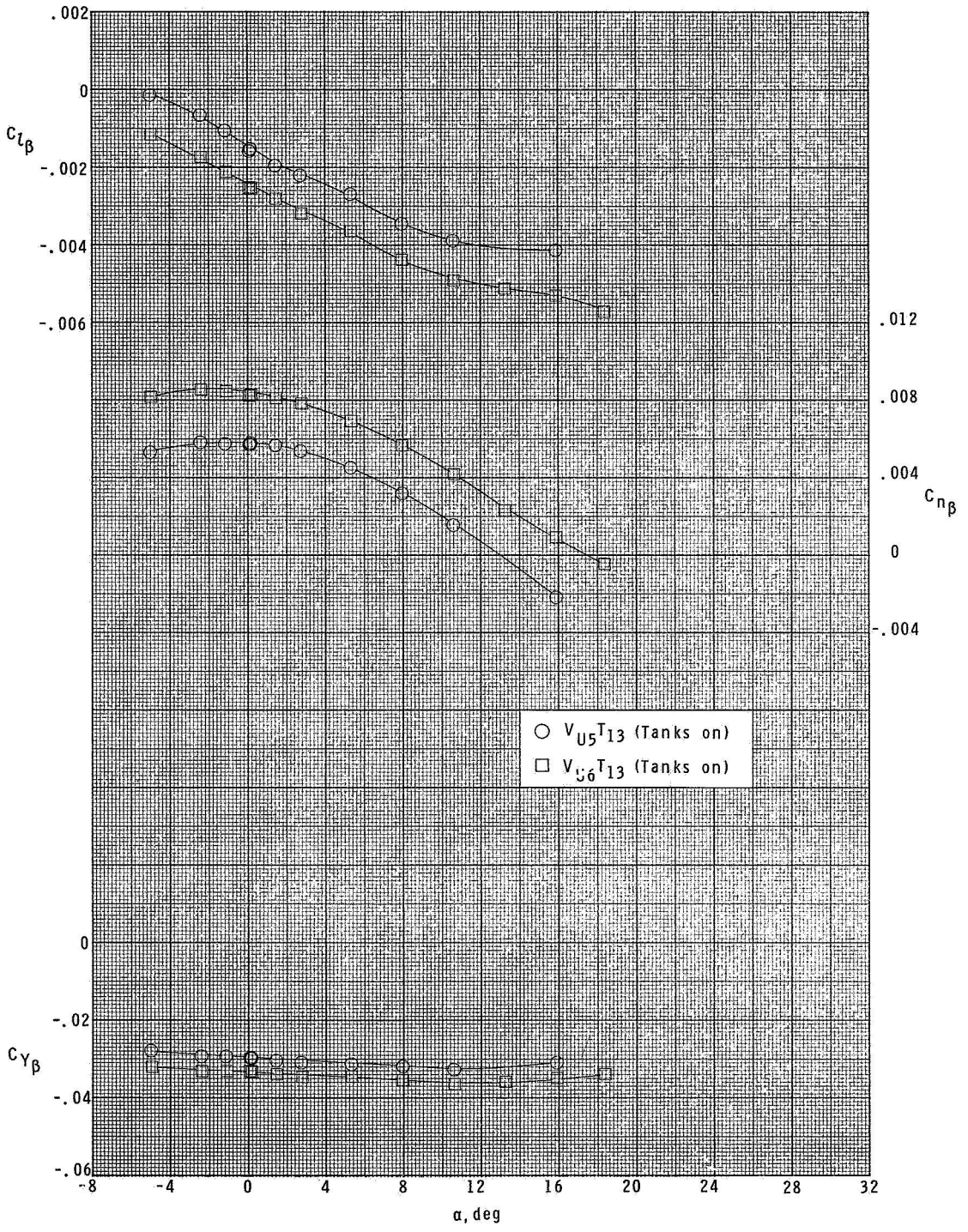
(e) M = 3.95.

Figure 23.- Continued.



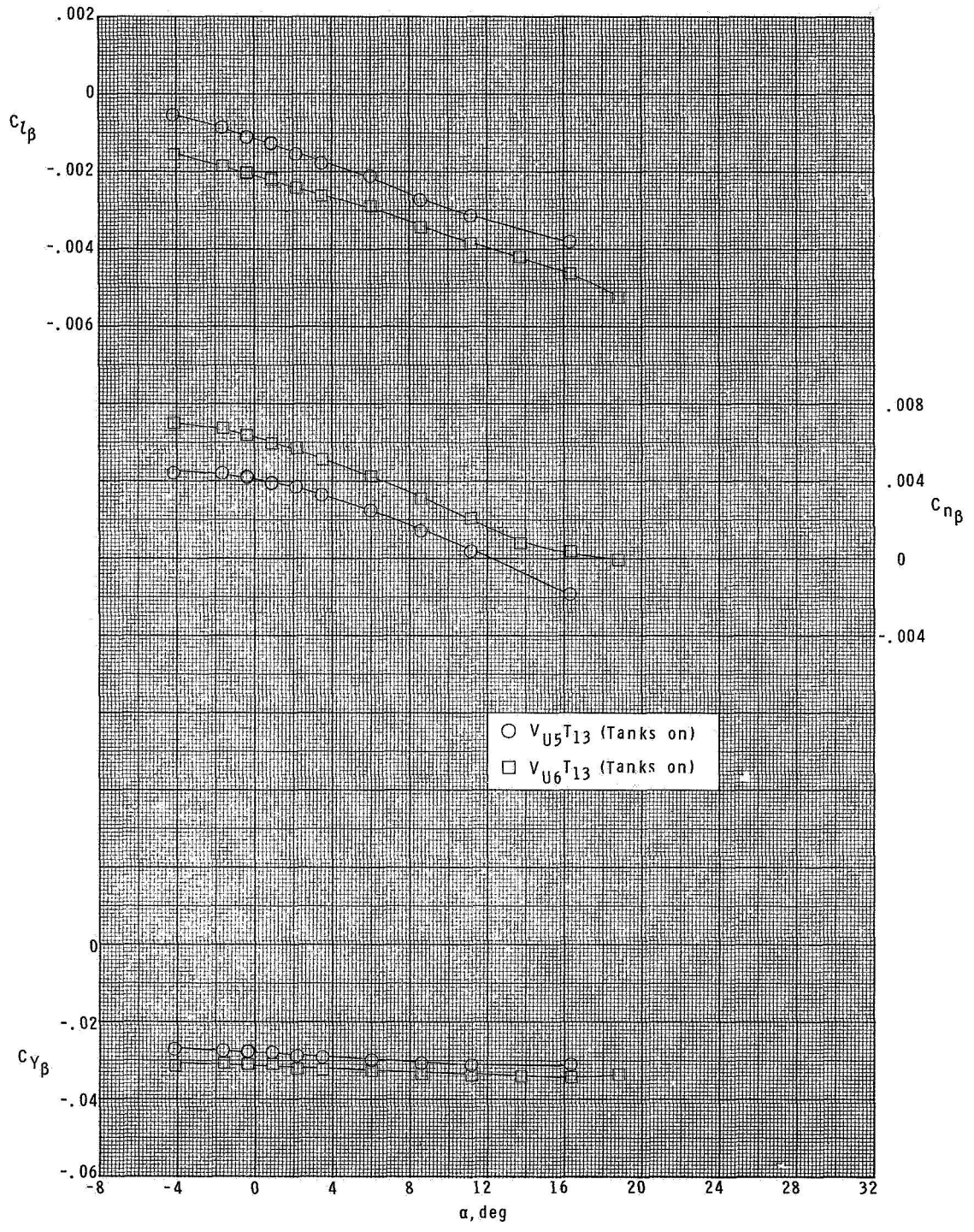
(f) M = 4.63.

Figure 23.- Concluded.



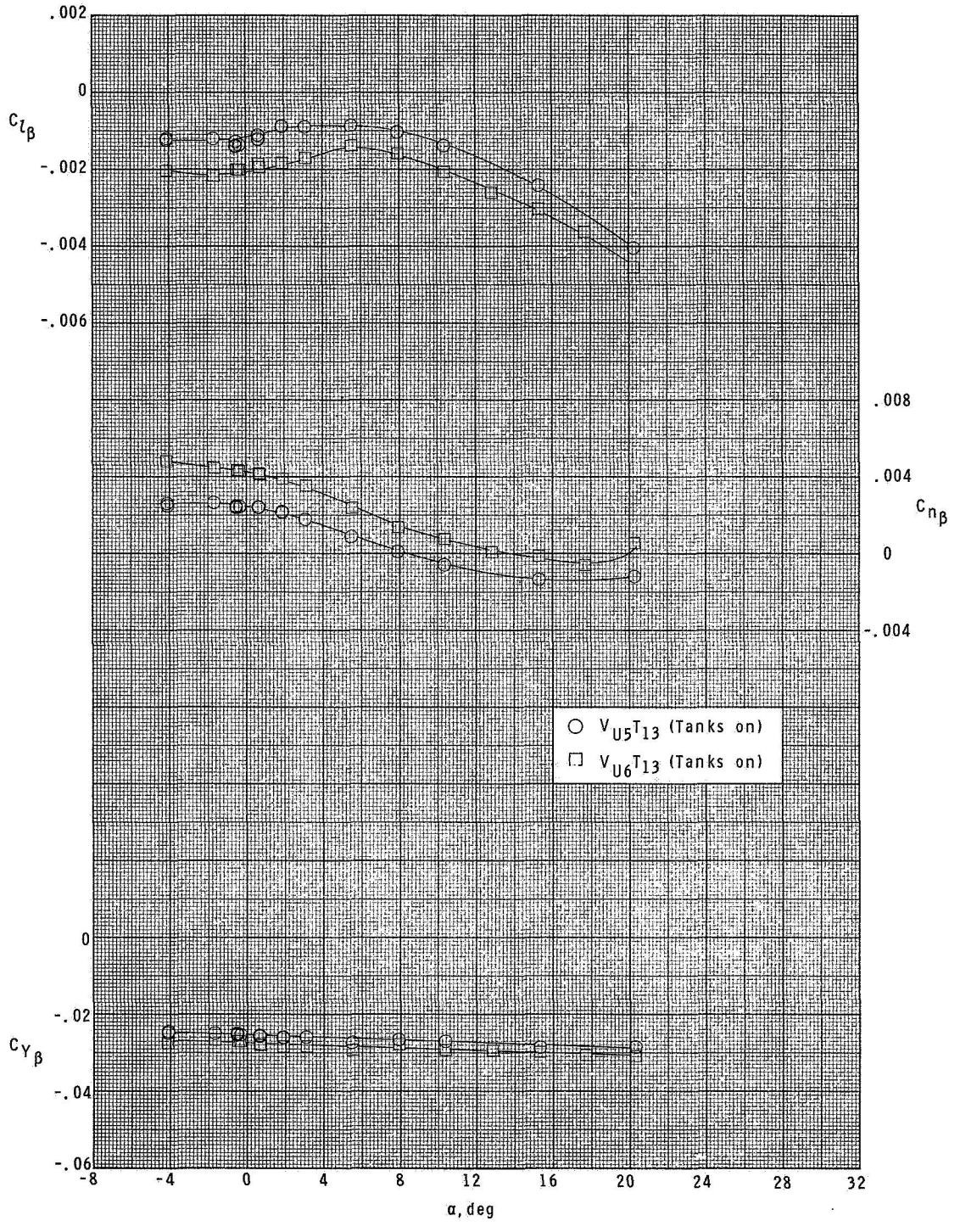
(a) M = 1.75.

Figure 24.- Effect of extended vertical tail on lateral stability parameters for $B_{11}X_{16}W_2H_9T_{12}Y_5N_{13}$.



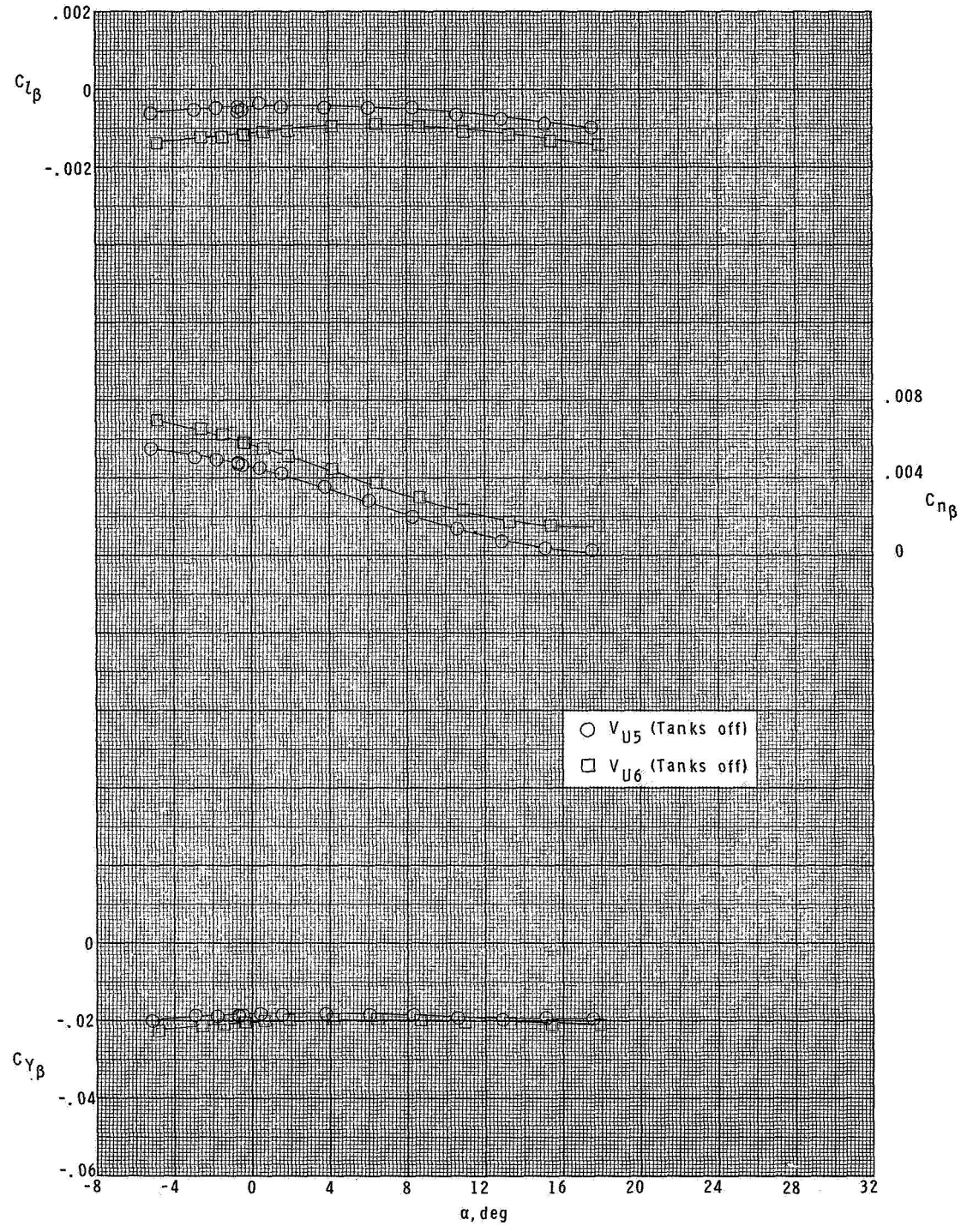
(b) M = 2.00.

Figure 24.- Continued.



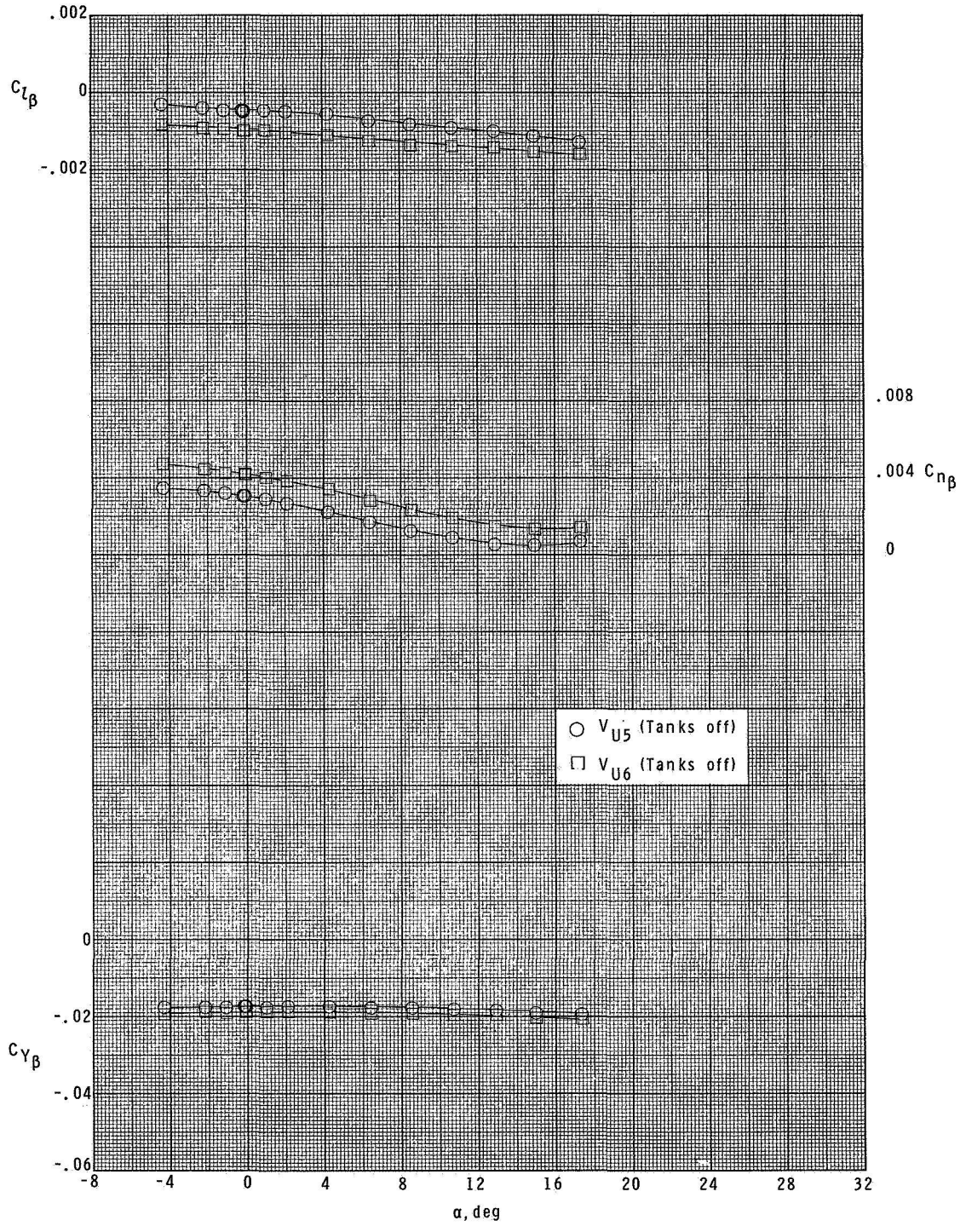
(c) M = 2.50.

Figure 24.- Continued.



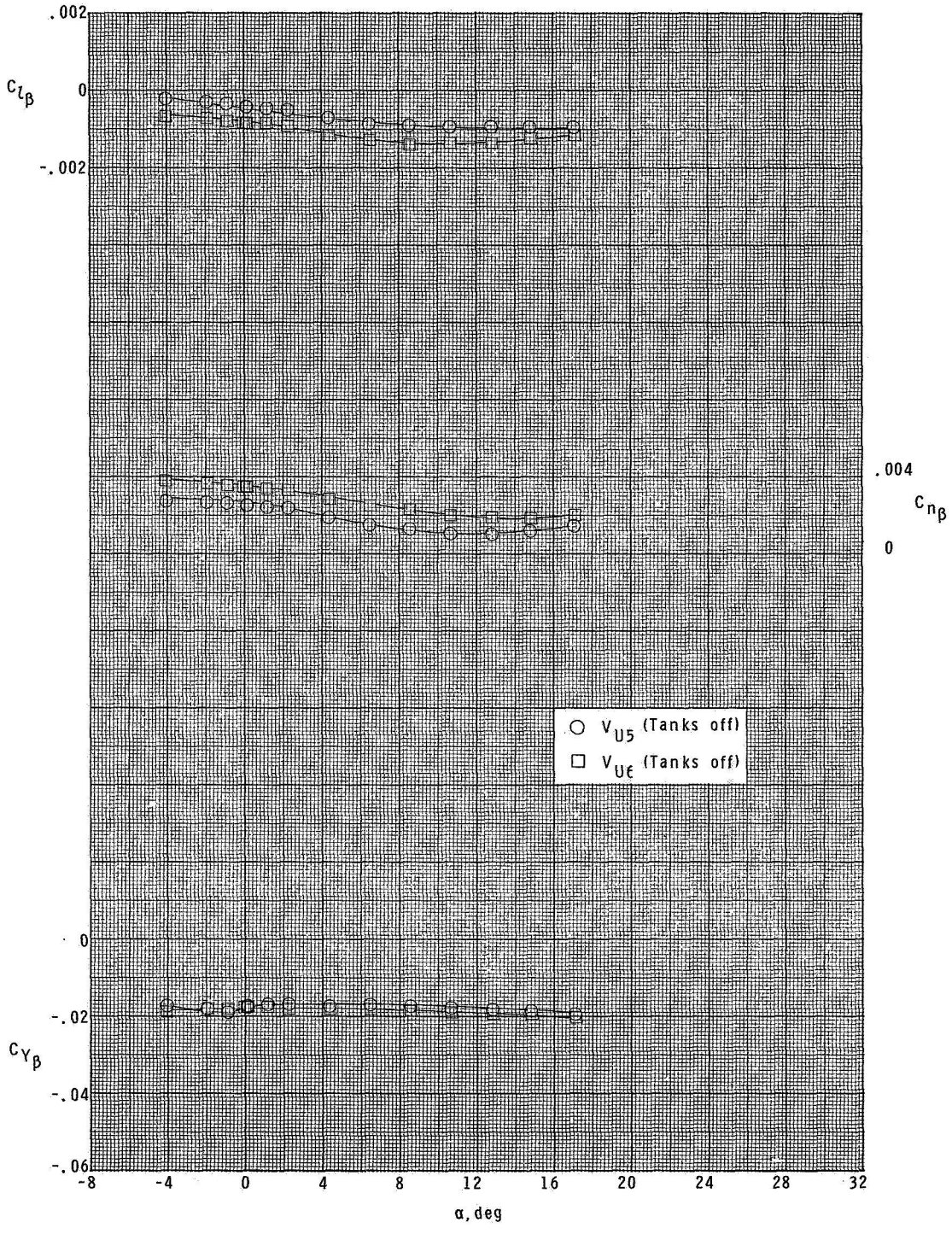
(d) M = 2.86.

Figure 24.- Continued.



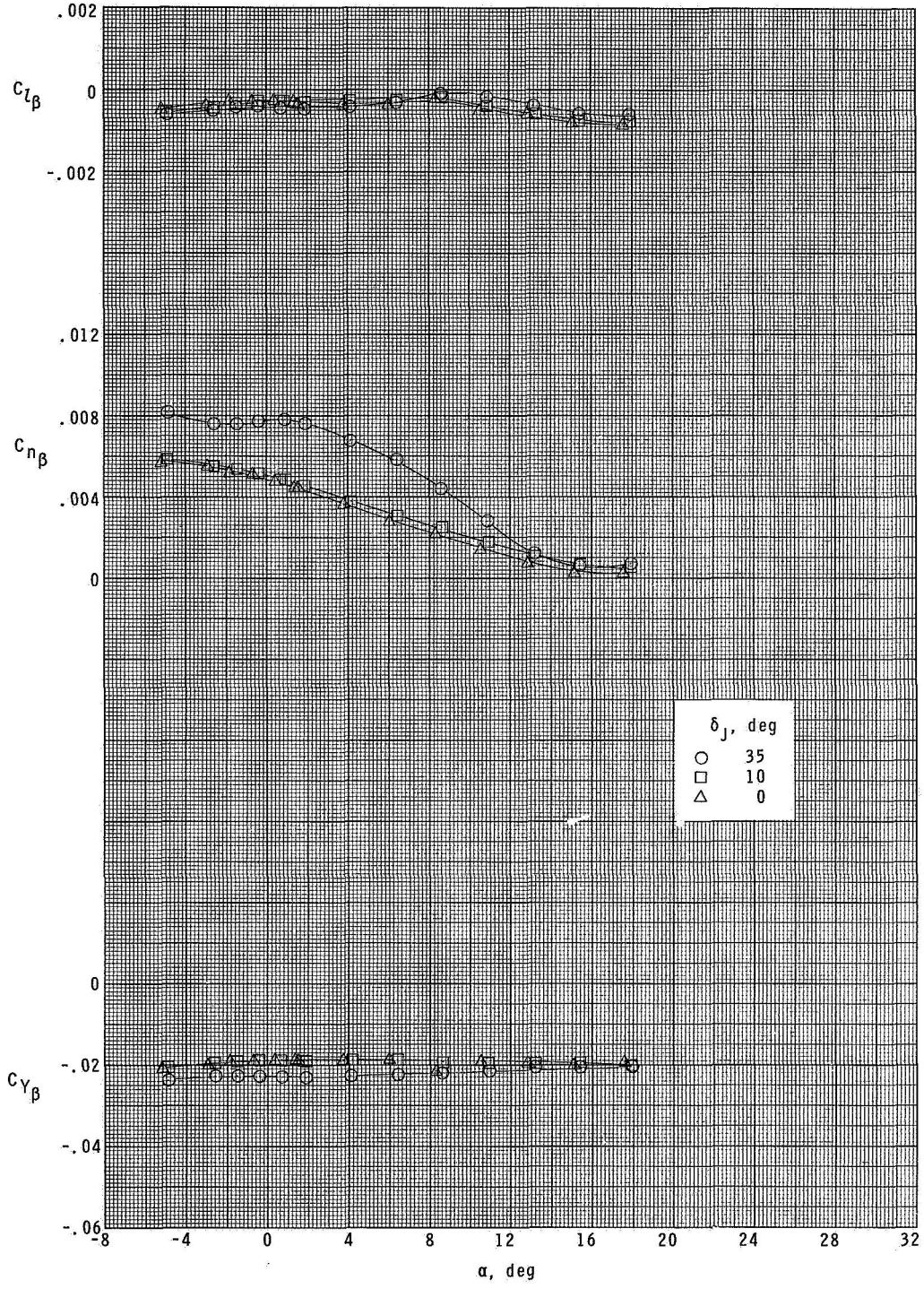
(e) M = 3.95.

Figure 24.- Continued.



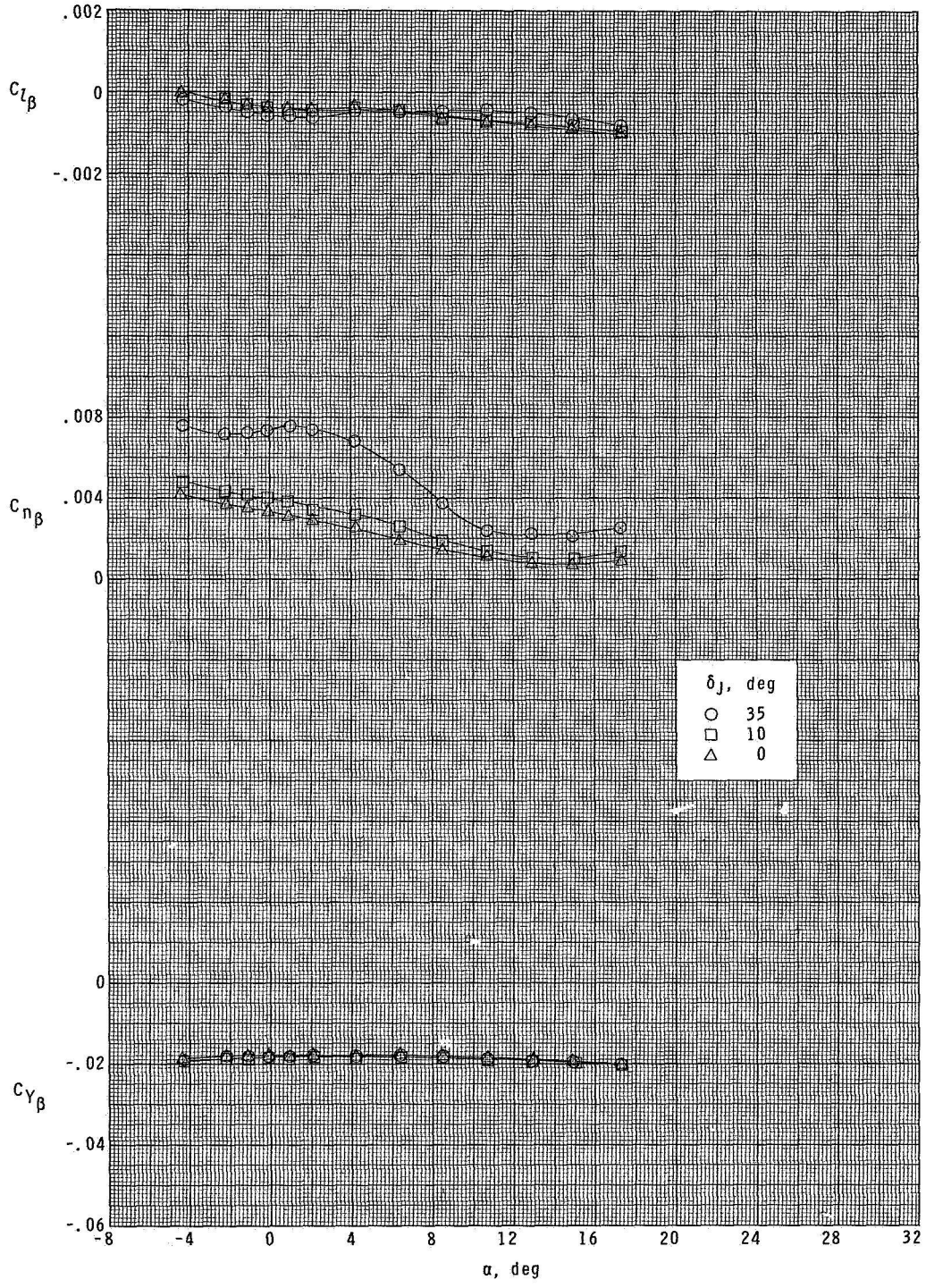
(f) M = 4.63.

Figure 24.- Concluded.



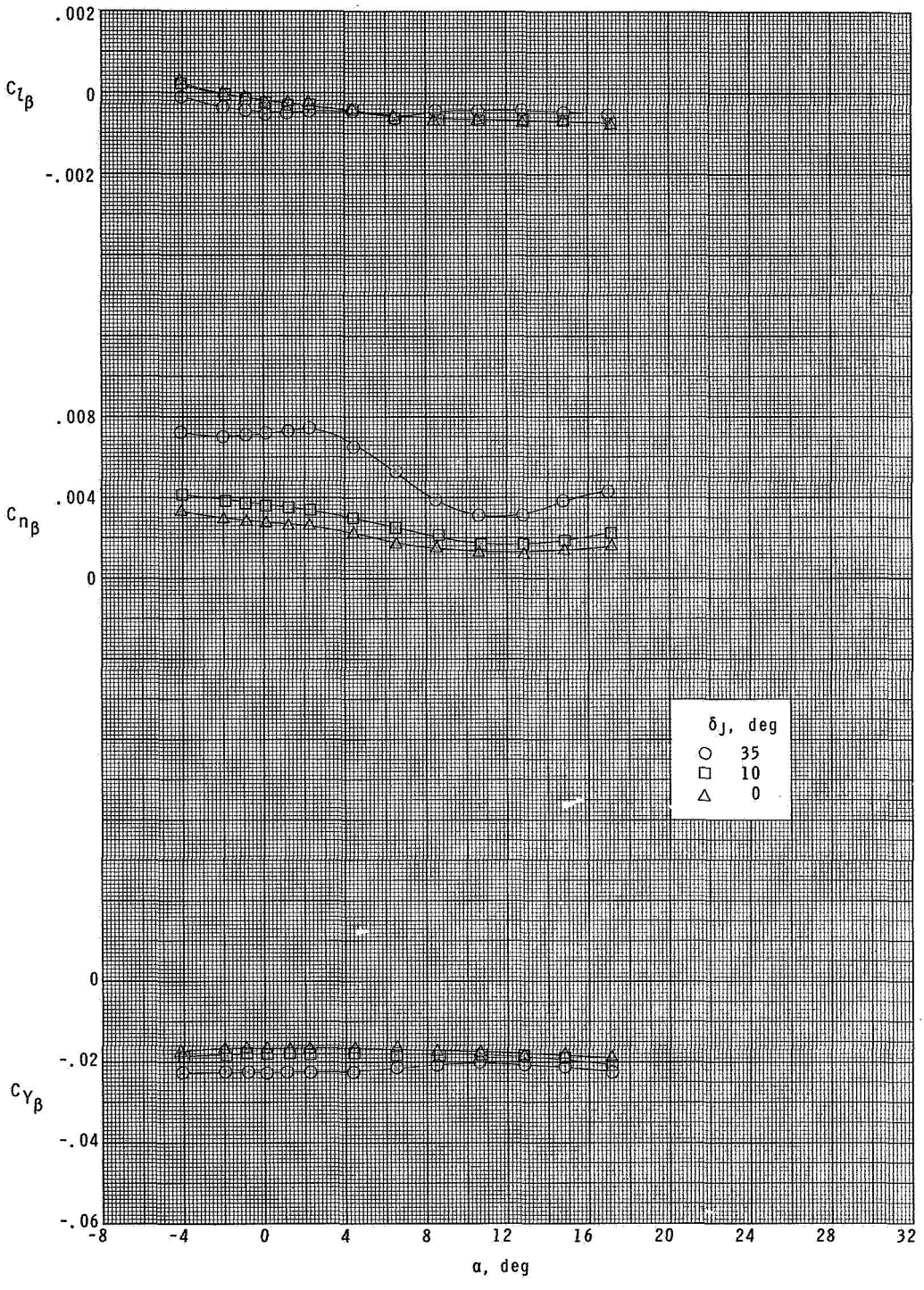
(a) M = 2.86.

Figure 25.- Effect of speed-brake deflection on lateral stability parameters for $B_{11}X_{16}W_2H_9T_{12}V_{U5}Y_5N_{13}$ (HRE on) with $\delta_h = -10^0$.



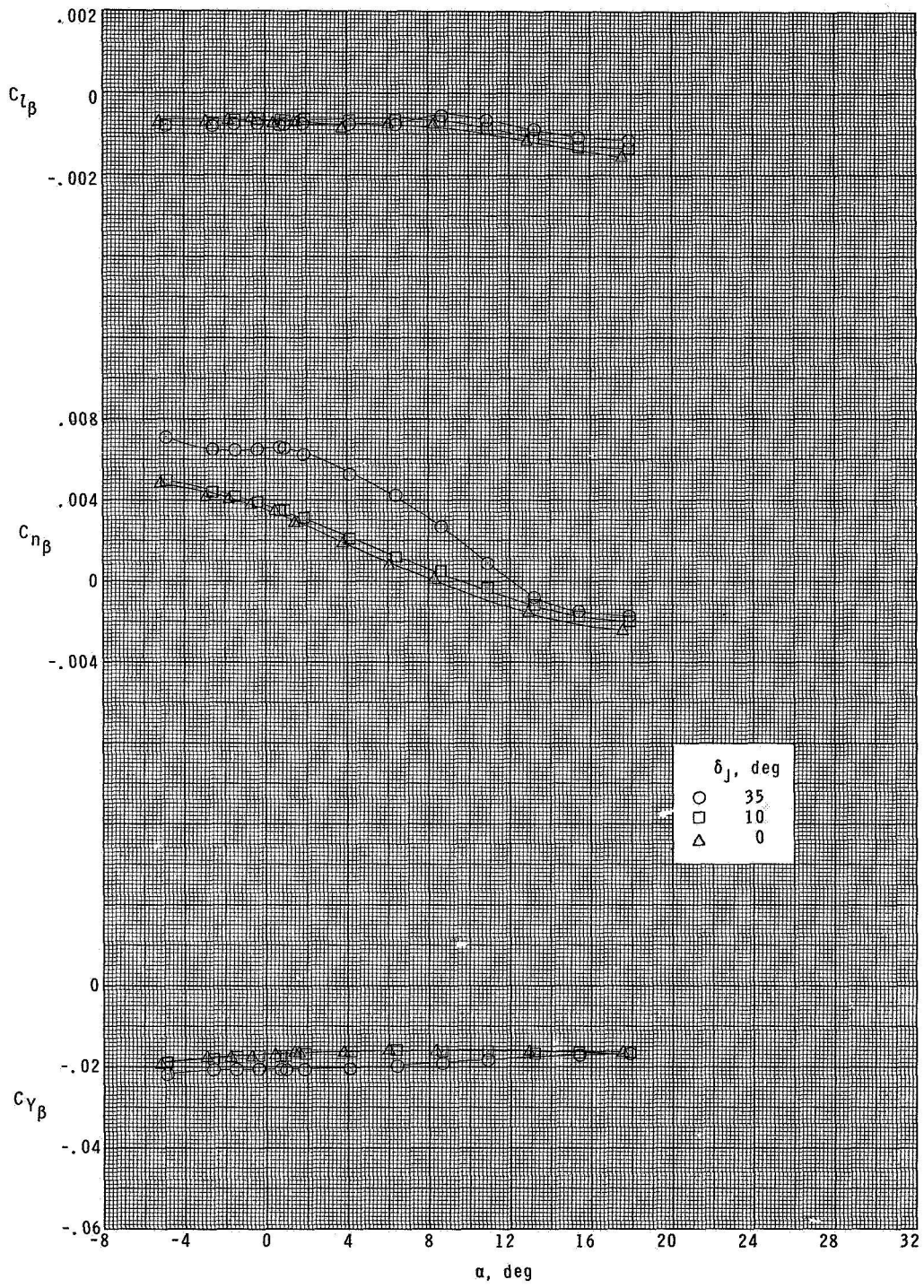
(b) M = 3.95.

Figure 25.- Continued.



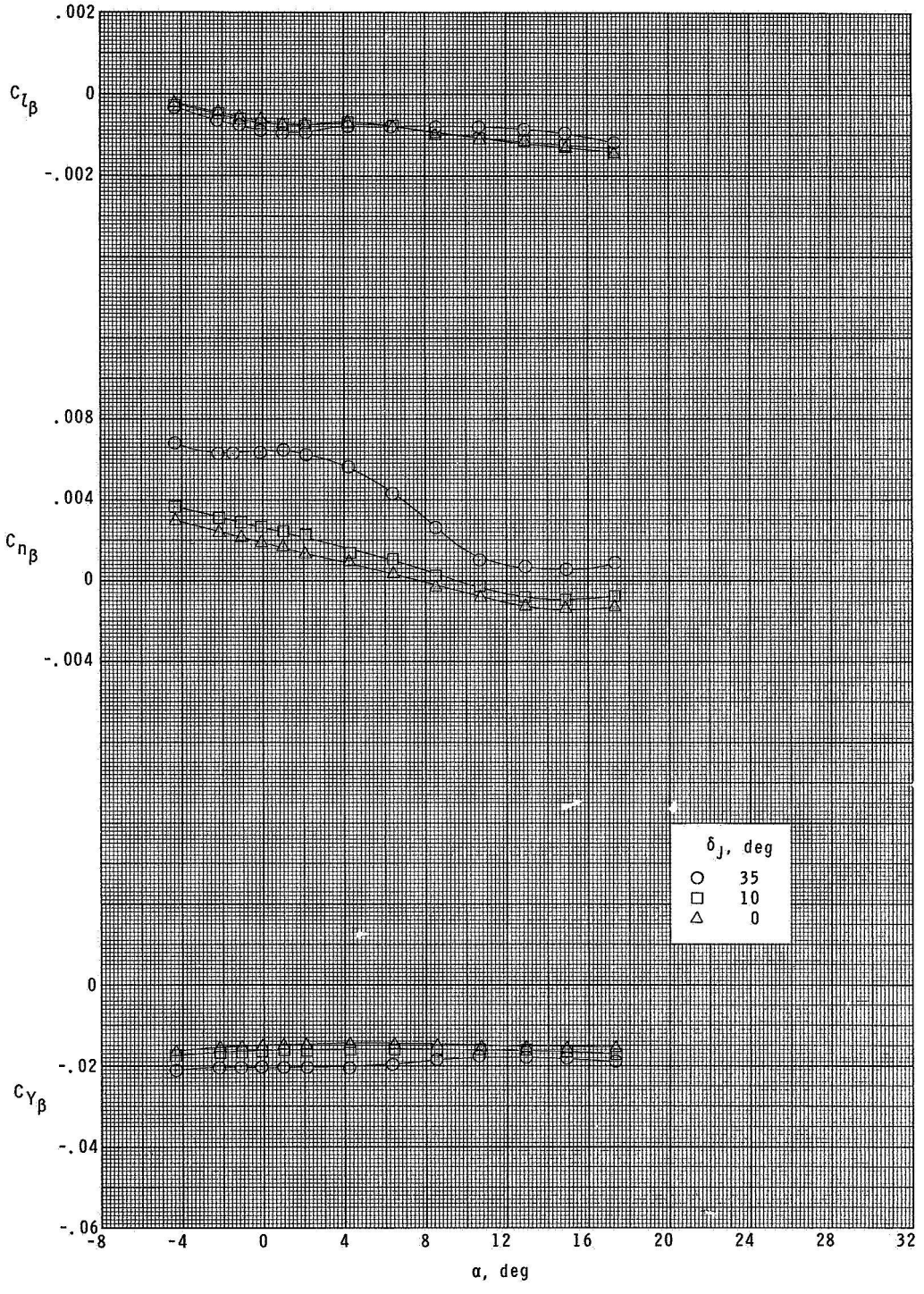
(c) M = 4.63.

Figure 25.- Concluded.



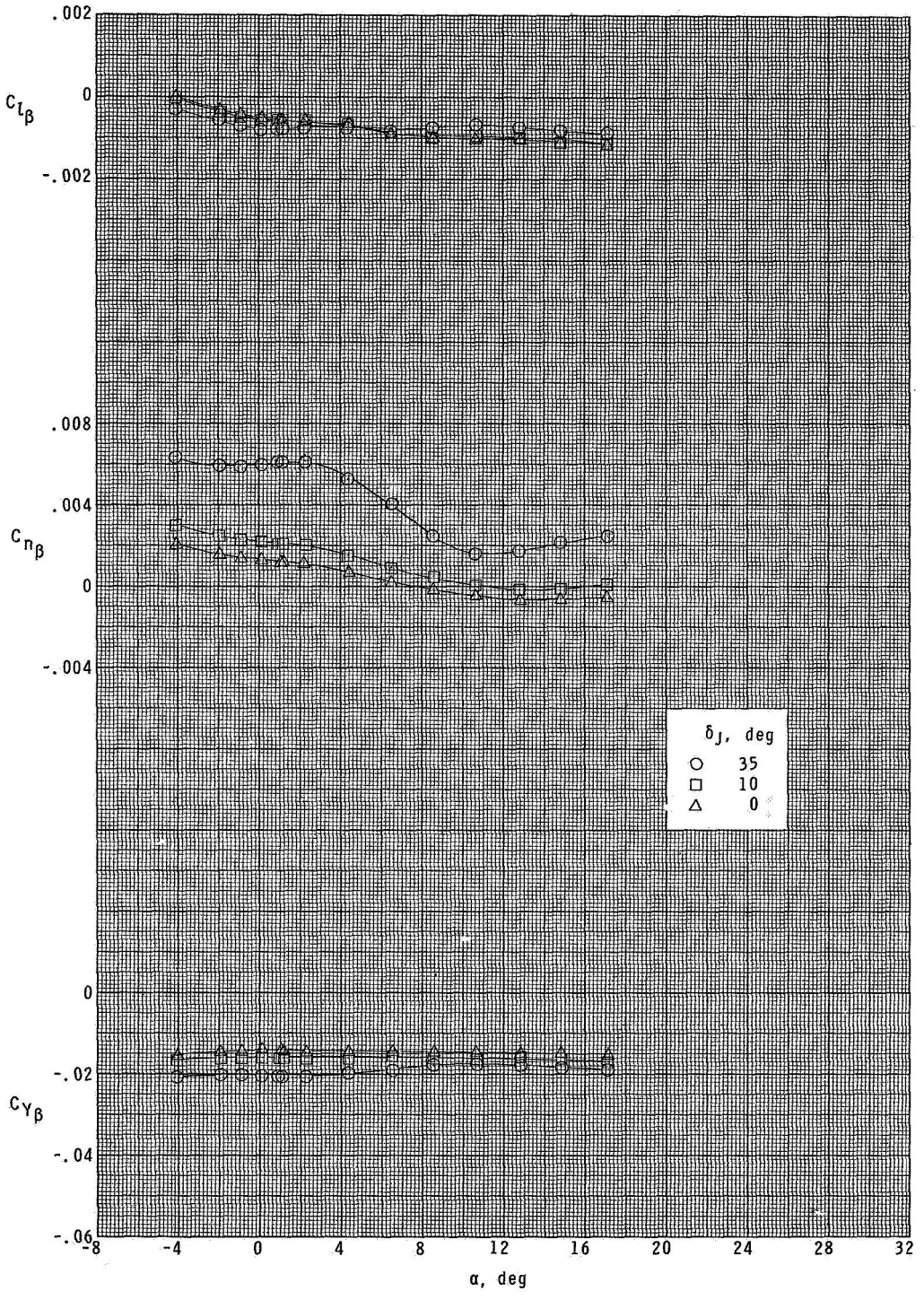
(a) M = 2.86.

Figure 26.- Effect of speed-brake deflection on lateral stability parameters for $B_{11}X_{16}W_2H_9T_{12}V_{U5}Y_5$ (HRE off) with $\delta_h = -10^0$.



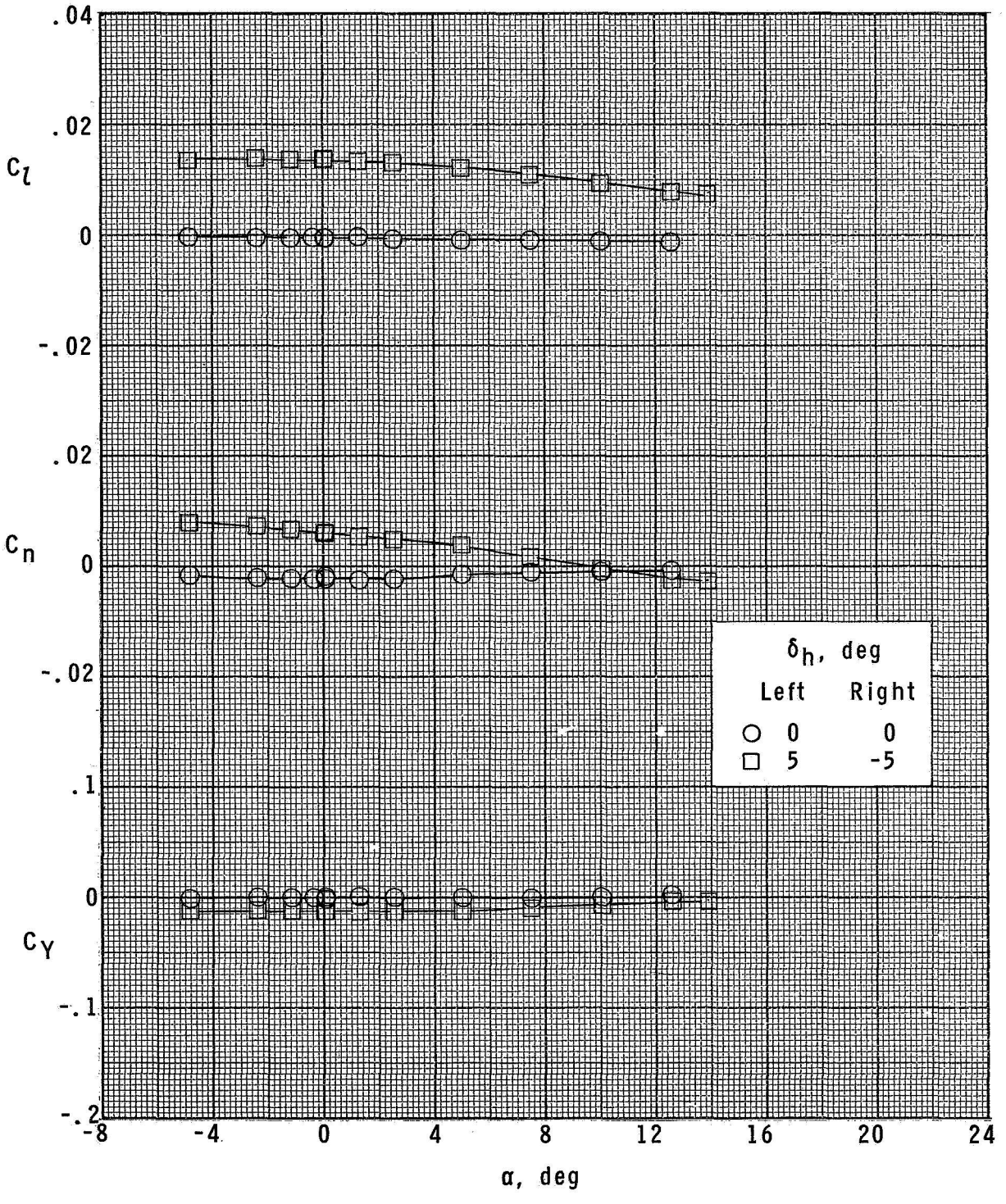
(b) M = 3.95.

Figure 26.- Continued.



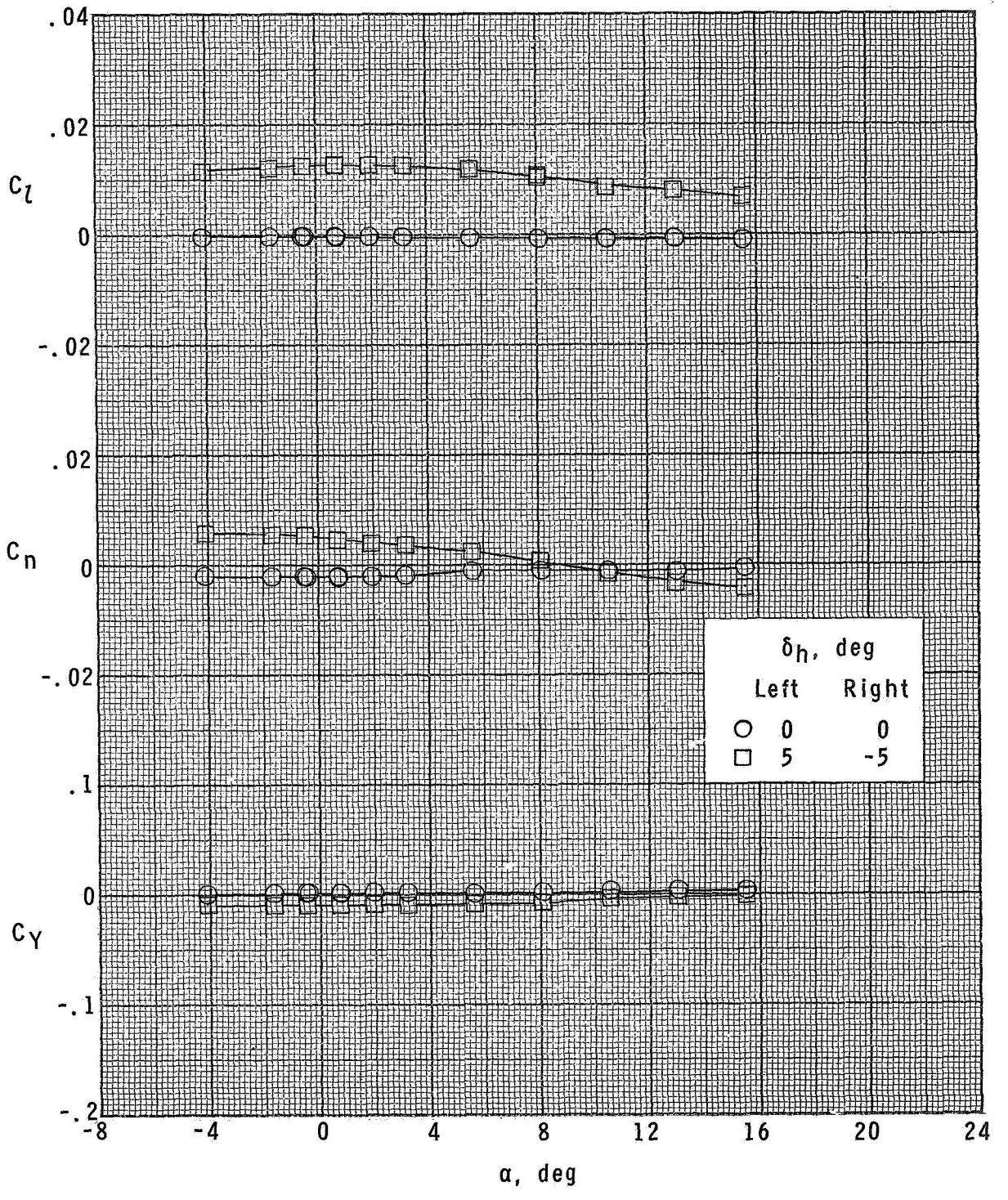
(c) M = 4.63.

Figure 26.- Concluded.



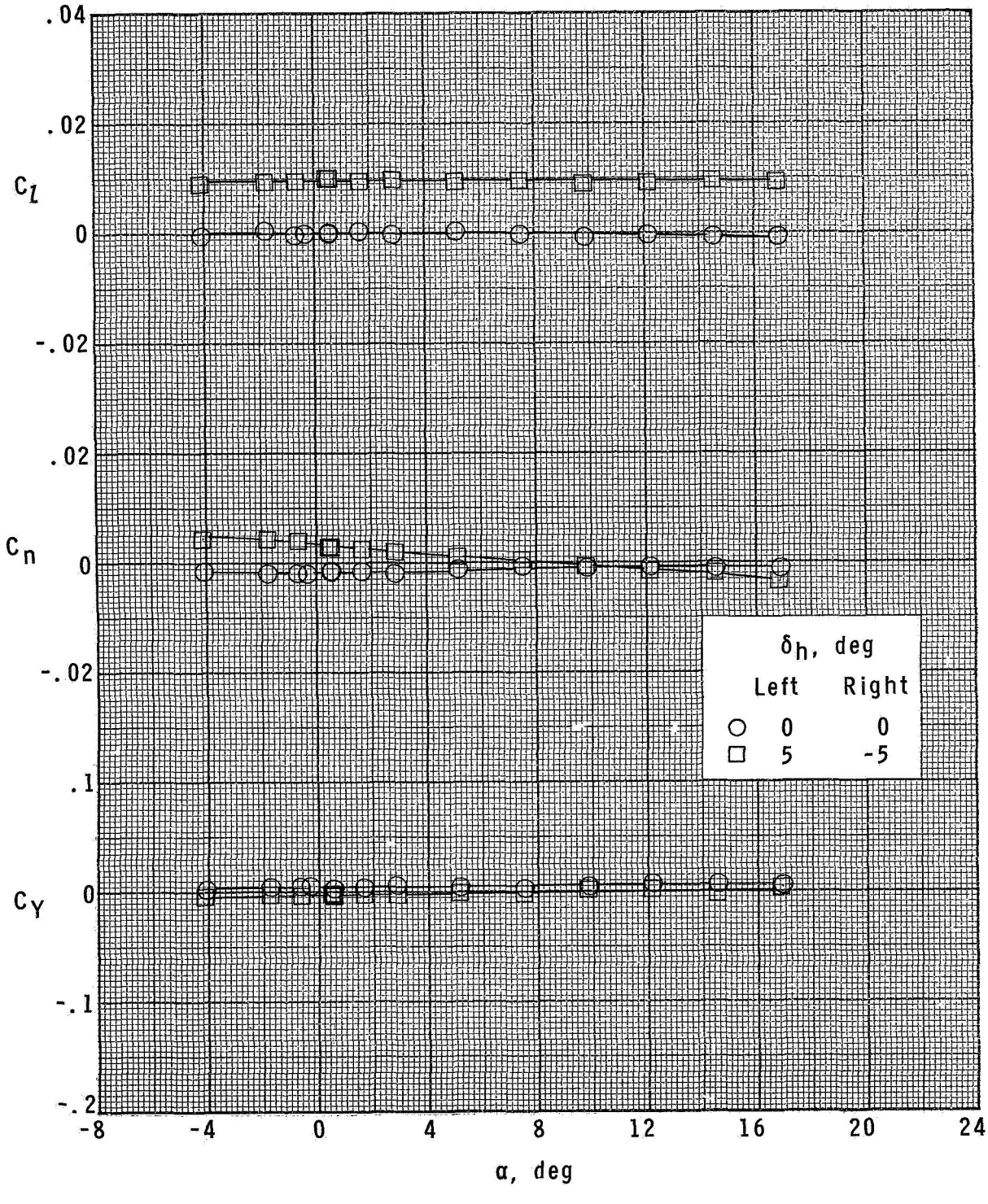
(a) M = 1.75.

Figure 27.- Roll control effectiveness of the horizontal tail for $B_{11}X_{16}W_2H_9T_{12}V_{U5}Y_5N_{13}$ (HRE on).



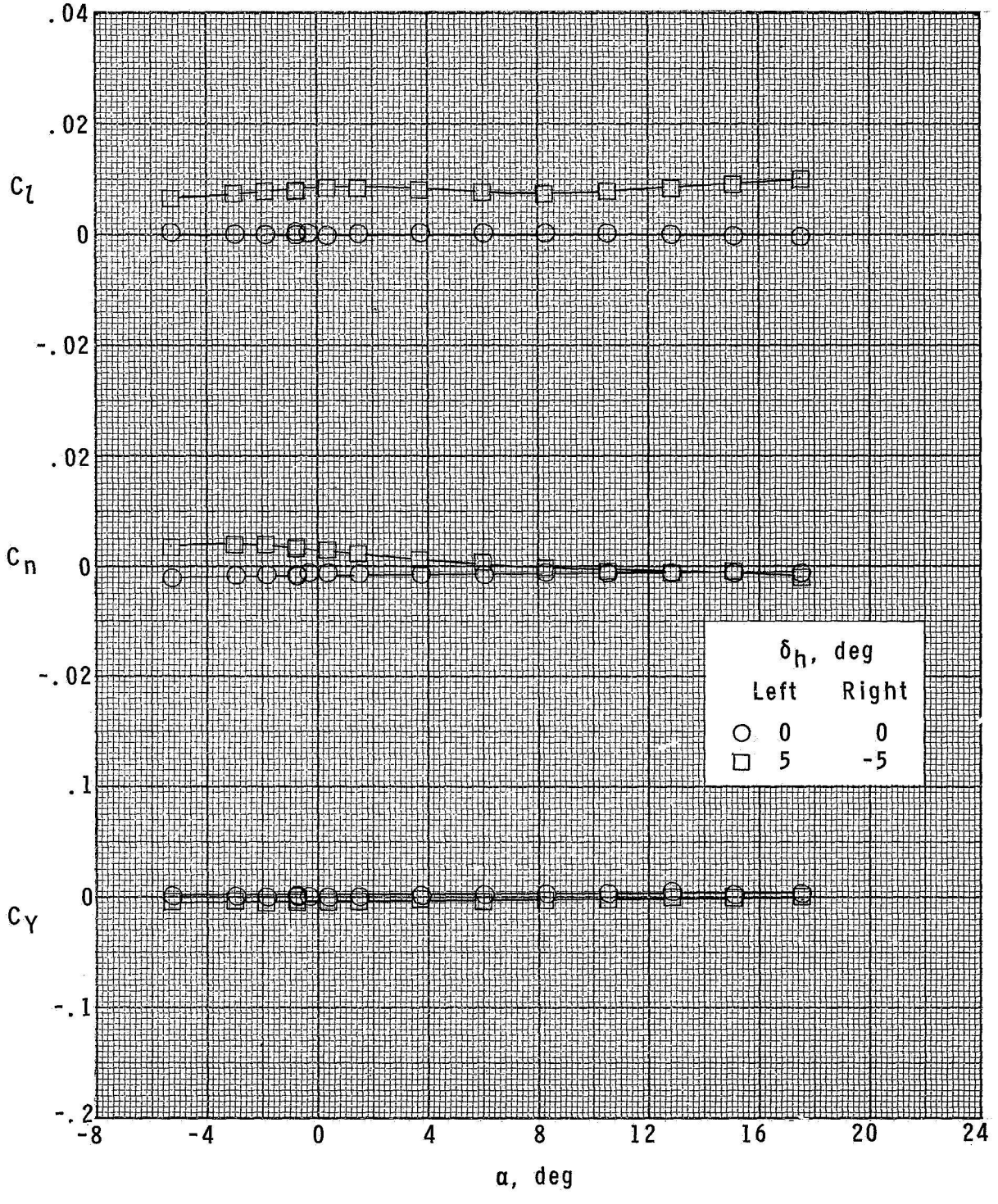
(b) M = 2.00.

Figure 27.- Continued.



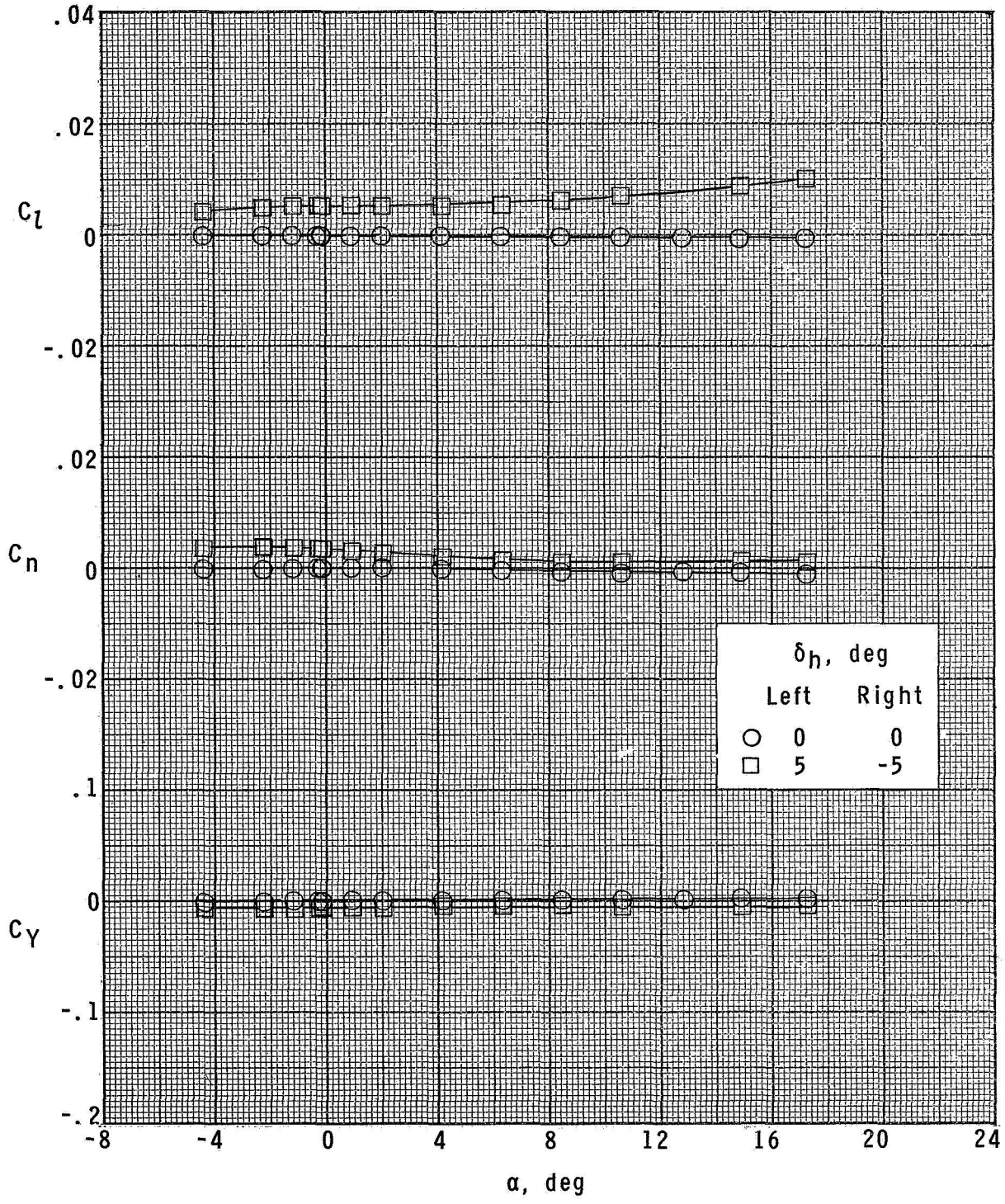
(c) M = 2.50.

Figure 27.- Continued.



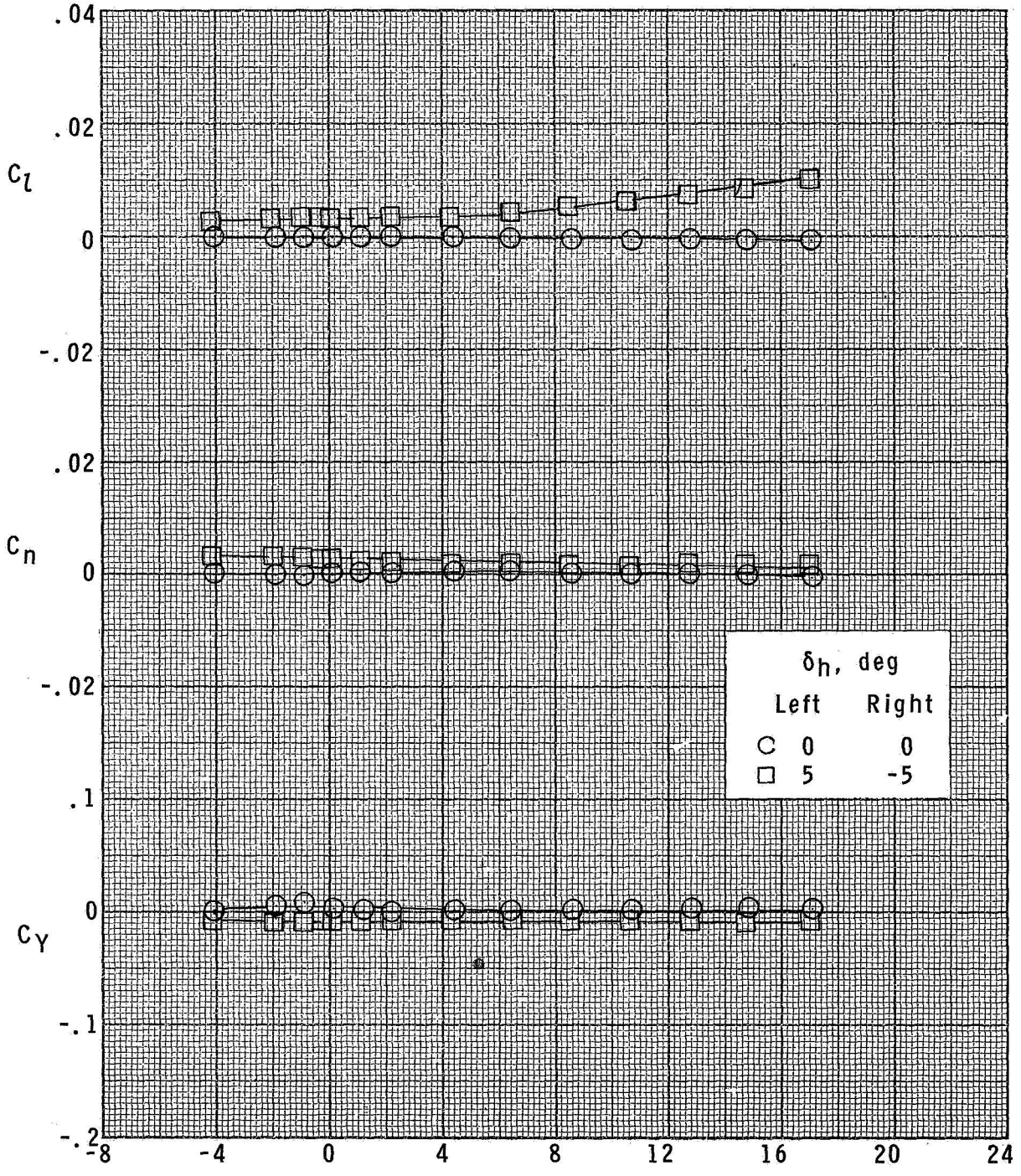
(d) M = 2.86.

Figure 27.- Continued.



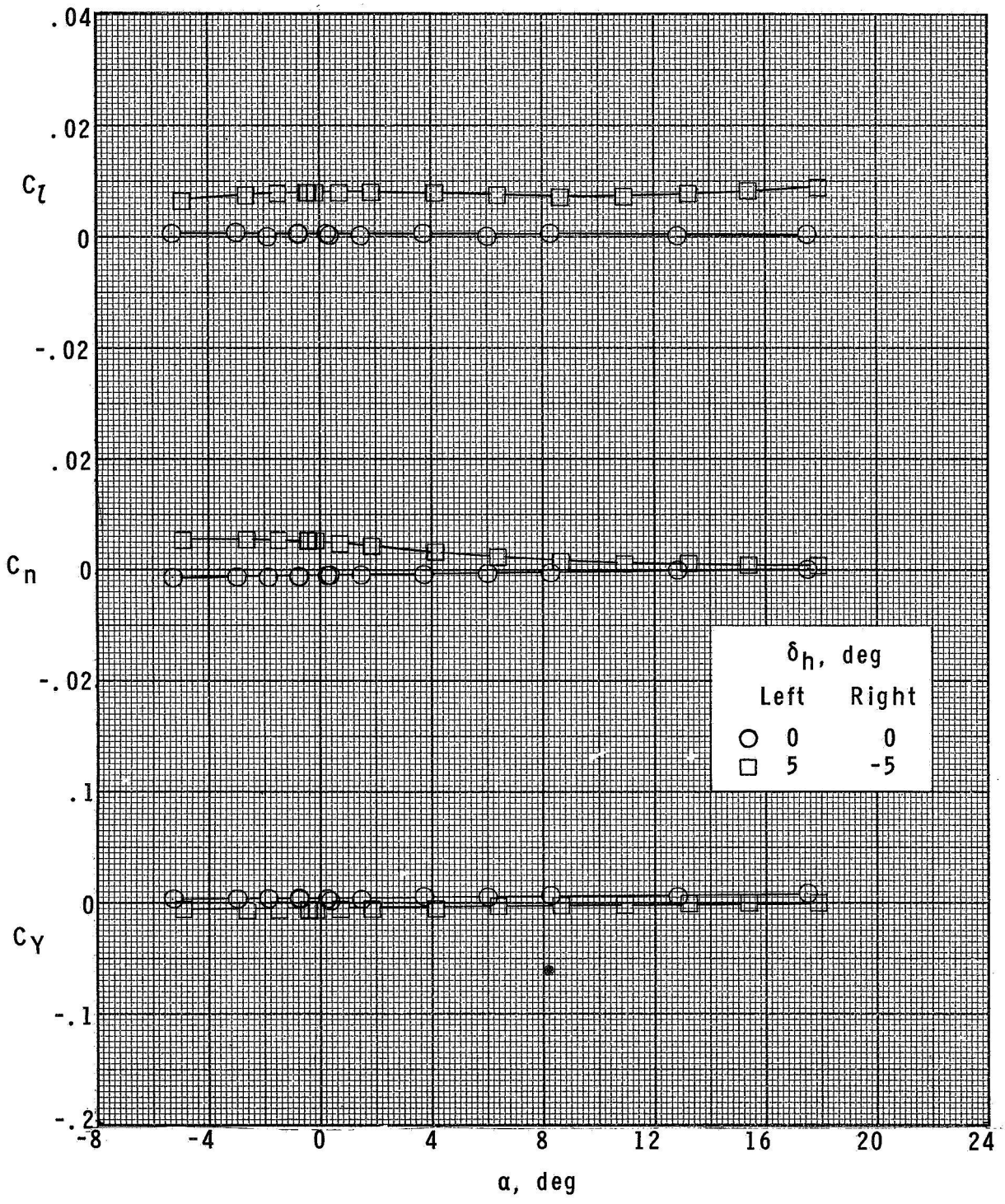
(e) M = 3.95.

Figure 27.- Continued.



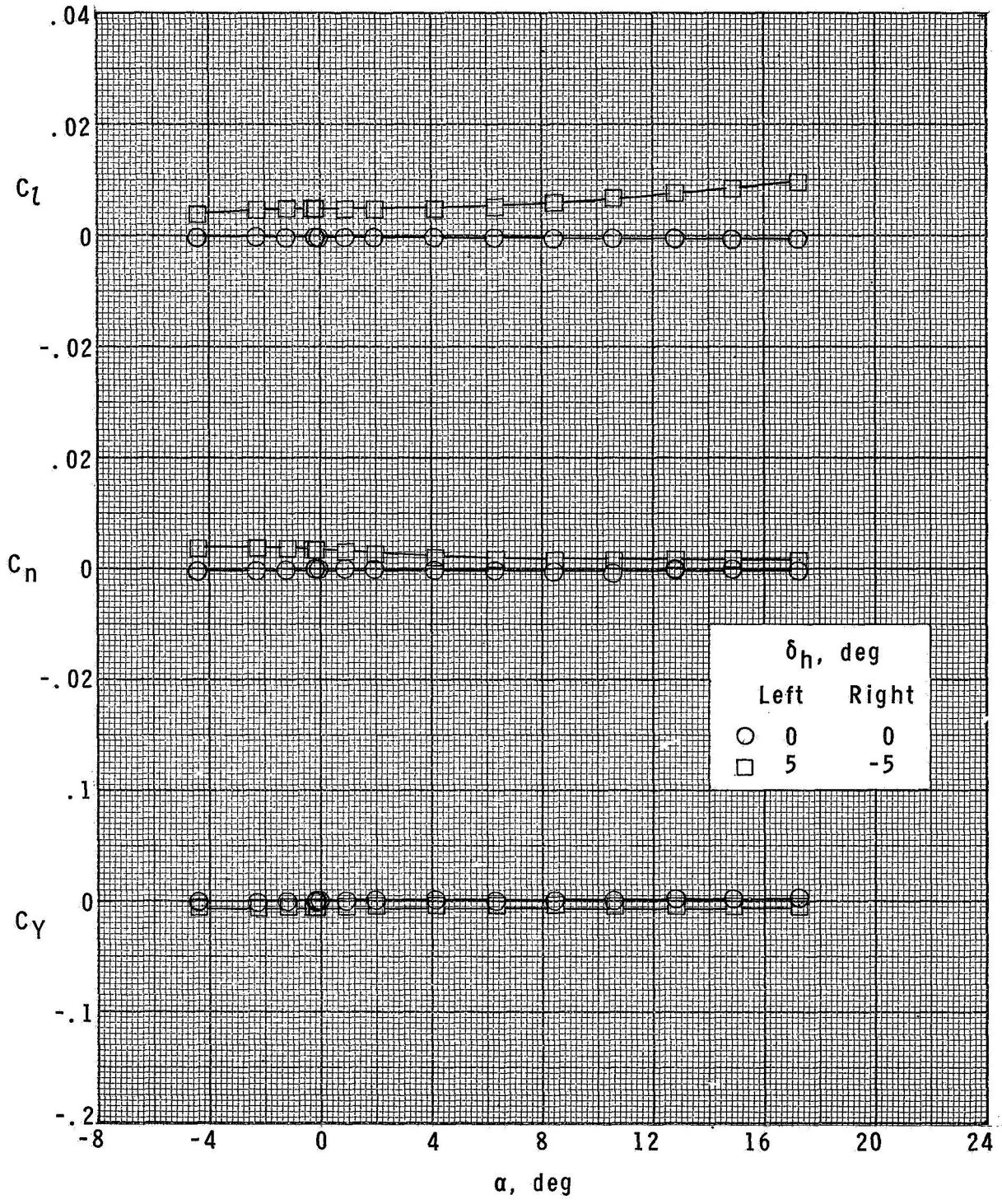
(f) M = 4.63.

Figure 27.- Concluded.



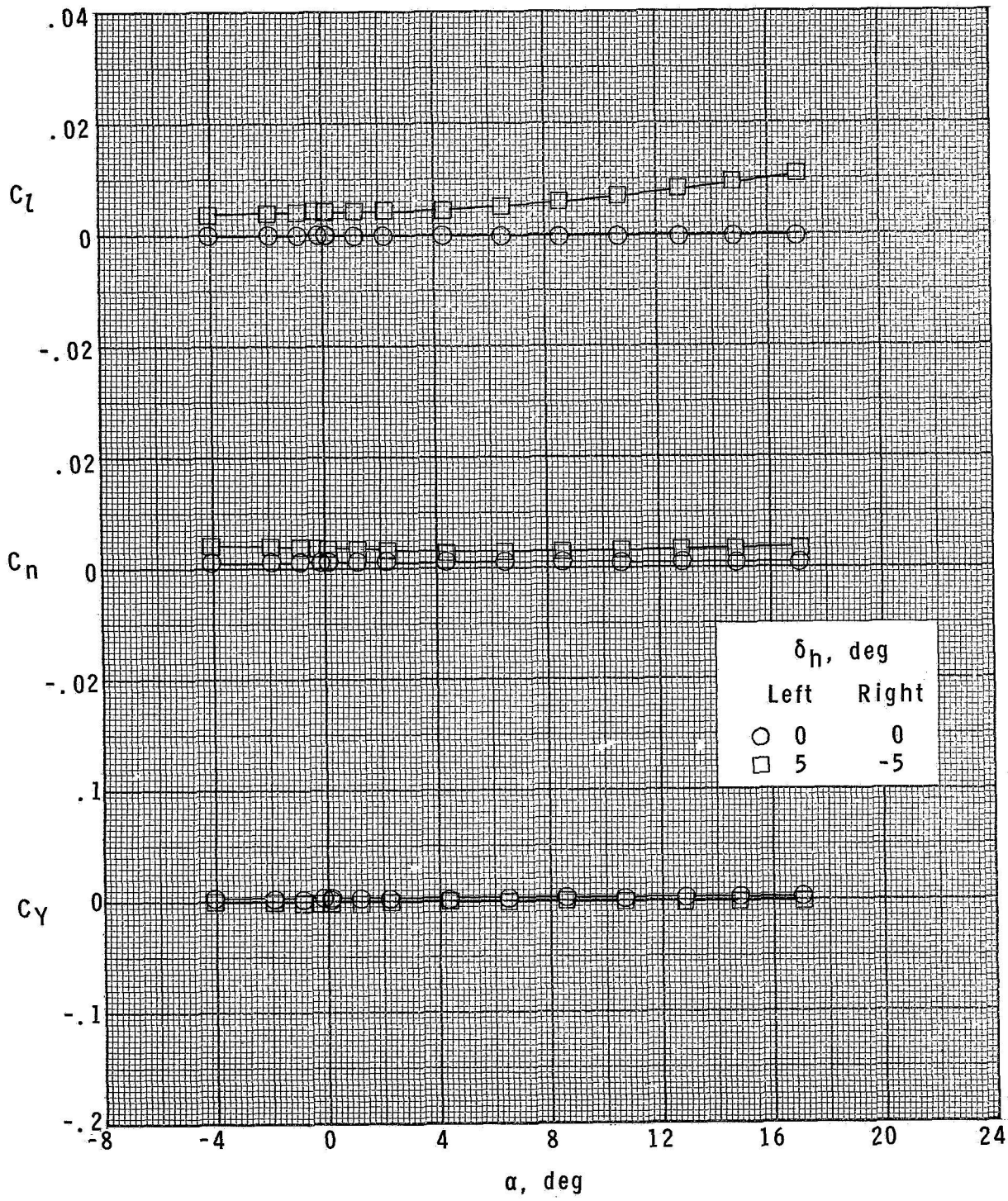
(a) M = 2.86.

Figure 28.- Roll control effectiveness of the horizontal tail for $B_{11}X_{16}W_2H_9T_{12}V_{U5}Y_5$ (HRE off).



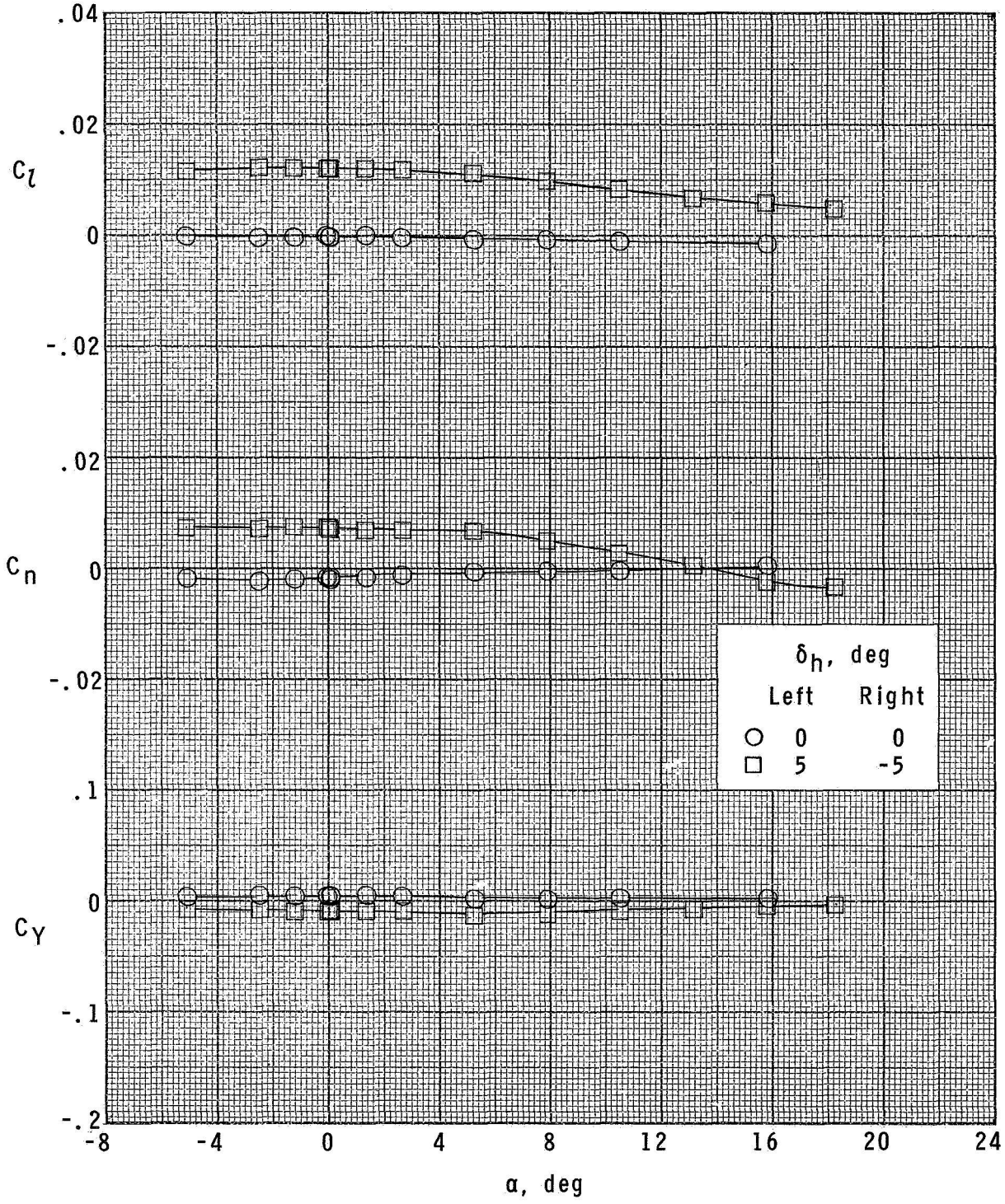
(b) M = 3.95.

Figure 28.- Continued.



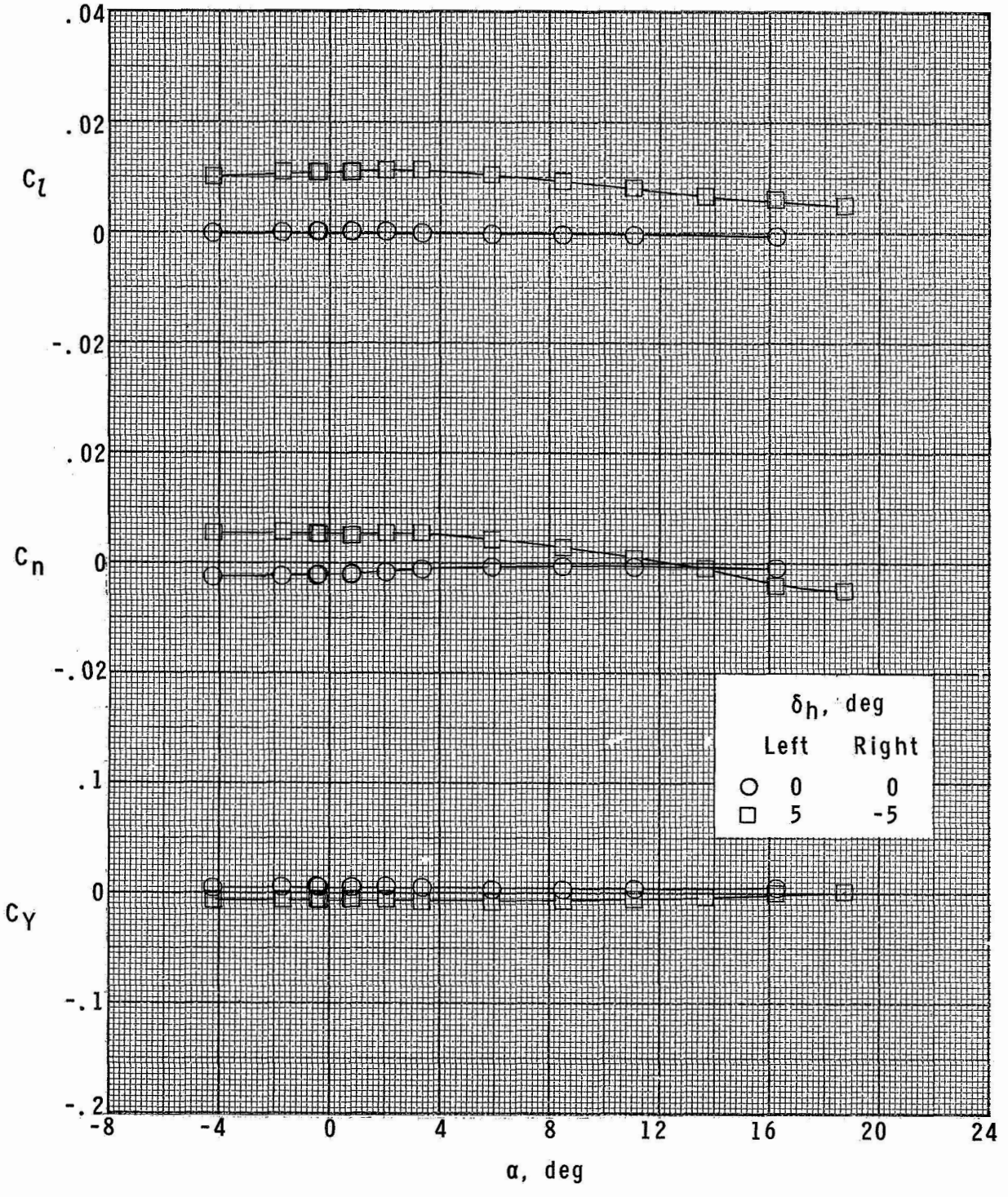
(c) M = 4.63.

Figure 28.- Concluded.



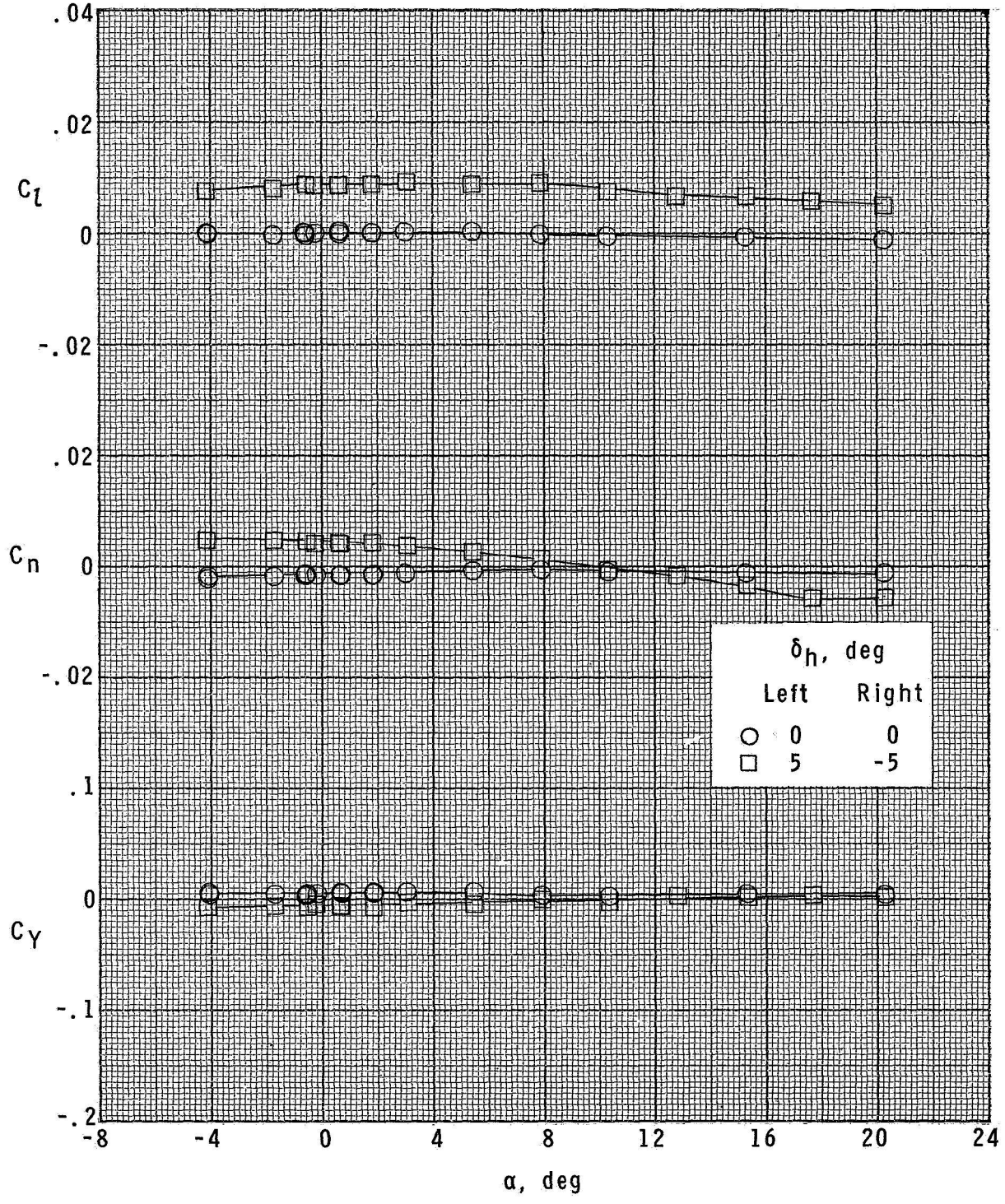
(a) M = 1.75.

Figure 29.- Roll control effectiveness of the horizontal tail for $B_{11}X_{16}W_2H_9T_{12}V_{U5}Y_5N_{13}T_{13}$ (HRE and tanks on).



(b) M = 2.00.

Figure 29.- Continued.



(c) M = 2.50.

Figure 29.- Concluded.

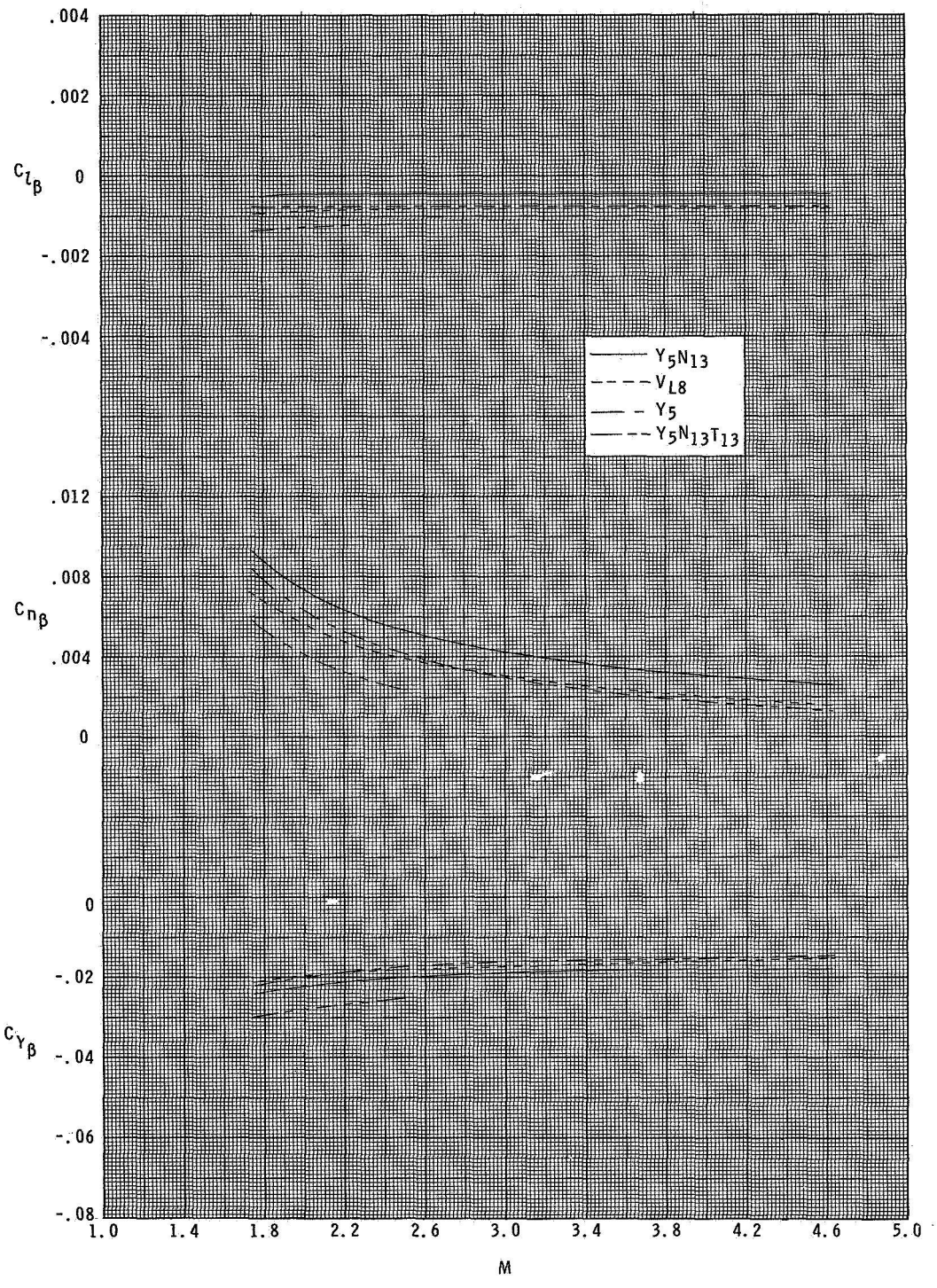
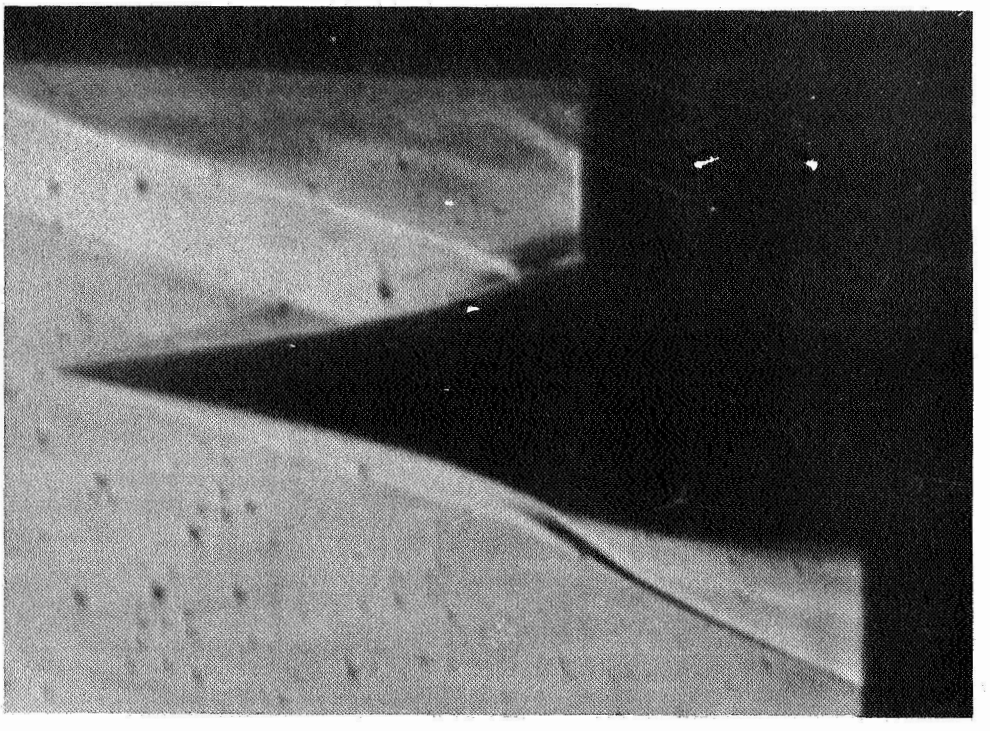


Figure 30.- Summary of lateral stability parameters for $B_{11}X_{16}W_2H_9T_{12}V_{U5}$.



(a) $B_{11}X_{16}W_2H_9T_{12}V_{U5}Y_5N_{13}$; $\alpha \approx 0^0$; M = 4.63.



(b) Blowup of HRE from above photograph. L-69-1375

Figure 31.- Schlieren photographs.

NASA-Langley, 1969 —— 1

NATIONAL AERONAUTICS AND SPACE ADMINISTRATION
WASHINGTON, D.C. 20546

OFFICIAL BUSINESS

FIRST CLASS MAIL

POSTAGE AND FEES PAID
NATIONAL AERONAUTICS AN
SPACE ADMINISTRATION

POSTMASTER: If Undeliverable (Section 15
Postal Manual) Do Not Retu

"The aeronautical and space activities of the United States shall be conducted so as to contribute . . . to the expansion of human knowledge of phenomena in the atmosphere and space. The Administration shall provide for the widest practicable and appropriate dissemination of information concerning its activities and the results thereof."

—NATIONAL AERONAUTICS AND SPACE ACT OF 1958

NASA SCIENTIFIC AND TECHNICAL PUBLICATIONS

TECHNICAL REPORTS: Scientific and technical information considered important, complete, and a lasting contribution to existing knowledge.

TECHNICAL NOTES: Information less broad in scope but nevertheless of importance as a contribution to existing knowledge.

TECHNICAL MEMORANDUMS: Information receiving limited distribution because of preliminary data, security classification, or other reasons.

CONTRACTOR REPORTS: Scientific and technical information generated under a NASA contract or grant and considered an important contribution to existing knowledge.

TECHNICAL TRANSLATIONS: Information published in a foreign language considered to merit NASA distribution in English.

SPECIAL PUBLICATIONS: Information derived from or of value to NASA activities. Publications include conference proceedings, monographs, data compilations, handbooks, sourcebooks, and special bibliographies.

TECHNOLOGY UTILIZATION PUBLICATIONS: Information on technology used by NASA that may be of particular interest in commercial and other non-aerospace applications. Publications include Tech Briefs, Technology Utilization Reports and Notes, and Technology Surveys.

Details on the availability of these publications may be obtained from:

SCIENTIFIC AND TECHNICAL INFORMATION DIVISION

NATIONAL AERONAUTICS AND SPACE ADMINISTRATION

Washington, D.C. 20546